frontiers | Research Topics

Insights in nutrition and food science technology

Edited by
Elena Ibañez and Alejandro Cifuentes

Published in
Frontiers in Nutrition

ISSN 1664-8714
ISBN 978-2-83251-404-7
DOI 10.3389/978-2-83251-404-7

About Frontiers

Frontiers is more than just an open access publisher of scholarly articles: it is a pioneering approach to the world of academia, radically improving the way scholarly research is managed. The grand vision of Frontiers is a world where all people have an equal opportunity to seek, share and generate knowledge. Frontiers provides immediate and permanent online open access to all its publications, but this alone is not enough to realize our grand goals.

Frontiers journal series

The Frontiers journal series is a multi-tier and interdisciplinary set of open-access, online journals, promising a paradigm shift from the current review, selection and dissemination processes in academic publishing. All Frontiers journals are driven by researchers for researchers; therefore, they constitute a service to the scholarly community. At the same time, the *Frontiers journal series* operates on a revolutionary invention, the tiered publishing system, initially addressing specific communities of scholars, and gradually climbing up to broader public understanding, thus serving the interests of the lay society, too.

Dedication to quality

Each Frontiers article is a landmark of the highest quality, thanks to genuinely collaborative interactions between authors and review editors, who include some of the world's best academicians. Research must be certified by peers before entering a stream of knowledge that may eventually reach the public - and shape society; therefore, Frontiers only applies the most rigorous and unbiased reviews. Frontiers revolutionizes research publishing by freely delivering the most outstanding research, evaluated with no bias from both the academic and social point of view. By applying the most advanced information technologies, Frontiers is catapulting scholarly publishing into a new generation.

What are Frontiers Research Topics?

Frontiers Research Topics are very popular trademarks of the *Frontiers journals series*: they are collections of at least ten articles, all centered on a particular subject. With their unique mix of varied contributions from Original Research to Review Articles, Frontiers Research Topics unify the most influential researchers, the latest key findings and historical advances in a hot research area.

Find out more on how to host your own Frontiers Research Topic or contribute to one as an author by contacting the Frontiers editorial office: frontiersin.org/about/contact

Insights in nutrition and food science technology

Topic editors

Elena Ibañez — Institute of Food Science Research, Spanish National Research Council (CSIC), Spain

Alejandro Cifuentes — Foodomics Lab, CIAL, Spanish National Research Council, Spain

Citation

Ibañez, E., Cifuentes, A., eds. (2023). *Insights in nutrition and food science technology*. Lausanne: Frontiers Media SA. doi: 10.3389/978-2-83251-404-7

Table of contents

frontiers | Frontiers in Nutrition

TYPE Editorial
PUBLISHED 09 January 2023
DOI 10.3389/fnut.2022.1129011

OPEN ACCESS

EDITED AND REVIEWED BY
Tai Boon Tan,
Universiti Putra Malaysia, Malaysia

*CORRESPONDENCE
Alejandro Cifuentes
✉ a.cifuentes@csic.es

SPECIALTY SECTION
This article was submitted to Nutrition and Food Science Technology, a section of the journal Frontiers in Nutrition

RECEIVED 21 December 2022
ACCEPTED 28 December 2022
PUBLISHED 09 January 2023

CITATION
Ibañez E and Cifuentes A (2023) Editorial: Insights in Nutrition and Food Science Technology.
Front. Nutr. 9:1129011.
doi: 10.3389/fnut.2022.1129011

Editorial: Insights in Nutrition and Food Science Technology

Elena Ibañez and Alejandro Cifuentes*

Foodomics Laboratory, Institute of Food Science Research (CIAL-CSIC), Madrid, Spain

KEYWORDS

sustainability, food safety and quality, healthy diets, food production, Sustainable Development Goals (SDGs)

Editorial on the Research Topic
Insights in Nutrition and Food Science Technology

Nutrition and Food Science and Technology is facing important challenges nowadays, mainly related to the roadmap toward the achievement of the Sustainable Development Goals (SDGs) such as zero hunger (SDG-2), good health and wellbeing (SDG-3), responsible consumption and production (SDG-12), climate action (SDG-13), life below water (SDG-14), and life on land (SDG-15), among others. To be able to advance in these goals, sustainable food production systems are needed, while ensuring food safety (1) and more healthy diets (2). This Research Topic focuses on new insights, novel developments, current challenges, latest discoveries, recent advances, and future perspectives in the field of Nutrition and Food Science and Technology. The main goal of this special Research Topic is therefore, to shed light on the progress made in the past decade in the Nutrition and Food Science & Technology field, and on its future challenges to provide a thorough overview of the field. Based on all the above, the following 10 works were included in the current Research Topic. Specifically, two review papers were dedicated to describe the effects of microwave heating on the structure, properties, and functions of macromolecular nutrients in novel food (Deng et al.) and to revise the effect of resistant starch on non-alcoholic fatty liver disease *via* the gut-liver axis (Zhu et al.). One brief research report was devoted to analyse the accumulation of flavonoids in *Dendrobium moniliforme* (L.) Sw. (a valuable herbal crop) by the integration of metabolomic and transcriptomic approaches (Yuan et al.). The other seven papers were published as original research contributions and were focused on (i) the integrated analysis of metabolome and transcriptome data for uncovering flavonoid components of *Zanthoxylum bungeanum* Maxim leaves under drought stress (Hu et al.); (ii) the integrated metabolomic and transcriptomic analyses to reveal novel insights of anthocyanin biosynthesis on color formation in cassava tuberous roots (Fu et al.); (iii) the identification of iron and zinc responsive genes in pearl millet using genome-wide RNA-sequencing approach (Goud et al.); (iv) the identification and analysis of major flavor compounds in radish taproots by widely targeted metabolomics (Mei et al.); (v) the development of a new indicator of overeating saturated fat based on serum fatty acids and

amino acids and its association with incidence of type 2 diabetes using two randomized controlled feeding trials and a prospective study (Wei et al.); (vi) the optimization of the ultrasound-assisted extraction of naturally occurring glucosinolates from by-products of *Camelina sativa* L. and their effect on human colorectal cancer cells (Pagliari et al.) and (vii) the investigation of the molecular mechanisms of flavonoid accumulation in germinating common bean (*Phaseolus vulgaris*) under salt stress (Zhang et al.). We hope this article collection may help, inform and provide direction and guidance to many colleagues working in this hot field of research.

Author contributions

EI and AC acted as editors of all the manuscript submitted to the Research Topic *Insights in Nutrition and Food Science Technology*. AC supervised and wrote the editorial article. EI reviewed the final version of the editorial article. Both authors approved the final version of the manuscript for publication.

Funding

This work was supported by the Ministry of Science and Innovation of Spain (Grant Nos. PID2020-113050RB-I00 and PDC2021-120814-I00).

Acknowledgments

As editors of this Research Topic devoted to *Insights in Nutrition and Food Science Technology*, we would like to thank all the authors for their suitable contributions, all reviewers for the time they devoted to the evaluation of the papers, Marta Klinska for her continuous help and support, and to those of Frontiers in Nutrition team who contributed with their effort for the preparation of this Research Topic. Muchas gracias a todos!

Conflict of interest

The authors declare that the research was conducted in the absence of any commercial or financial relationships that could be construed as a potential conflict of interest.

Publisher's note

References

1. Ballesteros-Vivas D, Socas-Rodríguez B, Mendiola JA, Ibañez E, Cifuentes A. Green food analysis: current trends and perspectives. *Curr Opin Green Sustain Chem.* (2021) 31:100522. doi: 10.1016/j.cogsc.2021.100522

2. Willett W, Rockström J, Loken B, Springmann M, Lang T, Vermeulen S, et al., Food in the Anthropocene: the EAT–Lancet Commission on healthy diets from sustainable food systems. *Lancet.* (2019) 393:447–92. doi: 10.1016/S0140-6736(18)31788-4

frontiers in Nutrition

ORIGINAL RESEARCH
published: 04 February 2022
doi: 10.3389/fnut.2021.801244

Integrated Analysis of Metabolome and Transcriptome Data for Uncovering Flavonoid Components of *Zanthoxylum bungeanum* Maxim. Leaves Under Drought Stress

Haichao Hu[1,2†], *Xitong Fei*[1,2†], *Beibei He*[3], *Yingli Luo*[1,2], *Yichen Qi*[1,2] *and Anzhi Wei*[1,2*]

[1] College of Forestry, Northwest Agriculture and Forestry University, Xianyang, China, [2] Research Centre for Engineering and Technology of Zanthoxylum State Forestry Administration, Xianyang, China, [3] College of Horticulture, Northwest Agriculture and Forestry University, Xianyang, China

OPEN ACCESS

Edited by:
Elena Ibañez,
Institute of Food Science Research, Spanish National Research Council (CSIC), Spain

Reviewed by:
Anna Lisa Piccinelli, University of Salerno, Italy
Lidia Montero, University of Duisburg-Essen, Germany
Gerardo Alvarez Rivera, Spanish National Research Council (CSIC), Spain

***Correspondence:**
Anzhi Wei
weianzhi@nwafu.edu.cn

† These authors have contributed equally to this work

Specialty section:
This article was submitted to Nutrition and Food Science Technology, a section of the journal Frontiers in Nutrition

Received: 25 October 2021
Accepted: 03 December 2021
Published: 04 February 2022

Citation:
Hu H, Fei X, He B, Luo Y, Qi Y and Wei A (2022) Integrated Analysis of Metabolome and Transcriptome Data for Uncovering Flavonoid Components of Zanthoxylum bungeanum Maxim. Leaves Under Drought Stress. Front. Nutr. 8:801244. doi: 10.3389/fnut.2021.801244

Zanthoxylum bungeanum Maxim. leaves (ZBLs) are rich in flavonoids and have become popular in nutrition, foods and medicine. However, the flavonoid components in ZBLs and the mechanism of flavonoid biosynthesis under drought stress have received little attention. Here, we performed an integrative analysis of the metabolome and transcriptome of ZBLs from HJ (*Z. bungeanum* cv. "Hanjiao") and FJ (*Z. bungeanum* cv. "Fengjiao") at four drought stages. A total of 231 individual flavonoids divided into nine classes were identified and flavones and flavonols were considered the most abundant flavonoid components in ZBLs. The total flavonoid content of ZBLs was higher in FJ; it increased in FJ under drought stress but decreased in HJ. Nine-quadrant analysis identified five and eight differentially abundant flavonoids in FJ and HJ leaves, respectively, under drought stress. Weighted gene correlation network analysis (WGCNA) identified nine structural genes and eight transcription factor genes involved in the regulation of flavonoid biosynthesis. Moreover, qRT-PCR results verified the accuracy of the transcriptome data and the reliability of the candidate genes. Taken together, our results reveal the flavonoid components of ZBLs and document changes in flavonoid metabolism under drought stress, providing valuable information for nutrition value and food utilization of ZBLs.

Keywords: ***Zanthoxylum bungeanum*** **Maxim. leaves, flavonoids, metabolome, drought stress, WGCNA**

INTRODUCTION

Zanthoxylum bungeanum Maxim. is a native shrub from the Rutaceae family in east Asian countries and is also named Chinese prickly ash (1). As an economically important plant, *Z. bungeanum* is widely planted in water-deficit areas because of its high drought stress tolerance and the high nutrition value of its products. *Z. bungeanum* cv. "Fengjiao" (FJ) and *Z. bungeanum* cv. "Hanjiao" (HJ) are the main breeding cultivars in the northwest region of China. Like the *Z. bungeanum* pericarp, the leaf is another main *Z. bungeanum* product that is generally used in nutrition, food and medicine because of its abundant flavonoid content and health benefits to the human body. As a food additive and condiment, *Z. bungeanum* leaf (ZBL) is widely introduced into food products

for its special flavor and distinctive numbing taste (2). The fresh sprouts and young leaves of *Z. bungeanum* are popular vegetables in Chinese cuisine (3). In addition, ZBLs can be made into a green tea and oral liquid for drinking, and ZBL extract oil can be made into an edible essence for foods (3).

Flavonoids are an important type of polyphenolic secondary metabolite with a common 3-C chemical structure (C6-C3-C6) (4). Flavonoids are present throughout the plant kingdom, and over 6000 different flavonoids have been discovered to date (5). Flavonoids in plants are widely used in the fields of nutrition, food and medicine. Catechins were reported to be the most powerful flavonoids in green and black tea for protecting the body against reactive oxygen species (6, 7). Quercetin, kaempferol, and isorhamnetin in *Ginkgo biloba* leaves are considered to be effective flavonoids for reducing the risks of non-alcoholic fatty liver disease (NAFLD) (8). Flavonoid biosynthesis involves both the phenylpropanoid metabolic pathway and the flavonoid biosynthetic pathway. It has been comprehensively elucidated in several model plants, such as *Arabidopsis thaliana* L. (9) and *Zea mays* L. (10). In the phenylpropanoid metabolic pathway, phenylalanine is transformed into p-coumaryl CoA in a series of reactions catalyzed by phenylalanine ammonia lyase (PAL), cinnamate 4-hydroxylase (C4H), and 4-coumaroyl CoA ligase (4CL). In the flavonoid biosynthetic pathway, p-coumaryl-CoA is transformed into naringin by chalcone synthase (CHS) and chalcone isomerase (CHI), and naringenin, which serves as a core substrate, is transformed into many other classes of flavonoids by the corresponding enzymes: dihydroflavonols by flavanone 3 β-hydroxylase (F3H), leucoanthocyanidins by dihydroflavonol-4-reducatse (DFR), flavonols by flavonol synthase (FLS), flavones by flavone synthase (FNS), flavanols by leucoanthocyanidin reductase (LAR), and anthocyanidins by anthocyanidin synthase (ANS) and anthocyanidin reductase (ANR) (11). In addition, the transcription of flavonoid biosynthesis structural genes is largely regulated by transcription factors (TFs), especially MYB, bHLH, and WD40 proteins (MBW) (12).

To date, increasing efforts have been made to identify the chemical compositions of ZBLs, with particular attention given to flavonoid compounds (2, 13). However, only several flavonoid components of ZBLs have been identified to date; most are still unknown, which could restrict the development of ZBL products in the food industry. Moreover, as important secondary metabolites, flavonoids participate in many physiological functions in response to biotic and abiotic stress (14) and are easily affected by environmental variation. For instance, Guo et al. (15) found that higher solar radiation in the northwestern areas of China increased flavonol content and decreased leaf dry mass, and Deluc et al. (16) reported that water deficit promoted the accumulation of anthocyanin in red grapes. The water-deficient environment in which *Z. bungeanum* is typically grown makes drought its major abiotic stress. Nonetheless, the effects of drought stress on flavonoids in ZBLs remain unexplored.

Here, an integrative analysis of widely targeted metabolome and transcriptome data from ZBLs was performed to investigate flavonoid compositions in ZBLs and examine flavonoid metabolism under drought stress. Several key candidate structural genes and TF genes involved in the regulation of flavonoid synthesis were identified by weighted gene correlation network analysis (WGCNA). The results improved the understanding of nutrition value and provide valuable information for food utilization of ZBLs.

MATERIALS AND METHODS

Plant Materials and Treatments

Mature seeds of FJ (*Z. bungeanum* cv. "Fengjiao") and HJ (*Z. bungeanum* cv. "Hanjiao") were collected from the Prickly Ash Experimental Station of Northwest Agriculture and Forestry University in Fengxian, Shannxi Province, China (N33°59′6.55″, E106°39′29.38″). After cleaning and pretreatment, the seeds were sown in trays (38 cm × 25 × 15 cm) in a soil mix of perlite, vermiculite, and chernozem and germinated at 25 ± 2 °C and 60–70% humidity in an experimental greenhouse at Northwest A&F University in Yangling, Shannxi Province, China. Two weeks after germination, healthy seedlings were transplanted separately into pots (32 cm high and 28 cm in diameter) and then cultivated with a soil water content of 85%.

Sixty three-month-old healthy seedlings of each cultivar with uniform growth were selected for treatment and sampling. The water supply to the seedlings was stopped at the onset of the drought treatment; leaves were sampled from the seedlings at 4 stages, 0 d (D1), 6 d (D2), 9 d (D3), and 15 d (D4) and immediately placed in liquid nitrogen. Three biological replicates of five seedlings each were sampled at each stage. The samples were stored in a −80°C freezer for further study.

Flavonoid Metabolite Profiling of ZBLs by UPLC-MS/MS

Flavonoid metabolites were extracted and identified by the Metware Biotechnology Co. Ltd. (Wuhan, China). The leaf samples were vacuum freeze-dried in a freeze drier (Scientz-100F, Zhejiang, China) and then ground into powder using a grinding mill (MM 400, Retsch, Germany). One-hundred milligrams of powder was dissolved in 1.2 mL 70% aqueous methanol (*v/v*) and mixed well with a Vortex-6 (Kylin-Bell, Jiangsu, China). The homogenate was extracted overnight at 4 °C and then centrifuged (5424R, Eppendorf Co., Shanghai, China) at 12,000 rpm at 4°C for 10 min. The obtained supernatant was filtered through a 0.22-μm organic nylon needle filter (SCAA-104, ANPEL, Shanghai, China) and stored in a sample bottle.

Ultra-performance liquid chromatography (UPLC) was performed using the Shimadzu Nexera X2 instrument (Shimadzu, Japan) equipped with an Agilent SB-C18 column (1.8 μm, 2.1 × 100 mm). The mobile phase was composed of ultrapure water with 0.1% formic acid (solvent A) and acetonitrile with 0.1% formic acid (solvent B). The gradient of solvent B was as follows: 0 min, 5%; 0–9 min, raised to 95%; 9–10 min, 95%; 10–11.10 min, reduced to 5%; 11.10–14 min, 5% (17). The column temperature was set to 40°C, and the injection volume was 4 μL.

The tandem mass spectrometry (MS/MS) analysis was performed using the Applied Biosystems 4,500 QTRAP

instrument (ABI, Framingham, USA). Linear ion trap (LIT) and triple quadrupole (QQQ) scans were obtained with the API 4500 QTRAP UPLC–MS/MS system, which was equipped with an ESI turbo ion-spray interface. The ESI source operations were carried out as follows: turbo spray in ion source, 550°C for source temperature; ion spray (IS) voltage, 5,500 V (positive ion mode)/−4500 V (negative ion mode); ion source gas I (GSI), ion source gas II (GSII), and curtain gas (CUR) set to 50, 60, and 25 psi, respectively; high ionization induction parameters. In addition, 10μM polypropylene glycol solutions in QQQ mode and 100μM polypropylene glycol solutions in LIT mode were used for instrument calibration.

Flavonoid Metabolite Data Analysis

Qualitative data analysis was performed based on secondary spectrum information from the MWDB database compiled by Metware Biotechnology Co., Ltd. (Wuhan, China). Flavonoids with variable importance in projection (VIP) ≥ 1 and fold change (FC) > 2 were defined as differentially accumulated flavonoids (DAFs). The Kyoto Encyclopedia of Genes and Genomes (KEGG) and the Plant Metabolic Network (PMN) databases were used to perform pathway enrichment analysis of these flavonoids.

RNA-Seq Analysis

RNA-Seq was performed by Biomarker Technologies Co., Ltd. (Beijing, China). Total RNA was extracted from ZBL samples using the Tiangen RNA Pure kit for plants (Tiangen, Beijing, China). RNA integrity and concentration were assessed using an Agilent 2100 Bioanalyzer (Agilent Technologies, Inc., Santa Clara, CA, USA). The cDNA libraries were constructed according to the manufacturer's instructions of the NEBNext Ultra RNA Library Prep Kit for Illumina (New England Biolabs, Ipswich, USA). The resulting ZBL libraries were sequenced on a flow cell of the Illumina HiSeq 2500 platform (Illumina, Inc., San Diego, USA).

Genes with FC ≥ 2 and false discovery rate (FDR) < 0.01 were identified as differentially expressed genes (DEGs). Gene functional annotation and pathway analysis were performed based on seven databases: GO (Gene Ontology), KO (KEGG Ortholog database), KOG/COG (Clusters of Orthologous Groups of proteins), Nr (NCBI non-redundant protein sequences), Nt (NCBI non-redundant nucleotide sequences), Pfam (Protein family), and Swiss-Prot (a manually annotated and reviewed protein sequence database).

Co-expression Network Analysis of Flavonoid Metabolome and Transcriptome

Co-expression network analysis was performed based on the transcriptome data using the WGCNA R package (v1.68) (18). Genes with FPKM > 1 were used as the input file, and nine classes of flavonoids were used as the trait file to generate the co-expression network and modules. Network construction and module identification were performed based on topological overlap measure (TOM) similarity. The modules were used to calculate the relationships among gene expression levels and flavonoid abundances in the 24 samples. The co-expression network was visualized using Cytoscape v3.8.0 with threshold $= 0.25$.

Quantitative Real-Time PCR (qRT-PCR) Analysis

Total RNA was extracted from ZBL samples according to the instructions of the Tiangen RNA Pure kit for plants (Tiangen, Beijing, China). The purity, concentration, and integrity of total RNA were measured on a NanoDrop 2000 spectrophotometer (Thermo Scientific, Wilmington, DE, USA). First-strand cDNA was synthesized using the PrimeScript RT reagent kit with gDNA Eraser (Takara Biotechnology Inc., Dalian, China). The qRT-PCR analysis was performed using TB Green Premix Ex Taq II (Cat. No. RR820A, Takara Biotechnology Inc., Dalian, China) on a CFX96 Real-Time System (Bio-Rad Laboratories, Inc., Hercules, USA). The reaction protocol followed the manufacturer's instructions: 1 cycle at 98°C for 30 s; 38 cycles at 95°C for 5 s, 56°C for 30 s, and 72°C for 30 s; and 4°C until removal. The specific quantitative primers (**Supplementary Table 1**) were designed using Primer Premier 6.0 (PREMIER Biosoft, CA, USA). The relative expression levels were calculated by the $2^{-\Delta\Delta}$CT method using *ZbUBA* and *ZbUBQ* as internal standards.

Statistical Analysis

The experimental data from three independent biological replicates were analyzed by one-way analysis of variance (ANOVA), and significant differences were determined by Duncan's multiple range test ($p < 0.05$) using SPSS 22.0 Statistics (SPSS Inc., Chicago, IL, USA). Hierarchical clustering analysis (HCA) was constructed using online software with default value at https://cloud.metware.cn/toolCustom/3. Principal component analysis (PCA) and orthogonal partial least squares discriminant analysis (OPLS-DA) were performed using software available at https://www.omicshare.com/tools/Home/Soft/getsoft. Bar graphs were created in OriginPro 2021 (OriginLab, Northampton, Massachusetts, USA). Log10 conversion is used to standardize our data in HCA, PCA and OPLS-DA.

RESULTS

Flavonoid Metabolomic Analysis of ZBLs

FJ and HJ leaves were sampled at four drought treatment stages (**Figure 1A**). At the second stage (F2), FJ showed slightly curled leaves caused by water loss, and this symptom became increasingly severe at the third (F3) and final (F4) stages. By contrast, HJ first displayed leaf curl under drought stress at the third stage (H3) and showed a less severe response to drought than FJ at every stage other than D0. These results indicated that HJ was more tolerant to drought stress than FJ.

In total, 231 flavonoids were identified from leaves of both FJ and HJ. In FJ, quercetin-3-O-(6″-malonyl)-galactoside was the most abundant flavonoid, followed by keracyanin, kaempferol-7-O-rhamnoside, isovitexin, and rutin. In HJ, guaijaverin was the most abundant flavonoid, followed by spiraeoside, kaempferol-7-O-rhamnoside, hesperetin-5-O-glucoside, and quercetin-7-O-glucoside (**Supplementary Figure 1**). Based on

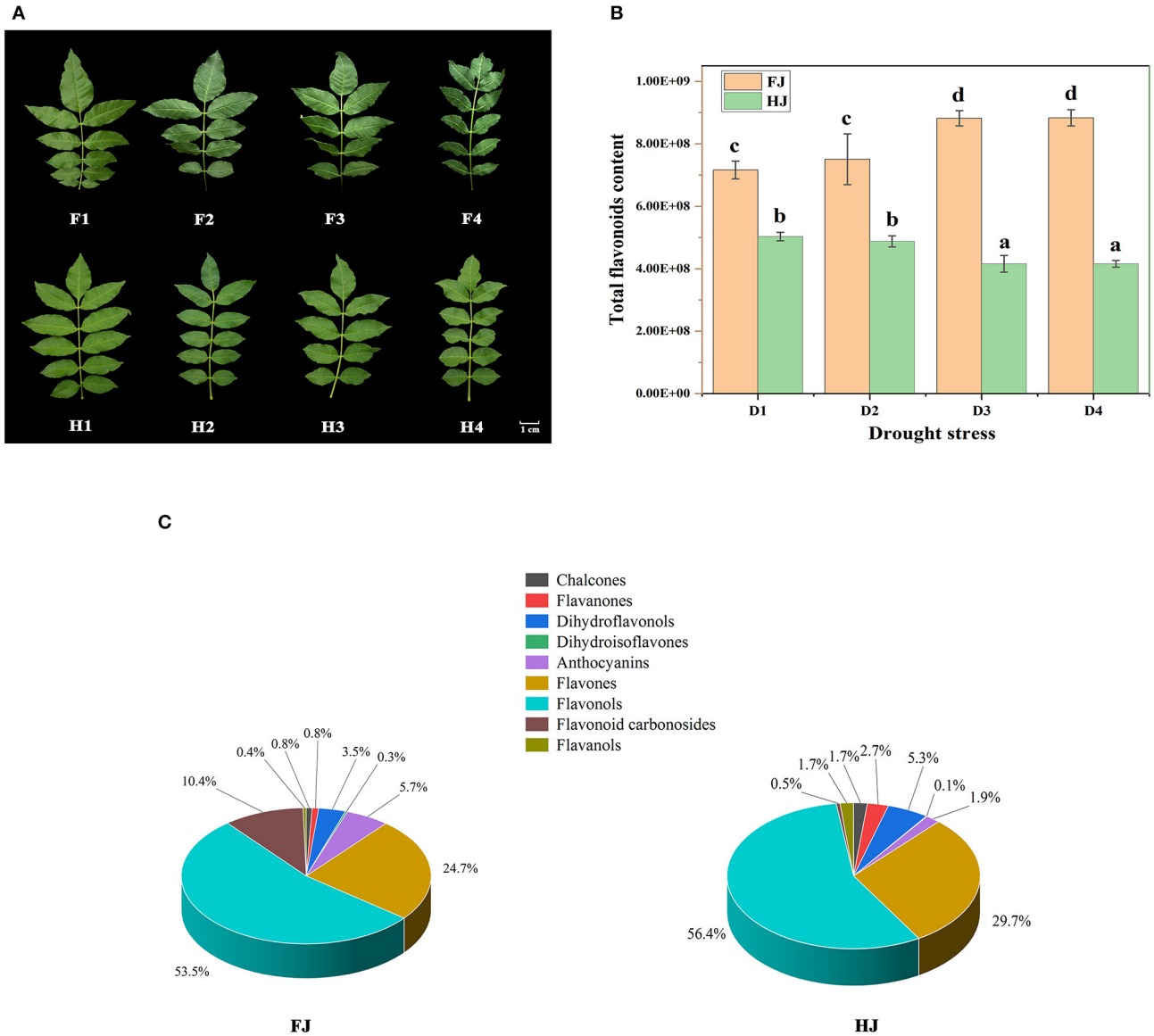

FIGURE 1 | The variation in flavonoid compositions of ZBLs under drought stress. **(A)**: the phenotype of ZBLs under drought stress. F1–F4 indicate FJ leaves exposed to drought treatment for 0 d, 6 d, 9 d, and 12 d; H1–H4 indicate HJ leaves exposed to drought treatment for 0 d, 6 d, 9 d, and 12 d. **(B)**: the relative content of total flavonoid of ZBLs from FJ and HJ under drought stress. D1–D4 indicate the four drought treatment stages. **(C)**: Classifications and proportions of 231 flavonoids detected in ZBLs. The mean values and SDs were calculated using one-way ANOVA followed by Duncan's multiple range test.

modifications of the C6-C3-C6 structure, the 231 flavonoids were divided into 9 classes: 7 chalcones, 19 flavanones, 2 dihydroisoflavones, 10 dihydroflavonols, 3 anthocyanins, 91 flavones, 80 flavonols, 10 flavonoid carbonosides, and 9 flavanols (**Supplementary Table 2**). The total flavonoid content increased steadily from D1 to D4 in FJ but decreased in HJ (**Figure 1B**). The total flavonoid content was significantly lower in HJ than in FJ at every time point. Among the nine classes, flavonols made up the highest proportion of total flavonoids (53.5 and 56.4%) in both FJ and HJ (**Figure 1C**), followed by flavones (24.7% and 29.7%). Flavonoid carbonosides and anthocyanins made up 10.4 and 5.7% of the total flavonoid content in FJ but only 4.5 and 0.9% in HJ. However, the proportion of flavanols was significantly higher in HJ (1.7%) than in FJ (0.4%).

The relative contents of the nine flavonoid classes changed differently under drought stress (**Supplementary Figure 2**). Chalcones and flavanones decreased in both cultivars under drought, whereas dihydroisoflavones and dihydroflavonols changed slightly. The content of flavonoid carbonosides increased in FJ during drought stress but not in HJ. The contents of the other four classes increased in FJ but decreased in HJ.

Differentially Accumulated Flavonoids in ZBLs Under Drought Stress

Hierarchical clustering analysis (HCA) and principal component analysis (PCA) were performed to investigate the flavonoid profiles of the eight sample types (**Figures 2A,B**). In the HCA, the 231 flavonoids were clustered into 5 groups based on differences in flavonoid contents among different samples. The contents of flavonoids in group I and group II were higher in FJ than in HJ. Most flavonoids in group III increased in FJ but decreased in HJ in response to drought stress. Contents of flavonoids in group IV and group V were higher in HJ than in FJ, and those in group V decreased under drought stress. In **Figure 2B**, the first two principal components accounted for 94.4% (PC1) and 2.5% (PC2) of the total variation, respectively, and the 24 samples (including 3 replicates) were divided into two groups by cultivar along PC1. Sample positions along PC2 were affected by drought stress, especially for FJ. These results suggested that observed differences in flavonoid profiles were related to cultivar and drought stress treatment. Correlation analysis based on the flavonoid profiles demonstrated that Pearson's correlation coefficient (PCC) was > 0.9 within the same cultivar, suggesting that the obtained data were repeatable and credible (**Figure 2C**). Besides, OPLS-DA was used to evaluate the differences between F1 and F4 ($Q2 = 0.982$; **Figure 2D**), H1 and H4 ($Q2 = 0.975$; **Figure 2E**), F1 and H1 ($Q2 = 0.997$; **Figure 2F**), and F4 and H4 ($Q2 = 0.998$; **Figure 2G**). The four comparisons with $Q2 > 0.9$ suggested that the OPLS-DA modules were stable and reliable and that the differences in flavonoid contents could be subjected to further analysis.

Volcano diagrams were used to illustrate the DAFs between the two cultivars and under drought stress (**Supplementary Figure 3**). Twenty DAFs (16 upregulated and 4 downregulated) were identified in F1 vs. F4, and 15 DAFs (3 upregulated and 12 downregulated) were identified in H1 vs. H4. The greater number of DAFs in F1 vs. F4 than in H1 vs. H4 suggested that flavonoids may have been more sensitive to drought stress in FJ. Only one flavonoid (tricetin) overlapped between the F1 vs. F4 and H1 vs. H4 comparisons with downregulation. When the cultivars were compared at specific drought time points, 126 DAFs (61 upregulated and 65 downregulated) were identified in H1 vs. F1, and 134 DAFs (85 upregulated and 49 downregulated) were identified in H4 vs. F4. There were 107 DAFs (61 upregulated and 46 downregulated) shared between the H1 vs. F1 and H4 vs. F4 comparisons. These 107 DAFs constituted the main flavonoids whose content differed between the two cultivars regardless of drought stress.

Transcriptomic Analysis of ZBLs

RNA sequencing was performed on 24 samples to investigate the molecular regulation of flavonoid synthesis under drought stress. In FJ, the largest number of DEGs were identified in F1 vs. F2 (4237), followed by F3 vs. F4 (3106) and F2 vs. F3 (675) (**Figures 3A,D**). In HJ, the largest number of DEGs were identified in H3 vs. H4 (4048), followed by H1 vs. H2 (3077) and H2 vs. H3 (886) (**Figures 3B,E**). Compared to downregulated DEGs, there were more upregulated DEGs in H1 vs. H2 but fewer in H2 vs. H3 and H3 vs. H4 (**Supplementary Figure 4**). In addition, 184 and 172 DEGs were identified in all drought stages of FJ and HJ, respectively. There were large numbers of DEGs between the two cultivars at all stages (**Figures 3C,F**), and there were more upregulated DEGs than downregulated DEGs in the four comparison groups (**Supplementary Figure 4C**), indicating that the cultivars may have different response patterns to drought stress.

In GO annotation analysis, there were 6863 DEGs annotated in the biological process, molecular function, and cellular component categories (**Figure 4A**). In the biological process category, the majority of DEGs were annotated under metabolic process (3560) and cellular process (3050). In the cellular component category, the cell (2829) and membrane (2654) GO terms were most common. For the molecular function category, most DEGs were assigned to binding (3414) and catalytic function (3479). TopGO analysis further revealed that the molecular function terms dioxygenase activity (GO0051213) and transferase activity (GO0016758) (**Supplementary Figure 5A**), the biological process terms flavonoid glucuronidation (GO0052696) and flavonoid biosynthetic process (GO009813) (**Supplementary Figure 5B**), and the cellular component term extracellular matrix (GO0031012) were among the most highly enriched terms (**Supplementary Figure 5C**).

Based on KEGG enrichment analysis, the top 20 enriched metabolic pathways are presented in the form of a bubble diagram (**Figure 4**). During drought stress, the DEGs were enriched mainly in plant hormone signal transduction (ko04075), starch and sucrose metabolism (ko00500), photosynthesis - antenna proteins (ko00196), photosynthesis (ko00195), ribosome biogenesis in eukaryotes (ko03008), and flavonoid biosynthesis (ko00941). Plant hormone signal transduction (ko04075) was strongly enriched in both cultivars (**Figures 4B,C**). In addition, KEGG analysis of DEGs between F4 and H4 showed that these genes were strongly enriched in flavonoid biosynthesis (ko00941) and phenylpropanoid biosynthesis (ko00940) (**Figure 4D**). Notably, phenylpropanoid biosynthesis is the source of precursors for the flavonoid biosynthesis pathway (19). These results suggested that the transcription level of flavonoid biosynthesis genes was influenced by drought stress and differed significantly between the two cultivars under drought stress.

Gene Expression and Metabolite Accumulation in the Flavonoid Biosynthesis Pathway

On the basis of the flavonoid biosynthetic pathway reported in model plants, we constructed a pathway diagram showing the expression of structural genes and the contents of flavonoids in ZBLs. In total, 30 structural genes and 9 classes of flavonoids were mapped to the pathway (**Figure 5**). Seven structural genes (3 *ZbPAL*s, 2 *ZbC4H*s, and 2 *Zb4CL*s) participated in the phenylpropanoid pathway, and 23 structural genes (2 *ZbCHS*s,

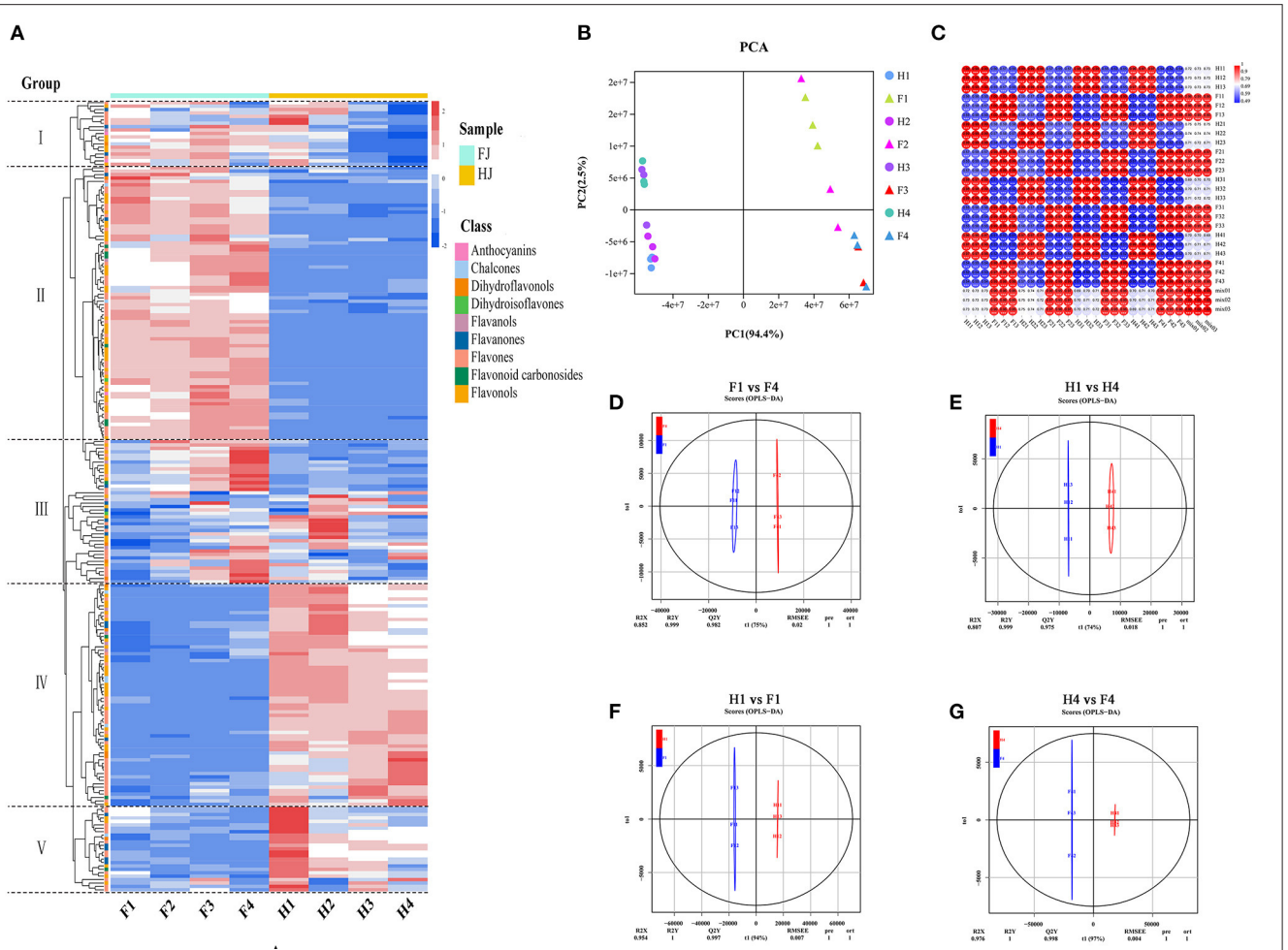

FIGURE 2 | Analysis of flavonoid metabolites in FJ and HJ leaves under drought stress. **(A)**: Heat map cluster analysis of 231 flavonoids. High and low abundance are indicated by red and blue colors, respectively. **(B)**: PCA score plot of 24 samples based on flavonoid abundances. **(C)**: Correlation coefficient graph of 24 samples. **(D–G)**: OPLS-DA plots for F1 vs. F4, H1 vs. H4, H1 vs. F1, and H4 vs. F4, respectively.

2 *ZbCHI*s, 1 *ZbIFS*, 2 *ZbF3H*s, 1 *ZbFNS*, 3 *ZbFLS*s, 2 *ZbDFR*s, 3 *ZbF3′H*s, 3 *ZbF3′5′H*s, 1 *ZbANS*, and 3 *ZbLAR*s) participated in the flavonoid pathway.

Naringenin chalcone is synthesized from phenylalanine through the phenylpropanoid pathway, in which PAL, C4H, 4CL, and CHS are the key rate-limiting enzymes. It is then transformed into naringenin by CHI. The higher expression levels of two *ZbCHS*s and two *ZbCHI*s in HJ than in FJ could explain its greater content of naringenin chalcone and naringenin. Naringenin, a core metabolite of the flavonoid pathway, can be transformed into dihydroisoflavones by IFS, flavones and flavone carbonosides by FNS, and dihydrokaempferol by F3H. Dihydrokaempferol can be transformed into flavonols by FLS and into anthocyanins and flavanols by F3′H, DFR, F3′5′H, and special enzymes (ANS for anthocyanins, LAR for flavanols). The higher content of dihydroisoflavones, flavonols, and anthocyanins and the lower content of flavanols in FJ were consistent with the expression levels of the corresponding enzyme genes. However, the higher content of flavones and flavone carbonosides was accompanied by a lower expression level of ZbFNS in FJ than in HJ.

Integrative Analysis of DAMs and DEGs in Response to Drought Stress

DEGs and DAMs in H1 vs. H4 and F1 vs. F4 with Pearson's correlation coefficients (PCCs) > 0.8 were used to generate nine-quadrant diagrams (**Figures 6A,B**). In the diagram, genes and metabolites with no difference are located in quadrant 5; genes and metabolites with a positive correlation are located in quadrants 3 and 7, and those with a negative correlation are located in quadrants 1 and 9. Up-regulated metabolites coupled with unchanged genes are located in quadrant 2, unchanged metabolites coupled with down-regulated genes are located in quadrant 4, and unchanged metabolites coupled with up-regulated genes are located in quadrant 6. Finally, down-regulated metabolites coupled with unchanged genes are located in quadrant 8. Most DEGs were found in quadrant 2 in F1 vs. F4 (5013), and most DEGs were found in quadrant 6 in

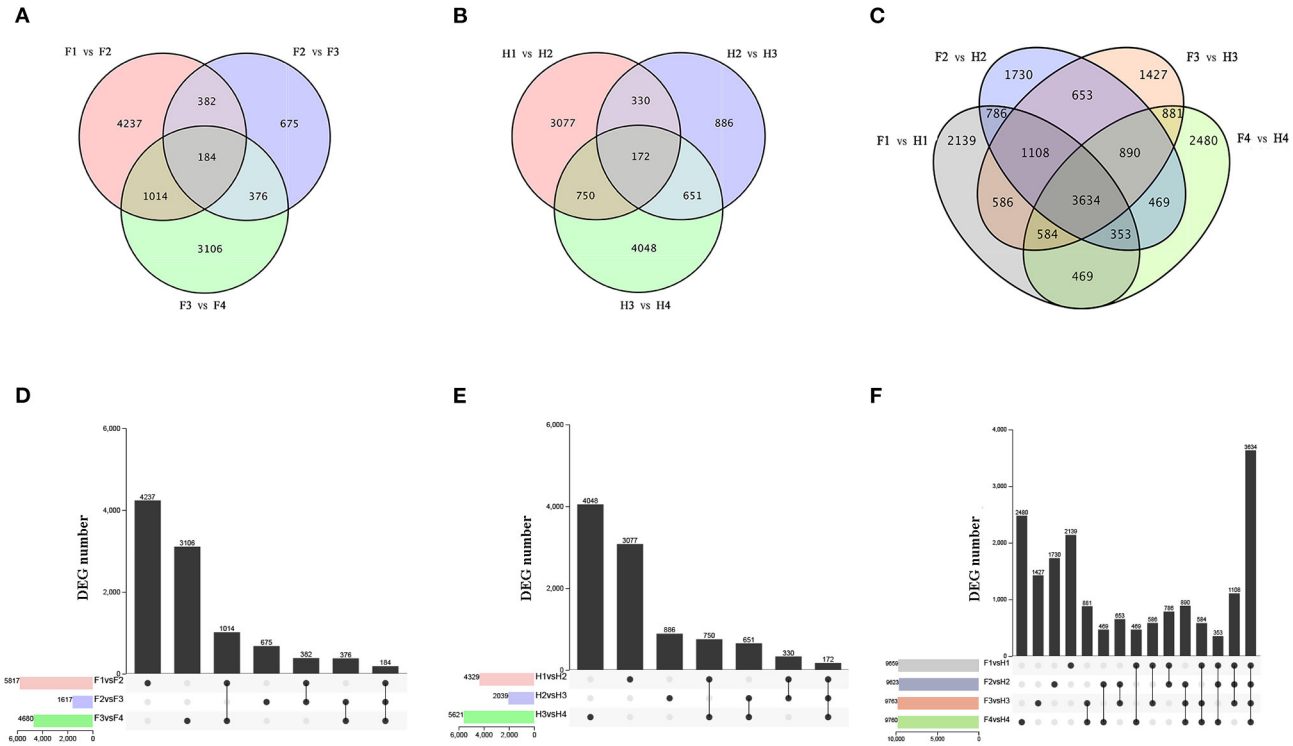

FIGURE 3 | Analysis of differentially expressed genes (DEGs) under drought stress in two cultivars. **(A–C)**: Venn diagrams of DEGs; **(D–F)**: Bar graphs of DEGs.

H1 vs. H4 (4913) (**Figures 6C,D**). However, most DAMs were found in quadrant 4 in both groups (319 DAMs for F1 vs. F4; 387 DAMs for H1 vs. H4). Notably, the DAMs in quadrants 3 and 7 were possibly regulated by the corresponding genes. In F1 vs. F4, 1831 DEGs and 76 DAMs were up-regulated in quadrant 3, and 2197 DEGs and 45 DAMs were down-regulated in quadrant 7. In H1 and H4, 1321 DEGs and 58 DAMs were up-regulated in quadrant 3, and 1875 DEGs and 29 DAMs were down-regulated in quadrant 7. With respect to flavonoids in F1 vs. F4, four individual flavonoids (hesperetin-7-O-(6″-malonyl)glucoside, syringetin, apigenin-6-C-rhamnoside, and kaempferol-3-O-arabinoside) were identified in quadrant 3, and one individual flavonoid, tricetin, was identified in quadrant 7. In H1 vs. H4, one individual flavonoid, dihydroquercetin, was identified in quadrant 3, and seven flavonoids were identified in quadrant 7 (butin, persicogenin, eriodictyol-7-O-(6″-O-galloyl)-glucoside, cyanidin-3-O-glucoside, cyanidin-3-O-rutinoside, cyanidin-3-O-(2″-O-glucosyl) glucoside, and tricetin) (**Figure 6E**). Among these, tricetin was present in quadrant 7 in both FJ and HJ. We performed KEGG enrichment analysis of the DEGs in quadrants 3 and 7 and found that nine DEGs were enriched in the flavonoid synthesis pathway (4 up-regulated and 5 down-regulated) in F1 vs. F4 (**Supplementary Figure 6A**), and six DEGs were enriched in the flavonoid synthesis pathway (1 up-regulated and 5 down-regulated) in H1 vs. H4 (**Supplementary Figure 6B**).

Co-expression Network Analysis Associated With Flavonoid Biosynthesis Under Drought Stress

To investigate the gene regulatory network of flavonoid synthesis in ZBLs, WGCNA was performed using 4426 filtered DEGs (with FPKM $>$ 1). These DEGs were clustered into eight modules labeled with different colors (**Figures 7A,B**, **Supplementary Figure 7A**), and each module contained DEGs with similar expression patterns. The cluster heatmap of traits highlighted the DAFs that differed significantly between the two cultivars: the contents of charcone, flavanones, and flavanols were higher in HJ, and the contents of dihydroisoflavones, anthocyanins, flavones, flavonols, and flavonoid carbonosides were higher in FJ. However, there was no significant difference in dihydroflavonol content between the two cultivars (**Supplementary Figure 7C**). Among the eight modules, the brown module with the most DEGs (1130) and the most TFs (66) had the highest correlation with most dihydroisoflavones, anthocyanins, flavones, flavonols, and flavonoid carbonosides ($r > 0.9$, $p < 0.001$) (**Figure 7C**). The relationship between the module and gene significance ($r = 0.97$, $p < e^{-200}$) suggested that the members of the brown module were well representative (**Supplementary Figure 7B**). In addition, the greenyellow module was positively correlated with the contents of chalcones ($r = 0.61$, $p = 0.001$) and flavanones ($r = 0.64$, $p < 0.001$), and the black module was

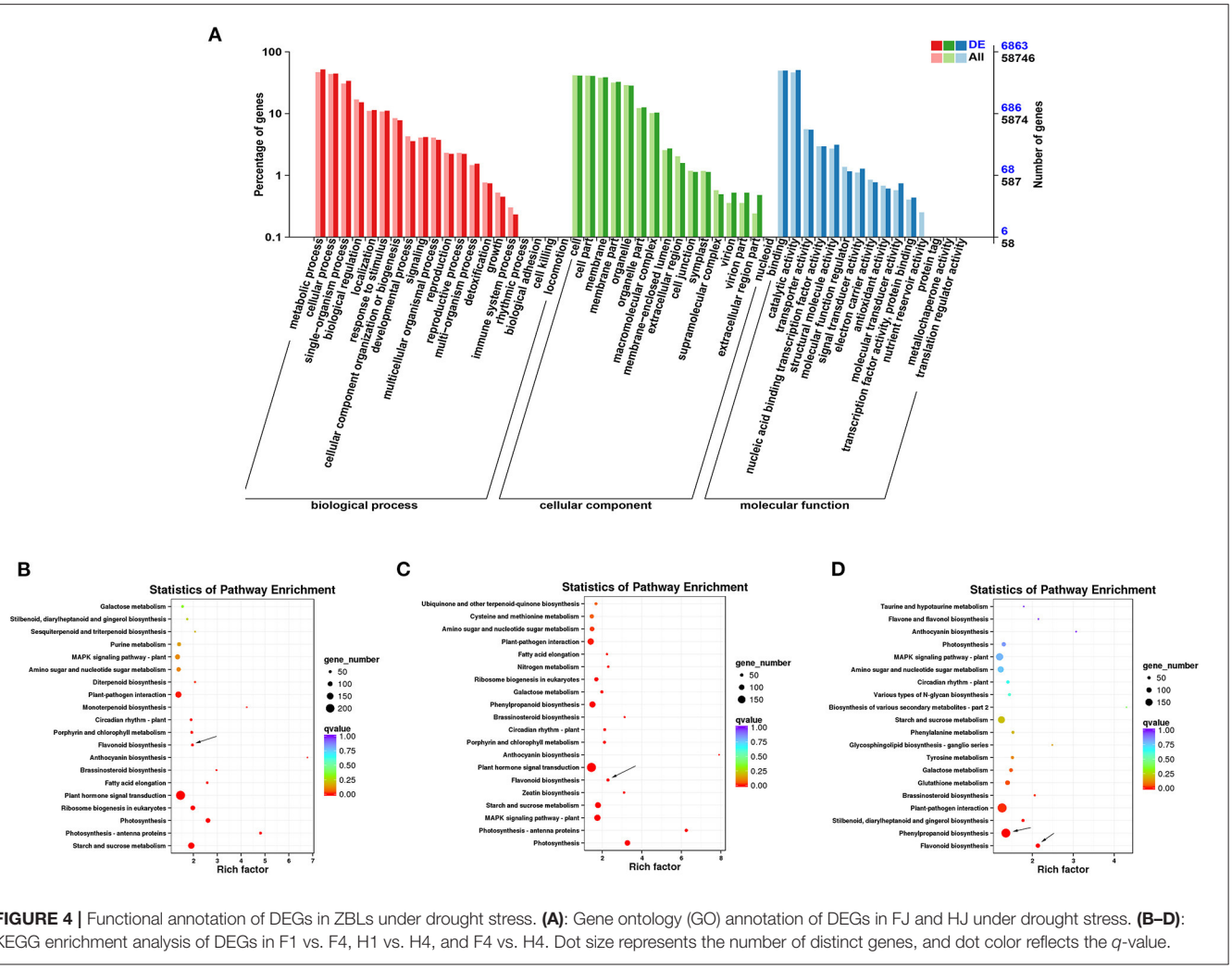

FIGURE 4 | Functional annotation of DEGs in ZBLs under drought stress. **(A)**: Gene ontology (GO) annotation of DEGs in FJ and HJ under drought stress. **(B–D)**: KEGG enrichment analysis of DEGs in F1 vs. F4, H1 vs. H4, and F4 vs. H4. Dot size represents the number of distinct genes, and dot color reflects the *q*-value.

positively correlated with flavanol contents ($r = 0.061$, $p = 0.002$). However, no modules were positively correlated with dihydroflavonol contents ($r > 0.6$).

The DEGs in the brown module were selected for further study. Heat map analysis based on FPKM values showed that all these DEGs were up-regulated under drought stress, but their expression levels were higher in FJ than in HJ (**Figure 7D**). GO analysis of the brown module showed that its DEGs were significantly enriched in metabolic process in the biological process category and binding and catalytic activity in the molecular function category (**Supplementary Figure 7A**). KEGG enrichment analysis revealed that the ribosome and flavonoid biosynthesis pathways were most strongly enriched in the brown module genes (**Supplementary Figure 7B**).

A Cytoscape representation of genes with edge weight > 0.5 and five classes of flavonoids indicated that genes in the brown module were highly positively connected to flavonoid contents (**Figure 7E**). In the interaction network diagram, the outer layer consisted of 17 TF genes (3 *bHLH*s, 2 *Bzip*s, 2 *C2H2*s, 1 *C3H*, 1 *HB-BELL*, 1 *HB-HD-ZIP*, 1 *LIM*, 1 *MYB*, 1 *NF-YB*, 1 *RB*, 1 *TCP*, 1 *Trihilix*, and 2 *WRKY*s), which were identified based on their orthologs in *Arabidopsis* and *Citrus* (**Supplementary Figure 7C**). In the middle of the network diagram, eight flavonoid synthesis genes were identified (*ZbANR* [*EVM0027590*], *ZbF3'5'H* [*EVM008863*], 2 *ZbHST*s [*EVM0095288*, *EVM0093603*], *ZbCHI* [*EVM0070967*], 2 *ZbCHS*s [*EVM0001110*, *EVM0064391*], and Zb*FLS* [*EVM0059890*]). The TF genes and eight structural genes showed the highest node connectivity with the five classes of flavonoids, which were located at the center of the network diagram.

By the same method, one gene associated with flavonoid synthesis (*EVM0070192*), one gene associated with phenylpropanoid biosynthesis (*EVM0046095*), and one *ZbbHLH* gene (*EVM0089951*) were identified in the black module. Likewise, one structural gene associated with phenylpropanoid biosynthesis (*EVM0083091*), one *ZbbHLH* gene (*EVM0090556*), and one *ZbMYB* gene (*EVM0039353*) were identified in the greenyellow module.

To validate the expression patterns of these flavonoid-related genes, four hub structural genes and four hub

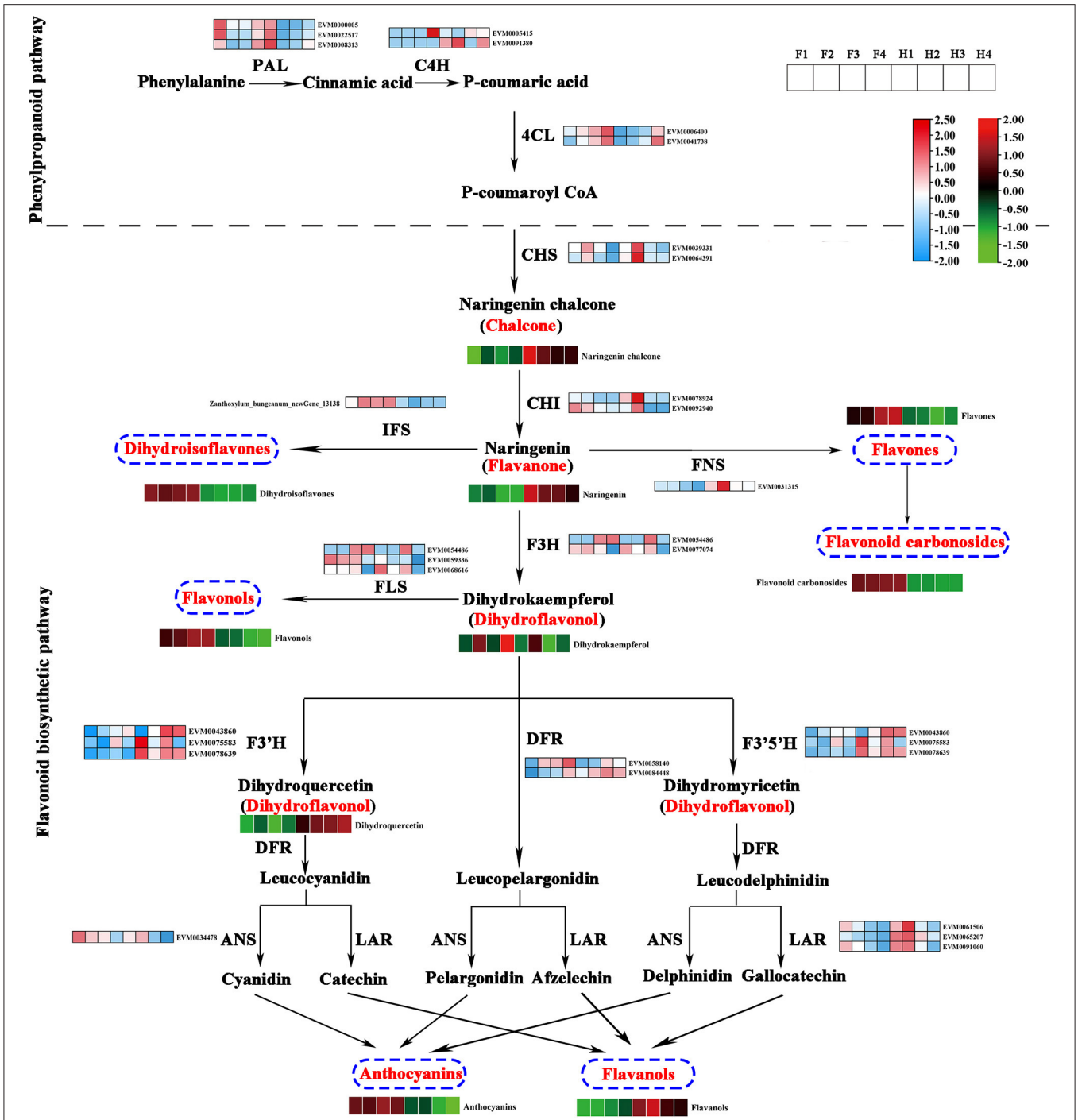

FIGURE 5 | Flavonoid biosynthesis pathway in ZBLs from two cultivars under drought stress. Gene expression is displayed in heatmaps based on the mean FPKM of three biological replicates; blue indicates low expression, and pink represents high expression. Flavonoid content is shown in heatmaps based on the abundance in the metabolite profile. Flavonoids with high abundance are indicated in red, and those with low abundance are indicated in green. PAL, phenylalanine ammonia lyase; C4H, cinnamate 4-hydroxylase; 4CL, 4-coumaroyl CoA ligase; CHS, chalcone synthase; CHI, chalcone isomerase; F3H, flavanone 3 β-hydroxylase; DFR, dihydroflavonol-4-reducatse; FLS, flavonol synthase; FNS, flavone synthase; LAR, leucoanthocyanidin reductase; ANS, anthocyanidin synthase; ANR, anthocyanidin reductase.

TF genes from the WGCNA co-expression network were selected for qRT-PCR (**Figure 8**). Their relative expression levels in qRT-PCR were consistent with their FPKM values in the transcriptomic data, confirming the accuracy of the transcriptome data and repeatability of the expression patterns.

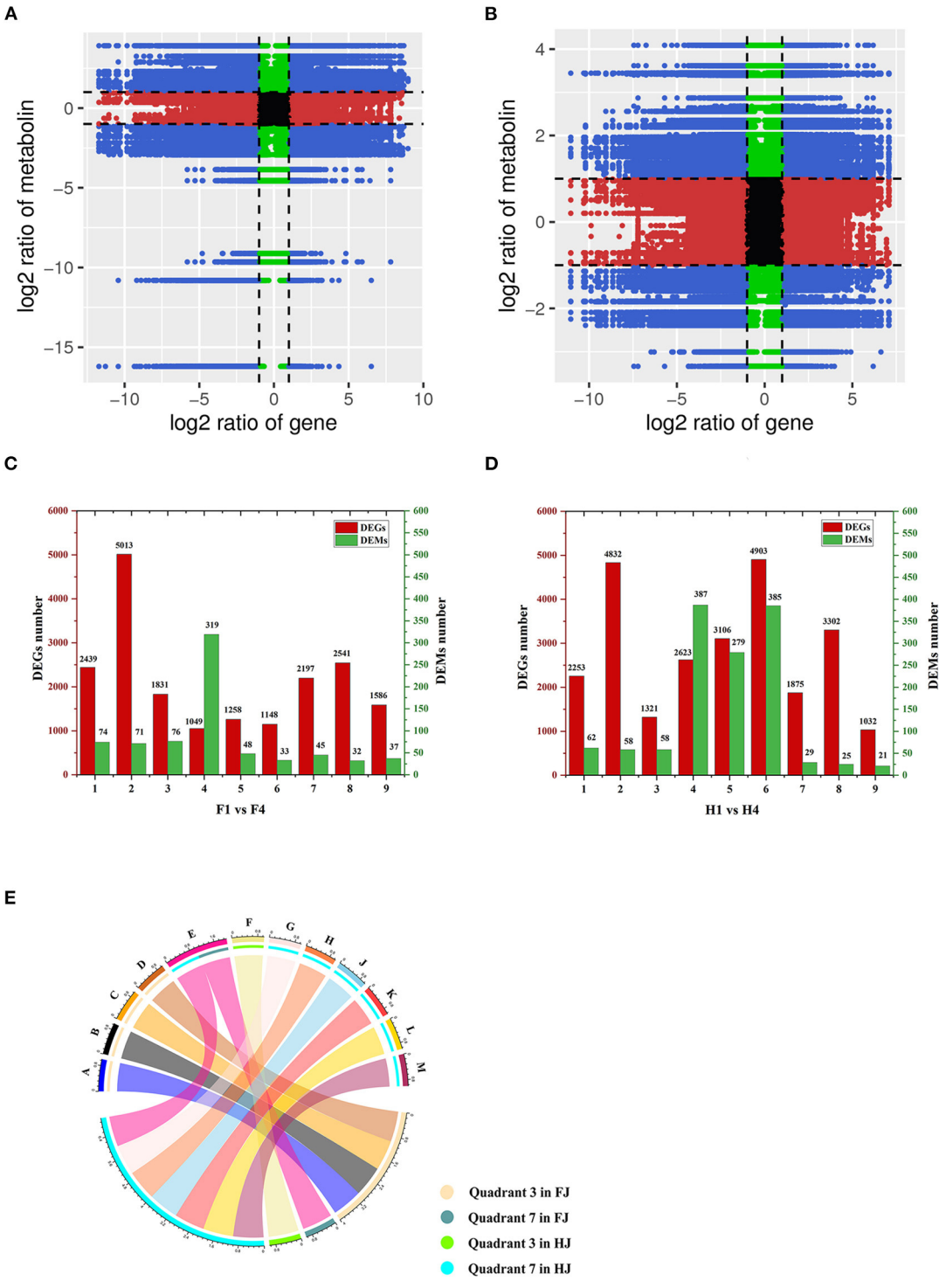

FIGURE 6 | Integrative analysis of DEGs and DAMs under drought stress in FJ and HJ. **(A, B)**: Nine-quadrant diagram of DEGs and DAMs in F1 vs. F4 and H1 vs. H4, respectively. **(C, D)**: The number of DEGs and DAMs in each quadrant in F1 vs. F4 and H1 vs. H4, respectively. **(E)**: DAFs in quadrant 3 and quadrant 7 in FJ and HJ.

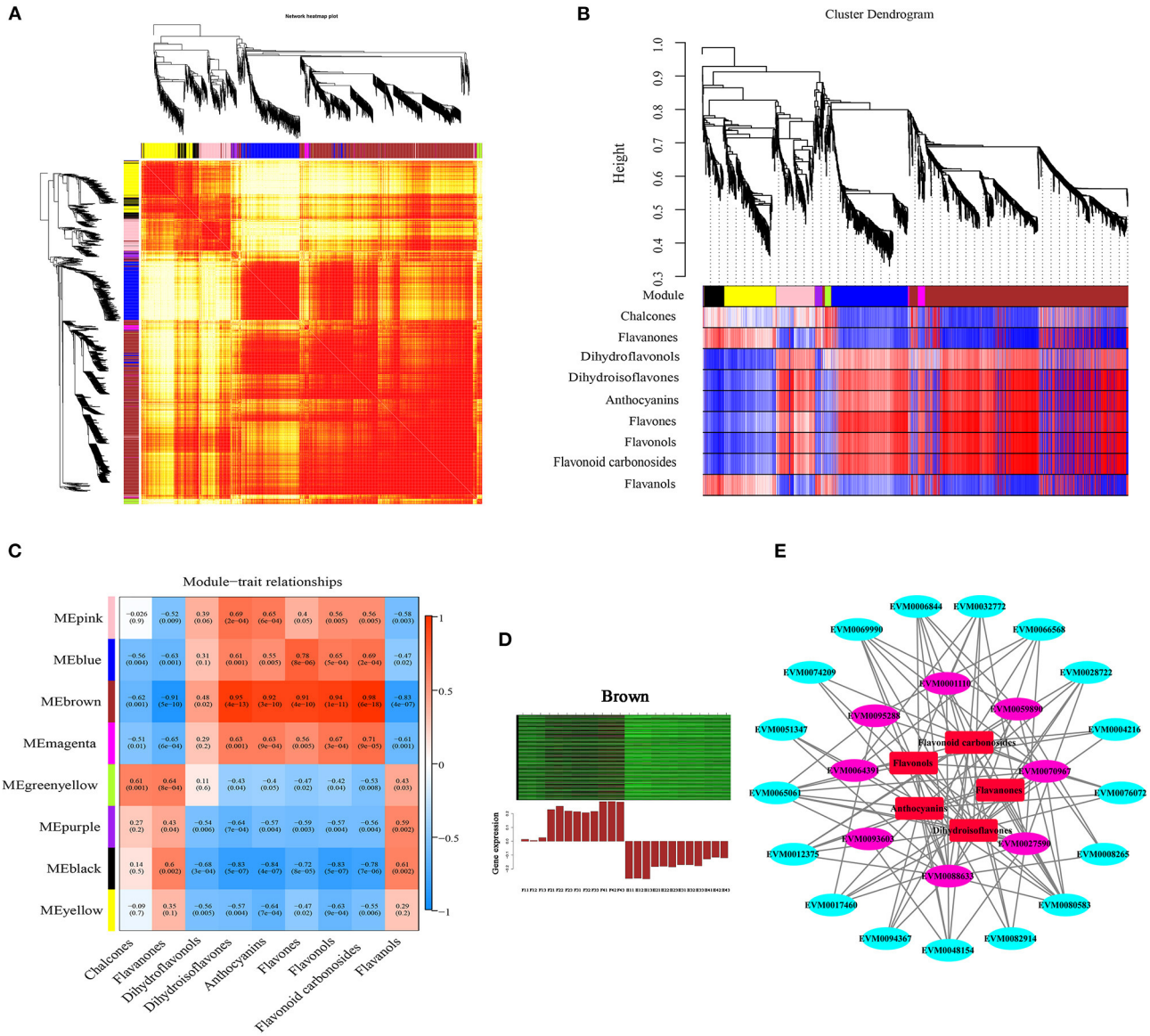

FIGURE 7 | Weighted gene co-expression network analysis of DEGs related to flavonoid content under drought stress. **(A)**: Network heatmap. **(B)**: Cluster dendrogram. **(C)**: Module-trait relationship heat map. Blue indicates low correlation, and red indicates high correlation. **(D)**: Eigengene expression profile for the brown module in different samples. The heat map above shows the expression profiles of all co-expressed genes in the brown module. The bar graph below shows the common expression patterns of co-expressed genes. **(E)**: Co-expression network between flavonoid contents and flavonoid-related gene expression.

DISCUSSION

ZBLs are popular among Chinese consumers as vegetables or food additives because of their high nutritional value and unique flavor. Flavonoids are a main secondary metabolite of ZBLs, and this has been verified in previous research. In addition, flavonoids are known to function as reductants in the plant's antioxidant system during abiotic stress, especially drought stress. In our research, widely targeted metabolite profiles were combined with transcriptome data to explore flavonoid accumulation and its underlying molecular regulation in ZBLs under drought stress.

Flavonoid Components in ZBLs and the Effects of Drought Stress on Flavonoids

Several studies have investigated the flavonoid components of ZBLs, and increasing numbers of flavonoid components have been identified by LC-MC (13). However, the number of identified flavonoid components in ZBLs remains quite limited. Widely targeted metabolomics is a new method that has been widely applied in food research (17, 20). To the best of our knowledge, the present study is the first widely targeted metabolomic analysis of ZBLs. The results showed that there were 231 flavonoid components

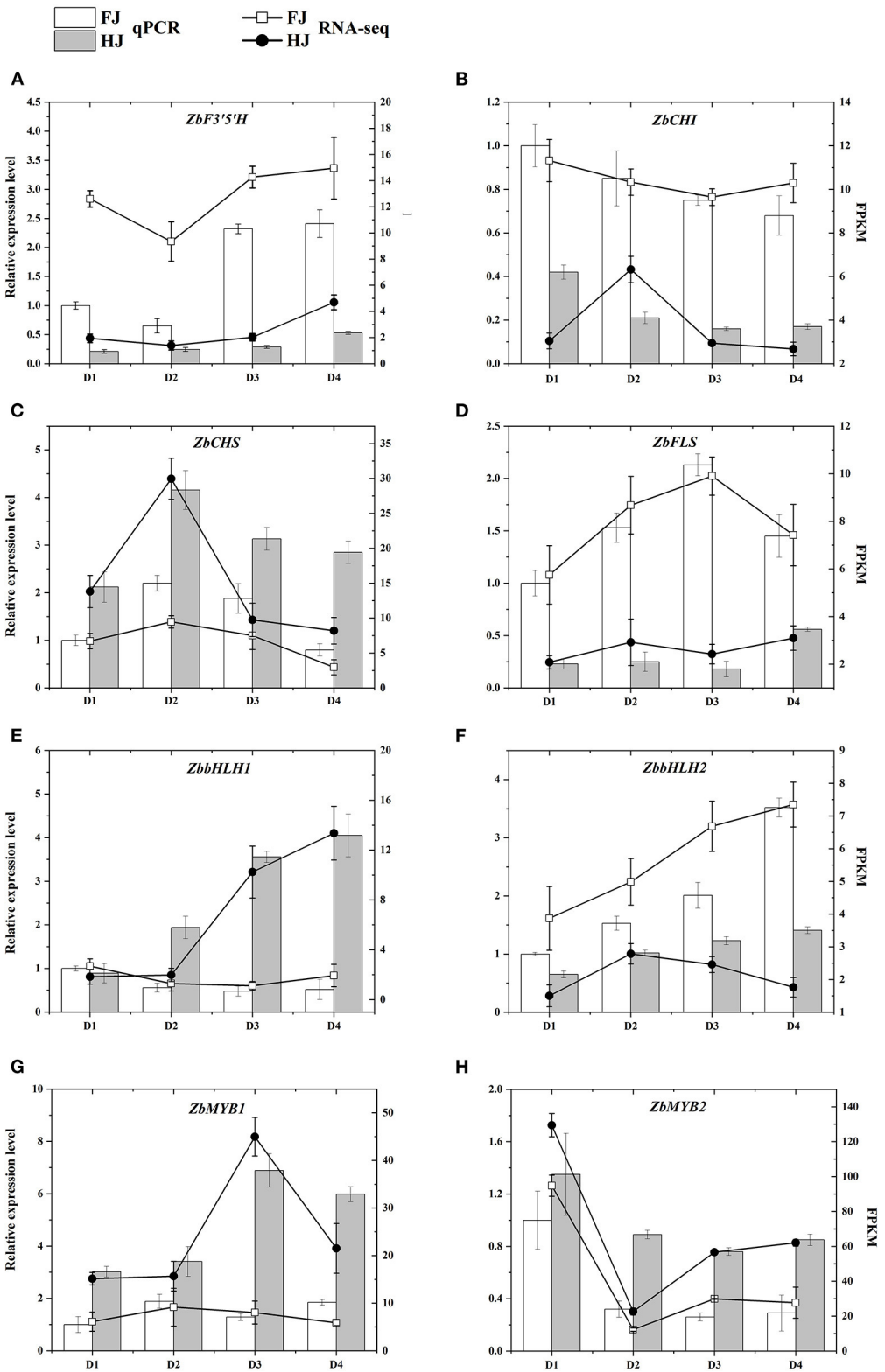

FIGURE 8 | (A–H) qRT-PCR validation of the expression patterns of candidate genes that participated in the regulation of flavonoid content in FJ and HJ leaves. The bar graphs present the results of the qRT-PCR, and the line graphs present the RNA-seq results. The scale on the left axis represents the relative expression level and the scale on the right axis represents the FPKM value. Data are means ± SD of three biological replicates.

in the ZBLs, and these were divided into nine classes: chalcones, flavanones, dihydroisoflavones, dihydroflavonols, anthocyanins, flavones, flavonols, flavanols, and flavonoid carbonosides (**Supplementary Table 2**, **Figure 2A**). We suspect that the diversity of flavonoids may be responsible for the various biological functions of ZBLs. Flavonols and flavones accounted for 77.9 and 86.1% of the total flavonoids in FJ and HJ (**Figure 1C**), indicating that they are the major flavonoid classes in ZBLs.

Flavonoid carbonosides, also called flavonoid glycosides, are a stable form of flavonoids in which sugar groups are bound to an aglycone carbon; they are vital phytochemicals in the human diet and are of great interest in human medicine (21). Vitexin and isovitexin have been reported to be active components of many traditional Chinese medicines and have a wide range of pharmacological effects, including anti-inflammatory (22), antioxidant (23) and anti-AD (AD, Alzheimer's disease) properties (24). In our research, 10 flavonoid carbonoside components were identified in leaves of FJ and HJ; isovitexin and vitexin were the most abundant flavonoid carbonosides in FJ but not in HJ. Moreover, the proportion of flavonoid carbonosides was 10.4% in FJ, higher than that in HJ (0.5%) (**Figure 1C**), and total flavonoids were also higher in FJ than in HJ (**Figure 1B**). Thus, we suspect that the leaves of FJ may have greater nutrition value for the human body and more potential for functional food production.

Flavanols are the 3-hydroxy derivatives of flavanones (25). Flavanols can be readily absorbed by the human body and are the major polyphenol antioxidants in green tea (6) and red wine (26). Preclinical studies showed that a high-flavanol dietary supplement improved cerebral blood flow and mitochondrial function, and enhanced activity in brain regions (27). In this paper, flavanols, with catechin and epicatechin as the major components, were present at higher levels in HJ (**Figure 1C**). Therefore, we inferred that the ZBLs of HJ may have greater potential for the development of natural functional beverages such as green tea and oral liquid.

Drought stress is a major environmental challenge for crops and influences their quality and yield, especially in water-deficit areas. Flavonoids, as stress-responsive metabolites, could alleviate the oxidative injury of abiotic stress by reducing various forms of reactive oxygen species ROS (28). Thus, plant flavonoid accumulation is generally influenced by drought stress, as demonstrated in Bupleurum chinense DC (29), *Camellia sinensis* (30) and rice (31). In our research, total flavonoid content increased continuously during drought stress in FJ, with elevated levels of flavanols, flavonols, flavones, and flavonoid carbonosides (**Figure 1B**). This result suggests that drought stress induces the accumulation of ROS in FJ plants, promoting the subsequent accumulation of flavonoids to protect the plant cell from oxidative injury. By contrast, the total flavonoid content declined under drought stress in HJ. In drought-tolerant plants, a strong ROS-scavenging system is activated under drought stress. It includes oxidative enzymes, such as peroxidase (POD), catalase (CAT), and superoxide dismutase (SOD), as well as osmoprotective substances such as soluble sugars and proline (32). As a drought-tolerant cultivar, HJ may have reduced the accumulation of ROS by strengthening the antioxidant system, and consequently, lower ROS levels obviated the need to activate flavonoid biosynthesis. Energy and reducing power are required for gene transcription and translation. In addition, the precursors of flavonoid biosynthesis may also participate in other pathways. Therefore, we speculate that the competition for energy and precursors by the strengthened ROS-scavenging system may have reduced the efficiency of flavonoid accumulation, leading to reduced flavonoid levels in HJ. Consistently, under salt stress, more carbon was allocated to flavonoids in the salt-sensitive *Myrtus communis* than in the salt-tolerant *Pistacia lentiscu* (33). Besides, tricetin was significantly downregulated with many related genes enriched in flavonoids biosynthesis in both FJ and HJ under drought stress (**Figure 6**), suggesting tricetin was the common flavonoid suffering damage from drought stress. A role for tricetin in drought resistance has seldom been reported. However, tricetin can be transformed into tricin by O-methyltransferases (34). Tricin accumulated under drought stress and played an important role in protecting the plant cell against abiotic stresses (35). Thus, we supposed that the reduced tricetin in ZBLs may contribute to increased accumulation of tricin in response to drought stress. Interestingly, tricin-7-O-Glucoside, one of the tricin derivatives, increased in both FJ and HJ and is negatively correlated with tricetin variation, which could support our hypothesis.

Gene Regulation Underlying Flavonoid Accumulation in ZBLs Under Drought Stress

Under environmental stresses, plant cells initiate gene expression programs at the transcriptional level, which regulate metabolite accumulation to adapt to the new conditions (36). Detailed gene expression profiles from transcriptomes can help to identify pivotal genes in targeted pathways. Here, transcriptome data revealed the molecular mechanisms underlying flavonoid content in ZBLs under drought stress. GO annotation analyses identified biological process, molecular function, and cellular component terms that were enriched under drought stress (**Figure 4A**), suggesting that drought stress influenced the transcription level and modulated the accumulation and transport of primary and secondary metabolites. KEGG enrichment analysis suggested that drought stress induced significant variation in the expression of genes from the flavonoid biosynthesis pathway in both cultivars (**Figures 4B–D**), suggesting that flavonoid variation under drought stress in ZBLs results from regulation at the molecular level.

The flavonoid biosynthetic pathway has been clearly delineated in some model plants (9, 10). Although Sun et al. (2) tentatively explored the flavonoid pathway in ZBLs, the pathway was restricted to six flavonoid components, and genes encoding F3′5′H were absent in flavonoid biosynthetic pathway in ZBLs. Here, 231 flavonoids and their related genes were used to construct the biosynthetic pathway, and 58 structural genes were identified using the NR database, including 3 *ZbF3′5′Hs* (**Figure 5**). Thus, our research supplements previous work on the flavonoid biosynthetic pathway in ZBLs. As reported

previously, the overexpression of *AgFNS* increased the content of apigenin, a natural flavone, in celery (37), and the overexpression of *MnFNS* promoted flavone accumulation in tobacco leaves (38). However, we observed higher expression of *ZbFNS* but lower flavone content in HJ than in FJ in this research. Flavone biosynthesis may be post-translationally regulated, or the regulated FNS structural gene may not have been identified in our transcriptome data.

In the present research, the DEGs were divided into eight modules according to the similarity of their expression patterns using WGCNA (**Figure 7**). The brown module was most correlated with five flavonoid classes (dihydroisoflavones, anthocyanins, flavones, flavonols, and flavonoid carbonosides), indicating that candidate genes involved in the regulation of flavonoid accumulation were present in the brown module. Furthermore, the co-expression network contained five structural genes that were highly correlated with these flavonoids: *ZbF3'5'H* (*EVM008863*), *ZbCHI* (*EVM0070967*), *ZbCHS* (*EVM0001110*, *EVM0064391*), and *ZbFLS* (*EVM0059890*). Likewise, one structural gene (*EVM0083091*) was identified in the greenyellow module and two (*EVM0070192, EVM0046095*) in the black module. Hence, these eight hub genes were considered to be the major genes that influenced flavonoid biosynthesis in ZBLs under drought stress. Environmental factors can regulate gene expression by influencing TFs, which bind specifically to their target gene promoters (39). The MWD complex is considered to be an important regulator of gene expression in the flavonoid pathway (12). For instance, VvMYBPA2 activates the promoters of *VvANR* and *VvLAR1*, thereby promoting proanthocyanidin biosynthesis in grapevine (40). In this study, three *ZbbHLH*s (*EVM0082914*, *EVM0008265*, *EVM0094367*) and one *ZbMYB* (*EVM0069990*) were identified as highly related to structural genes and five classes of flavonoids based on WGCNA. For chalcones and flavanones, one *ZbbHLH* (*EVM0090556*) and one *ZbMYB* (*EVM0039353*) were identified; for flavanols, one *ZbbHLH* (*EVM0089951*) was identified. Consequently, these seven TF genes were considered to be important in regulating the flavonoid content of ZBLs. Although qRT-PCR results showed good consistency with transcriptome data (**Figure 8**), future work is required to determine the function of these genes in flavonoid biosynthesis.

CONCLUSIONS

This study represents the first integration of widely targeted metabolomic data with transcriptome data from ZBLs. In total, 231 flavonoids were identified from ZBLs, including 7 chalcones, 19 flavanones, 2 dihydroisoflavones, 10 dihydroflavonols, 3 anthocyanins, 91 flavones, 80 flavonols, 10 flavonoid carbonosides, and 9 flavanols. Flavonols and flavones were the most abundant flavonoids. The total flavonoid content increased in FJ but decreased in HJ under drought stress. In addition, our results suggested that FJ leaves were more suitable for functional food and medicine, whereas HJ leaves were more suitable for producing green tea and oral liquid. Nine-quadrant analysis identified five and eight differentially flavonoids in FJ and HJ leaves. Furthermore, eight candidate structural genes and seven TF genes that regulated flavonoid biosynthesis in ZBLs were identified using WGCNA. qRT-PCR results for eight candidate genes were consistent with the transcriptome data, verifying the accuracy of the transcriptome sequencing and the reliability of the candidate genes. In total, our research revealed the flavonoid compositions of ZBLs and shed light on the molecular regulation of flavonoid accumulation under drought stress. These results will improve the knowledge of nutrition value in ZBLs and provide a basis for the development and utilization of ZBLs in the food and nutrition industry.

DATA AVAILABILITY STATEMENT

The original contributions presented in the study have been uploaded to an online repository. This data can be found here: https://dataview.ncbi.nlm.nih.gov/object/PRJNA784034?reviewer=v79bcipc97tajk7ppuam33d88t.

AUTHOR CONTRIBUTIONS

HH: methodology, software, data curation, and writing—original draft. XF: supervision and writing—review and editing. BH: validation and investigation. YL: investigation. YQ: data curation. AW: funding acquisition and resources. All authors contributed to the article and approved the submitted version.

FUNDING

This study was financially supported by The Technology Innovation Guidance Special Foundation of Shaanxi Province (2020QFY07-01).

ACKNOWLEDGMENTS

We would like to thank Jinjiao Yan for her help in qRT-PCR.

SUPPLEMENTARY MATERIAL

The Supplementary Material for this article can be found online at: https://www.frontiersin.org/articles/10.3389/fnut.2021.801244/full#supplementary-material

REFERENCES

1. Fei X, Qi Y, Lei Y, Wang S, Hu H, Wei A. Transcriptome and metabolome dynamics explain aroma differences between green and red prickly ash fruit. *Foods.* (2021) 10:391. doi: 10.3390/foods10020391

2. Sun L, Yu D, Wu Z, Wang C, Yu L, Wei A, et al. Comparative transcriptome analysis and expression of genes reveal the biosynthesis and accumulation patterns of key flavonoids in different varieties of *Zanthoxylum bungeanum* Leaves. *J Agric Food Chem.* (2019) 67:13258–68. doi: 10.1021/acs.jafc.9b05732

3. Zhong K, Li X-J, Gou A-N, Huang Y-N, Bu Q, Gao H. Antioxidant and cytoprotective activities of flavonoid glycosides-rich extract from the leaves of *Zanthoxylum bungeanum*. *J Food Nutr Res.* (2014) 2:349–56. doi: 10.12691/jfnr-2-7-4
4. Nabavi SM, Šamec D, Tomczyk M, Milella L, Russo D, Habtemariam S, et al. Flavonoid biosynthetic pathways in plants: Versatile targets for metabolic engineering. *Biotechnol Adv.* (2020) 38:107316. doi: 10.1016/j.biotechadv.2018.11.005
5. Ferrer JL, Austin MB, Stewart C, Noel JP. Structure and function of enzymes involved in the biosynthesis of phenylpropanoids. *Plant Physiol Biochem.* (2008) 46:356–70. doi: 10.1016/j.plaphy.2007.12.009
6. Wang H, Cao X, Yuan Z, Guo G. Untargeted metabolomics coupled with chemometrics approach for Xinyang Maojian green tea with cultivar, elevation and processing variations. *Food Chem.* (2021) 352:129359–129359. doi: 10.1016/j.foodchem.2021.129359
7. Huang A, Jiang Z, Tao M, Wen M, Xiao Z, Zhang L, et al. Targeted and nontargeted metabolomics analysis for determining the effect of storage time on the metabolites and taste quality of keemun black tea. *Food Chem.* (2021) 359:129950–129950. doi: 10.1016/j.foodchem.2021.129950
8. Wei T. Xiong F-f, Wang S-d, Wang K, Zhang Y-y, Zhang Q-h. Flavonoid ingredients of Ginkgo biloba leaf extract regulate lipid metabolism through Sp1-mediated carnitine palmitoyltranferase 1A up-regulation. *J Biomed Sci.* (2014) 21:87. doi: 10.1186/s12929-014-0087-x
9. Saito K, Yonekura-Sakakibara K, Nakabayashi R, Higashi Y, Yamazaki M, Tohge T, et al. The flavonoid biosynthetic pathway in *Arabidopsis*: structural and genetic diversity. *Plant Physiol Biochem.* (2013) 72:21–34. doi: 10.1016/j.plaphy.2013.02.001
10. Andersen JR, Zein I, Wenzel G, Darnhofer B, Eder J, Ouzunova M. et al. Characterization of phenylpropanoid pathway genes within European maize (Zea mays L) inbreds. *BMC Plant Biol.* (2008) 8:2–2. doi: 10.1186/1471-2229-8-2
11. Forkmann G, Martens S. Metabolic engineering and applications of flavonoids. *Curr Opin Biotechnol.* (2001) 12:155–60. doi: 10.1016/S0958-1669(00)00192-0
12. Hichri I, Barrieu F, Bogs J, Kappel C, Delrot S, Lauvergeat V. Recent advances in the transcriptional regulation of the flavonoid biosynthetic pathway. *J Exp Bot.* (2011) 62:2465–83. doi: 10.1093/jxb/erq442
13. Chen X, Wang W, Wang C, Liu Z, Sun Q, Wang D. Quality evaluation and chemometric discrimination of Zanthoxylum bungeanum Maxim leaves based on flavonoids profiles, bioactivity and HPLC-fingerprint in a common garden experiment. *Ind Crops Prod.* (2019) 134:225–33. doi: 10.1016/j.indcrop.2019.04.017
14. Moschen S, Rienzo JAD, Higgins J, Tohge T, Watanabe M, González S. et al. Integration of transcriptomic and metabolic data reveals hub transcription factors involved in drought stress response in sunflower (Helianthus annuus L). *Plant Mol Biol.* (2017) 94:549–64. doi: 10.1007/s11103-017-0625-5
15. Guo Y, Gao C, Wang M. Fu F-f, El-Kassaby YA, Wang T, et al. Metabolome and transcriptome analyses reveal flavonoids biosynthesis differences in Ginkgo biloba associated with environmental conditions. *Ind Crops Products.* (2020) 158:112963. doi: 10.1016/j.indcrop.2020.112963
16. Deluc LG, Quilici DR, Decendit A, Grimplet J, Wheatley MD, Schlauch KA, et al. Water deficit alters differentially metabolic pathways affecting important flavor and quality traits in grape berries of *Cabernet Sauvignon* and *Chardonnay*. *BMC Genomics.* (2009) 10:212–212. doi: 10.1186/1471-2164-10-212
17. Wang H, Hua J, Yu Q, Li J, Wang J, Deng Y, et al. Widely targeted metabolomic analysis reveals dynamic changes in non-volatile and volatile metabolites during green tea processing. *Food Chem.* (2021) 363:130131. doi: 10.1016/j.foodchem.2021.130131
18. Langfelder P, Horvath S, WGCNA. an R package for weighted correlation network analysis. *BMC Bioinform.* (2008) 9:559–559. doi: 10.1186/1471-2105-9-559
19. Falcone Ferreyra ML, Rius S, Casati P. Flavonoids: biosynthesis, biological functions, and biotechnological applications. *Front Plant Sci.* (2012) 3:222. doi: 10.3389/fpls.2012.00222
20. Fan F-Y, Huang C-S, Tong Y-L, Guo H-W, Zhou S-J, Ye J-H, et al. Widely targeted metabolomics analysis of white peony teas with different storage time and association with sensory attributes. *Food Chem.* (2021) 362:130257. doi: 10.1016/j.foodchem.2021.130257
21. Kumar S, Pandey AK. Chemistry and biological activities of flavonoids: an overview. *Sci World J.* (2013) 2013:162750–162750. doi: 10.1155/2013/162750
22. Rosa SIG, Rios-Santos F, Balogun SO. Martins DTdO Vitexin reduces neutrophil migration to inflammatory focus by down-regulating pro-inflammatory mediators via inhibition of p38, ERK1/2 and JNK pathway. *Phytomedicine.* (2016) 23:9–17. doi: 10.1016/j.phymed.2015.11.003
23. Zhang J, Yuan K, Zhou W-L, Zhou J, Yang P. Studies on the active components and antioxidant activities of the extracts of *Mimosa pudica* Linn. from southern China. *Pharmacogn Mag.* (2011) 7:35–9. doi: 10.4103/0973-1296.75899
24. Choi JS, Islam MN, Ali MY, Kim EJ, Kim YM, Jung HA. Effects of C-glycosylation on anti-diabetic, anti-Alzheimer's disease and anti-inflammatory potential of apigenin. *Food Chem Toxicol.* (2014) 64:27–33. doi: 10.1016/j.fct.2013.11.020
25. Panche AN, Diwan AD, Chandra SR. Flavonoids: an overview. *J Nutr Sci.* (2016) 5:e47. doi: 10.1017/jns.2016.41
26. Pimentel FA, Nitzke JA, Klipel CB. Jong EVd. Chocolate and red wine - A comparison between flavonoids content. *Food Chem.* (2010) 120:109–12. doi: 10.1016/j.foodchem.2009.09.078
27. Bonetti F, Brombo G, Zuliani G. *Nootropics, Functional Foods, and Dietary Patterns for Prevention of Cognitive Decline.*In*:* Frontiers in Plant Science. (2017) p. 211–232. doi: 10.1016/B978-0-12-805376-8.00019-8
28. Agati G, Azzarello E, Pollastri S, Tattini M. Flavonoids as antioxidants in plants: Location and functional significance. *Plant Sci.* (2012) 196:67–76. doi: 10.1016/j.plantsci.2012.07.014
29. Yang L-l, Yang L, Yang X, Zhang T, Lan Y-m, Zhao Y, et al. Drought stress induces biosynthesis of flavonoids in leaves and saikosaponins in roots of *Bupleurum chinense* DC. *Phytochemistry*. (2020) 177:112434. doi: 10.1016/j.phytochem.2020.112434
30. Wang W, Xin H, Wang M, Ma Q, Wang L, Kaleri NA, et al. Transcriptomic analysis reveals the molecular mechanisms of drought-stress-induced decreases in *Camellia sinensis* leaf quality. *Front Plant Sci.* (2016) 7:385. doi: 10.3389/fpls.2016.00385
31. Chen Z, Chen H, Jiang Y, Wang J, Khan A, Li P, et al. Metabolomic analysis reveals metabolites and pathways involved in grain quality traits of high-quality rice cultivars under a dry cultivation system. *Food Chem.* (2020) 326:126845. doi: 10.1016/j.foodchem.2020.126845
32. Ahanger MA, Siddique KHM, Ahmad P. Understanding drought tolerance in plants. *Physiol Plant.* (2021) 172:286–8. doi: 10.1111/ppl.13442
33. Tattini M, Remorini D, Pinelli P, Agati G, Saracini E, Traversi ML, et al. Morpho-anatomical, physiological and biochemical adjustments in response to root zone salinity stress and high solar radiation in two Mediterranean evergreen shrubs, *Myrtus communis* and *Pistacia lentiscus*. *New Phytol.* (2006) 170:779–94. doi: 10.1111/j.1469-8137.2006.01723.x
34. Zhou J-M, Ibrahim RK. Tricin—a potential multifunctional nutraceutical. *Phytochem Rev.* (2010) 9:413–24. doi: 10.1007/s11101-009-9161-5
35. Moheb A, Agharbaoui Z, Kanapathy F, Ibrahim RK, Roy R, Sarhan F. Tricin biosynthesis during growth of wheat under different abiotic stresses. *Plant Sci.* (2013) 201:115–20. doi: 10.1016/j.plantsci.2012.12.005
36. López-Maury L, Marguerat S, Bähler J. Tuning gene expression to changing environments: from rapid responses to evolutionary adaptation. *Nat Rev Genet.* (2008) 9:583–93. doi: 10.1038/nrg2398
37. Tan G-F, Ma J, Zhang X-Y, Xu Z-S, Xiong A-S. AgFNS overexpression increase apigenin and decrease anthocyanins in petioles of transgenic celery. *Plant Sci.* (2017) 263:31–8. doi: 10.1016/j.plantsci.2017.07.001
38. Li H, Li D, Yang Z, Zeng Q, Luo Y, He N. Flavones produced by mulberry flavone synthase type I constitute a defense line against the ultraviolet-B stress. *Plants.* (2020) 9:215. doi: 10.3390/plants9020215
39. Hassani D, Fu X, Shen Q, Khalid M, Rose JKC, Tang K. Parallel transcriptional regulation of artemisinin and flavonoid biosynthesis. *Trends Plant Sci.* (2020) 25:466–76. doi: 10.1016/j.tplants.2020.01.001
40. Terrier N, Torregrosa L, Ageorges A, Vialet S, Verriès C, Cheynier V, et al. Ectopic expression of VvMybPA2 promotes proanthocyanidin biosynthesis in

grapevine and suggests additional targets in the pathway. *Plant Physiol.* (2009) 149:1028–41. doi: 10.1104/pp.108.131862

Conflict of Interest: The authors declare that the research was conducted in the absence of any commercial or financial relationships that could be construed as a potential conflict of interest.

Publisher's Note: All claims expressed in this article are solely those of the authors and do not necessarily represent those of their affiliated organizations, or those of the publisher, the editors and the reviewers. Any product that may be evaluated in this article, or claim that may be made by its manufacturer, is not guaranteed or endorsed by the publisher.

frontiers | Frontiers in Nutrition

ORIGINAL RESEARCH
published: 05 April 2022
doi: 10.3389/fnut.2022.842693

Integrated Metabolomic and Transcriptomic Analyses Reveal Novel Insights of Anthocyanin Biosynthesis on Color Formation in Cassava Tuberous Roots

Lili Fu[1,2†], Zehong Ding[1,2,3†], Weiwei Tie[1,2,3], Jinghao Yang[1,2], Yan Yan[1,2] and Wei Hu[1,2,3*]*

[1] Hainan Key Laboratory for Biosafety Monitoring and Molecular Breeding in Off-Season Reproduction Regions, Key Laboratory of Biology and Genetic Resources of Tropical Crops, Institute of Tropical Bioscience and Biotechnology, Chinese Academy of Tropical Agricultural Sciences, Haikou, China, [2] Hainan Key Laboratory for Protection and Utilization of Tropical Bioresources, Hainan Institute for Tropical Agricultural Resources, Chinese Academy of Tropical Agricultural Sciences, Haikou, China, [3] Sanya Research Institute of Chinese Academy of Tropical Agricultural Sciences, Sanya, China

OPEN ACCESS

Edited by:
Alberto Valdés, Spanish National Research Council (CSIC), Spain

Reviewed by:
Ramesh S. V, Indian Council of Agricultural Research (ICAR), India
Chunpeng (Craig) Wan, Jiangxi Agricultural University, China

***Correspondence:**
Zehong Ding
dingzehong@itbb.org.cn
Wei Hu
huwei2013@itbb.org.cn

[†] *These authors have contributed equally to this work*

Specialty section:
This article was submitted to Nutrition and Food Science Technology, a section of the journal Frontiers in Nutrition

Received: *24 December 2021*
Accepted: *03 March 2022*
Published: *05 April 2022*

Citation:
Fu L, Ding Z, Tie W, Yang J, Yan Y and Hu W (2022) Integrated Metabolomic and Transcriptomic Analyses Reveal Novel Insights of Anthocyanin Biosynthesis on Color Formation in Cassava Tuberous Roots. Front. Nutr. 9:842693. doi: 10.3389/fnut.2022.842693

Yellow roots are of higher nutritional quality and better appearance than white roots in cassava, a crucial tropical and subtropical root crop. In this work, two varieties with yellow and white cassava roots were selected to explore the mechanisms of color formation by using comparative metabolome and transcriptome analyses during seven developmental stages. Compared with the white-rooted cassava, anthocyanins, catechin derivatives, coumarin derivatives, and phenolic acids accumulated at higher levels in yellow-rooted cassava. Anthocyanins were particularly enriched and displayed different accumulation patterns during tuberous root development. This was confirmed by metabolic comparisons between five yellow-rooted and five white-rooted cassava accessions. The integrative metabolomic and transcriptomic analysis further revealed a coordinate regulation of 16 metabolites and 11 co-expression genes participating in anthocyanin biosynthesis, suggesting a vital role of anthocyanin biosynthesis in yellow pigmentation in cassava tuberous roots. In addition, two transcriptional factors, i.e., *MeMYB5* and *MeMYB42*, were also identified to co-express with these anthocyanin biosynthesis genes. These findings expand our knowledge on the role of anthocyanin biosynthesis in cassava root color formation, and offer useful information for the genetic breeding of yellow-rooted cassava in the future.

Keywords: cassava tuberous roots, color formation, anthocyanin biosynthesis, metabolome, transcriptome, coordinate regulation

INTRODUCTION

Cassava (*Manihot esculenta*) is one of the highly used tropical and subtropical root crops, providing staple food for more than 800 million people worldwide (1). Cassava tuberous roots are high in starch but very low in protein, micronutrients, and bioactive compounds such as carotenoids and anthocyanins (2, 3). Cassava is typically white rooted, although a few yellow landraces have been

reported in Amazonia, Brazil (4). Compared with white cassava roots, yellow cassava roots usually have higher levels of carotenoid contents (2, 5), flavanones, anthocyanins, and proanthocyanidins (6). In addition to the higher nutritional values, yellow cassava roots are also gaining popularity among consumers for their striking color compared to the white cassava roots (7). To date, the molecular mechanisms of color formation in cassava tuberous roots remain elusive, which greatly limits its breeding for higher nutritional contents.

Many studies have been conducted to investigate the color formation of yellow cassava roots. For instance, Carvalho et al. (5) characterized carotenoid profiles in 23 landraces of cassava tuberous roots with white-to-yellow-to-pink color. They established potential links of low transcript abundance of *LCYb* and *HYb* to the pink and yellow landraces, respectively. Similarly, Olayide et al. (8) found that carotenoid biosynthesis genes were expressed in both yellow and white cassava roots. Still, only lycopene-ε-cyclase (*LCY*ε), phytoene synthase 2 (*PSY2*), and β-carotenoid hydroxylase (*CHY*β) showed higher expression in yellow roots. Welsch et al. (2) revealed that a single nucleotide polymorphism in *PSY2* resulted in the accumulation of provitamin A carotenoids and induced yellow color to the cassava roots. Beyene et al. (9) enhanced β-carotene contents in cassava tuberous roots by co-expression of transgenes for deoxy-D-xylulose-5-phosphate synthase (*DXS*) and bacterial phytoene synthase (*crtB*). This resulted in color change of the cassava tuberous roots from white to yellow. These studies mainly focused on the carotenoid pathways; however, the carotenoid contents were not always higher in yellow cassava roots than white cassava roots (5), indicating that other pigments may also influence the coloring of yellow cassava roots.

Anthocyanins are well-known water-soluble phenolic pigments that color the fruits and flowers of many plants (10, 11). These pigments are present in vacuoles, and their hue and stability are usually influenced by intravacuolar environments, including pH, co-pigmentation, and complex formation with metal ions (11). In addition to the red, blue, and purple color formation, anthocyanins are reported to participate in color formation of yellow flowers in Herbaceous peony (12) and yellow peel in several fruits (13, 14). Similarly, in cassava, the anthocyanins and proanthocyanidins were more accumulated in yellow tuberous roots than white tuberous roots. Moreover, the expression of several anthocyanin biosynthesis genes, including *CHI, F3′5′H*, *F3H*, and *DFR*, was up-regulated in yellow cassava roots than white cassava roots (6). These results suggested that anthocyanins might also participate in the color formation of yellow cassava roots; however, the underlying key genes and regulatory networks remain unknown.

Due to the advantage of multi-omics in explaining complex biological problems, the integrated metabolomic and transcriptomic analyses have been widely applied to identify crucial genes and pathways controlling pigment accumulation in plants. For example, combined metabolome and transcriptome analyses were performed in pepper and asparagus cultivars, respectively, to demonstrate the roles of carotenoid and anthocyanin biosynthesis genes in color formation (15, 16). Similarly, the mechanisms underlying peel and pulp color formation were unveiled in pitaya fruit by an integrated transcriptome and metabolome approach, providing several candidate genes and metabolites for further functional characterization (13). In addition, network analysis of the metabolomic and transcriptomic profiles has been demonstrated as a powerful approach to uncover novel genes and regulatory pathways in potato pigmentation (17). However, no multi-omics studies have been conducted to determine the color formation in cassava tuberous roots, although there have been reports on drought response, root development, and nutritional properties (6, 18, 19).

In this work, comparative transcriptome and metabolome analyses were performed in seven developmental stages of SC205 (white-rooted cassava) and SC9 (yellow-rooted cassava), respectively, to explore the mechanisms of color formation in cassava tuberous roots. The findings will provide novel insights of anthocyanin biosynthesis on color formation in cassava tuberous roots and offer useful information for the genetic breeding of yellow-rooted cassava.

MATERIALS AND METHODS

Plant Materials and Sample Collection

Two cassava varieties, i.e., SC9 and SC205, which have yellow and white tuberous roots, respectively, were used in this study. Cassava stems were sectioned with a length of about 15 cm each and planted in the Chinese Academy of Tropical Agricultural Sciences experimental farm under normal field conditions at Danzhou, China. As described previously (18), seven experimental blocks were designed. Each block consisted of four rows, and each row was planted with seven individual plants, which were regarded as different biological replicates. The typical roots of five plants cultivated in the middle of each row were sampled at ∼9 am, respectively, at a total of seven developmental stages (S1-S7) including 100, 140, 180, 220, 260, 300, and 340 days after planting. These time points roughly represented three critical stages of early (S1-S3), middle (S4), and late (S5-S7) during cassava production (20). Only one main root was collected for each plant. Each root was dissected into pieces of ∼3 mm thick from the middle, and then 5–6 pieces were immediately frozen in liquid nitrogen and stored at −80°C until analyzed.

Metabolome Analysis

The untargeted metabolic experiments were performed at the Wuhan Metware Biotechnology Co., Ltd., as previously described (18, 21). Briefly, 100 mg powder was weighed and added to 1.2 ml 70% aqueous methanol for overnight extraction at 4°C. After centrifugation for 10 min at 10,000 *g*, the extracted solution was absorbed and filtrated. The quality control samples were prepared by mixing equal volumes of sample extracts and analyzed every 10 samples to monitor the repeatability. An ultra-performance liquid chromatography (UPLC) system (Shim-pack UFLC SHIMADZU CBM30A) and an MS/MS system (Applied Biosystems 6500 Q TRAP) were used to analyze the sample extracts under following conditions: UPLC column, Waters ACQUITY UPLC HSS T3 C18 (1.8 μm, 0.21 cm × 10 cm).

The mobile phase consisted of pure water with 0.04% acetic acid as eluent A and acetonitrile with 0.04% acetic acid as eluent B. Sample measurement was executed with a gradient program employing the initial conditions of 95% A and 5% B. A linear gradient to 5% A and 95% B was programmed within 10 min, and the composition of 5% A and 95% B was maintained for 1 min. Subsequently, a composition of 95% A and 5% B was adjusted within 0.1 min and maintained for 2.9 min. The injection volume was fixed to 2 μL, and the column temperature was controlled at 40°C. The effluents were alternatively connected to electrospray ionization (ESI)-triple quadrupole-linear ion trap (Q TRAP)-MS.

The acquisitions of linear ion trap (LIT) and triple quadrupole (QQQ) scans were executed on a triple quadrupole-linear ion trap MS API 6500 Q TRAP LC/MS/MS system, equipped with a Turbo Ion-Spray interface (operating in positive ion mode and negative ion mode) and controlled by Analyst 1.6.3 software (AB Sciex). The ESI source operation parameters were following: ion source, turbo spray; source temperature, 550°C; ion spray voltage, 5,500 V for positive ion mode and −4,500 V for negative ion mode; ion source gas I, gas II, and curtain gas were set at 50, 60, and 30 psi, respectively; the collision gas was high. Instrument tuning and mass calibration were analyzed in QQQ and LIT modes using 10 and 100 μmol/L polypropylene glycol solutions, respectively. The acquisition of QQQ scan was executed during MRM experiment with collision gas (nitrogen) at 5 psi.

Metabolites were identified and relative quantified by searching the self-built MetWare database[1] constructed based on the standard materials and purified compounds and the public databases (including MassBank, KNApSAcK, HMDB, MoTo DB, and METLIN), based on the accurate precursor ion (Q1) and production (Q3) values, m/z and MSMS spectra, retention time, and fragmentation pattern. The peak area of each chromatographic peak represented the relative content of the corresponding metabolite. All identified metabolites were used to conduct principle component analysis and orthogonal partial least squares discriminate analysis, and differentially accumulated metabolites (DAMs) were identified by setting the variable importance in projection (VIP) ≥ 1 and $|\log2(\text{fold-change})| \geq 1$. Each sample was performed with three biological replications.

Transcriptome Analysis

Library construction and RNA-seq sequencing were executed at the Annoroad Gene Technology Corporation (Beijing, China). In brief, total RNA was isolated from each sample to construct transcriptome libraries using Illumina TruSeq RNA sample prep Kit (Illumina, San Diego), according to the manufacturer's instructions. RNA-seq libraries were sequenced on an Illumina Hiseq 4000 platform to generate 150 bp pair-end reads. Each sample was performed with three biological replicates.

As previously described (22, 23), sequence quality was checked by FastQC software[2]. Sequencing adaptors and low-quality bases were filtered by FASTX-toolkit[3]. Clean reads were mapped to the cassava reference genome (version 6.1) by HISAT2 v2.1.0 (24) with default parameters and then assembled by Stringtie v1.3.4 (24) with reference genome-based strategy. Differentially expressed genes (DEGs) were identified by DESeq2 (25) setting false discovery rate < 0.05 and $\log2|\text{fold-change}| > 1$. Gene expression was measured in fragments per kilobase per million mapped reads (FPKM).

Metabolomic and Transcriptomic Integrative Analysis

The levels of metabolites and genes were log2-transformed for metabolomic and transcriptomic integrative analysis. The abundance patterns of metabolites and genes were determined by the standard procedure of WGCNA (26) based on the Pearson correlation coefficient and then visualized by R package "pheatmap." Cassava genes were classified into distinct hierarchical categories using the MapMan annotation system (27) for their biological function interpretation. The significantly enriched categories were identified by Fisher's exact test as previously reported (22, 23). WGCNA was also applied to identify the association between genes and metabolites, while Cytoscape software (28) was used for network visualization.

qRT-PCR Analysis

The qRT-PCR experiments were executed as previously described (19) to verify the expression of RNA-seq. Total RNA was isolated using RNAiso reagent (OMEGA), and then reversely transcribed to obtain cDNA using PrimeScript RT reagent Kit with gDNA Eraser (Takara, Dalian, China). Eleven genes related to anthocyanin biosynthesis were selected and analyzed by qRT-PCR. The primers were listed in **Supplementary Table 1**.

The qRT-PCR was executed on a Stratagene Mx3000P machine (Stratagene, CA, United States) using SYBR Premix Ex Taq (Takara, Dalian, China) with the following processes: 30 s at 95°C, then 40 cycles of 10 s at 95°C and 30 s at 60°C. A thermal denaturing step was executed to produce the melt curves for verification of amplification specificity. The cassava actin gene was used as an internal control (19). Each sample was measured in triplicates, and the relative gene expression was calculated by the $2^{-\Delta\Delta Ct}$ method (23).

RESULTS

Metabolomic Profiling of Cassava Tuberous Roots With Different Colors Across the Developmental Stages

In total, 488 metabolic compounds were identified and quantified in tuberous roots of SC9 and SC205 across seven developmental stages (S1-S7, **Figure 1A**). These metabolites were divided into fifteen categories with the three most abundant were flavones (108), amino acid derivatives (60), and lipids (56). Principle component analysis revealed that tuberous root samples of SC9 and SC205 were separated while different replicates were closely grouped (**Figure 1B**), indicating high reliability of our

[1] http://www.metware.cn/

[2] http://www.bioinformatics.babraham.ac.uk/projects/fastqc/

[3] http://hannonlab.cshl.edu/fastx_toolkit/index.html

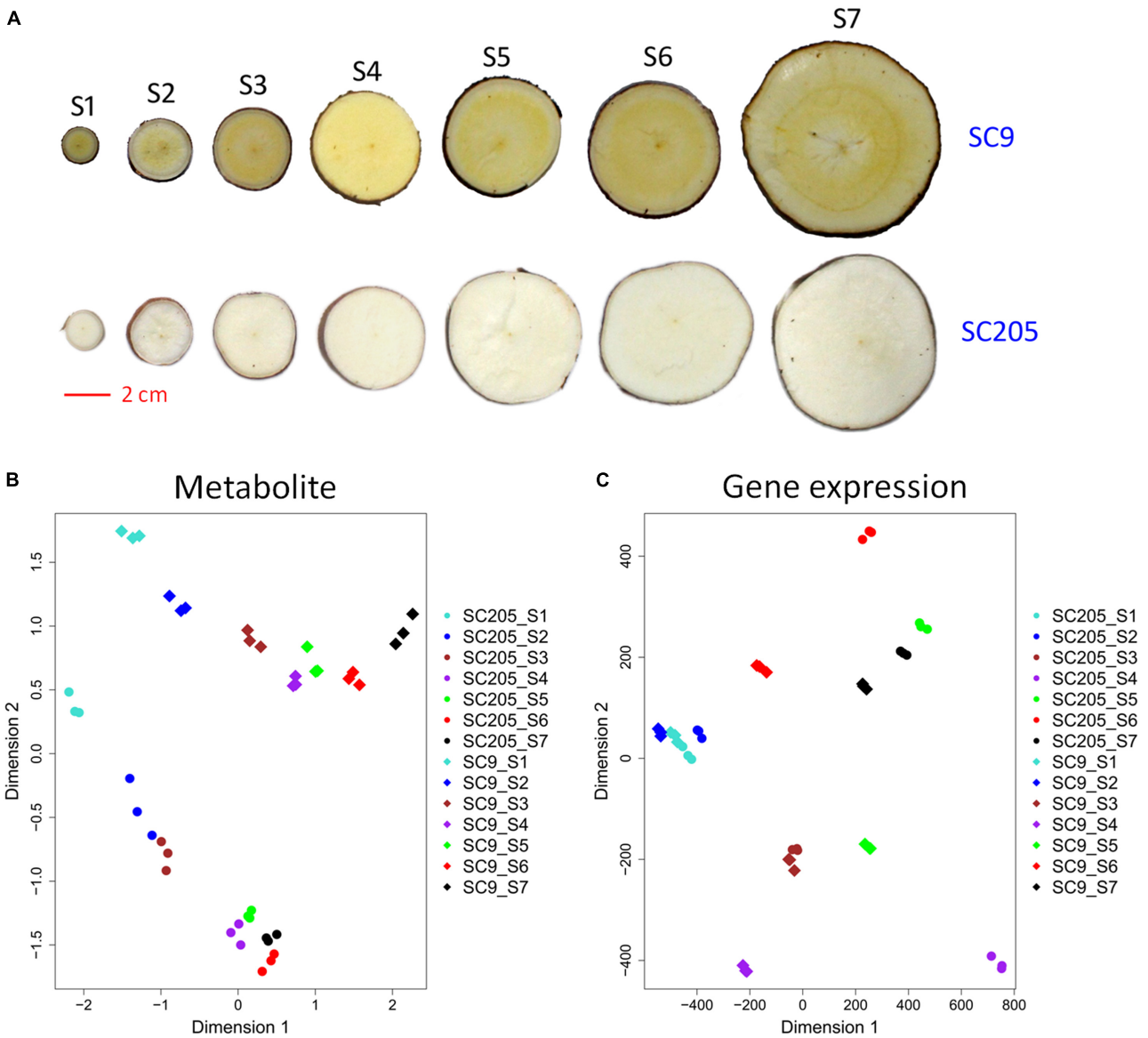

FIGURE 1 | Overview of tuberous roots of SC9 and SC205. **(A)** Phenotypes of SC9 and SC205 tuberous roots collected at seven developmental stages from 100–340 days after planting: S1, 100; S2, 140; S3, 180; S4, 220; S5, 260; S6, 300; and S7, 340. The scale bar equals 2 cm. **(B,C)** Clustering of tuberous root samples based on the metabolite levels and gene expression profiles, respectively. The symbols with the same color represent different replicates of a sample.

metabolomic data and a significant impact of metabolites on the color of tuberous roots.

A total of 335 differentially accumulated metabolites (DAMs) were identified by metabolomic comparisons between SC9 and SC205 at seven developmental stages, respectively (**Supplementary Table 2**). Most metabolites were higher accumulated in SC9 compared with SC205 from S1 to S6, while this trend was reversed at S7 (**Figure 2A**). On average, the categories with most DAMs were flavones (22.84%) and lipids (12.27%), followed by amino acid derivatives (8.69%), organic acids (8.10%), hydroxycinnamoyl derivatives (7.2%), phenolic acids (6.32%), nucleotide and its derivatives (5.23%), catechin derivatives (4.79%), coumarin and its derivatives (3.60%), and anthocyanins (3.57%). However, their frequencies varied slightly across different developmental stages (**Figure 2B**).

The metabolomic changes in each category were also observed. Notably, anthocyanin-related DAMs were increased in SC9 than SC205 across all the developmental stages (**Figure 2C**). Likely, most DAMs related to catechin derivatives, coumarin and its derivatives, phenolic acids, and hydroxycinnamoyl derivatives were higher accumulated in SC9 than SC205 at different stages (**Figures 2D–G**). In addition, most flavone-related DAMs were also increased in SC9 compared with SC205 from stage S1 to S3; however, this trend was not apparent during the remaining

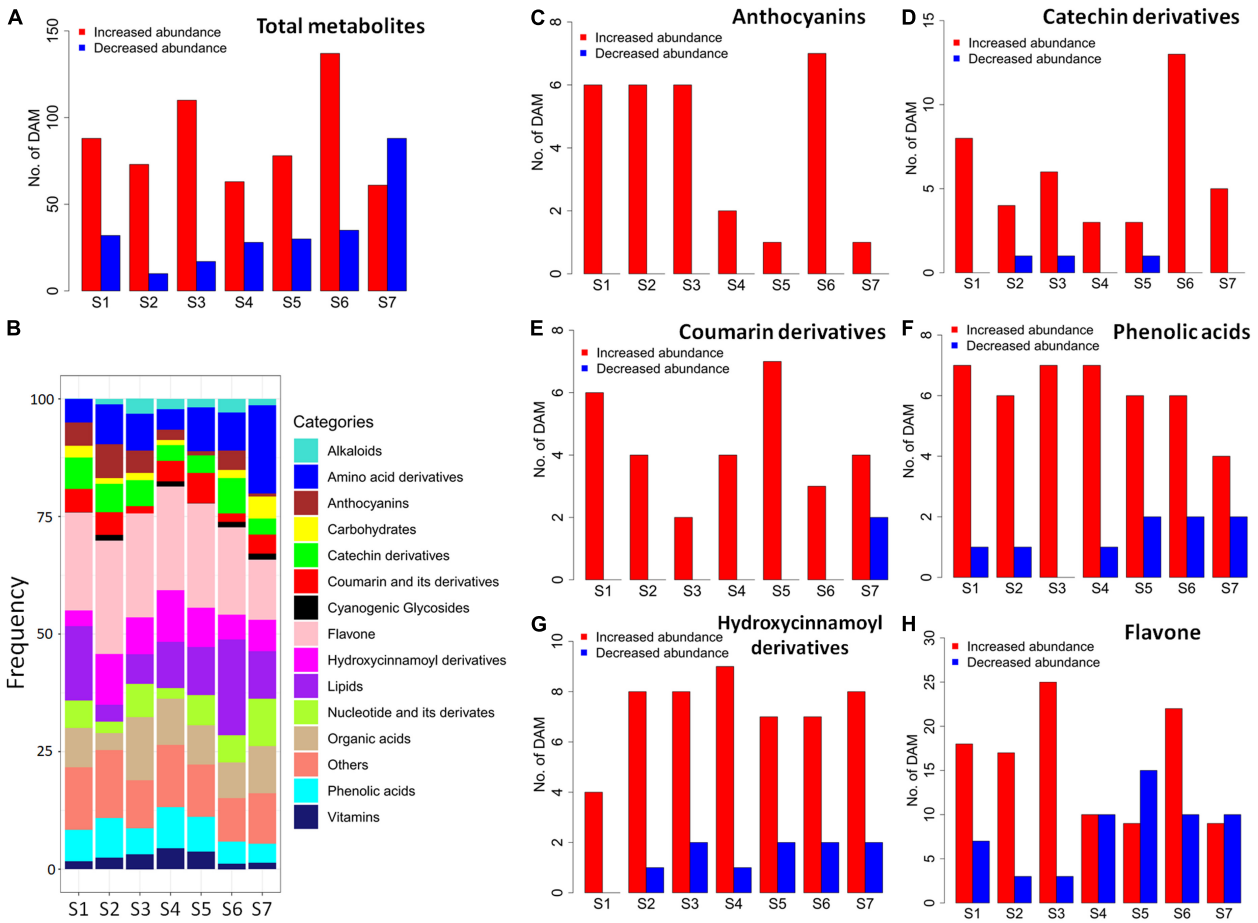

FIGURE 2 | Differentially accumulated metabolites between SC9 and SC205 during tuberous root development. **(A)** Number of all abundance-increased and abundance-decreased DAMs, which showed higher and lower metabolite levels in SC9 than SC205, respectively. **(B)** Category frequency of all DAMs. **(C–H)** Number of abundance-increased and abundance-decreased DAMs relevant to anthocyanins, catechin derivatives, coumarin derivatives, phenolic acids, hydroxycinnamoyl derivatives, and flavones, respectively.

developmental stages (**Figure 2H**). Together, these results revealed a comprehensive change of metabolites between yellow and white cassava roots across different developmental stages.

Developmental Effects on Metabolites in Cassava Tuberous Roots With Different Colors

A total of five groups (M1-M5) of metabolites were identified according to their profiles in SC205 and SC9 across seven different development stages (**Figure 3A** and **Supplementary Table 2**).

Metabolites from M1 were gradually accumulated from S1 to S4 and then declined until S7 in SC205, while these metabolites displayed a time-shift pattern in SC9 as they were accumulated from S1 to S6 and decreased at S7 (**Figure 3A**). These metabolites were significantly enriched in lipids (**Figure 3B**). As expected, 68% (21/31) metabolites from this group belonged to diverse forms of lysophosphatidylcholine (LPC) and lysophosphatidylethanolamine (LPE).

Metabolites from M2 were highly accumulated at late stages (S3-S6) than early stages (S1-S2) in both SC205 and SC9, while there was a sharp decrease at S7 in SC9 (**Figure 3A**). These metabolites were significantly enriched in amino acid derivatives (**Figure 3B**). A total of ten amino acids, including phenylalanine, homocysteine, methionine, tyrosine, asparagines, tryptophan, isoleucine, leucine, citrulline, and arginine, were included in this group.

Metabolites from M3 and M5 exhibited very similar patterns between SC205 and SC9 during tuberous root development, although they were highly accumulated at S4-S7 and S1-S3, respectively (**Figure 3A**). The metabolites from M3 were significantly enriched in anthocyanins, and anthocyanin-related metabolites such as pelargonin, procyanidin B2, and procyanidin B3 were found in this group (**Figure 3C**). The enriched categories of M5 were lipids and flavones (**Figure 3B**). A large number of metabolites relevant to monoacylglycerol (MAG, 18:1, 18:2, 18:3, and 18:4), digalactosylmonoacylglycerol (DGMG, 18:1 and 18:2), and monogalactosylmonoglyceride (MGMG, 18:2) were included in this group. In addition, flavones such as naringenin,

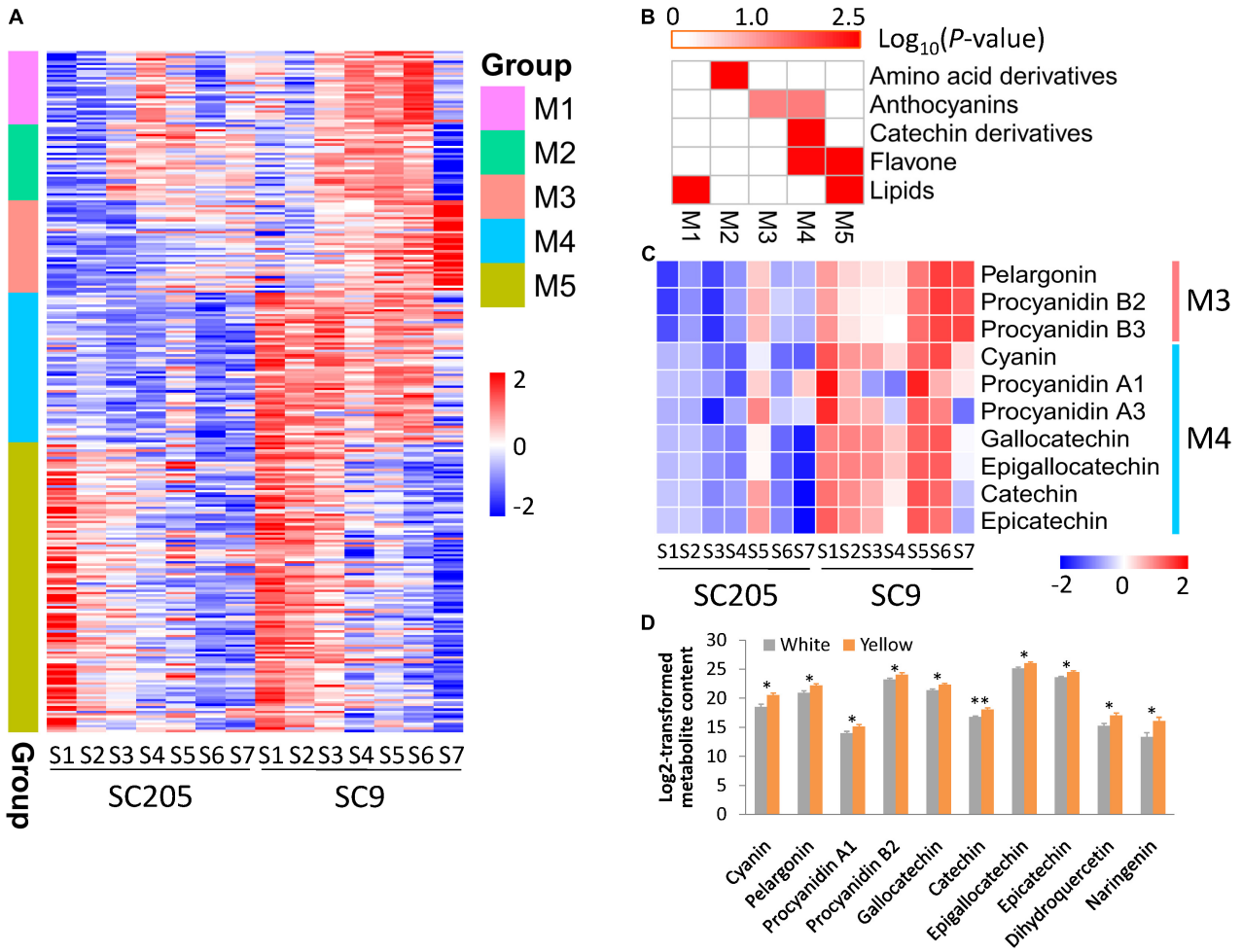

FIGURE 3 | Metabolite profiles of cassava tuberous roots with different colors during seven developmental stages. **(A)** Metabolite profiles of SC205 and SC9 during tuberous root development. A total of five groups (M1-M5) were determined. **(B)** Metabolite enrichment analysis of the groups presented in panel **(A)**. **(C)** Changes of metabolites relevant to anthocyanins and catechin derivatives during tuberous root development. **(D)** DAMs identified between five white-rooted and five yellow-rooted cassava accessions at the developmental stage S7 with at least two biological replicates. The values represent the mean ± SD, and ** and * represent significant differences at $P < 0.01$ and $P < 0.05$, respectively, based on the Student's *t*-test.

dihydroquercetin, quercetin 3-*O*-glucoside, quercetin 3-*O*-rutinoside, kaempferol 3-*O*-galactoside, and kaempferol 3-*O*-rutinoside were also included (**Supplementary Table 2**).

Although no obvious trends were observed for the metabolites from M4, their levels were overall higher in SC9 than SC205. The metabolites of this group were enriched in anthocyanins, catechin derivatives, and flavones (**Figure 3B**). Cyanin, procyanidin A1, and procyanidin A3 relevant to anthocyanins, and gallocatechin, epigallocatechin, catechin, and epicatechin related to catechin derivatives, were found in this group (**Figure 3C**). Collectively, these results revealed a dynamic change of metabolites in yellow and white cassava tuberous roots during different developmental stages.

We also found that anthocyanin-related metabolites were significantly higher in SC9 than SC205 (**Figure 3C**). Moreover, the higher levels of anthocyanins in yellow-rooted cassava were further confirmed by metabolic comparisons between five yellow-rooted and five white-rooted cassava accessions (**Figure 3D**). These results suggested a significant role of anthocyanin-related metabolites in the yellow pigment formation of cassava tuberous roots.

Transcriptomic Profiling of Cassava Tuberous Roots With Different Colors Across the Developmental Stages

The samples used for metabolic assay were subjected to RNA-seq analysis, to investigate the transcriptomic mechanisms underlying color formation of cassava tuberous roots. Principle component analysis showed that transcriptomic samples of SC9 and SC205 tuberous roots were well separated, whereas three replicates of the same sample were clustered (**Figure 1C**). In total, ∼1,086 million clean reads were obtained after removing the adaptors and low-quality reads, and 78.1% on average were mapped to the cassava reference genome. Low-expressed

genes with FPKM < 1 across samples were discarded for further analysis.

Differentially expressed genes (DEGs) were identified between SC9 and SC205 at each developmental stage, and functional category enrichment was subsequently analyzed for the up-regulated and down-regulated genes, respectively (**Figures 4A,B**). A total of 13,537 DEGs were identified (**Supplementary Table 3**). Overall, the number of DEGs was higher at S4-S7 than S1-S3, indicating that more genes were required to maintain the differentiation of tuberous roots between SC9 and SC205 at late developmental stages. In addition, the number of up-regulated DEGs was higher than those down-regulated at each stage, in accord with the changes of metabolites (**Figures 2A**, **4A**). Functional enrichment found that secondary metabolism pathways (including flavonoids, phenylpropanoids, and simple phenols) were commonly enriched in the up-regulated DEGs at S1-S2 and S4-S6, which provided a strong hint to further investigate the expression of genes involved in phenylpropanoid-flavonoid (anthocyanin biosynthesis) pathways.

In total, 41 genes from fourteen key enzymes participating in anthocyanin biosynthesis were found in the cassava genome (**Figure 4C** and **Supplementary Table 4**). Fifteen of them were excluded from further analysis since they were not or low expressed during the whole developmental stages. Although similar expression patterns were observed for most of the remaining genes between SC9 and SC205, their expression levels were higher in SC9 than SC205 (especially from S3 to S6), suggesting the involvement of anthocyanin biosynthesis pathways in color formation of cassava tuberous roots.

To verify the expression levels of RNA-seq data, eleven genes involved in anthocyanin biosynthesis were examined by the qRT-PCR method in SC205. The correlation coefficients ranged from 0.86 to 0.99 between these two independent methods (**Supplementary Table 1**), indicating the high reliability of gene expression profiles detected by RNA-seq.

Integrative Metabolomic and Transcriptomic Analysis for Anthocyanin Biosynthesis Pathways

In total, 16 metabolites involved in anthocyanin biosynthesis were identified (**Figure 5A**), including three flavones (naringenin, dihydroquercetin, and afzelechin), six anthocyanins (cyanin, pelargonin, procyanidin A1, procyanidin A3, procyanidin B2, and procyanidin B3), five catechin derivatives (gallocatechin, epigallocatechin, catechin, epicatechin, and epiafzelechin), one amino acid (phenylalanine), and one hydroxycinnamoyl metabolite (4-coumarate). These metabolites accumulated at higher levels in SC9 than SC205 during tuberous root development. Correspondingly, eleven co-expressed DEGs (namely *MePAL1*, *MeC4H1*, *Me4CL1*, *MeCHS1*, *MeCHS2*, *MeCHI*, *MeF3H*, *MeF3'5'H*, *MeDFR1*, *MeANS*, and *MeANR*) covering the whole anthocyanin biosynthesis pathways were also identified and showed higher expression levels in SC9 than SC205 during the developmental stages (**Figures 5B,C** and **Supplementary Table 5**).

In addition, five flavanols (including kaempferol 3-*O*-glucoside, kaempferol 3-*O*-rutinoside, kaempferol 3-*O*-galactoside, quercetin 3-*O*-glucoside, and quercetin 3-*O*-rutinoside) were identified. However, they accumulated at lower levels in SC9 than SC205 during tuberous root development. Flavonol synthase (FLS) is a key enzyme involved in the conversion of dihydroflavonols (e.g., dihydrokaempferol and dihydroquercetin) to the corresponding flavonols (kaempferol and quercetin). Interestingly, in accord with the metabolic changes of the above five flavanols, we found a flavonol synthase gene (*MeFLS2*) exhibiting lower expression levels in SC9 than SC205 (**Supplementary Table 4**). These results suggested that *MeFLS2* was a crucial gene controlling the metabolic flows of dihydroflavonols (such as dihydrokaempferol and dihydroquercetin) toward anthocyanin biosynthesis in cassava tuberous roots.

Together, these results revealed a coordinate regulation of anthocyanin biosynthesis at the metabolomic and transcriptomic levels.

Identification of Transcriptional Factors Modulating the Expression of Anthocyanin Biosynthesis Genes

The expression levels of genes in a co-expression network are usually regulated by the same transcriptional factors (TFs). Therefore, the eleven co-expressed anthocyanin biosynthesis genes were used as queries to perform a co-expression network analysis, to identify the crucial TFs participating in anthocyanin biosynthesis.

Two MYB members (*MeMYB5* and *MeMYB42*), whose homologs (such as *VvMYB5* and *AtMYB42*) were previously reported to be involved in anthocyanin biosynthesis regulation (29, 30), were identified to highly co-express with eight and nine anthocyanin biosynthesis genes, respectively (**Figure 5D**). Moreover, MYB *cis*-element was found in the 2-kb promoter region of these anthocyanin biosynthesis genes (except *MeC4H1*, **Supplementary Table 5**). *MeMYB5* and *MeMYB42* were also co-expressed with 4-coumarate, naringenin, and dihydroquercetin, located on the anthocyanin biosynthesis pathways (**Figure 5D**). These results suggested that *MeMYB5* and *MeMYB42* were the key TFs participating in the regulation of anthocyanin biosynthesis in cassava tuberous roots.

DISCUSSION

Discovery of Candidate Genes and Pathways for the Coloring of Cassava Roots

It is well established that the yellow cassava roots have higher nutritional values and are more popular with consumers than white cassava roots (5, 7). Thus, the primary goal of our study is to explore key genes and pathways responsible for the color formation in yellow cassava roots. This is a crucial and fundamental step for the molecular breeding of cassava varieties with improved nutrition.

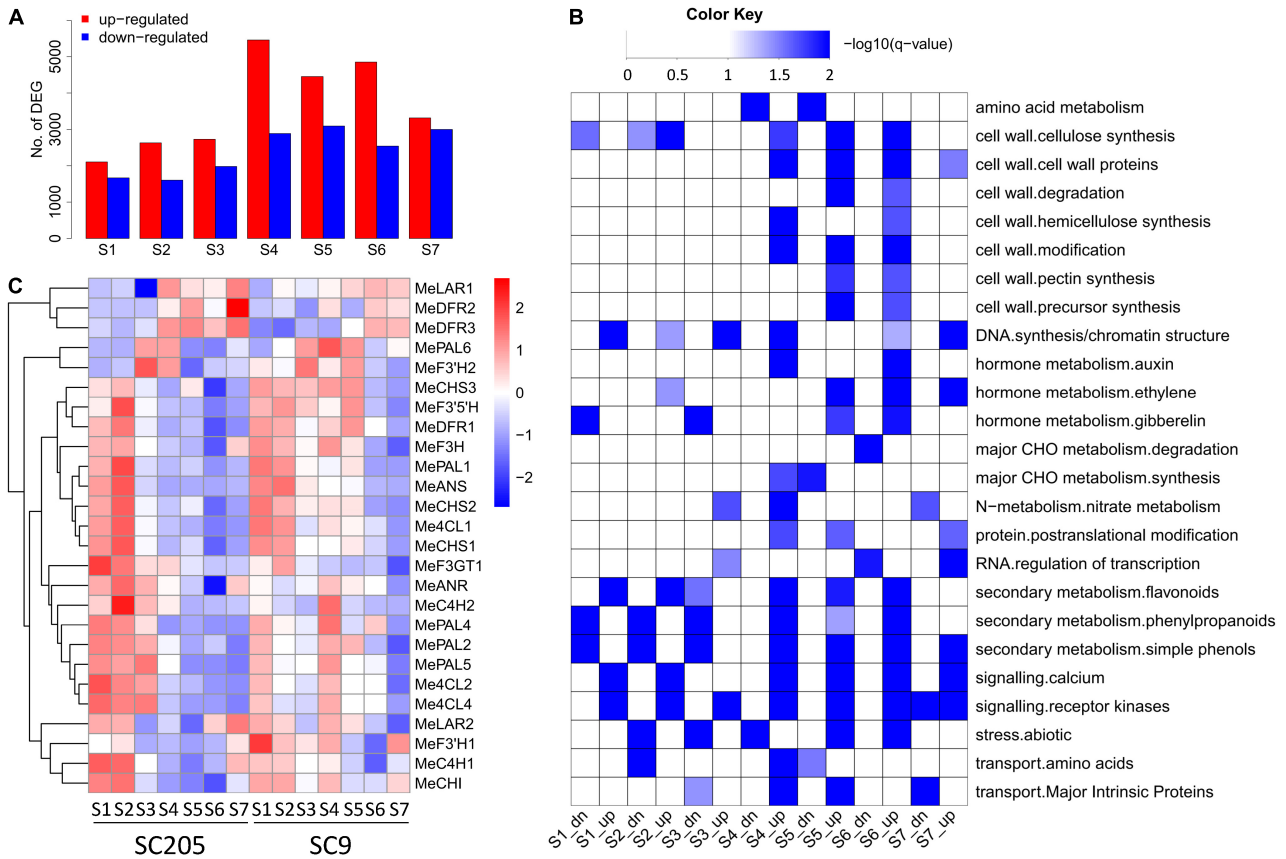

FIGURE 4 | Differentially expressed genes between SC9 and SC205 during tuberous root development. **(A)** Number of up-regulated and down-regulated DEGs, which showed higher and lower expression levels in SC9 than SC205, respectively. **(B)** Functional category enrichment of the up-regulated (suffixed with "up") and down-regulated (suffixed with "dn") DEGs presented in panel **(A)**. **(C)** Expression profiles of anthocyanin biosynthesis genes during tuberous root development.

In the past decades, many progresses have been achieved concerning the mechanisms of yellow cassava roots. Carotenoid pathways were found as a major factor for yellow pigmentation, and several related genes were identified and functionally characterized (2, 9). However, the carotenoid contents were not always higher in yellow cassava roots than white cassava roots (5), indicating that other genes and pathways might be involved in the yellow pigment formation of cassava roots.

With the availability of cassava genome, the members derived from a gene family or involved in a biological pathway are identified (31). However, it is still hard to systematically determine the key players without an assistance of other omics approaches (e.g., transcriptome and metabolome), which define a biosystem at distinct molecular layers (32). Multi-omics studies have been performed to identify candidate genes and pathways controlling pigment accumulation in many plants (13, 15, 16). Similar studies were also performed in cassava in response to drought, cold, root development, and nutritional properties (6, 18, 19, 33). In this study, 355 DAMs and 13,537 DEGs were reported by comparative transcriptomic and metabolomic analyses during cassava tuberous root development between SC9 and SC205 (**Supplementary Tables 2, 3**). Integrated transcriptome and metabolome analyses helped in the exploration of anthocyanin metabolic pathways, since many genes and metabolites referred to the anthocyanin biosynthesis showed a coordinated change between yellow cassava roots and white cassava roots (**Figure 5A**). In addition, *MeFLS2* was determined as a vital gene controlling the metabolic flows of dihydroflavonols to the direction of anthocyanin biosynthesis in cassava roots (**Figure 5A**), in accordance with the roles of *MlFLS* in competition between anthocyanin and flavonol biosynthesis (34). By co-expression network analysis, *MeMYB5* and *MeMYB42* were identified as the key TFs to transcriptionally regulate anthocyanin biosynthesis genes in cassava (**Figure 5D**). These results expand our knowledge on yellow pigmentation formation in cassava tuberous roots and also suggest that multi-omics integrative analysis is a promising tool for discovering candidate genes and pathways especially with the availability of genome sequences.

Roles of Carotenoid Synthesis Genes in the Coloring of Cassava Tuberous Roots

Carotenoid synthesis genes have been demonstrated to involve in the color formation of cassava roots (2, 5, 8). However, the full members referred to carotenoid synthesis pathways have not yet

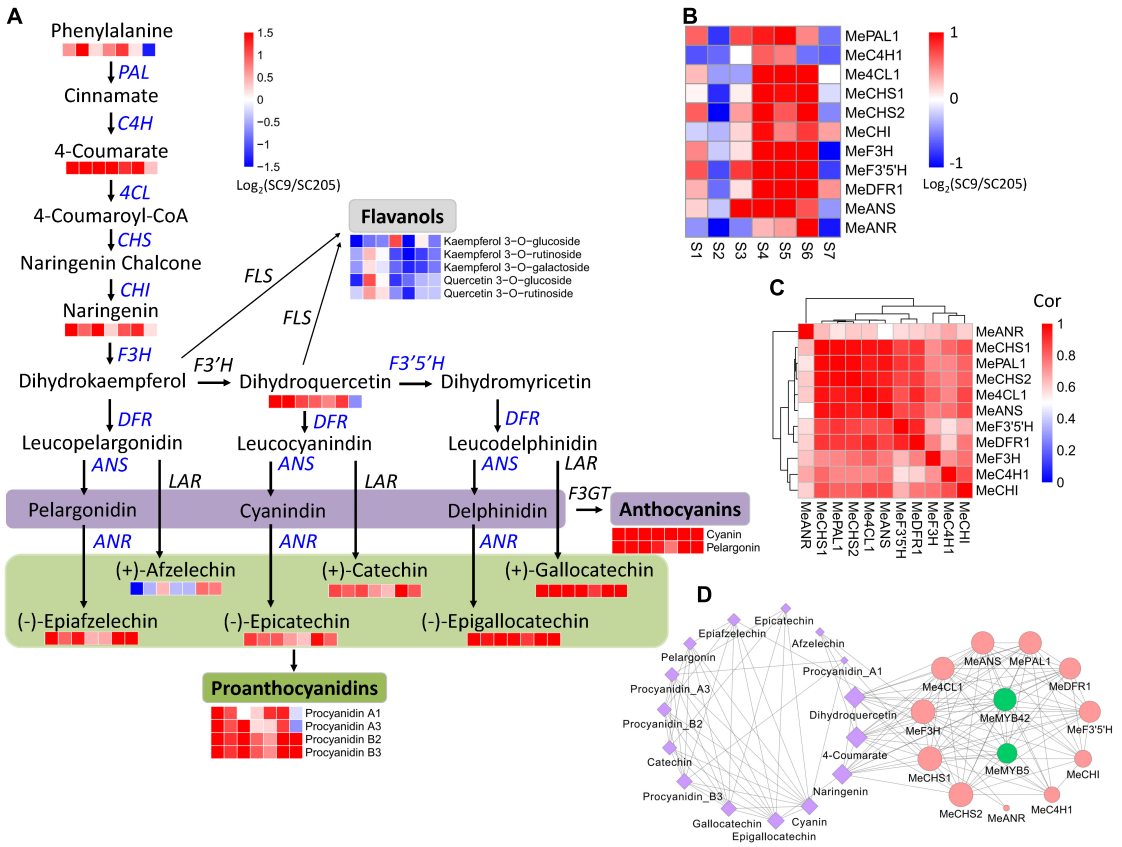

FIGURE 5 | Abundance changes of metabolites and genes relevant to anthocyanin biosynthesis during tuberous root development. **(A)** Summary of anthocyanin biosynthesis pathways. Heatmaps are shown where the metabolite levels changed significantly between SC9 and SC205 during tuberous root development. Co-expressed anthocyanin biosynthesis genes are indicated in blue. **(B)** Expression fold-change of co-expressed anthocyanin biosynthesis genes between SC9 and SC205 during tuberous root development. **(C)** Expression correlation of anthocyanin biosynthesis genes shown in panel **(B)**. **(D)** The network of co-expressed genes and metabolites relevant to anthocyanin biosynthesis. The edges were shown by setting the threshold = 0.65. Node size represents its connectivity to other genes/metabolites. Metabolites are colored by purple, while anthocyanin biosynthesis genes and transcription factors are colored by red and green, respectively.

been systematically identified and their roles in color formation remain largely unknown.

In this work, 23 genes were found from eleven gene families located on the carotenoid synthesis pathways in the cassava genome (**Figure 6A** and **Supplementary Table 6**). Three genes, including *MePSY3*, *MeZDS2*, and *MeZEP2*, were extremely low expressed (FPKM < 0.1) during seven stages of tuberous root development in SC205 and SC9, indicating a minimal role of these genes in cassava tuberous roots. According to their different expression patterns, the remaining 20 genes were grouped into three clusters (C1-C3, **Figure 6B**). The genes from cluster C1 expressed higher in SC205 than SC9, especially during S4 to S7 stages. It seems that the genes in this cluster were not relevant to the yellow formation of cassava tuberous roots; however, a previously suggested candidate gene *MeLCYE* was included in this group (8). The genes from cluster C2 exhibited similar expression patterns between SC205 and SC9, i.e., the expression levels were higher at stages S1 and S2 but lower at S3 to S7. Notably, *MeLCYB1* from this group expressed lower in SC205 than SC9 in most of the developmental stages, supporting a possible role of this gene in the color formation of cassava roots (5).

A total of six genes, including *MePSY2*, *MeCRTISO2*, *MeLCYB2*, *MeCHYB3*, *MeZEP1*, and *MeNXS*, were included in cluster C3. These genes covered most enzymes responsible for the carotenoid biosynthesis and expressed lower in SC205 than SC9 during cassava tuberous root development, with *MeLCYB2* and *MeNXS* being the most significantly changed genes (**Figure 6C**). These two genes exhibited significantly higher expression levels in yellow cassava roots than white cassava roots (5). In addition, their homologs have also been characterized in color formation in watermelon and Chinese kale (35, 36), indicating a similar role of these two genes in cassava roots. A key gene *MePSY2*, which was responsible for cassava roots with yellow color by provitamin A accumulation (2), was included in this group. Another carotenoid synthesis gene *MeCRTISO2*, which expressed higher in yellow cassava roots than white cassava roots (5), was also included. Moreover, positive correlations were observed between the total carotenoid content and the expression of *MeLCYB2* and *MePSY2*, respectively (5, 8). Together, these results strongly suggested that

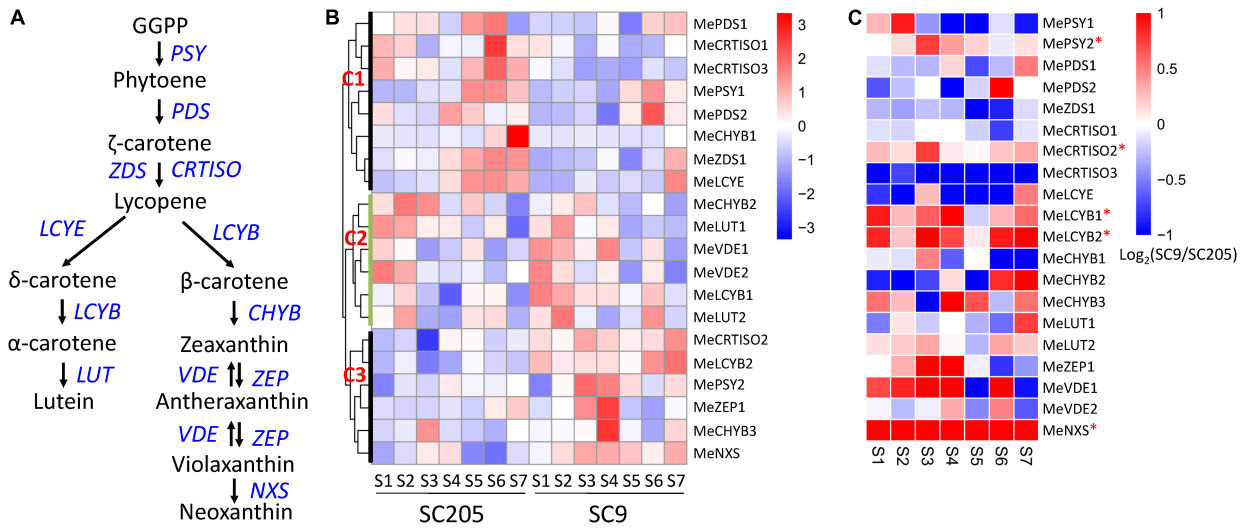

FIGURE 6 | Expression changes of carotenoid biosynthesis genes during tuberous root development. **(A)** Summary of carotenoid biosynthesis pathways, in which the genes are highlighted in blue. **(B)** Expression profiles of carotenoid biosynthesis genes between SC9 and SC205 during tuberous root development. **(C)** Expression fold-change of carotenoid biosynthesis genes between SC9 and SC205 during tuberous root development. The genes suffixed with a star (*) are up-regulated in SC9 than SC205 during most developmental stages and may participate in the yellow formation of cassava tuberous roots.

the six genes in cluster C3 might participate in the yellow pigment formation of cassava tuberous roots *via* carotenoid synthesis.

Roles of Anthocyanin Biosynthesis Genes in Color Formation of Cassava Tuberous Roots

Anthocyanins are water-soluble pigments responsible for coloring plant flowers and fruits (10, 11). To date, anthocyanin biosynthesis genes and pathways have been demonstrated to play an important role in color formation in pepper (16), cucumber (14), asparaguses (15), jujube fruit (37, 38), cowpea (39), potato (40, 41), tea (42), longan (43), and pitaya (13). In cassava, Xiao et al. (6) found that anthocyanins and proanthocyanidins were significantly lower in white cassava roots than yellow cassava roots. Although several anthocyanin biosynthesis genes were uncovered in response to stresses and leaf and root development in cassava (18, 19, 22), the changes of anthocyanins and proanthocyanidins during cassava root development as well as the related key genes and regulatory networks remain largely unknown.

In this work, six metabolites referred to anthocyanins and proanthocyanidins were higher accumulated in yellow cassava roots than white cassava roots (**Figures 3C,D**). Furthermore, these metabolites exhibited distinct accumulation patterns in white and yellow cassava roots during tuberous root development (**Figure 3C**). To demonstrate their possible roles in color formation of cassava roots, a total of 41 anthocyanin biosynthesis genes derived from fourteen enzyme families were systematically identified throughout the cassava genome (**Supplementary Table 4**). Excluding fifteen low- or non-expressed genes, the majority of the remaining genes were expressed higher in SC9 than SC205. Notably, eleven DEGs covering the whole anthocyanin biosynthesis pathways were co-expressed during cassava root development (**Figure 5D**). *MePAL1* and *MeANS* catalyzed the first and the last steps of anthocyanin biosynthesis, respectively (44). Together with *MeF3H*, *MeCHS1*, and *MeCHS2*, these two genes ranked as the top hub genes in the co-expression network (**Figure 5D**), supporting that they were vital members in anthocyanin biosynthesis in cassava (45). These results also suggested that anthocyanin biosynthesis genes play a crucial role in the color formation of cassava roots *via* a coordinated expression regulation.

Anthocyanin biosynthesis genes are transcriptionally coordinated by the "MYB-bHLH-WDR (MBW)" complex that regulates their expression levels through specific *cis*-element binding in the promoter regions (46). Our co-expression network analysis revealed that *MeMYB5* and *MeMYB42* were closely related to many anthocyanin biosynthesis genes (including *MePAL1*, *MeANS*, and *MeF3H*). Moreover, MYB *cis*-element was present in the promoter region of these genes. These results suggested that *MeMYB5* and *MeMYB42* might regulate the expression of anthocyanin biosynthesis genes *via* binding to the MYB *cis*-element in cassava, in accordance with previous reporters in other species (29, 30). However, this conclusion has not been verified and deserves further investigations.

The ratio of anthocyanins and carotenoids was a major factor determining the fruit color (47). Although several crucial anthocyanin biosynthesis genes were identified to participate in color formation of cassava tuberous roots in this work, the relationships between anthocyanin and carotenoid biosynthesis genes were still not explored. Therefore, one feasible strategy for yellow-rooted cassava breeding is to examine the effect of candidate genes (especially for the TFs) individually by transgenic methods, and then to introduce multiple anthocyanin and carotenoid biosynthesis genes into a commercial cassava cultivar.

CONCLUSION

In summary, the mechanisms of color formation in cassava tuberous roots were investigated by metabolomic and transcriptomic approaches during seven developmental stages. Compared with white-rooted cassava (SC205), anthocyanins, catechin derivatives, coumarin derivatives, and phenolic acids were higher accumulated in yellow-rooted cassava (SC9). Anthocyanins were particularly enriched and displayed different accumulation patterns during tuberous root development. Further analysis found that 16 metabolites participating in anthocyanin biosynthesis, as well as 11 co-expression genes covering the whole anthocyanin biosynthesis pathways, showed higher accumulation levels in SC9 than SC205 at most developmental stages, suggesting a major role of anthocyanin biosynthesis in yellow pigmentation formation of cassava tuberous roots *via* coordinate regulation. These findings expand our knowledge of anthocyanin biosynthesis on color formation in cassava tuberous roots and offer useful candidate genes for genetic breeding of yellow-rooted cassava in the future.

DATA AVAILABILITY STATEMENT

The RNA-seq datasets generated in this work were submitted to the NCBI SRA database under the accessions SRR10480882-SRR10480904 and SRR17267560-SRR17267580. The metabolomics data were deposited to the EMBL-EBI MetaboLights database with the identifier MTBLS4361.

AUTHOR CONTRIBUTIONS

ZD and WH designed the project and finalized the manuscript. LF, ZD, WT, JY, and YY analyzed the data. LF and ZD drafted the manuscript. All authors read and approved the final manuscript.

FUNDING

This research was funded by the 2020 Research Program of Sanya Yazhou Bay Science and Technology City (No. SKJC-2020-02-002), the National Key Research and Development Program of China (No. 2019YFD1001105), the High Level Talents Project of Hainan Basic and Applied Research Program (Natural Science, No. 2019RC289), the earmarked fund for Modern Agro-industry Technology Research System (No. nycytx-11), and the Central Public-Interest Scientific Institution Basal Research Fund for Chinese Academy of Tropical Agricultural Sciences (No. 1630052017021).

SUPPLEMENTARY MATERIAL

The Supplementary Material for this article can be found online at: https://www.frontiersin.org/articles/10.3389/fnut.2022.842693/full#supplementary-material

REFERENCES

1. Tappiban P, Smith DR, Triwitayakorn K, Bao J. Recent understanding of starch biosynthesis in cassava for quality improvement: a review. *Trends Food Sci Tech.* (2019) 83:167–80. doi: 10.1016/j.tifs.2018.11.019
2. Welsch R, Arango J, Bar C, Salazar B, Al-Babili S, Beltran J, et al. Provitamin a accumulation in cassava (*Manihot esculenta*) roots driven by a single nucleotide polymorphism in a phytoene synthase gene. *Plant Cell.* (2010) 22:3348–56. doi: 10.1105/tpc.110.077560
3. Uarrota VG, Maraschin M. Metabolomic, enzymatic, and histochemical analyzes of cassava roots during postharvest physiological deterioration. *BMC Res Notes.* (2015) 8:648. doi: 10.1186/s13104-015-1580-3
4. Ferreira CF, Alves E, Pestana KN, Junghans DT, Kobayashi AK, de Jesus Santos V, et al. Molecular characterization of cassava (*Manihot esculenta* Crantz) with yellow-orange roots for beta-carotene improvement. *Crop Breed Appl Biot.* (2008) 8:23–9. doi: 10.12702/1984-7033.v08n01a04
5. Carvalho LJ, Agustini MA, Anderson JV, Vieira EA, de Souza CR, Chen S, et al. Natural variation in expression of genes associated with carotenoid biosynthesis and accumulation in cassava (*Manihot esculenta* Crantz) storage root. *BMC Plant Biol.* (2016) 16:133. doi: 10.1186/s12870-016-0826-0
6. Xiao L, Cao S, Shang X, Xie X, Zeng W, Lu L, et al. Metabolomic and transcriptomic profiling reveals distinct nutritional properties of cassavas with different flesh colors. *Food Chem Mol Sci.* (2021) 2:100016. doi: 10.1016/j.fochms.2021.100016
7. Bechoff A, Chijioke U, Westby A, Tomlins KI. 'Yellow is good for you': consumer perception and acceptability of fortified and biofortified cassava products. *PLoS One.* (2018) 13:e0203421. doi: 10.1371/journal.pone.0203421
8. Olayide P, Large A, Stridh L, Rabbi I, Baldermann S, Stavolone L, et al. Gene expression and metabolite profiling of thirteen Nigerian cassava landraces to elucidate starch and carotenoid composition. *Agronomy.* (2020) 10:424. doi: 10.3390/agronomy10030424
9. Beyene G, Solomon FR, Chauhan RD, Gaitan-Solis E, Narayanan N, Gehan J, et al. Provitamin a biofortification of cassava enhances shelf life but reduces dry matter content of storage roots due to altered carbon partitioning into starch. *Plant Biotechnol J.* (2018) 16:1186–200. doi: 10.1111/pbi.12862
10. Kayesh E, Shangguan L, Korir NK, Sun X, Bilkish N, Zhang Y, et al. Fruit skin color and the role of anthocyanin. *Acta Physiol Plant.* (2013) 35:2879–90. doi: 10.1007/s11738-013-1332-8
11. Oren-Shamir M. Does anthocyanin degradation play a significant role in determining pigment concentration in plants? *Plant Sci.* (2009) 177:310–6. doi: 10.1152/japplphysiol.00626.2005
12. Zhao D, Jiang Y, Ning C, Meng J, Lin S, Ding W, et al. Transcriptome sequencing of a chimaera reveals coordinated expression of anthocyanin biosynthetic genes mediating yellow formation in herbaceous peony (*Paeonia lactiflora* Pall.). *BMC Genomics.* (2014) 15:689. doi: 10.1186/1471-2164-15-689
13. Zhou Z, Gao H, Ming J, Ding Z, Lin X, Zhan R. Combined transcriptome and metabolome analysis of pitaya fruit unveiled the mechanisms underlying peel and pulp color formation. *BMC Genomics.* (2020) 21:734. doi: 10.1186/s12864-020-07133-5
14. Chen C, Zhou G, Chen J, Liu X, Lu X, Chen H, et al. Integrated metabolome and transcriptome analysis unveils novel pathway involved in the formation of yellow peel in cucumber. *Int J Mol Sci.* (2021) 22:1494. doi: 10.3390/ijms22031494
15. Dong T, Han R, Yu J, Zhu M, Zhang Y, Gong Y, et al. Anthocyanins accumulation and molecular analysis of correlated genes by metabolome and transcriptome in green and purple asparaguses (*Asparagus officinalis*, L.). *Food Chem.* (2019) 271:18–28. doi: 10.1016/j.foodchem.2018.07.120
16. Liu Y, Lv J, Liu Z, Wang J, Yang B, Chen W, et al. Integrative analysis of metabolome and transcriptome reveals the mechanism of color formation in pepper fruit (*Capsicum annuum* L.). *Food Chem.* (2020) 306:125629. doi: 10.1016/j.foodchem.2019.125629

17. Cho K, Cho KS, Sohn HB, Ha IJ, Hong SY, Lee H, et al. Network analysis of the metabolome and transcriptome reveals novel regulation of potato pigmentation. *J Exp Bot.* (2016) 67:1519–33. doi: 10.1093/jxb/erv549
18. Ding Z, Fu L, Tie W, Yan Y, Wu C, Dai J, et al. Highly dynamic, coordinated, and stage-specific profiles are revealed by a multi-omics integrative analysis during tuberous root development in cassava. *J Exp Bot.* (2020) 71:7003–17. doi: 10.1093/jxb/eraa369
19. Ding Z, Fu L, Tie W, Yan Y, Wu C, Hu W, et al. Extensive post-transcriptional regulation revealed by transcriptomic and proteomic integrative analysis in cassava under drought. *J Agric Food Chem.* (2019) 67:3521–34. doi: 10.1021/acs.jafc.9b00014
20. Li Y, Pan YH, Sun CB, Dong HT, Luo XL, Wang ZQ, et al. An ordered EST catalogue and gene expression profiles of cassava (*Manihot esculenta*) at key growth stages. *Plant Mol Biol.* (2010) 74:573–90. doi: 10.1007/s11103-010-9698-0
21. Chen W, Gong L, Guo Z, Wang W, Zhang H, Liu X, et al. A novel integrated method for large-scale detection, identification, and quantification of widely targeted metabolites: application in the study of rice metabolomics. *Mol Plant.* (2013) 6:1769–80. doi: 10.1093/mp/sst080
22. Ding Z, Zhang Y, Xiao Y, Liu F, Wang M, Zhu X, et al. Transcriptome response of cassava leaves under natural shade. *Sci Rep.* (2016) 6:31673. doi: 10.1038/srep31673
23. Fu L, Ding Z, Han B, Hu W, Li Y, Zhang J. Physiological investigation and transcriptome analysis of polyethylene glycol (PEG)-induced dehydration stress in cassava. *Int J Mol Sci.* (2016) 17:283. doi: 10.3390/ijms17030283
24. Pertea M, Kim D, Pertea GM, Leek JT, Salzberg SL. Transcript-level expression analysis of RNA-SEQ experiments with HISAT, stringtie and ballgown. *Nat Protoc.* (2016) 11:1650–67. doi: 10.1038/nprot.2016.095
25. Love MI, Huber W, Anders S. Moderated estimation of fold change and dispersion for RNA-SEQ data with DESeq2. *Genome Biol.* (2014) 15:550. doi: 10.1186/s13059-014-0550-8
26. Langfelder P, Horvath S. WGCNA: an R package for weighted correlation network analysis. *BMC Bioinformatics.* (2008) 9:559. doi: 10.1186/1471-2105-9-559
27. Thimm O, Blasing O, Gibon Y, Nagel A, Meyer S, Kruger P, et al. MAPMAN: a user-driven tool to display genomics data sets onto diagrams of metabolic pathways and other biological processes. *Plant J.* (2004) 37:914–39. doi: 10.1111/j.1365-313x.2004.02016.x
28. Su G, Morris JH, Demchak B, Bader GD. Biological network exploration with cytoscape 3. *Curr Protoc Bioinformatics.* (2014) 47:8.13.11–24. doi: 10.1002/0471250953.bi0813s47
29. Amato A, Cavallini E, Walker AR, Pezzotti M, Bliek M, Quattrocchio F, et al. The MYB5-driven MBW complex recruits a wrky factor to enhance the expression of targets involved in vacuolar hyper-acidification and trafficking in grapevine. *Plant J.* (2019) 99:1220–41. doi: 10.1111/tpj.14419
30. Geng P, Zhang S, Liu J, Zhao C, Wu J, Cao Y, et al. MYB20, MYB42, MYB43, and MYB85 regulate phenylalanine and lignin biosynthesis during secondary cell wall formation. *Plant Physiol.* (2020) 182:1272–83. doi: 10.1104/pp.19.01070
31. Zhao H, Wu C, Yan Y, Tie W, Ding Z, Liu G, et al. Genomic analysis of the core components of ABA signaling reveals their possible role in abiotic stress response in cassava. *Environ Exp Bot.* (2019) 167:103855. doi: 10.1016/j.envexpbot.2019.103855
32. Zenda T, Liu S, Dong A, Li J, Wang Y, Liu X, et al. Omics-facilitated crop improvement for climate resilience and superior nutritive value. *Front Plant Sci.* (2021) 12:774994. doi: 10.3389/fpls.2021.774994
33. Li S, Yu X, Cheng Z, Zeng C, Li W, Zhang L, et al. Large-scale analysis of the cassava transcriptome reveals the impact of cold stress on alternative splicing. *J Exp Bot.* (2020) 71:422–34. doi: 10.1093/jxb/erz444
34. Yuan YW, Rebocho AB, Sagawa JM, Stanley LE, Bradshaw HD Jr. Competition between anthocyanin and flavonol biosynthesis produces spatial pattern variation of floral pigments between *Mimulus* species. *Proc Natl Acad Sci USA.* (2016) 113:2448–53. doi: 10.1073/pnas.1515294113
35. Bang H, Kim S, Leskovar D, King S. Development of a codominant CAPS marker for allelic selection between canary yellow and red watermelon based on SNP in lycopene β-cyclase (LCYB) gene. *Mol Breed.* (2007) 20:63–72. doi: 10.1007/s11032-006-9076-4
36. Jian Y, Zhang C, Wang Y, Li Z, Chen J, Zhou W, et al. Characterization of the role of the neoxanthin synthase gene BoaNXS in carotenoid biosynthesis in Chinese Kale. *Genes.* (2021) 12:1122. doi: 10.3390/genes12081122
37. Zhang Q, Wang L, Liu Z, Zhao Z, Zhao J, Wang Z, et al. Transcriptome and metabolome profiling unveil the mechanisms of *Ziziphus jujuba* Mill. peel coloration. *Food Chem.* (2020) 312:125903. doi: 10.1016/j.foodchem.2019.125903
38. Shi Q, Du J, Zhu D, Li X, Li X. Metabolomic and transcriptomic analyses of anthocyanin biosynthesis mechanisms in the color mutant *Ziziphus jujuba* cv. Tailihong. *J Agric Food Chem.* (2020) 68:15186–98. doi: 10.1021/acs.jafc.0c05334
39. Li Y, Chen Q, Xie X, Cai Y, Li J, Feng Y, et al. Integrated metabolomics and transcriptomics analyses reveal the molecular mechanisms underlying the accumulation of anthocyanins and other flavonoids in cowpea pod (*Vigna unguiculata* L.). *J Agric Food Chem.* (2020) 68:9260–75. doi: 10.1021/acs.jafc.0c01851
40. Wang A, Li R, Ren L, Gao X, Zhang Y, Ma Z, et al. A comparative metabolomics study of flavonoids in sweet potato with different flesh colors (*Ipomoea batatas* (L.) Lam). *Food Chem.* (2018) 260:124–34. doi: 10.1016/j.foodchem.2018.03.125
41. Gutierrez-Quequezana L, Vuorinen AL, Kallio H, Yang B. Impact of cultivar, growth temperature and developmental stage on phenolic compounds and ascorbic acid in purple and yellow potato tubers. *Food Chem.* (2020) 326:126966. doi: 10.1016/j.foodchem.2020.126966
42. Shi J, Simal-Gandara J, Mei J, Ma W, Peng Q, Shi Y, et al. Insight into the pigmented anthocyanins and the major potential co-pigmented flavonoids in purple-coloured leaf teas. *Food Chem.* (2021) 363:130278. doi: 10.1016/j.foodchem.2021.130278
43. Yi D, Zhang H, Lai B, Liu L, Pan X, Ma Z, et al. Integrative analysis of the coloring mechanism of red longan pericarp through metabolome and transcriptome analyses. *J Agric Food Chem.* (2021) 69:1806–15. doi: 10.1021/acs.jafc.0c05023
44. Davies KM, Jibran R, Zhou Y, Albert NW, Brummell DA, Jordan BR, et al. The evolution of flavonoid biosynthesis: a bryophyte perspective. *Front Plant Sci.* (2020) 11:7. doi: 10.3389/fpls.2020.00007
45. Fu L, Ding Z, Tie W, Yan Y, Hu W, Zhang J. Large-scale RNAseq analysis reveals new insights into the key genes and regulatory networks of anthocyanin biosynthesis during development and stress in cassava. *Ind Crop Prod.* (2021) 169:113627. doi: 10.1016/j.indcrop.2021.113627
46. Zhu Z, Wang H, Wang Y, Guan S, Wang F, Tang J, et al. Characterization of the cis elements in the proximal promoter regions of the anthocyanin pathway genes reveals a common regulatory logic that governs pathway regulation. *J Exp Bot.* (2015) 66:3775–89. doi: 10.1093/jxb/erv173
47. Filyushin M, Dzhos E, Shchennikova A, Kochieva E. Dependence of pepper fruit colour on basic pigments ratio and expression pattern of carotenoid and anthocyanin biosynthesis genes. *Russ J Plant Physiol.* (2020) 67:1054–62. doi: 10.1134/s1021443720050040

Conflict of Interest: The authors declare that the research was conducted in the absence of any commercial or financial relationships that could be construed as a potential conflict of interest.

Publisher's Note: All claims expressed in this article are solely those of the authors and do not necessarily represent those of their affiliated organizations, or those of the publisher, the editors and the reviewers. Any product that may be evaluated in this article, or claim that may be made by its manufacturer, is not guaranteed or endorsed by the publisher.

frontiers | Frontiers in Nutrition

REVIEW
published: 17 May 2022
doi: 10.3389/fnut.2022.861854

Amelioratory Effect of Resistant Starch on Non-alcoholic Fatty Liver Disease *via* the Gut-Liver Axis

Weifeng Zhu[1], Ying Zhou[1], Rong Tsao[2], Huanhuan Dong[1] and Hua Zhang[1]**

[1] Department of Food Nutrition and Safety, College of Pharmacy, Jiangxi University of Traditional Chinese Medicine, Nanchang, China, [2] Guelph Research and Development Centre, Agriculture and Agri-Food Canada, Guelph, ON, Canada

Non-alcoholic fatty liver disease (NAFLD) is a hepatic manifestation of metabolic syndrome with a global prevalence. Impaired gut barrier function caused by an unhealthy diet plays a key role in disrupting the immune-metabolic homeostasis of the gut-liver axis (GLA), leading to NAFLD. Therefore, dietary interventions have been studied as feasible alternative therapeutic approaches to ameliorate NAFLD. Resistant starches (RSs) are prebiotics that reduce systemic inflammation in patients with metabolic syndrome. The present review aimed to elucidate the mechanisms of the GLA in alleviating NAFLD and provide insights into how dietary RSs counteract diet-induced inflammation in the GLA. Emerging evidence suggests that RS intake alters gut microbiota structure, enhances mucosal immune tolerance, and promotes the production of microbial metabolites such as short-chain fatty acids (SCFAs) and secondary bile acids. These metabolites directly stimulate the growth of intestinal epithelial cells and elicit GPR41/GPR43, FXR, and TGR5 signaling cascades to sustain immune-metabolic homeostasis in the GLA. The literature also revealed the dietary-immune-metabolic interplay by which RSs exert their regulatory effect on the immune-metabolic crosstalk of the GLA and the related molecular basis, suggesting that dietary intervention with RSs may be a promising alternative therapeutic strategy against diet-induced dysfunction of the GLA and, ultimately, the risk of developing NAFLD.

Keywords: resistant starch, NAFLD, gut-liver axis, gut microbiota, gut metabolites

OPEN ACCESS

Edited by:
Elena Ibañez, Institute of Food Science Research, Nutrition and Food Science Technology (CSIC), Spain

Reviewed by:
Giovanni Tarantino, University of Naples Federico II, Italy
Pietro Vajro, University of Salerno, Italy

****Correspondence:***
Huanhuan Dong
donghh@jxutcm.edu.cn
Hua Zhang
20191002@jxutcm.edu.cn;
sunnymay_z@hotamil.com

Specialty section:
This article was submitted to Nutrition and Food Science Technology, a section of the journal Frontiers in Nutrition

Received: *25 January 2022*
Accepted: *19 April 2022*
Published: *17 May 2022*

Citation:
Zhu W, Zhou Y, Tsao R, Dong H and Zhang H (2022) Amelioratory Effect of Resistant Starch on Non-alcoholic Fatty Liver Disease via the Gut-Liver Axis. Front. Nutr. 9:861854. doi: 10.3389/fnut.2022.861854

INTRODUCTION

Diets high in sugar and fats cause microbiota dysbiosis, which impairs gut immune tolerance and contributes to increased risk of metabolic disorders (1). Being the primary metabolic organ, high-fat diet (HFD)-induced impairment in the metabolic profile of the liver can promote lipogenesis and inhibit free fatty acid (FFA) oxidation, which eventually progresses to non-alcoholic fatty liver disease (NAFLD) (2). NAFLD is a hepatic manifestation of metabolic syndrome and has become one of the most common causes of liver disease worldwide (3), accounting for a considerable burden on healthcare systems (4). Intracellular fat accumulation-induced steatosis and altered metabolic homeostasis are the primary features of NAFLD (5). A high prevalence of NAFLD (33.6%) was observed in patients with inflammatory bowel disease (IBD) (6). This suggests that an integrated coordination of the gut-liver axis (GLA) exists and is important for

the maintenance of immune-metabolic homeostasis. This makes the GLA a promising therapeutic target for treating NAFLD.

As disturbances in gut integrity and dysbiosis impair the physiological function of the liver along the GLA, restoration of the microenvironment in the lower gut can be a potential and efficacious approach to ameliorating NAFLD (7), including dietary interventions aimed at maintaining gut microbiota composition, mucosal function, and barrier integrity, particularly prebiotics. Resistant starches (RSs) have been widely found in food sources rich in carbohydrates, such as corn, potato, and banana, which are often processed into a broad variety of foods (i.e., breads, cereals, pasta, snacks, and beverages). RSs are indigestible carbohydrates but fermentable for gut microbiota; thus, they are widely believed to be effective prebiotics that improve the production of short-chain fatty acids (SCFAs), which benefits the gut microbiome structure and overall human health (8). Current findings suggest that dietary supplementation with probiotics, functional oligosaccharides, and dietary fibers can help maintain gut bacterial balance and improve immune homeostasis in the gut, which is potentially beneficial for NAFLD amelioration (5, 9). However, the role and underlying mechanism of RSs in ameliorating NAFLD by enhancing gut microenvironment homeostasis remain largely unknown. This review aims to provide insights into RSs as a dietary strategy to alleviate liver disease conditions of NAFLD, with a particular focus on intestinal microecological changes from the perspective of the GLA (10).

PATHOGENESIS OF NON-ALCOHOLIC FATTY LIVER DISEASE VIA THE GUT-LIVER AXIS

The underlying mechanisms for the development and progression of NAFLD are complex. The interdependence between the gut and liver forms a close integration of their molecular and physiological functions, playing a key role in the integrated pathogenesis of NAFLD, as shown in **Figure 1** (10, 11). The excessive intake of high calories promotes the accumulation of fat in visceral and subcutaneous adipose tissues, where the amounts of FFAs and total glycerol are dramatically increased. As such, NAFLD eventually developed. Moreover, there is a clear causal link between NAFLD and dysbiosis of the gut microbiota. Patients with NAFLD tend to have increased intestinal permeability and microbiota dysbiosis (12, 13). Dysfunction and dysregulation of the intestinal barrier and dysbiosis impair mucosal immune tolerance, leading to systemic inflammation and disturbing liver immune metabolism homeostasis.

The intestinal barrier is a complex functional unit composed of lumen and mucosal components (i.e., epithelial cell layer, mucosal barrier, and innate and acquired immune components), neurointestinal, vascular, and endocrine systems, digestive enzymes, and gut microbiota (14). In addition to the epithelial layer and mucus, recent evidence has characterized the gut-vascular barrier, which prevents the translocation of bacteria directly into portal circulation (15). However, the loss of gut barrier integrity and mediated translocation of the gut microbiome evokes a toll-like receptors (TLR)-mediated pro-inflammatory cascade in the liver (16–18). In addition, pathogenic bacteria from the intestinal microbiota can interactively regulate IL-17A production from immune or non-immune cells, which plays a major role in regulating gut mucosal immunity and pathogenesis of NAFLD, and thus accelerates the progression of NAFLD, a highly related complication of atherosclerosis (19–22). Moreover, pathogenic bacterial metabolites [i.e., lipopolysaccharides (LPS) and ethanol] from the lumen to the circulation rapidly relay information to the brain and damage the periphery, mainly in the liver and adipose tissues, by altering the central neurotransmitter systems (5). The vagus nerve in the gut can be directly activated by inflammatory signals to impair insulin sensitivity and hepatic steatosis associated with liver inflammation by altering the central neurotransmitter system (23). Available research demonstrates the role of enterohepatic axis dysfunction in the development of NAFLD; the underlying mechanisms can be summarized as: (1) alterations in the gut microbiome profile and immune responses; (2) the effects of gut bacterial components and metabolites, such as LPS, endogenous ethanol (EnEth), and SCFAs; and (3) the impairment of intestinal barrier function and bile acid (BA) homeostasis (24). Owing to the inflammatory tone, metabolic homeostasis and functionality of the liver are impaired, leading to an increased risk of developing metabolic disorders, particularly NAFLD.

RESISTANT STARCH

Resistant starches are defined as the total amount of starch and starch degradation products that resist digestion in the small intestine, and are therefore recognized as a typical prebiotic (25). Naturally occurring RSs are widely found in cereal grains, seeds, heated starches, and starch-containing foods (26). Furthermore, RSs are classified into five types (RS1–RS5) according to their source and processing procedure. RS1 are starch granules that occur in some indigestible plant materials, such as whole grains; RS2 are native granular starches, such as raw potatoes, green bananas, gingko, or high-amylose maize; RS3 are retrograded amylose starch or crystallized starches, such as cooked and cooled starchy foods; RS4 are chemically modified starches produced via esterification, cross-linking, or transglycosylation; and RS5 are amylose-lipid complex, amylose, and long branch chains of amylopectin from single-helical complexes with fatty acids and fatty alcohols when the starch molecules interact with lipids (27, 28). As humans do not have the enzymes to digest RSs, gut microbes ferment RSs to benefit the host by selectively stimulating the growth of intestinal epithelial cells and probiotic strains in the lower gut, thereby improving the overall health of the host (29). The gut bacterial fermentation of prebiotics increases the concentration of SCFAs in the cecum and portal vein blood, which are eventually transported through the blood circulation to various internal organs and tissues, as shown in **Figure 2**. Simultaneously, the altered intestinal metabolomic profiles and associated bioactive metabolites may be involved

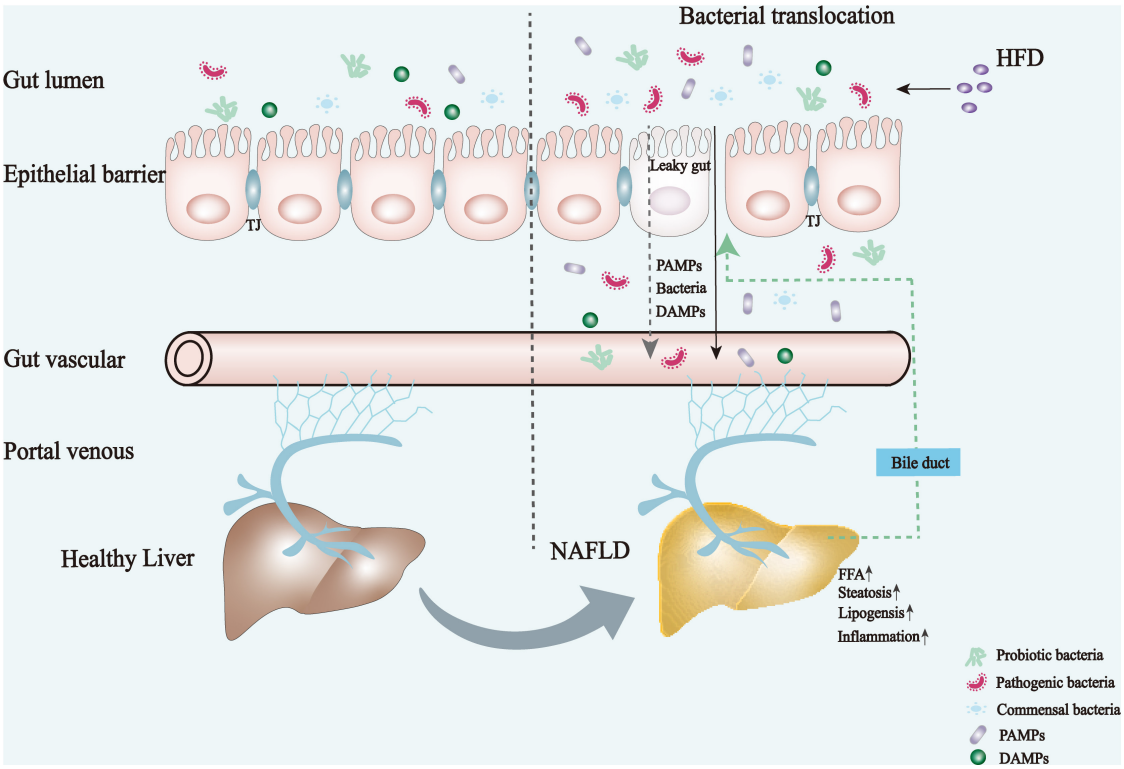

FIGURE 1 | Mechanism underlying the pathogenesis and physiological alterations of NAFLD. High-caloric diets lead to an imbalanced intestinal flora, which in turn elicits an impaired gut barrier function and increased permeability, followed by bacterial translocation and an increase of harmful metabolites or bacterial products that eventually enter the liver through the portal vein. These factors together promote the development of NAFLD by exacerbating hepatic steatosis, lipogenesis, and inflammatory responses. DAMPs, damage-associated molecular patterns; FFA, free fatty acid; HFD, high-fat diet; TJ, tight junctions; PAMPs, pathogen-associated molecular patterns.

in the regulation of signaling cascades in the GLA, exerting beneficial effects on the host (**Figure 2**). Emerging evidence from animal studies strongly demonstrates the efficacy of RSs in the prevention or treatment of various diseases [e.g., IBD, inflammatory bowel syndrome, colon cancer, obesity, type 2 diabetes mellitus (T2DM) and cardiovascular disease]; however, the data in humans remain ambiguous. The possible mechanism of RSs in ameliorating NAFLD from the perspective of the GLA is still unknown, warranting further in-depth studies.

THERAPEUTIC POTENTIAL OF RESISTANT STARCHES ON AMELIORATING NON-ALCOHOLIC FATTY LIVER DISEASE

Lifestyle interventions, such as eating a healthy diet and regular exercise, are among the most effective and safe ways to mitigate NAFLD, as well as other types of metabolic disorders. Recent evidence has highlighted the preventive and therapeutic effects of some plant foods, particularly those rich in bioactive polyphenols, carotenoids, oleic acid, n-3 polyunsaturated fatty acids, and fiber (30–32). RSs, being food components, have physiological properties similar to those of fermentable dietary fibers. It has been found that RS intake reduces fat accumulation to improve insulin sensitivity, thereby maintaining blood glucose levels and lipid metabolic homeostasis (27, 33). A human study confirmed that RSs significantly improved insulin and low-density lipoprotein cholesterol (LDL-C) levels in obese patients (34). Furthermore, supplementation of green bananas rich in RSs in NAFLD model mice was shown to improve SCFAs production and reduce hepatic steatosis by regulating the transporters involved in lipid excretion and adipogenesis (35). A previous finding illustrated that RSs exhibit the ability to lower serum cholesterol by interacting with BAs, which might be related to the increased expression of hepatic cholesterol 7α-hydroxylase (CYP7A1) and fecal BA excretion (33). Overall, RSs may be a promising dietary approach for the alleviation of NAFLD by maintaining lipid metabolic homeostasis (**Table 1**). However, the understanding of how RS intake contributes to ameliorating NAFLD remains scarce. It is necessary to explore the molecular basis of RSs sustaining the integrated gut homeostasis involved in the symbiotic microbiota, mucosal immune response, and metabolism toward prevention or mitigate NAFLD. Moreover, clinical studies are needed to investigate the regulatory effects of RS intake in patients with NAFLD.

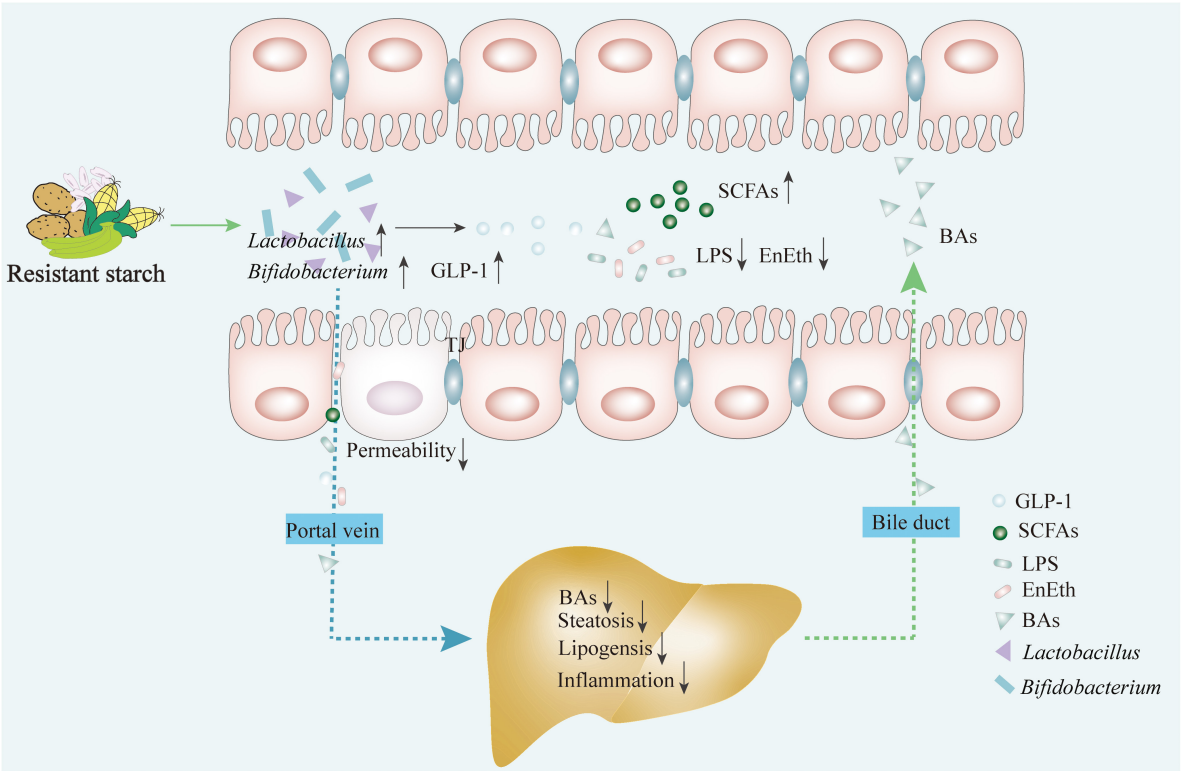

FIGURE 2 | RSs exert the effects on ameliorating NAFLD via restoring the gut microbiota structure and regulating bacterial metabolites through the link between gut and liver. Intake of RSs contributes to: (1) improving the growth of probiotics (e.g., *Lactobacillus* and *Bifidobacterium*); (2) promoting the production of metabolites (e.g., short chain fatty acids and glucagon-like peptide-1); (3) inhibiting harmful metabolites production (e.g., LPS and EnEth); and (4) maintaining the homeostasis of the BAs. This regulates the enterohepatic axis homeostasis by modulating flora metabolite and intestinal hormone productions to inhibit hepatic steatosis, lipogenesis, and inflammatory responses. BAs, bile acids; EnEth, endogenous ethanol; GLP-1, glucagon-like peptide-1; LPS, lipopolysaccharide; RS, resistant starch; SCFAs, short-chain fatty acids.

POTENTIAL MECHANISMS OF RESISTANT STARCHES ON REGULATING THE GUT-LIVER AXIS HOMEOSTASIS TOWARD NON-ALCOHOLIC FATTY LIVER DISEASE MITIGATION

The intestinal microecology, consisting of intestinal microbiota, intestinal epithelial cells, and the immune system, may play a role in energy metabolism (36). Recent human and rodent studies on obesity-related metabolic disorders have suggested that the gut microbiome plays a key role in NAFLD pathogenesis (37). The long-term consumption of diets high in calories and saturated fat may lead to dysbiosis in the gut microbiota. This, in turn, would evoke an imbalance in the BA pool and a dysfunctional intestinal barrier, followed by increased translocation of bacteria and accumulation of bacterial-derived products in the liver, which play significant roles in the development of NAFLD as summarized in **Figure 2**. RSs are an energy source for symbiotic microbiota and are fermented to release SCFAs, which in turn are beneficial for the growth of colonic cells, thus enhancing the mucosal barrier function. The regulatory effects of RSs on NAFLD mainly occur in the gut, where RSs contribute to the restoration of microbiota structure, an increase in SCFA release, and enhanced gut barrier integrity. The specific mechanisms by which RSs alleviate NAFLD by promoting overall gut health are described in the following sections.

Intake of Resistant Starches Contributes to the Modulation of the Gut Microbiota Structure

A growing body of evidence from several animal and human studies suggests a direct causal link between NAFLD and dysbiosis of gut microbiota. It has been noticed that patients suffering from NAFLD tend to have an increased intestinal permeability along with microbiota dysbiosis (12). A significantly elevated abundance of various species of gut microbiota was identified in NAFLD patients, including *Firmicutes* (i.e., *Erysipelotrichia, Lachnospiraceae,* and *Lactobacillus*) and *Bacteroidetes* (i.e., *Prevotella* and *Parabacteroides*) (38). Patients with NAFLD have a reduced population of *Bacteroidetes* and an increased proportion of *Prevotella* and *Porphyromonas spp.* compared with healthy individuals (39). In an animal model of NAFLD, decreased abundance of *Akkermansia muciniphila* was

TABLE 1 | Effect of RS on NAFLD.

	Model	Dose	Time	NAFLD-related parameters	References
Rice starch-oleic acid complex	Male Sprague-Dawley rats (non-obese) fed HFD	54.5% in HFD	8 weeks	TG↓; TC↓; HDL-C↑; SOD↑; GSH-PX↑; MDA↓; AST↓; and ALT↓	(47)
Raw potato starch	Duroc × Landrace × Large White growing barrows	230 (growing) or 280 g/kg (finishing)	100 days	Fatty acid biosynthesis↓; acid β-oxidation↑; FABP1↑; fatty acid intake ↓; fatty acid synthesis↓; fatty acid oxidation↑; and glycerophospholipid synthesis↑	(97)
High amylose maize starch	Male Wistar rats (non-obese) fed a high-fat, high-sucrose diet	2 g/day	6 weeks	Blood glucose↓; TC↓; TG↓; HDL-C↑; LDL-C↓; T-AOC↑; T-SOD↑; MDA↓; GSH-PX↑; AST↓; ALT ↓; AKP↓; SREBP-1↓; FAS↓; LXRα↓; and FABP4↓	(98)
Purple yam RS	Male golden hamsters fed HFD	0.5 g/100 g, 1.5 g/100 g	4 weeks	HDL-C↑; TG↓; TC↓; LDL-C↓; and liver fat accumulation↓	(99)
Maize RS	Male Sprague–Dawley rats fed HFD	1.2 g/day	6 weeks	Liver weight ↓; TG↓; TC↓; LDL-C↓; PPAR-γ↓; LXR↓; SREBP-c↓; FAS↓; and ACC↓	(100)
Maize RS	Female ob/ob mice fed HFD	10%, 15%, and 20% in HFD	12 weeks	Liver weight↓; lipid droplet accumulation↓; TBA↓; LPS↓; TG↓; TC↓; AST↓; ALT↓; PPAR↑; and AMPK pathways↑	(86)
Microwave–toughening treatment starch	Male C57BL/6J (B6) mice fed HFD	MTT starch in HFD	5 weeks	Liver index↓; fasting glucose↓; and fat vacuoles↓	(101)
Sorghum RS	Female Sprague–Dawley rats given Formestane for 50 mg/kg BW/d, fed with no soy feed or ordinary feed	0.9 g/kg, 1.8 g/kg, and 2.7 g/kg	6 weeks	Liver steatosis↓; FXR↓; SREBP-1↓; ACC↓; FAS↓; and SCD1↓;	(102)
Green banana (*Musa* sp.) RS	Male C57BL/6 mice fed HFD	15% RS in HFD	14 weeks	Liver steatosis↓; fasting glucose↓; HOMA-IR↓; TG↓; TC↓; p-AMPK/AMPK↑; and HMG CoA-R↓	(35)
Buckwheat RS	Male C57BL/6 mice fed HFD	33.4% RS in HFD	6 weeks	Liver index ↓; HDL-C↑; TG↓; TC↓; LDL-C↓; IL-6↓; TNF-α↓; LPS↓; SOD↑; T-AOC↑; and MDA↓	(65)
Maize RS	Male Wistar rats fed HFD	41.6% RS in HFD	9 weeks	TG↓;TC↓;NEFA↓; HOMA-IR; IRS1↓; IRS2↓; and PPARGC1α↑	(103)
High amylose starch or Esterified high amylose starch	Male Wistar rats (non-obese) fed a high-fat	2 g/day	6 weeks	TC↓; TG↓; HDL-C↑; LDL-C↓; AST↓; ALT↓; MDA↓; GSH-PX↑; T-AOC↑; T-SOD↑; ACC↓; SREBP-1↓; PPAR γ↓; and LXRα↓	(104)

ACC, acetyl CoA carboxylase; ALT, alanine aminotransferase; AMPK, adenosine 5′-monophosphate (AMP)-activated protein kinase; AST, aspartate aminotransferase; FABP, fatty acid-binding protein; FAS, fatty acid synthase; GSH-Px, glutathione peroxidase; HDL-C, high density lipoprotein cholesterol; HFD, high-fat diet; HMG-CoA, 3-hydroxy-3-methylglutaryl coenzyme A; HOMA-IR, homeostatic model assessment for insulin resistance; IL-6, interleukin-6; ISR, insulin receptor substrate; LDL-C, low density lipoprotein cholesterol; LPS, lipopolysaccharides; LXR, liver X receptors; MDA malondialdehyde; NEFA, non-esterified fatty acid; PPAR, peroxisome proliferators-activated receptors; PPARGC1α, peroxisome proliferator-activated receptor, gamma, coactivator 1 alpha; RS, resistant starch; SCD1, stearoyl-CoA desaturase-1; SOD, superoxide dismutase; SREBP, sterol regulatory element-binding protein; T-AOC, total antioxidant capacity; TBA, total bile acids; TC, total cholesterol; TG, triglyceride; TNF-α, tumor necrosis factor-α; T-SOD, total superoxide dismutase. The symbol ↑ is upregulated, and the symbol ↓ is downregulated.

observed (40). It was also found that *A. muciniphila* prevents fatty liver disease by regulating the expression of genes that regulate fat synthesis and inflammation in the liver (41). Moreover, a recent human study showed that the intake of RSs promotes the abundance of *A. muciniphila* (42). Notably, one of the most important findings is that the microbiota of patients with NAFLD is generally enriched in gram-negative bacteria, whereas gram-positive bacterial counts are reduced, implying a reduced abundance of butyric acid-producing bacteria (7). The collective findings suggest an association between the composition of the bacterial community, the abundance of distinct taxa, and NAFLD (24).

Findings from a fecal microbiota transplantation (FMT) NAFLD mouse model showed that the gut microbiota obtained from lean mice augmented the abundance of probiotic strains, inhibited systemic inflammation, and ultimately attenuated HFD-induced steatohepatitis (43). In contrast, germ-free obese mice receiving FMT developed low-grade inflammation and hepatic macrovascular steatosis (44). The results obtained from this study demonstrated that the gut microbiota has a significant effect on the development of NAFLD, potentially related to damage to the intestinal barrier to elicit systemic inflammation and exacerbate steatosis (45). The role of the gut microbiome structure in maintaining liver homeostasis is attributed to a dynamic interaction between the gastrointestinal tract and liver.

Patients suffering from NAFLD are affected by the structural disruption of intestinal microbes via the GLA. Hence, restoration of gut microbiota structure may be beneficial for the amelioration of NAFLD. Emerging evidence from rodent and minipig models has demonstrated that RS interventions have therapeutic efficacy in attenuating HFD-induced liver damage, thereby preventing NAFLD (46). The intake of a diet rich in RSs effectively restored the composition of the intestinal microbiome (**Table 2**), beneficial for gut microbial communities (47). After entering the lower gut, RSs are fermented by the intestinal microbiota to release bioactive metabolites, primarily SCFAs, which contribute to improved homeostasis of host immune metabolism (48, 49). RSs are the primary energy resources for the gut microbiota, particularly for the glycolytic bacteria in the lower gut (50). The degradation of RSs by microbiomes provides SCFAs, particularly butyrate, an energy source for colonocytes to maintain the proper structure and function of the intestinal barrier (51, 52). SCFAs can travel through the gut-brain axis, across the blood–brain barrier into the central nervous system, and affect the cellular biological mechanism of neural development, thereby resulting in various physiological processes in the liver, including gluconeogenesis, insulin sensitivity, and adenosine 5′-monophosphate activated protein kinase (AMPK) activity (53, 54). Moreover, it has been found that the SCFAs pentanoate can reduce IL-17A production in $CD4^+$ T cells by inhibiting histone deacetylase activity (55). Similarly, probiotics that synthesize SCFA, particularly acetate, are involved in reducing IL-17A in hepatic type 3 innate lymphoid cells (ILC3s) (56). It was also found that dietary intake of RS and decreased colonic IL-17A stimulate intestinal immune and endocrine responses that may alter liver health (48).

Notably, the abundance of butyric acid-producing bacteria is suppressed in NAFLD patients (24). This suggests that RS intervention has the potential to alleviate NAFLD features by promoting the growth of butyric acid-producing bacteria. A recent finding validated that supplementation with RS5 augments the abundance of butyrate-producing bacteria (*Coprococcus*, *Roseburia*, *Bifidobacterium,* and *Butyrivibrio*) in an HFD-induced rat model (47). Moreover, RSs derived from purple yam were found to increase the abundance of *Bifidobacteria, Lactobacillus*, *Coprococcus,* and *Allobaculum* while decreasing the abundance of *Parabacteroides* and *Dorea*. Among these, the alleviated abundance of probiotics, including *Bifidobacteria* and *Lactobacillus,* has been implicated in mitigating blood hyperlipidemia in an HFD-induced hamster model (57). Finally, intervention with green banana-derived RSs promoted the release of SCFAs and helped restore the gut microbiota structure by increasing the abundance of *Lactobacillus*, *Bifidobacterium*, and *Enterococcus*, while inhibiting the growth of *Escherichia coli*, which resulted in ameliorating NAFLD in an obese mouse model (35). Despite these findings, the molecular basis underlying the observed anti-NAFLD effect of RSs mediated by maintaining gut microbiota structure and released SCFA is still not well established.

In addition to maintaining the gut microbiota structure, RS intervention also contributes to enhanced gut barrier function and regulation of BA metabolic homeostasis, as well as the reduction of harmful metabolites produced by intestinal pathogens (58, 59). RSs were found to bind to BAs with high affinity, resulting in suppressed BA reabsorption in the colon and lowered intestinal cholesterol absorption (60). Furthermore, symbiotic bacteria can exploit RS fermentation to produce bacterial metabolites that prevent colonic mucin depletion, thus maintaining healthy mucosa (25, 61). Mucin, in turn, promotes host-microbe symbiosis and enhances gut barrier integrity. Taken together, RS supplementation potentially regulates the release of various metabolites by symbiotic bacteria, including bioactive peptides, BAs, and EnEth, which are beneficial to the host as vital modulators of immunometabolism (62–66). This further indicated that dietary RSs can alleviate NAFLD through the GLA.

Regulatory Activity of Metabolites Derived From the Gut Microbiota Fermentation of Resistant Starches in the Gut-Liver Axis Toward Alleviating Liver Damage in Non-alcoholic Fatty Liver Disease

Regulatory Role of Short-Chain Fatty Acids Upregulated by the Intake of Resistant Starches

The intestinal barrier protects the host against bacterial invasion while harboring commensal bacterial colonization in the lower gut. Hence, a functionally intact intestinal barrier plays a vital role in sustaining overall host health. The metabolites released by the fermentation of commensal bacteria mainly contain a variety of FFA SCFAs (i.e., acetate, propionate, and butyrate), an energy source for intestinal epithelial cells and, more importantly, key molecules involved in regulating chemo-sensing activities and subsequent cell signaling cascades in the

TABLE 2 | Intake of resistant starch (RS)-induced alterations of gut microbiota structure.

RS type	Model	Bacterial flora changes	References
Rice starch-oleic acid complex	HFD-induced male Sprague–Dawley rats (non-obese)	*Bacteroidetes*↓; *Firmicutes*↑; *Bifidobacterium*↑; *Lactobacillus*↓; *Coprococcus*↑; *Roseburia*↑; *Bifidobacterium*↑; and *Butyrivibrio*↑	(47)
Purple yam RS	HFD-induced male golden hamsters	*Veillonella*↑; *Lactobacillus*↑; *Coprococcus*↑; *Allobaculum*↑; *Parabacteroides*↓; and *Dorea*↓	(99)
Maize RS	HFD-induced female ob/ob mice	*Bifidobacteriales*↑ and *Prevotellaceae*↓	(86)
Buckwheat RS	HFD-induced male C57BL/6 mice	*Lactobacillus*↑; *Bifidobacterium*↑; *Enterococcus*↑; and *Escherichia coli*↓	(65)

intestinal mucosal layer, thereby sustaining gut homeostasis (67). Numerous studies have established that SCFAs are involved in regulating immune-metabolic homeostasis by activating metabolite-sensing G-protein coupled receptors (GPCRs) (67, 68). A recent study demonstrated that GPR41 and GPR43 regulate molecular events associated with inflammation, gut homeostasis, and metabolic alterations (69). Moreover, GPR43 activation has the potential to improve hepatic steatosis associated with high-fat obesity (70). Both GPR41 and GPR43 can be activated by acetate, butyrate, and propionate to regulate molecular events associated with inflammation, gut homeostasis, and metabolic alterations (69). In the liver, SCFAs stimulate GPR41 and GPR43 to activate AMPK in a peroxisome proliferator-activated receptor (PPAR)-γ-dependent manner, leading to regulation of hepatic glycolipid homeostasis via increased hepatic lipid oxidation (71). SCFA-induced serotonin release from enterochromaffin cells can influence gastrointestinal motility (72, 73). SCFAs might directly influence the brain by crossing the blood-brain barrier, reinforcing blood-brain barrier integrity, modulating neurotransmission, increasing anorexigenic neuropeptide expression, and enhancing satiety (74, 75). RS in mice markedly increases gut microbiome-derived tryptophan, a precursor of serotonin that can cross the blood–brain barrier and increase the production of cerebral serotonin; this means that the more RS intake in the diet, the more satiety can be enhanced by promoting SCFAs production while reducing caloric intake. Altogether, intake of RSs can lead to increased SCFAs by promoting mucus secretion, enhancing intestinal epithelial tight junctions (TJs), preventing dysbiosis of the intestinal microbiota, preventing endotoxins, and reducing caloric intake, inflammation, and oxidative stress in the liver, thereby lowering the risk of developing NAFLD.

Resistant Starches Exerting Modulatory Effects on Bile Acid Metabolism and Signaling

There is increasing evidence that a high correlation exists between BAs and SCFAs, and that their cross-talk involves the regulation of the interactive physiological status between the liver and the intestine (76). BAs may exist as primary BAs [i.e., chenodeoxycholic acid (CDA) or cholic acid (CA)] produced as glycine or taurine conjugates in the liver, and secondary BAs synthesized by the gut microbiota [i.e., deoxycholic acid (DCA) or lithocholic acid (LCA)] (76). Most gram-positive gut bacteria (i.e., *Clostridium*, *Enterococcus*, *Bifidobacterium*, and *Lactobacillus*) with bile salt hydrolase activity can produce secondary BAs (77). As previously mentioned, RS intake increases the excretion rate of primary BAs, leading to lowered blood LDL and total cholesterol levels. Meanwhile, RSs were found to contribute to the enhanced release of secondary BAs because of the increased abundance of *Lactobacillus* and *Bifidobacterium* (35). However, at high physiological concentrations, secondary BAs negatively affect the gut by augmenting oxidative stress and stimulating apoptosis and mutations, resulting in an increased risk of developing colon cancer (76, 78, 79). In contrast, a moderate level of secondary BAs inhibits colonic inflammation by downregulating pro-inflammatory cytokines (80). Reduced levels of secondary BAs and their production *Ruminococcaceae* have been detected in ulcer colitis (UC) patients, and supplementation with secondary BAs has been shown to ameliorate disease status in a TGR5 dependent manner (66, 79). It is worth noting that TGR5 activation significantly suppressed the TLR4/NF-κB pathway against inflammatory damage in the liver (81). Below toxic concentrations, a higher proportion of secondary BAs may inhibit the adipogenesis pathway and enhance bile flow in the liver, which is beneficial for preventing NAFLD (82). A recent study revealed that RSs derived from green bananas contributed to the increased abundance of *Ruminococcaceae* (83). This suggests a complex and integrated link between the gut microbiota and their metabolites, which collaboratively govern the host immune-metabolic responses along the GLA and related physiological alterations by the actions of GPCRs such as TGR5 or FXR. In this case, the RS-induced bacterial metabolites in the lower gut played a key role in regulating immune metabolism homeostasis via integrated cellular, molecular targets and mediated pathways along the GLA, eventually improving liver physiological functionality.

Resistant Starches Modulating the Molecular Events Involved in Immune-Metabolic Homeostasis in the Liver

The symbiotic relationship and communication between the host and gut microbiota are believed to occur via exchange of signals of bacteria-produced metabolites and molecular biomarkers synthesized by the host. The intake of RSs may have therapeutic efficacy in maintaining liver function by providing beneficial metabolites produced from colonic fermentation. More specifically, RS supplementation was shown to significantly promote the release of fecal butyrate, which has anti-inflammatory properties in the intestinal epithelium

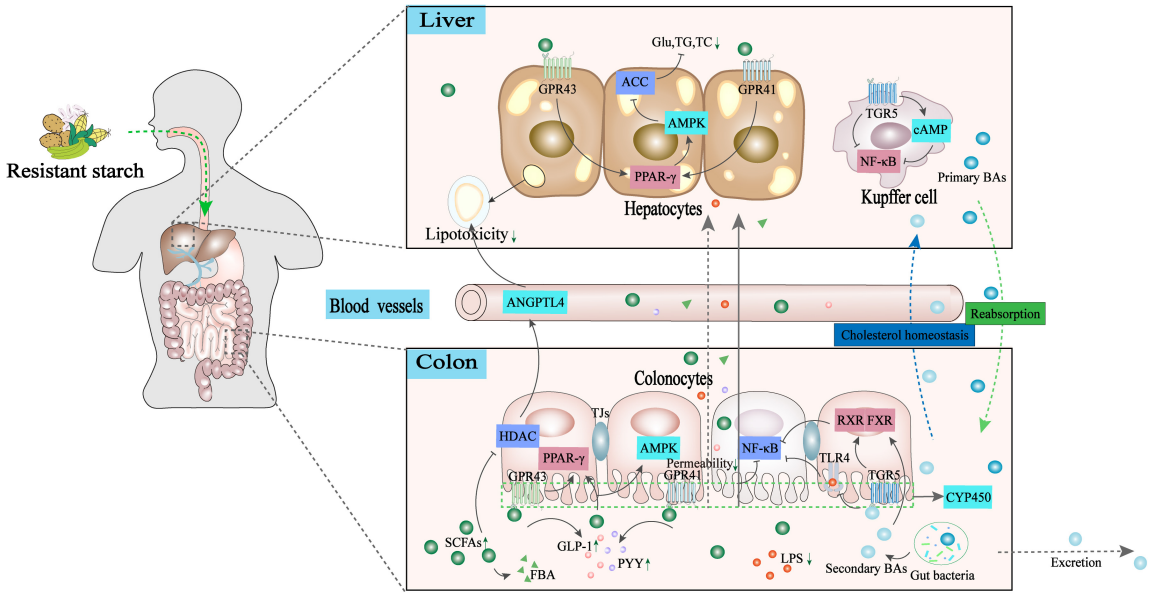

FIGURE 3 | Potential mechanisms underlying RSs regulating the GLA immune-metabolic homeostasis toward NAFLD mitigation. The gut bacterial metabolites released after intake of RSs act as crucial molecules that interact with a broad range of sensing receptors along with the GLA. (1). Secondary BAs bind to TGR5/FXR receptors in the intestine, inhibiting the TLR4/NF-κB inflammatory signaling pathway to ameliorate NAFLD. (2). SCFAs binding with GPR41/GPR43 receptors in the intestine and hepatic activates PPAR-γ/AMPK signaling pathway to inhibit acetyl CoA carboxylase. As such, the production of glucose triglyceride and total cholesterol production is inhibited. (3). SCFAs can enhance the release of pro-peptide YY (PYY)/glucagon-like peptide 1 (GLP-1) by ligand binding with GPR43, which contributes to regulating appetite to maintain energy homeostasis. (4). SCFAs act as a histone deacetylase inhibitor to strengthen intestinal barrier functions, or elevate angiopoietin-like 4 secretions to reduce lipotoxicity and inflammation by potentially activating PPAR-γ. ACC, acetyl-CoA carboxylase; AMPK, adenosine 5′-monophosphate (AMP)-activated protein kinase; ANGPTL4, recombinant human angiopoietin-like protein 4; BAs, bile acids; CAT, catalase; FBA, N-(1-carbamoyl-2-phenyl-ethyl) butyramide; FXR, farnesoid X receptor; GPCR, G protein-coupled receptors; GLP-1, glucagon-like peptide 1; GPR43, G protein-coupled receptor 43; HDAC, histone deacetylase; NF-κB, nuclear factor kappa-B; PGC1α, peroxisome proliferator-activated receptor-γ coactivator-1α; PPAR-γ, peroxisome proliferator activated receptor-γ; SCFAs, short-chain fatty acids; SOD, superoxide dismutase; TC, total cholesterol; TG, triglyceride; TLR4, toll-like receptor 4; PYY, pro-peptide YY.

to maintain mucosal immune tolerance and enhance intestinal barrier functions by acting as a histone deacetylase (HDAC) inhibitor or signal molecule targeting GPCRs (58). It has been demonstrated that the uptake of butyrate and its synthetic derivative, N-(1-carbamoyl-2-phenyl-ethyl) butyramide (FBA), in the liver can enhance fatty acid oxidation by activating AMPK-acetyl-CoA carboxylase against fatty liver (84). In addition, butyrate exerts protective effects by activating the GPR43/β-arrestin-2/NF-κB network against LPS-induced liver injury in a mouse model (85).

Furthermore, RS intake plays a key role in maintaining BA homeostasis. A recent finding highlighted that consumption of maize RSs increased the biosynthesis of secondary BAs that enhanced cholesterol homeostasis, resulting in the mitigation of the metabolic syndrome of obesity in a dose-dependent manner (86). However, the underlying mechanism needs to be further elucidated. Unconjugated or secondary BAs can bind to a variety of receptors, including FXR, pregnane X receptor (PXR), and TGR5, to initiate signal transduction involved in regulating CYP450 enzymes, suggesting a regulatory role for BAs in host xenobiotic metabolism (87). These findings suggest that a feedback loop exists between secondary BAs and the gut microbiota structure, which is implicated in the modulation of host immune responses, energy, and xenobiotic metabolism. This ultimately results in the regulation of liver metabolic homeostasis, suggesting that dietary RSs can be a potential therapeutic strategy for NAFLD.

Resistant Starches Exerting Modulatory Effects on Endogenous Ethanol

Previous studies have shown that RSs have a positive effect on intestinal flora dysbiosis and a significant inhibitory effect on the EnEth content; the latter is higher in patients with NAFLD than in healthy individuals (43). The gut microbiomes from NAFLD patients are enriched in *E. coli*, which produces a high level of EnEth (88). A recent study indicated that EnEth can upregulate the expression of inflammatory cytokines and thus increase intestinal permeability to compromise intestinal barrier function (11). In addition, EnEth impedes the tricarboxylic acid cycle, which promotes fatty acid synthesis and exacerbates hepatic steatosis (5). Previous studies have shown that RSs have a significant modulatory effect in preventing dysbiosis by inhibiting the growth of intestinal pathogens such as *E. coli* (64, 65). Taken together, RSs may inhibit EnEth production by restoring the dysbiotic gut microbiome, thereby preventing hepatic steatosis. However, studies on the molecular basis and functional implications of EnEth in the GLA are limited. Therefore, it would be worthwhile to study this in the future.

Intake of Resistant Starches Modulates Energy Homeostasis and Related Hormone Signaling

Resistant starch supplementation has been clinically proven to effectively modulate metabolic endotoxemia, insulin resistance, and oxidative stress in patients with T2DM, implying a strong therapeutic potential of RSs (89). As the intake of RSs can improve the production of SCFAs from gut bacterial fermentation, SCFAs, key colonic metabolites of RSs, act as signaling molecules to regulate appetite and maintain glucose metabolic homeostasis by upregulating proglucagon and pro-peptide YY (PYY) gene expression, increasing the levels of plasma glucagon-like peptide (GLP)-1 and PYY, two gut secreted hormones (90). GLP-1 is an anorexigenic intestinal hormone secreted by the intestinal endocrine cells that primarily controls nutrient and food intake. RS supplementation also induces the secretion of GLP-1 and PYY to inhibit body fat accumulation in mice (91). The molecular basis of the RSs triggering GLP-1 secretion depends on the interactions of SCFAs with GPR43, similar to that of the FFA receptor (FFAR)-2 through ligand binding (63). Findings from a FFAR2$^{-/-}$ mouse study demonstrated that colonic fermentation of inulin increases the secretion of GLP-1 and PYY in an FFAR2-dependent manner (92). Moreover, a GLP-1 agonist was shown to restore insulin sensitivity and reduce hepatic TC, TG, and LDL-C levels, suggesting the anti-obesity potential of GLP-1 (10, 93). As previously mentioned, SCFAs, particularly propionate, can stimulate intestinal enteroendocrine cells to release PYY, which is involved in the modulation of electrolytes and water absorption in both epithelial and neuronal cells (94, 95). The above findings suggest that FFA receptors play a crucial role in sensing the release of SCFAs from colonic fermentation of RSs to regulate the secretion of the intestinal hormones GLP-1 and PYY. The release of GLP-1 and PYY in turn inhibits appetite and food intake to prevent obesity. This finding implies a possible regulatory effect of RSs consumption on glucose homeostasis. Nonetheless, the molecular basis underlying RS intake regulation of gut hormone secretion and subsequent metabolic outcomes is not fully understood; therefore, further investigations are warranted.

CONCLUSION AND PERSPECTIVES

Non-alcoholic fatty liver disease imposes a substantial economic burden on developing or developed countries worldwide. The high prevalence of NAFLD and less effective pharmaceutical treatments have led to new and alternative therapeutic approaches for NAFLD based on multiple factors, including dietary impact, gut microbiota structure, hormone secretion, and intestinal and systemic immune responses (96). The mechanism underlying the development of impaired liver function depends on the host-microbe-metabolic interplay along the GLA, a critical basis for rationalizing the use of dietary supplementation as a therapeutic strategy. A review of recent literature shows that dietary RSs, as prebiotics, contribute to the restoration of a healthy gut microbiota structure, beneficial for maintaining gut barrier integrity and mucosal immune tolerance. This eventually leads to the prevention of pathogenic invasion and endotoxemia-mediated metabolic syndrome. Moreover, gut bacterial metabolites released after RS intake promote the growth of intestinal epithelial cells and act as key molecules that interact with a broad range of sensing receptors along the GLA, including GPR41, GPR43, FXR, PXR, and TGR5. Upon ligand binding, SCFAs and secondary BA elicit a series of signaling cascades in the intestine and liver to sustain immune metabolic homeostasis (**Figure 3**). These findings strengthen our understanding of how interactions between the gut microbiota and host regulate immune-metabolic crosstalk in the GLA at the molecular level. This provides insights into the dietary-immune-metabolic interplay by which the gut microbiome profiles and immune-metabolic homeostasis are well maintained. However, existing studies on the health-promoting effects of RSs on NAFLD are still scarce; thus, the differences among various types of RSs in NAFLD prevention are unclear. In addition, a variety of microbiota-derived metabolites may permeate the blood–brain barrier and enter the central nervous system; however, their implication in the pathogenesis of NAFLD is still unknown. Future research on the role of RSs in NAFLD should focus on the following: (1) elucidating the effect of different types of RSs and the roles of their distinct metabolite profiles after colonic fermentation; (2) analyzing the effect of the particular metabolic profile of different RSs on microbiota composition at the species level; and (3) understanding the relationship between specific RSs and typical gut microbial strains and how they modulate factors associated with NAFLD.

AUTHOR CONTRIBUTIONS

WZ: conceptualization and writing the review. YZ: data collection and original draft of the manuscript. RT: writing the review and editing. HD: writing and funding acquisition. HZ: project administration, manuscript revising and editing, and funding acquisition. All authors contributed to the article and approved the submitted version.

FUNDING

This research was supported by the National Key R&D Program Key Special Project, China (Grant no. 2019YFC1604905), Jiangxi Provincial Thousand Talents Plan Project (Grant no. jxsq2019101023), and Natural Science Foundation of Jiangxi Province (Grant No. 20202BABL205011).

REFERENCES

1. Zmora N, Bashiardes S, Levy M, Elinav E. The role of the immune system in metabolic health and disease. *Cell Metab.* (2017) 25:506–21. doi: 10.1016/j.cmet.2017.02.006
2. Mu W, Cheng X-F, Liu Y, Lv Q-Z, Liu G-l, Zhang J-G, et al. Potential nexus of non-alcoholic fatty liver disease and type 2 diabetes mellitus: insulin resistance between hepatic and peripheral tissues. *Front Pharmacol.* (2019) 9:1566. doi: 10.3389/fphar.2018.01566
3. Younossi ZM, Koenig AB, Abdelatif D, Fazel Y, Henry L, Wymer M. Global epidemiology of nonalcoholic fatty liver disease—meta-analytic assessment of prevalence, incidence, and outcomes. *Hepatology.* (2016) 64:73–84. doi: 10.1002/hep.28431
4. Younossi Z, Anstee QM, Marietti M, Hardy T, Henry L, Eslam M, et al. Global burden of NAFLD and NASH: trends, predictions, risk factors and prevention. *Nat Rev Gastroenterol Hepatol.* (2018) 15:11–20. doi: 10.1038/nrgastro.2017.109
5. Wang Z, Zeng M, Wang Z, Qin F, Chen J, He Z. Dietary polyphenols to combat nonalcoholic fatty liver disease via the gut–brain–liver axis: a review of possible mechanisms. *J Agric Food Chem.* (2021) 69:3585–600. doi: 10.1021/acs.jafc.1c00751
6. Sartini A, Gitto S, Bianchini M, Verga MC, Di Girolamo M, Bertani A, et al. Non-alcoholic fatty liver disease phenotypes in patients with inflammatory bowel disease. *Cell Death Dis.* (2018) 9:87. doi: 10.1038/s41419-017-0124-2
7. Chopyk DM, Grakoui A. Contribution of the intestinal microbiome and gut barrier to hepatic disorders. *Gastroenterology.* (2020) 159:849–63. doi: 10.1053/j.gastro.2020.04.077
8. DeMartino P, Cockburn DW. Resistant starch: impact on the gut microbiome and health. *Curr Opin Biotechnol.* (2020) 61:66–71. doi: 10.1016/j.copbio.2019.10.008
9. Wang Z, Zhong J, Meng X, Gao J, Sun J, Li X, et al. The gut microbiome-immune axis as a target for nutrition-mediated modulation of food allergy. *Trends Food Sci Technol.* (2021) 114:116–32. doi: 10.1016/j.tifs.2021.05.021
10. Bauer PV, Hamr SC, Duca FA. Regulation of energy balance by a gut–brain axis and involvement of the gut microbiota. *Cell Mol Life Sci.* (2016) 73:737–55. doi: 10.1007/s00018-015-2083-z
11. Ji Y, Yin Y, Sun L, Zhang W. The molecular and mechanistic insights based on gut-liver axis: nutritional target for Non-Alcoholic Fatty Liver Disease (NAFLD) improvement. *Int J Mol Sci.* (2020) 21:3066. doi: 10.3390/ijms21093066
12. Belei O, Olariu L, Dobrescu A, Marcovici T, Marginean O. The relationship between non-alcoholic fatty liver disease and small intestinal bacterial overgrowth among overweight and obese children and adolescents. *J Pediatr Endocrinol Metab.* (2017) 30:1161–8. doi: 10.1515/jpem-2017-0252
13. Henao-Mejia J, Elinav E, Jin C, Hao L, Mehal WZ, Strowig T, et al. Inflammasome-mediated dysbiosis regulates progression of NAFLD and obesity. *Nature.* (2012) 482:179–85. doi: 10.1038/nature10809
14. Paolella G, Mandato C, Pierri L, Poeta M, Di Stasi M, Vajro P. Gut-liver axis and probiotics: their role in non-alcoholic fatty liver disease. *World J Gastroenterol.* (2014) 20:15518–31. doi: 10.3748/wjg.v20.i42.15518
15. Spadoni I, Zagato E, Bertocchi A, Paolinelli R, Hot E, Di Sabatino A, et al. A gut-vascular barrier controls the systemic dissemination of bacteria. *Science.* (2015) 350:830–4. doi: 10.1126/science.aad0135
16. Miele L, Marrone G, Lauritano C, Cefalo C, Gasbarrini A, Day C, et al. Gut-liver axis and microbiota in NAFLD: insight pathophysiology for novel therapeutic target. *Curr Pharm Design.* (2013) 19:5314–24. doi: 10.2174/13816128130307
17. Kawada M, Arihiro A, Mizoguchi E. Insights from advances in research of chemically induced experimental models of human inflammatory bowel disease. *World J Gastroenterol.* (2007) 13:5581. doi: 10.3748/wjg.v13.i42.5581
18. Torres DM, Harrison SA. Diagnosis and therapy of nonalcoholic steatohepatitis. *Gastroenterology.* (2008) 134:1682–98. doi: 10.1053/j.gastro.2008.02.077
19. Tarantino G, Costantini S, Finelli C, Capone F, Guerriero E, La Sala N, et al. Is serum Interleukin-17 associated with early atherosclerosis in obese patients?. *J Transl Med.* (2014) 12:214. doi: 10.1186/s12967-014-0214-1
20. Douzandeh-Mobarrez B, Kariminik A. Gut microbiota and IL-17A: physiological and pathological responses. *Probiotics Antimicrob Proteins.* (2019) 11:1–10. doi: 10.1007/s12602-017-9329-z
21. Mao J-W, Tang H-Y, Zhao T, Tan X-Y, Bi J, Wang B-Y, et al. Intestinal mucosal barrier dysfunction participates in the progress of nonalcoholic fatty liver disease. *Int J Clin Exp Pathol.* (2015) 8:3648.
22. Harley IT, Stankiewicz TE, Giles DA, Softic S, Flick LM, Cappelletti M, et al. IL-17 signaling accelerates the progression of nonalcoholic fatty liver disease in mice. *Hepatology.* (2014) 59:1830–9. doi: 10.1002/hep.26746
23. Mighiu PI, Filippi BM, Lam TK. Linking inflammation to the brain-liver axis. *Diabetes.* (2012) 61:1350–2. doi: 10.2337/db12-0330
24. Kolodziejczyk AA, Zheng D, Shibolet O, Elinav E. The role of the microbiome in NAFLD and NASH. *EMBO Mol Med.* (2019) 11:e9302. doi: 10.15252/emmm.201809302
25. Zaman SA, Sarbini SR. The potential of resistant starch as a prebiotic. *Crit Rev Biotechnol.* (2016) 36:578–84.
26. Homayouni A, Amini A, Keshtiban AK, Mortazavian AM, Esazadeh K, Pourmoradian S. Resistant starch in food industry: a changing outlook for consumer and producer. *Starch.* (2014) 66:102–14. doi: 10.1002/star.201300110
27. Zhang L, Li HT, Li S, Fang QC, Qian LL, Jia WP. Effect of dietary resistant starch on prevention and treatment of obesity-related diseases and its possible mechanisms. *Biomed Environ Sci.* (2015) 28:291–7. doi: 10.3967/bes2015.040
28. Snelson M, Kellow NJ, Coughlan MT. Modulation of the gut microbiota by resistant starch as a treatment of chronic kidney diseases: evidence of efficacy and mechanistic insights. *Adv Nutr.* (2019) 10:303–20. doi: 10.1093/advances/nmy068
29. Maier TV, Lucio M, Lee LH, VerBerkmoes NC, Brislawn CJ, Bernhardt J, et al. Impact of dietary resistant starch on the human gut microbiome, metaproteome, and metabolome. *mBio.* (2017) 8:e01343–17. doi: 10.1128/mBio.01343-17
30. Fan JG, Cao HX. Role of diet and nutritional management in non-alcoholic fatty liver disease. *J Gastroenterol Hepatol.* (2013) 28:81–7. doi: 10.1111/jgh.12244
31. Romero-Gómez M, Zelber-Sagi S, Trenell M. Treatment of NAFLD with diet, physical activity and exercise. *J Hepatol.* (2017) 67:829–46. doi: 10.1016/j.jhep.2017.05.016
32. Zelber-Sagi S, Salomone F, Mlynarsky L. The Mediterranean dietary pattern as the diet of choice for non-alcoholic fatty liver disease: evidence and plausible mechanisms. *Liver Int.* (2017) 37:936–49. doi: 10.1111/liv.13435
33. Han K-H, Iijuka M, Shimada K-I, Sekikawa M, Kuramochi K, Ohba K, et al. Adzuki resistant starch lowered serum cholesterol and hepatic 3-hydroxy-3-methylglutaryl-CoA mRNA levels and increased hepatic LDL-receptor and cholesterol 7α-hydroxylase mRNA levels in rats fed a cholesterol diet. *Br J Nutr.* (2005) 94:902–8. doi: 10.1079/bjn20051598
34. Eshghi F, Bakhshimoghaddam F, Rasmi Y, Alizadeh M. Effects of resistant starch supplementation on glucose metabolism, lipid profile, lipid peroxidation marker, and oxidative stress in overweight and obese adults: randomized, double-blind, crossover trial. *Clin Nutr Res.* (2019) 8:318–28. doi: 10.7762/cnr.2019.8.4.318
35. Rosado CP, Rosa VHC, Martins BC, Soares AC, Santos IB, Monteiro EB, et al. Resistant starch from green banana (Musa sp.) attenuates non-alcoholic fat liver accumulation and increases short-chain fatty acids production in high-fat diet-induced obesity in mice. *Int J Biol Macromol.* (2020) 145:1066–72. doi: 10.1016/j.ijbiomac.2019.09.199
36. Lin S, Wang Z, Lam K-L, Zeng S, Tan BK, Hu J. Role of intestinal microecology in the regulation of energy metabolism by dietary polyphenols and their metabolites. *Food Nutr Res.* (2019) 63. doi: 10.29219/fnr.v63.1518
37. Boursier J, Rawls JF, Diehl AM. Obese humans with nonalcoholic fatty liver disease display alterations in fecal microbiota and volatile organic compounds. *Clin Gastroenterol Hepatol.* (2013) 11:876–8. doi: 10.1016/j.cgh.2013.04.016
38. Bashiardes S, Shapiro H, Rozin S, Shibolet O, Elinav E. Non-alcoholic fatty liver and the gut microbiota. *Mol Metab.* (2016) 5:782–94. doi: 10.1016/j.molmet.2016.06.003

39. McCullough AJ. The clinical features, diagnosis and natural history of nonalcoholic fatty liver disease. *Clin Liver Dis.* (2004) 8:521–33. doi: 10.1016/j.cld.2004.04.004
40. Moreira GV, Azevedo FF, Ribeiro LM, Santos A, Guadagnini D, Gama P, et al. Liraglutide modulates gut microbiota and reduces NAFLD in obese mice. *J Nutr Biochem.* (2018) 62:143–54. doi: 10.1016/j.jnutbio.2018.07.009
41. Warman DJ, Jia H, Kato H. The potential roles of probiotics, resistant starch, and resistant proteins in ameliorating inflammation during aging (Inflammaging). *Nutrients.* (2022) 14:747. doi: 10.3390/nu14040747
42. Zhang L, Ouyang Y, Li H, Shen L, Ni Y, Fang Q, et al. Metabolic phenotypes and the gut microbiota in response to dietary resistant starch type 2 in normal-weight subjects: a randomized crossover trial. *Sci Rep.* (2019) 9:4736. doi: 10.1038/s41598-018-38216-9
43. Zhou D, Pan Q, Shen F, Cao H-X, Ding W-J, Chen Y-W. Total fecal microbiota transplantation alleviates high-fat diet-induced steatohepatitis in mice via beneficial regulation of gut microbiota. *Sci Rep.* (2017) 7:1529. doi: 10.1038/s41598-017-01751-y
44. Le Roy T, Llopis M, Lepage P, Bruneau A, Rabot S, Bevilacqua C, et al. Intestinal microbiota determines development of non-alcoholic fatty liver disease in mice. *Gut.* (2013) 62:1787–94. doi: 10.1136/gutjnl-2012-303816
45. Chiu C-C, Ching Y-H, Li Y-P, Liu J-Y, Huang Y-T, Huang Y-W, et al. Nonalcoholic fatty liver disease is exacerbated in high-fat diet-fed gnotobiotic mice by colonization with the gut microbiota from patients with nonalcoholic steatohepatitis. *Nutrients.* (2017) 9:1220. doi: 10.3390/nu9111220
46. Mohamed AB, Rémond D, Chambon C, Sayd T, Hébraud M, Capel F, et al. A mix of dietary fermentable fibers improves lipids handling by the liver of overfed minipigs. *J Nutr Biochem.* (2019) 65:72–82. doi: 10.1016/j.jnutbio.2018.12.002
47. Zheng B, Wang T, Wang H, Chen L, Zhou Z. Studies on nutritional intervention of rice starch-oleic acid complex (resistant starch type V) in rats fed by high-fat diet. *Carbohydr Polym.* (2020) 246:116637. doi: 10.1016/j.carbpol.2020.116637
48. Barouei J, Bendiks Z, Martinic A, Mishchuk D, Heeney D, Hsieh YH, et al. Microbiota, metabolome, and immune alterations in obese mice fed a high-fat diet containing type 2 resistant starch. *Mol Nutr Food Res.* (2017) 61:1700184. doi: 10.1002/mnfr.201700184
49. Upadhyaya B, McCormack L, Fardin-Kia AR, Juenemann R, Nichenametla S, Clapper J, et al. Impact of dietary resistant starch type 4 on human gut microbiota and immunometabolic functions. *Sci Rep.* (2016) 6:28797. doi: 10.1038/srep28797
50. Pérez-Montes de Oca A, Julián MT, Ramos A, Puig-Domingo M, Alonso N. Microbiota, fiber, and NAFLD: is there any connection?. *Nutrients.* (2020) 12:3100. doi: 10.3390/nu12103100
51. Corrêa-Oliveira R, Fachi JL, Vieira A, Sato FT, Vinolo MAR. Regulation of immune cell function by short-chain fatty acids. *Clin Transl Immunol.* (2016) 5:e73. doi: 10.1038/cti.2016.17
52. Venkataraman A, Sieber J, Schmidt A, Waldron C, Theis K, Schmidt T. Variable responses of human microbiomes to dietary supplementation with resistant starch. *Microbiome.* (2016) 4:33. doi: 10.1186/s40168-016-0178-x
53. Koh A, De Vadder F, Kovatcheva-Datchary P, Bäckhed F. From dietary fiber to host physiology: short-chain fatty acids as key bacterial metabolites. *Cell.* (2016) 165:1332–45. doi: 10.1016/j.cell.2016.05.041
54. Mitchell RW, On NH, Del Bigio MR, Miller DW, Hatch GM. Fatty acid transport protein expression in human brain and potential role in fatty acid transport across human brain microvessel endothelial cells. *J Neurochem.* (2011) 117:735–46. doi: 10.1111/j.1471-4159.2011.07245.x
55. Luu M, Pautz S, Kohl V, Singh R, Romero R, Lucas S, et al. The short-chain fatty acid pentanoate suppresses autoimmunity by modulating the metabolic-epigenetic crosstalk in lymphocytes. *Nat Commun.* (2019) 10:760. doi: 10.1038/s41467-019-08711-2
56. Hu C, Xu B, Wang X, Wan WH, Lu J, Kong D, et al. Gut microbiota-derived short-chain fatty acids regulates group 3 innate lymphoid cells in hepatocellular carcinoma. *Hepatology.* (2022). [Online ahead of print]. doi: 10.1002/hep.32449
57. Li T, Teng H, An F, Huang Q, Chen L, Song H. The beneficial effects of purple yam (*Dioscorea alata* L.) resistant starch on hyperlipidemia in high-fat-fed hamsters. *Food Funct.* (2019) 10:2642–50. doi: 10.1039/c8fo02502a
58. Liu H, Wang J, He T, Becker S, Zhang G, Li D, et al. Butyrate: a double-edged sword for health? *Adv Nutr.* (2018) 9:21–9. doi: 10.1093/advances/nmx009
59. Zhang C, Ma S, Wu J, Luo L, Qiao S, Li R, et al. A specific gut microbiota and metabolomic profiles shifts related to antidiabetic action: the similar and complementary antidiabetic properties of type 3 resistant starch from Canna edulis and metformin. *Pharmacol Res.* (2020) 159:104985. doi: 10.1016/j.phrs.2020.104985
60. Dongowski G, Jacobasch G, Schmiedl D. Structural stability and prebiotic properties of resistant starch type 3 increase bile acid turnover and lower secondary bile acid formation. *J Agric Food Chem.* (2005) 53:9257–67. doi: 10.1021/jf0507792
61. Ridlon JM, Hylemon PB. A potential role for resistant starch fermentation in modulating colonic bacterial metabolism and colon cancer risk. *Cancer Biol Ther.* (2006) 5:273–4. doi: 10.4161/cbt.5.3.2728
62. Visekruna A, Luu M. The Role of Short-Chain Fatty Acids and Bile Acids in Intestinal and Liver Function, Inflammation, and Carcinogenesis. *Front Cell Dev Biol.* (2021) 9:703218. doi: 10.3389/fcell.2021.703218
63. Tolhurst G, Heffron H, Lam YS, Parker HE, Habib AM, Diakogiannaki E, et al. Short-chain fatty acids stimulate glucagon-like peptide-1 secretion via the G-protein–coupled receptor FFAR2. *Diabetes.* (2012) 61:364–71. doi: 10.2337/db11-1019
64. Rengadu D, Gerrano AS, Mellem JJ. Prebiotic effect of resistant starch from Vigna unguiculata (L.) Walp. (cowpea) using an in vitro simulated digestion model. *Int J Food Sci Technol.* (2019) 55:332–9. doi: 10.1111/ijfs.14304
65. Zhou Y, Zhao S, Jiang Y, Wei Y, Zhou X. Regulatory function of buckwheat-resistant starch supplementation on lipid profile and gut microbiota in mice fed with a high-fat diet. *J Food Sci.* (2019) 84:2674–81. doi: 10.1111/1750-3841.14747
66. Sinha SR, Haileselassie Y, Nguyen LP, Tropini C, Wang M, Becker LS, et al. Dysbiosis-induced secondary bile acid deficiency promotes intestinal inflammation. *Cell Host Microbe.* (2020) 27:659.–670. doi: 10.1016/j.chom.2020.01.021
67. Psichas A, Reimann F, Gribble FM. Gut chemosensing mechanisms. *J Clin Investig.* (2015) 125:908–17. doi: 10.1172/jci76309
68. Gill P, Van Zelm M, Muir J, Gibson P. Short chain fatty acids as potential therapeutic agents in human gastrointestinal and inflammatory disorders. *Aliment Pharmacol Ther.* (2018) 48:15–34. doi: 10.1111/apt.14689
69. Tan JK, McKenzie C, Mariño E, Macia L, Mackay CR. Metabolite-sensing G protein–coupled receptors—facilitators of diet-related immune regulation. *Annu Rev Immunol.* (2017) 35:371–402. doi: 10.1146/annurev-immunol-051116-052235
70. Dai X, Guo Z, Chen D, Li L, Song X, Liu T, et al. Maternal sucralose intake alters gut microbiota of offspring and exacerbates hepatic steatosis in adulthood. *Gut Microbes.* (2020) 11:1043–63. doi: 10.1080/19490976.2020.1738187
71. Sun L, Ma L, Ma Y, Zhang F, Zhao C, Nie Y. Insights into the role of gut microbiota in obesity: pathogenesis, mechanisms, and therapeutic perspectives. *Protein Cell.* (2018) 9:397–403. doi: 10.1007/s13238-018-0546-3
72. Cherbut C, Ferrier L, Rozé C, Anini Y, Blottière H, Lecannu G, et al. Short-chain fatty acids modify colonic motility through nerves and polypeptide YY release in the rat. *Am J Physiol.* (1998) 275:G1415–22. doi: 10.1152/ajpgi.1998.275.6.G1415
73. Fukumoto S, Tatewaki M, Yamada T, Fujimiya M, Mantyh C, Voss M, et al. Short-chain fatty acids stimulate colonic transit via intraluminal 5-HT release in rats. *Am J Physiol Regul Integr Comp Physiol.* (2003) 284:R1269–76. doi: 10.1152/ajpregu.00442.2002
74. Peng L, Li ZR, Green RS, Holzman IR, Lin J. Butyrate enhances the intestinal barrier by facilitating tight junction assembly via activation of AMP-activated protein kinase in Caco-2 cell monolayers. *J Nutr.* (2009) 139:1619–25. doi: 10.3945/jn.109.104638
75. Parikh M, Maddaford TG, Austria JA, Aliani M, Netticadan T, Pierce GN. Dietary flaxseed as a strategy for improving human health. *Nutrients.* (2019) 11:1171. doi: 10.3390/nu11051171
76. Zeng H, Umar S, Rust B, Lazarova D, Bordonaro M. Secondary bile acids and short chain fatty acids in the colon: a focus on colonic microbiome, cell proliferation, inflammation, and cancer. *Int J Mol Sci.* (2019) 20:1214. doi: 10.3390/ijms20051214

77. Ridlon JM, Harris SC, Bhowmik S, Kang D-J, Hylemon PB. Consequences of bile salt biotransformations by intestinal bacteria. *Gut Microbes.* (2016) 7:22–39. doi: 10.1080/19490976.2015.1127483
78. Milovic V, Stein J, Odera G, Gilani S, Murphy GM. Low-dose deoxycholic acid stimulates putrescine uptake in colon cancer cells (Caco-2). *Cancer Lett.* (2000) 154:195–200. doi: 10.1016/s0304-3835(00)00400-6
79. Stadler J, Stern HS, Yeung KS, McGuire V, Furrer R, Marcon N, et al. Effect of high fat consumption on cell proliferation activity of colorectal mucosa and on soluble faecal bile acids. *Gut.* (1988) 29:1326–31. doi: 10.1136/gut.29.10.1326
80. Ward JB, Lajczak NK, Kelly OB, O'Dwyer AM, Giddam AK, Ní Gabhann J, et al. Ursodeoxycholic acid and lithocholic acid exert anti-inflammatory actions in the colon. *Am J Physiol Gastrointest Liver Physiol.* (2017) 312:G550–8. doi: 10.1152/ajpgi.00256.2016
81. Yang H, Luo F, Wei Y, Jiao Y, Qian J, Chen S, et al. TGR5 protects against cholestatic liver disease via suppressing the NF-κB pathway and activating the Nrf2/HO-1 pathway. *Ann Transl Med.* (2021) 9:1158. doi: 10.21037/atm-21-2631
82. Petrov PD, Garcia-Mediavilla MV, Guzman C, Porras D, Nistal E, Martinez-Florez S, et al. A Network Involving Gut Microbiota, Circulating Bile Acids, and Hepatic Metabolism Genes That Protects Against Non-Alcoholic Fatty Liver Disease. *Mol Nutr Food Res.* (2019) 63:e1900487. doi: 10.1002/mnfr.201900487
83. Fu J, Wang Y, Tan S, Wang J. Effects of banana resistant starch on the biochemical indexes and intestinal flora of obese rats induced by a high-fat diet and their correlation analysis. *Front Bioeng Biotechnol.* (2021) 9:575724. doi: 10.3389/fbioe.2021.575724
84. Mollica MP, Raso GM, Cavaliere G, Trinchese G, De Filippo C, Aceto S, et al. Butyrate regulates liver mitochondrial function, efficiency, and dynamics in insulin-resistant obese mice. *Diabetes.* (2017) 66:1405–18. doi: 10.2337/db16-0924
85. Luo Q-J, Sun M-X, Guo Y-W, Tan S-W, Wu X-Y, Abassa K-K, et al. Sodium butyrate protects against lipopolysaccharide-induced liver injury partially via the GPR43/β-arrestin-2/NF-κB network. *Gastroenterol Rep.* (2021) 9:154–65. doi: 10.1093/gastro/goaa085
86. Wang A, Liu M, Shang W, Liu J, Dai Z, Strappe P, et al. Attenuation of metabolic syndrome in the ob/ob mouse model by resistant starch intervention is dose dependent. *Food Funct.* (2019) 10:7940–51. doi: 10.1039/c9fo01771b
87. Kliewer SA, Willson TM. Regulation of xenobiotic and bile acid metabolism by the nuclear pregnane X receptor. *J Lipid Res.* (2002) 43:359–64. doi: 10.1016/s0022-2275(20)30141-3
88. Cope K, Risby T, Diehl AM. Increased gastrointestinal ethanol production in obese mice: implications for fatty liver disease pathogenesis. *Gastroenterology.* (2000) 119:1340–7. doi: 10.1053/gast.2000.19267
89. Karimi P, Farhangi MA, Sarmadi B, Gargari B, Javid AZ, Pouraghaei M, et al. The therapeutic potential of resistant starch in modulation of insulin resistance, endotoxemia, oxidative stress and antioxidant biomarkers in women with type 2 diabetes: a randomized controlled clinical trial. *Ann Nutr Metab.* (2016) 68:85–93. doi: 10.1159/000441683
90. Nøhr MK, Pedersen MH, Gille A, Egerod KL, Engelstoft MS, Husted AS, et al. GPR41/FFAR3 and GPR43/FFAR2 as cosensors for short-chain fatty acids in enteroendocrine cells vs FFAR3 in enteric neurons and FFAR2 in enteric leukocytes. *Endocrinology.* (2013) 154:3552–64. doi: 10.1210/en.2013-1142
91. Zhou J, Martin RJ, Raggio AM, Shen L, McCutcheon K, Keenan MJ. The importance of GLP-1 and PYY in resistant starch's effect on body fat in mice. *Mol Nutr Food Res.* (2015) 59:1000–3. doi: 10.1002/mnfr.201400904
92. Brooks L, Viardot A, Tsakmaki A, Stolarczyk E, Howard JK, Cani PD, et al. Fermentable carbohydrate stimulates FFAR2-dependent colonic PYY cell expansion to increase satiety. *Mol Metab.* (2017) 6:48–60. doi: 10.1016/j.molmet.2016.10.011
93. Drucker DJ, Nauck MA. The incretin system: glucagon-like peptide-1 receptor agonists and dipeptidyl peptidase-4 inhibitors in type 2 diabetes. *Lancet.* (2006) 368:1696–705. doi: 10.1016/S0140-6736(06)69705-5
94. Okuno M, Nakanishi T, Shinomura Y, Kiyohara T, Ishikawa H, Tarui S. Peptide YY enhances NaCl and water absorption in the rat colon in vivo. *Experientia.* (1992) 48:47–50. doi: 10.1007/BF01923605
95. Martin-Gallausiaux C, Marinelli L, Blottière HM, Larraufie P, Lapaque N. SCFA: mechanisms and functional importance in the gut. *Proc Nutr Soc.* (2021) 80:37–49. doi: 10.1017/S0029665120006916
96. Poeta M, Pierri L, Vajro P. Gut–liver axis derangement in non-alcoholic fatty liver disease. *Children.* (2017) 4:66. doi: 10.3390/children4080066
97. Sun Y, Yu K, Zhou L, Fang L, Su Y, Zhu W. Metabolomic and transcriptomic responses induced in the livers of pigs by the long-term intake of resistant starch. *J Anim Sci.* (2016) 94:1083–94. doi: 10.2527/jas.2015-9715
98. Si X, Strappe P, Blanchard C, Zhou Z. Enhanced anti-obesity effects of complex of resistant starch and chitosan in high fat diet fed rats. *Carbohydr Polym.* (2017) 157:834–41. doi: 10.1016/j.carbpol.2016.10.042
99. Li T, Teng H, An F, Huang Q, Chen L, Song H. The beneficial effects of purple yam (*Dioscorea alata* L.) resistant starch on hyperlipidemia in high-fat-fed hamsters. *Food Funct.* (2019) 10:2642–650. doi: 10.1039/c8fo02502a
100. Shang W, Si X, Zhou Z, Wang J, Strappe P, Blanchard C. Studies on the unique properties of resistant starch and chito-oligosaccharide complexes for reducing high-fat diet-induced obesity and dyslipidemia in rats. *J Funct Foods.* (2017) 38:20–7. doi: 10.1016/j.jff.2017.08.032
101. Li YD, Xu TC, Xiao JX, Zong AZ, Qiu B, Jia M, et al. Efficacy of potato resistant starch prepared by microwave-toughening treatment. *Carbohydr Polym.* (2018) 192:299–307. doi: 10.1016/j.carbpol.2018.03.076
102. Ge YF, Wei CH, Wang WH, Cao LK. The resistant starch from sorghum regulates lipid metabolism in menopausal rats via equol. *J Food Biochem.* (2020) 44:e13295. doi: 10.1111/jfbc.13295
103. Polakof S, Díaz-Rubio ME, Dardevet D, Martin J-F, Pujos-Guillot E, Scalbert A, et al. Resistant starch intake partly restores metabolic and inflammatory alterations in the liver of high-fat-diet-fed rats. *J Nutr Biochem.* (2013) 24:1920–30. doi: 10.1016/j.jnutbio.2013.05.008
104. Si X, Zhou Z, Strappe P, Blanchard C. A comparison of RS4-type resistant starch to RS2-type resistant starch in suppressing oxidative stress in high-fat-diet-induced obese rats. *Food Funct.* (2017) 8:232–40. doi: 10.1039/c6fo01225f

Conflict of Interest: The authors declare that the research was conducted in the absence of any commercial or financial relationships that could be construed as a potential conflict of interest.

frontiers | Frontiers in Nutrition

ORIGINAL RESEARCH
published: 14 June 2022
doi: 10.3389/fnut.2022.897375

A Newly Developed Indicator of Overeating Saturated Fat Based on Serum Fatty Acids and Amino Acids and Its Association With Incidence of Type 2 Diabetes: Evidence From Two Randomized Controlled Feeding Trials and a Prospective Study

Wei Wei[1,2†], Tianqi Zi[1†], Ruiming Yang[1†], Jiaxu Xu[1], Yunyan Chen[1], XiTao Jiang[3], Xia Chu[1], Xue Yang[1] and Wenbo Jiang[1,4]**

[1] Department of Nutrition and Food Hygiene, National Key Discipline, School of Public Health, Harbin Medical University, Harbin, China, [2] Key Laboratory of Cardiovascular Research, Department of Pharmacology, College of Pharmacy, Ministry of Education, Harbin Medical University, Harbin, China, [3] College of Engineering, IT and Environment, Charles Darwin University, Darwin, NT, Australia, [4] Department of Cardiology, The First Affiliated Hospital of Harbin Medical University, Harbin, China

OPEN ACCESS

Edited by:
Jun Lu,
Auckland University of Technology,
New Zealand

Reviewed by:
Jennifer Rutkowsky,
University of California, Davis,
United States
Fredrik Rosqvist,
Uppsala University, Sweden
Reza Nemati,
Canterbury Health Laboratories,
New Zealand

***Correspondence:**
Xue Yang
yangxue1910@126.com
Wenbo Jiang
102593@hrbmu.edu.cn

† These authors have contributed equally to this work

Specialty section:
This article was submitted to Nutrition and Food Science Technology, a section of the journal Frontiers in Nutrition

Received: 16 March 2022
Accepted: 03 May 2022
Published: 14 June 2022

Citation:
Wei W, Zi T, Yang R, Xu J, Chen Y, Jiang X, Chu X, Yang X and Jiang W (2022) A Newly Developed Indicator of Overeating Saturated Fat Based on Serum Fatty Acids and Amino Acids and Its Association With Incidence of Type 2 Diabetes: Evidence From Two Randomized Controlled Feeding Trials and a Prospective Study. Front. Nutr. 9:897375. doi: 10.3389/fnut.2022.897375

Objective: Hyper-caloric intake of saturated fatty acids (SFAs) is common in modern societies, probably contributing to the epidemic of type 2 diabetes mellitus (T2DM). This study conducted two randomized controlled trials (RCTs) for developing a new indicator that can assess the nutritional status and examined its association with incidence of T2DM.

Methods: In RCT 1, healthy participants were randomly assigned into three groups, namely, control group (n = 40), overfeeding group 1 (100 g butter per day, n = 37), and overfeeding group 2 (120 g butter per day, n = 37). In RCT 2, healthy subjects were randomly assigned into two groups, namely, control group (n = 52) and high-fat group (300-extra kcal/day from diet that was designed by high-fat diet, n = 58). In the prospective cohort, 4,057 participants aged 20–74 years were enrolled and followed up over 5.3 years. Serum profiles of fatty acids and amino acids were measured.

Results: In RCT 1, serum fatty acids, including C14:0 and C18:0, increased, whereas C18:2, C20:4, C22:5, and C22:6 decreased; serum amino acids, including tyrosine, alanine, and aminobutyric acid, increased, whereas histidine and glycine decreased ($p < 0.05$). Among these serum fatty acids and amino acids, changes in C14:0, C20:4, tyrosine, histidine, and glycine were also observed in RCT 2. An indicator was developed based on the five fatty acids and amino acids, namely, C14:0 × tyrosine × 1,000/[C20:4 × (glycine + histidine)], and it significantly identified participants in the intervention group with area under the curve (AUC) (95% CI) being 0.85 (0.77–0.92). The indicator was significantly associated with incidence of T2DM in

the prospective cohort with HRs (95% CIs) from bottom quartile to top quartile being 1,1.21 (0.82–1.77), 1.60 (1.12–2.30), 2.04 (1.42–2.94).

Conclusion: The newly developed indicator in RCTs can be used in assessing the nutritional status of hypercaloric intake of SFA and predicting the development of T2DM.

Keywords: type 2 diabetes, biomarker, serum fatty acids, saturated fat intake, serum amino acid

INTRODUCTION

The rapid increase in the prevalence of diabetes mellitus and its complications have been major global health threats. Globally, it has been estimated that 1 of 11 adults currently have diabetes mellitus, and 90% of them have type 2 diabetes mellitus (T2DM) (1). A healthy diet has been demonstrated to play a critical role in the prevention of T2DM. The association between saturated fatty acids (SFAs) and T2DM has been one of the most vexed issues in this field (2, 3). Although the short-term randomized controlled trials (RCTs) have shown that overeating SFA promotes hepatic fat storage and insulin resistance (IR) (4, 5), evidence from a meta-analysis of long-term epidemiological studies frequently shows that dietary SFA is not associated with the incidence of T2DM (6, 7).

Dietary fat has been widely considered as one of the most difficult dietary components to assess through traditional nutritional methods (8). This may be the reason for the inconsistencies in the findings from the short-term RCTs and long-term epidemiological studies. Therefore, it is important to identify biomarkers that can assess the nutritional status of hypercaloric intake of dietary SFA objectively. Previous studies frequently focused on evaluating the utility of fatty acid profiles in serum as biomarkers of dietary SFA. However, serum SFA did not correlate well with dietary intake of SFA (9). Moreover, the total circulating fatty acids and other types of fatty acids, including monounsaturated fatty acids (MUFAs) and polyunsaturated fatty acids (PUFAs), also influence the circulating levels of SFA. Experimental evidence from human studies shows that it is energy intake that is a key mediator of serum fatty acids, rather than dietary fatty acid intake *per se*. The serum profiles of fatty acids may reflect the excessive intake of energy. In addition, recent studies have reported the impact of a high-fat diet on the catabolism of the amino acids (10–12), suggesting that serum profiles of amino acids may be related to the intake of SFA. However, whether and how serum profiles of amino acids would change during feeding of SFA have not been reported in previous RCTs. Examining the serum profiles of amino acids across different interventions of SFA feeding may aid in identifying some new biomarkers that are sensitive to the dietary intake of SFA, and it may be more accurate to evaluate the nutritional status of the hypercaloric intake of SFA by combination of serum fatty acids and amino acids.

In this study, two RCTs by feeding a hypercaloric diet rich in SFA with different intervention doses and sources were performed for identifying fatty acids and amino acids that could be used to assess this nutritional status. We aimed to develop a new indicator based on serum fatty acids and amino acids and examine the association between this newly developed indicator and the incidence of T2DM in a prospective cohort.

MATERIALS AND METHODS

Participants in the Two Randomized Controlled Trials

Participants in the two RCTs were recruited from voluntary and healthy students in Harbin Medical University from March to August 2019. The RCTs were registered at www.chictr.org as ChiCTR-1900021716 and ChiCTR-1900024931, respectively. Exclusion criteria included individuals who were older than 30 years, alcohol drinkers or smokers, had dysfunction of the liver, kidney, or digestive system, dyslipidemia, hypertension or taking medications, took nutritional supplements in the past 2 months, lost weight by restricting diet in the past 6 months, and had vigorous physical activity more than 5 h/week. Based on these exclusion criteria, 23 and 31 individuals were excluded in RCT 1 and RCT 2, respectively.

The participants in the two RCTs were provided with standard meals for 3 days, and then they were randomly assigned by a biostatistician to the intervention and control groups. In RCT 1, healthy participants were randomly assigned into three groups, namely, control group (2,150 kcal/day, 25% fat and 5% SFA, n = 40), overfeeding group 1 (100 g butter per day, n = 37), and overfeeding group 2 (120 g butter per day, n = 37). The same meals during the intervention in the three groups were provided, which is shown in **Supplementary Table 1**. The excess calories ranging from 100 to 120 g of butter were added to the meals, which contained 76% energy provided by SFA, 20% energy provided by MUFAs, and 4% energy provided by PUFAs), and the energy and macronutrients for the three groups are presented in **Supplementary Table 2**. In RCT 2, healthy subjects were randomly assigned into two groups, namely, the control group (2,250 kcal/day, 20% fat and 5% SFA, n = 52) and high-fat group (300 kcal/day extra energy, n = 58). The high-fat diet contained 35% energy provided by total fat and 15% energy provided by SFA, and the detailed information in terms of food groups and macronutrients is presented in **Supplementary Tables 3, 4**. The percentage of energy provided by protein was similar between the two groups. All the meals in the two RCTs were finished in the student canteen under the supervision of the study dietitian with the intervention periods in the two RCTs lasting for 7 days. Before the two RCTs, the food frequency questionnaire (FFQ) surveys were conducted to collect the dietary information of each participant for evaluating their habitus of dietary intake, and used as the reference for setting the energy and macronutrients

provided in the control group. The cooking menu was different between the two RCTs because of the different sources of SFA, making the energy provided in the control group of RCT 2 a bit higher than that of RCT 1 for controlling the overall carbohydrate and protein constant. Moreover, the degree of overnutrition in RCT 1 was greater than RCT 2 because RCT 1 aimed to capture more changes in the profiles of fatty acids and amino acids, and RCT 2 aimed to examine which fatty acids and amino acids could be still significantly changed if the overnutrition was relatively moderate. The overlapped serum fatty acids and amino acids between the two RCTs were used to develop the indicator for the hypercaloric intake of SFA.

Participants in the Prospective Cohort

The data of the Harbin Cohort Study on Diet, Nutrition and Chronic Non-communicable Disease (HDNNCDS) were used, which was launched in 2010, registered at www.chictr.org as ChiCTR-ECH-12002721. A total of 9,734 participants were recruited in the baseline survey of HDNNCDS. During 2015–2016, 8,913 participants completed the first in-person follow-up survey (13). Among the 8,913 participants, 4,958 participants' blood samples were randomly selected to measure the serum profiles of fatty acids and amino acids. After exclusion of the participants who had T2DM at baseline, a total of 4,057 subjects aged 20–74 years, including 1,352 men and 2,705 women, were enrolled in both the 2010 baseline survey and the 2016 follow-up survey, with a follow-up period of 5.3 years on average.

The study designs of the two RCTs and the prospective study were approved by the Ethics Committee of Harbin Medical University. The nature and potential risks of the study were explained to volunteers before obtaining written informed consent. The investigations were conducted in accordance with the Declaration of Helsinki. The methods in this study were in accordance with the approved guidelines.

Data Collection in a Prospective Cohort

In-person interviews were administered by trained personnel using a structured questionnaire to collect information on demographic characteristics, dietary habits, lifestyles, physical conditions, and anthropometric characteristics. Current smokers were defined as those who smoked at least 100 cigarettes in a lifetime or smoked every day or currently smoked some days. Current drinkers were defined as those who consumed $\geq$1 alcohol every month in 12 months before the survey. Regular exercise was defined as any kind of recreational or sports physical activity other than walking for work or life performed at least 30 min for $\geq$3 days/week. Family history of diabetes was defined as diabetes in first- or second-degree relatives.

Anthropometric and Biochemical Measurements

The measurement of height, weight, and waist circumferences (WCs) were conducted by well-trained professionals with participants wearing light, thin clothing, and no shoes. Bodyweight and height were measured to the nearest 0.1 kg and 0.1 cm, and body mass index (BMI) was calculated as weight (kg) divided by the square of the height in meters (m^2). Fat mass (FM) was measured by using the electric impedance method with a body FM analyzer (ACCUNIQ IOI-353, JAWON Medical Corporation, Korea). The blood samples were collected by venipuncture after a 12-h fast. Plasma and serum were centrifuged from the blood samples and immediately stored at –80°C for further analysis. Fasting serum (FS) glucose, triglyceride (TG), total cholesterol (TC), high-density lipoprotein cholesterol (HDL-C), and low-density lipoprotein cholesterol (LDL-C) were determined by an automatic analyzer (Hitachi 7100, Tokyo, Japan). Serum insulin was measured by Chemiluminescence Immune Analyzer (TOSOH AIA2000, Japan). Glycosylated hemoglobin (HbA1c) was determined by high-performance liquid chromatography (BIO-RAD VARIANT 2, United States). The homeostasis assessment model for IR (HOMA-IR) updated by the University of Oxford in 2004 was used to estimate IR (14). Serum preparation for fatty acids and amino acids quantitation was carried out as previously described (15, 16). Targeted analysis of serum fatty acids was performed by the TRACE GC/Polaris-Q MS system (Thermo Finnigan, Austin, TX, United States). Targeted analysis of serum amino acids was performed by a Waters ACQUITY Ultra performance liquid chromatography (UPLC) system (Waters Corporation, Milford, MA, United States) coupled to a Waters Xevo TQD mass spectrometer (MS) (Waters Corporation, Manchester, United Kingdom). Quality control was conducted using reference standards that were run concurrently with study samples to verify batch-to-batch variation. Absolute concentrations of fatty acids and amino acids were measured with mean interassay coefficients of variation 5.9 and 6.3%.

Ascertainment of Normal Glycemia, Prediabetes, Insulin Resistance, and Type 2 Diabetes Mellitus in a Prospective Cohort

Normal glycemia was defined as baseline FS glucose $<$5.5 mmol/L and 2-h glucose $<$7.8 mmol/L. Prediabetes was defined as baseline FS glucose $>$5.5 mmol/L, and/or 2-h glucose $>$7.8 mmol/L. IR was defined as the top quartiles of baseline HOMA-IR. T2DM was defined as self-reports of a history of T2DM diagnosis, FS glucose $\geq$7.0 mmol/L, 2-h glucose $\geq$11.1 mmol/L, and/or receiving treatment for T2DM.

Statistical Analysis

The sample size in RCT 1 was determined based on changes in HOMA-IR (as the primary outcome). At a 5% significance level with 80% statistical power, a sample size of 36 per group was required to detect a 0.60 difference in HOMA-IR with an SD of 0.9. The sample size in RCT 2 was determined based on the area under the curve (AUC) for discriminating the intervention group. At a 5% significance level with 80% statistical power, a sample size of 52 per group was required to detect an AUC value of 0.65. Before analyses, the Kolmogorov–Smirnov test was used to test the normality of distributions, and variables were log-transformed when necessary. The baseline characteristics in the two RCTs and the prospective cohort were compared by

Student's *t*-test for continuous variables and the Chi-square test for categorical variables. Among the two RCTs, the differences (△) between the baseline values and end-point values (end-point value – baseline value) for each participant in terms of anthropometric and biochemical indicators were calculated, and the differences in the △indicators between the control group and intervention group were compared using Student's *t*-test or one-way ANOVA. Meanwhile, the △fatty acids or △amino acids for each participant were also calculated, which were standardized by zero-mean normalization (*Z*-score) to eliminate the influence of the order of magnitude for different types of fatty acids and amino acids. After the indicator was developed, it was categorized into quartiles in the prospective cohort; the lowest quartile was used as the reference. Cox proportional hazards regression analyses were performed to examine the association between the quartiles of the indicator and incident T2DM in the total sample and subgroups of baseline normal glycemia, prediabetes, IR, men, and women. Three Cox models were conducted with adjustment for a series of covariates. In model 1, age, sex, BMI, WC, weight gain, smoke use, alcohol use, education level, family history of diabetes, energy intake, regular exercise habits, physical activity levels, and hypertension were included, and model 2 additionally adjusted for TG, HDL-C, TC, FS glucose, 2-h glucose, and HOMA-IR based on model 1. Furthermore, model 3 additionally adjusted for serum leucine, isoleucine, and valine based on model 2.

RESULTS

Baseline Characteristics of the Two Randomized Controlled Trials

In RCT 1, of the 143 participants assessed for eligibility, 120 participants were randomized, 3 dropped in the group with feeding 100 g butter and 3 dropped in the group with feeding 120 g butter during the study, and 114 participants completed the study. In RCT 2, of the 151 participants assessed for eligibility, 120 were randomized and 10 participants dropped during the intervention, leaving 110 participants in the study. The age, percentage of sex, and dietary intakes at baseline were similar in the two RCTs (**Supplementary Table 5**). After finishing the intervention, the energy, total fat intake, and saturated fat intake were significantly greater in the two RCTs (**Supplementary Table 6**).

Changes in the Body Composition and Biochemical Indicators in the Two Randomized Controlled Trials

The baseline body composition and biochemical indicators were similar across different groups of the two RCTs (**Table 1**). The mean absolute change of FS glucose in the intervention group of feeding 120 g of butter was significantly greater than that in the control group in RCT 1 (0.14 ± 0.37 vs. 0.33 ± 0.27; $p = 0.039$). Both FS insulin and HOMA-IR were significantly increased in the intervention groups compared with the control groups in the two RCTs (FS insulin: 0.38 ± 3.65 vs. 2.10 ± 4.31 vs. 2.56 ± 4.65, $p < 0.05$ in RCT 1; -0.72 ± 3.69 vs. 1.23 ± 3.63, $p < 0.01$ in RCT 2; HOMA-IR: 0.13 ± 0.79 vs. 0.50 ± 0.93 vs. 0.63 ± 0.97, $p < 0.01$ in RCT 1; -0.15 ± 0.81 vs. 0.29 ± 0.68, $p < 0.01$ in RCT 2).

Changes in the Serum Profiles of Fatty Acids and Amino Acids in the Two Randomized Controlled Trials

In RCT 1, the baseline serum profiles of fatty acids and amino acids were similar across the three groups (**Supplementary Table 7**). The significant differences for C14:0, C16:0, C18:0, C18:2, C20:3, C20:4, C22:5, and C22:6 across the three groups after the intervention were observed (**Supplementary Table 8**). Similarly, △C14:0 and △C18:0 significantly increased in the intervention group with *p*-values being $2.94e^{-9}$ and 0.010, and the △C18:2, △C20:4, △C22:5, and △C22:6 significantly decreased in the intervention group with *p*-values being 0.010, 0.001, $2.45e^{-3}$, and 0.044, respectively (**Figure 1A**). Meanwhile, the significant differences for the γ-aminobutyric acid, tyrosine, ornithine, histidine, glycine, citrulline, alanine, and L-aminobutyric acid across the three groups after the intervention were observed (**Supplementary Table 8**). Also, △tyrosine, △alanine, and △aminobutyric acid significantly increased in the intervention group with *p*-values being 0.027, 0.001, and 0.009, respectively, and the △glycine and △histidine significantly decreased in the intervention group with *p*-values being 0.017 and 0.014 (**Figure 1B**).

In RCT 2, the baseline serum profiles of fatty acids and amino acids were similar between the two groups (**Supplementary Table 7**). The significant differences for the C14:0, C18:2, C18:3α, and C20:4 between the two groups after the intervention were observed (**Supplementary Table 8**), and △C14:0 and △C16:0 significantly increased in the intervention group with *p*-values being 0.005 and 0.024, and the △C18:3α and △C20:4, significantly decreased in the intervention group with *p*-values being 0.034, and 0.010, respectively (**Figure 1C**). Meanwhile, the significant differences between the tyrosine, histidine, glycine, and citrulline between the two groups after the intervention were observed (**Supplementary Table 8**), and △tyrosine, △taurine, and △citrulline acid significantly increased in the intervention group with *p*-values being 0.044, 0.023, and 0.012, respectively, and the △glycine and △histidine significantly decreased in the intervention group with *p*-values being 0.016 and 0.01 (**Figure 1D**).

Assessment of the Ability for Discriminating Participants in Randomized Controlled Trial 2

Because the levels of C14:0, C18:0, C18:2, C20:4, C22:5, and C22:6 were significantly different after the intervention among the three groups, and their significant changing values in terms of △ were also observed in the intervention groups of RCT 1, we therefore further examined which of the above fatty acids could be used indiscriminate the participants who were in the intervention group in RCT 2, which is shown in **Figure 2A**. C14:0, C:18:2, and C20:4 could identify participants in the intervention group of RCT 2 with the AUCs (95% CI) being 0.73 (0.64–0.83), 0.62 (0.51–0.73), and 0.69 (0.59–0.79), whereas the AUCs (95% CIs)

TABLE 1 | The anthropometric and biochemical indicators at baseline and mean absolute change after 1 week in the two RCTs.

	RCT 1						RCT 2			
	Control (*N* = 40)		Overfeeding 100 g butter (*N* = 37)		Overfeeding 120 g butter (*N* = 37)		Control (*N* = 52)		HF-diet (35%) (*N* = 58)	
	Baseline	Mean absolute change	Baseline	Mean absolute change	Baseline	Mean absolute change	Baseline	Mean absolute change	Baseline	Mean absolute change
BMI (kg/m^2)	20.6 (2.5)	0.08 (0.31)	20.6 (2.6)	0.23 (0.58)	20.8 (2.7)	0.27 (0.37)	20.9 (2.3)	−0.08 (0.48)	20.8 (1.8)	−0.02 (0.72)
WC (cm)	69.2 (8.8)	1.94 (4.58)	67.5 (9.4)	2.31 (6.31)	70.5 (9.6)	1.68 (4.71)	73.3 (6.6)	−0.68 (2.76)	73.4 (8.6)	−1.30 (3.60)
BF (%)	21.1 (6.0)	−0.10 (2.48)	21.0 (5.7)	0.21 (1.75)	21.8 (5.5)	0.74 (2.35)	19.9 (6.4)	−0.03 (2.09)	19.3 (5.8)	0.31 (2.37)
Weight (kg)	56.5 (9.1)	−0.03 (0.66)	55.7 (9.7)	0.53 (1.28)*	57.9 (11.6)	0.72 (0.70)*	59.6 (8.4)	−1.05 (1.32)	60.0 (9.2)	0.16 (1.01)**
FPG (mmol/L)	4.17 (0.39)	0.14 (0.37)	4.26 (0.23)	0.21 (0.33)	4.18 (0.34)	0.33 (0.27)*	4.10 (0.68)	0.07 (0.71)	4.09 (0.38)	0.20 (0.33)
FINS (pmol/ml)	8.2 (4.0)	0.38 (3.65)	8.9 (4.4)	2.10 (4.31)*	8.5 (3.9)	2.56 (4.96)*	6.2 (3.9)	−0.72 (3.69)	6.1 (3.2)	1.23 (3.63)**
HOMA-IR	1.53 (0.79)	0.13 (0.79)	1.71 (0.87)	0.50 (0.93)**	1.59 (0.74)	0.63 (0.97)**	1.52 (0.91)	−0.15 (0.81)	1.39 (0.73)	0.29 (0.68)**
ALT (U/L)	9.1 (5.5)	2.5 (5.0)	8.8 (3.8)	13.1 (16.2)**	9.5 (5.4)	10.8 (13.2)**	17.2 (11.7)	0.42 (3.1)	19.4 (17.0)	0.21 (13.0)
AST (U/L)	18.8 (3.8)	−1.3 (2.7)	19.2 (3.1)	4.4 (8.9)**	19.8 (3.9)	4.5 (12.4)**	17.9 (4.4)	−0.35 (3.6)	18.5 (6.2)	−0.31 (4.2)
UA (μmol/L)	287.9 (59.1)	−26.9 (31.6)	293.9 (64.2)	−27.6 (28.3)	295.0 (46.2)	−24.9 (27.3)	324.2 (73.0)	6.4 (27.0)	343.8 (95.5)	3.2 (33.8)
TC (mmol/L)	3.90 (0.52)	−0.50 (0.29)	3.95 (0.61)	0.10 (0.30)**	3.99 (0.53)	0.10 (0.30)**	3.96 (0.67)	−0.02 (0.36)	4.11 (0.69)	0.35 (0.43)**
TG (mmol/L)	0.70 (0.21)	−0.07 (1.52)	0.73 (0.32)	−0.10 (0.20)	0.71 (0.18)	−0.15 (0.13)	0.84 (0.40)	0.12 (0.31)	0.98 (0.45)	−0.02 (0.46)
HDL-C (mmol/L)	1.47 (0.31)	−0.04 (0.25)	1.44 (0.26)	0.14 (0.14)**	1.46 (0.29)	0.15 (0.14)**	1.32 (0.25)	−0.07 (0.13)	1.30 (0.30)	0.09 (0.11)**
LDL-C (mmol/L)	2.35 (0.48)	−0.37 (0.29)	2.51 (0.61)	0.03 (0.26)**	2.53 (0.47)	0.04 (0.32)**	1.92 (0.44)	0.003 (0.21)	2.05 (0.52)	0.17 (0.29)**

Data are mean (SD); BMI, body mass index; WC, waist circumference; BF, percentage of body fat; FPG, fasting glucose; HOMA-IR, homeostasis model assessment for insulin resistance; UA, uric acid; TC, total cholesterol; TG, triglycerides; HDL-C, high-density lipoprotein cholesterol; LDL-C, low-density lipoprotein cholesterol.
$^*p < 0.05$ for the difference being different from 0.
$^{**}p < 0.01$ for the difference being different from 0.

for C18:2, C22:5, and C22:6 were 0.51 (0.40–0.62), 0.52 (0.41–0.63), and 0.53 (0.42–0.64), where 95% CIs crossed 0.5, suggesting that the discriminating abilities of these fatty acids were non-significant. Meanwhile, in RCT 2, no significant changes in C18:2 were observed during the intervention; we, therefore, excluded C18:2 as described in **Figure 1C** and **Supplementary Table 5**, and calculated the ratio of myristic acid (C14:0) to arachidonic acid (20:4) (MA) based on the direction of changes of the two fatty acids to examine whether the combination of the two fatty acids could elevate the discriminating abilities for identifying the participants with a high-fat diet. The MA could identify the participants more accurately with the AUC (95% CI) being 0.80 (0.71–0.89) (**Figure 2C**).

Similarly, because the levels of glycine, histidine, tyrosine, alanine, and L-aminobutyric were significantly different after the intervention among the three groups, and their significant changing values in terms of △ were also observed in the intervention groups of RCT 1, we therefore further examined which of the above amino acids could be used to indiscriminate the participants who were in the intervention group in RCT 2, which is shown in **Figure 2B**. Glycine, histidine, and tyrosine could identify participants in the intervention group of RCT 2 with the AUCs (95% CI) being 0.65 (0.55–0.76), 0.65 (0.54–0.74), and 0.65 (0.54–0.75), whereas the AUCs (95% CIs) for alanine and L-aminobutyric were 0.55 (0.44–0.66) and 0.59 (0.48–0.70), where the 95% CIs crossed 0.5, suggesting that the discriminating abilities of the two amino acids were non-significant. Based on the direction of changes of the three amino acids, the ratio of tyrosine to the sum of glycine and histidine (TGH) was calculated to examine whether the combination of the three amino acids could elevate the discriminating abilities for identifying the participants with a high-fat diet. The TGH could identify the participants more accurately with the AUC (95% CI) being 0.77 (0.68–0.87) (**Figure 2C**).

Furthermore, we also examined whether the combination of these fatty acids and amino acids could elevate the discriminating abilities, and the indicator was further developed by multiplying MA by TGH (MA-TGH): C14:0 × tyrosine × 1,000/[C20:4 × (glycine + histidine)], and we found that it has more accurate discriminating ability

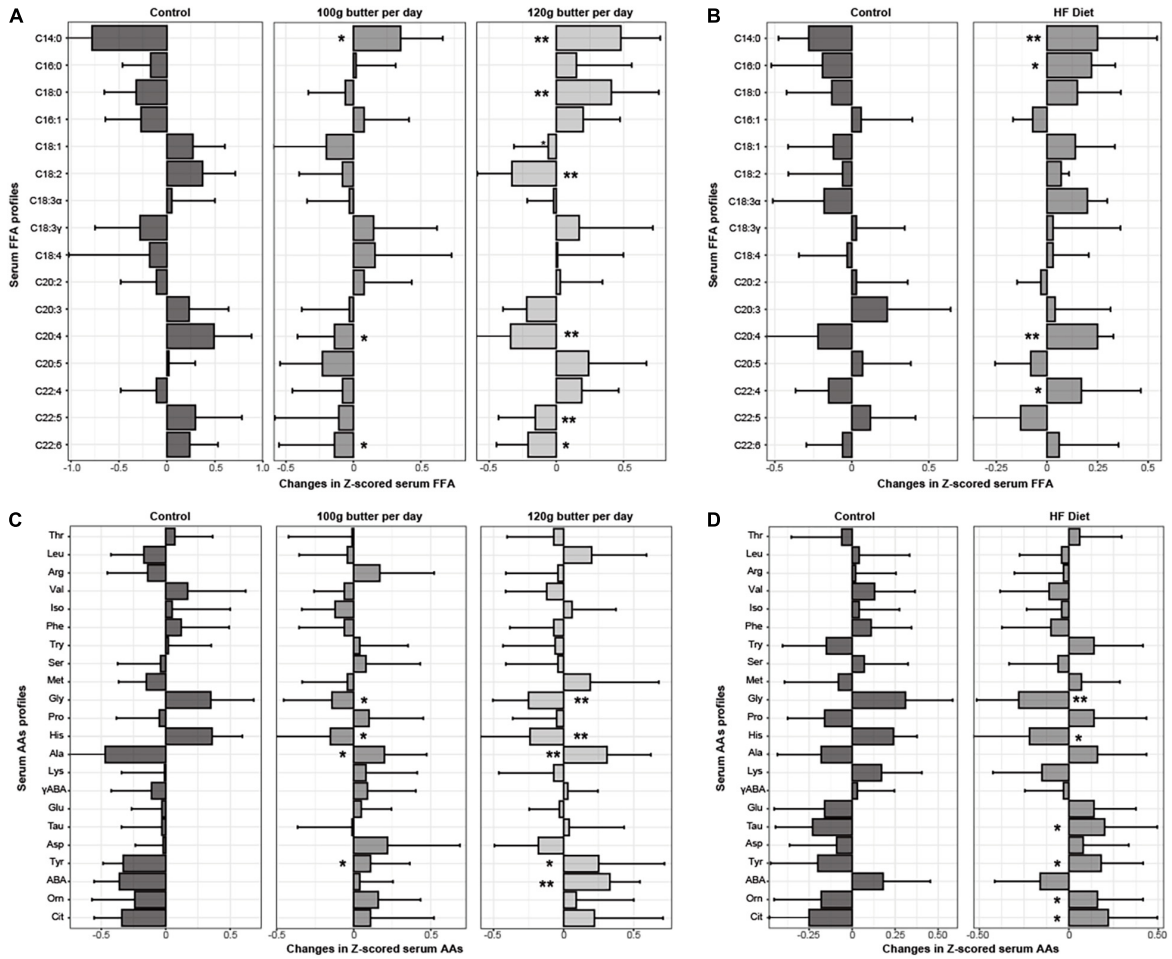

FIGURE 1 | Changes in *Z*-scored profiles of serum fatty acids and amino acids in the two RCTs. *$p < 0.05$ for the differences in the *Z*-scored serum fatty acids and amino acids between the intervention group and control group. **$p < 0.01$ for the differences in the *Z*-scored serum fatty acids and amino acids between the intervention group and control group. **(A)** Changes in the *Z*-scored profiles of fatty acids in the RCT1. **(B)** Changes in the *Z*-scored profiles of fatty acids in the RCT2. **(C)** Changes in the *Z*-scored profiles of amino acids in the RCT1. **(D)** Changes in the *Z*-scored profiles of amino acids in the RCT2.

than MA or TGH used alone with AUC (95% CI) being 0.85 (0.77–0.92) (**Figure 2C**).

Association of MA-TGH With the Incidence of Type 2 Diabetes Mellitus

In this longitudinal data, age, percentage of men, BMI, WC, the prevalence of hypertension, family history of diabetes, blood lipids, FS glucose, 2-h glucose, HOMA-IR, and serum BCAA at baseline were significantly greater in new cases of T2DM (**Supplementary Table 9**). MA-TGH was significantly associated with weight gain ($r = 0.136$, $p < 0.001$) (**Supplementary Figure 1**). The association of MA-TGH with the incidence of T2DM is presented in **Table 2**. After adjustment for age, sex, BMI, WC, smoke use, alcohol use, education level, family history of diabetes, energy intake, regular exercise habits, physical activity levels, hypertension, TG, HDL-C, TC, FS glucose, 2-h glucose, HOMA-IR, valine, leucine, isoleucine, and weight gain in model 4, MA-TGH was significantly associated with the incidence of T2DM in the total sample with HRs (95% CI) from bottom to the top quartiles being 1, 1.17 (0.82–1.72), 1.70 (1.21–2.39), and 2.09 (1.49–2.92). Meanwhile, among the participants with normal glycemia at baseline, MA-TGH was still associated with the incidence of T2DM with HR (95% CI) from bottom to the top quartiles being 1, 1.49 (0.89–2.50), 1.66 (0.99–2.77), and 2.75 (1.68–4.48) after adjustment for the covariates included in model 3 (**Table 2**), and sex had no effect on this association (**Supplementary Table 10**).

DISCUSSION

In this study, two RCTs with the intervention of hypercaloric intake of SFA from different doses and sources were conducted. In RCT 1, numbers of serum fatty acids and amino acids were significantly varied after overeating SFA. Among these serum fatty acids and amino acids, the significant changes in myristic acid (C14:0), arachidonic acid (C20:4), tyrosine, glycine, and

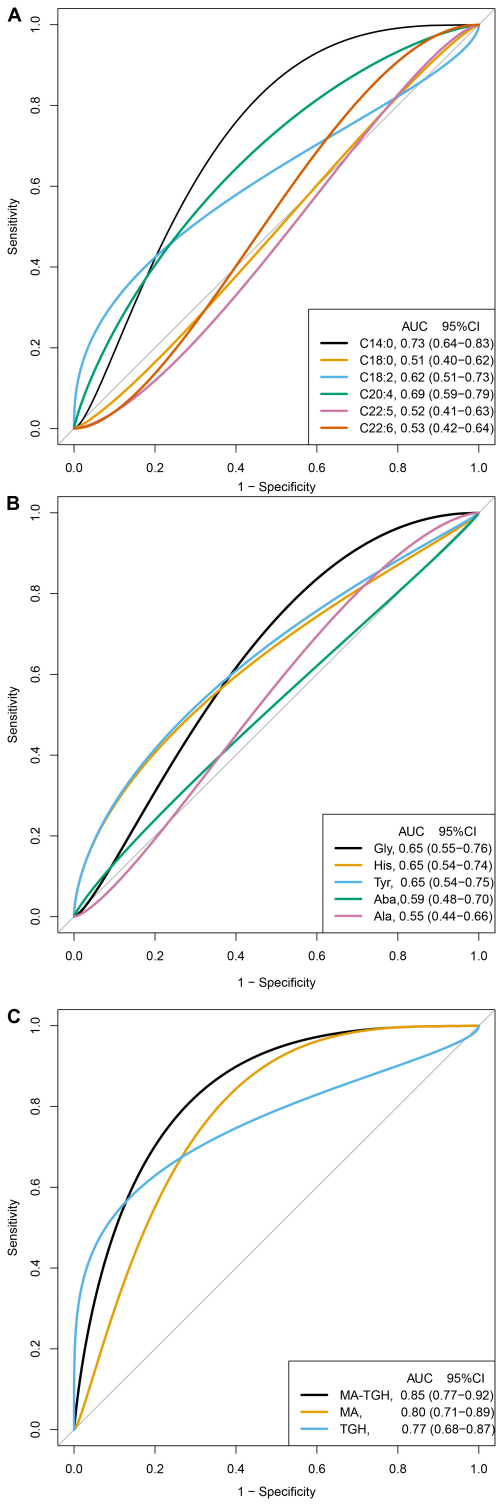

FIGURE 2 | Discrimination ability of the fatty acids, amino acids, and the indicator for identifying participants in the intervention group of RCT 2 (*N* = 110). MA, the ratio of myristic acid (C14:0) to arachidonic acid (20:4); TGH, the ration of tyrosine to the sum of glycine and histidine; MA-TGH, multiplying MA by TGH calculated by C14:0 × tyrosine × 1,000/[C20:4 × (glycine + histidine)]. **(A)** Discrimination ability of the fatty acids in the RCT2. **(B)** Discrimination ability of the amino acids in the RCT2. **(C)** Discrimination ability of combined indicators in the RCT2.

histidine during the intervention were consistently observed in RCT 2, which showed lower discrimination ability for identifying the participants with the hypercaloric intake of SFA. An indicator of hypercaloric intake of SFA was therefore developed based on the above five serum fatty acids and amino acids. This indicator could significantly identify participants with hypercaloric intake of SFA in RCT 2, and it was associated with the development of future risk of T2DM, independent of other risk factors, particularly glucose, IR, and branched-chain amino acids. To our knowledge, this is the first study to establish an indicator based on fatty acids and amino acids, which can assess the nutritional status of hypercaloric intake of SFA, and examine its association with T2DM.

The most important finding of this study is that an indicator of hypercaloric intake of SFA was developed in this study. To achieve this, two RCTs were conducted in this study, with one for developing the indicator and the other for validation. In RCT 1, 100 and 120 g butter was provided as the main source of SFA to the participants. Compared to previous studies that reported the composition of serum FFA, this study examined the absolute changed values of serum FFA. We found that serum myristic acid (C14:0), stearic acid (C18:0), tyrosine, alanine, and L-aminobutyric acid increased, and linoleic acid (C18:2), arachidonic acid (C20:4), EPA (C22:5), DHA (C22:6), histidine, and glycine decreased among the participants in the group of 120 g butter per day, and only myristic acid (C14:0), linoleic acid (C18:2), arachidonic acid (C20:4), and EPA (C22:5) among the fatty acids and tyrosine, histidine, and glycine among the amino acids were significantly varied among the participants in the group of 100 g butter per day. This observation suggested that the number of significant changed fatty acids and amino acids gradually decreased with the stimulation of hypercaloric intake of SFA, and myristic acid (C14:0), arachidonic acid (C20:4), EPA (C22:5), tyrosine, histidine, and glycine probably had dose-response manner in relation to the hypercaloric intake of SFA from butter. These observations were consistent with previous studies, all indicating that serum long-chain SFAs increased, and serum unsaturated fatty acids decreased during hypercaloric intake of SFA (4, 5, 17–19). Also, these observations suggested that hypercaloric intake of SFA could influence the metabolic pathways of amino acids, and these amino acids were probably associated with hypercaloric intake of SFA.

Compared to RCT 1, RCT 2 adopted a more moderate degree of hypercaloric intake of SFA with a high-fat diet as the main source of SFA. We observed that myristic acid (C14:0), palmitic acid (C16:0), tyrosine, taurine, and citrulline acid increased, and α-linolenic acid (C18:3α), arachidonic acid (C20:4), histidine, and glycine were decreased. Although the different varied fatty acids and amino acids were observed, probably because of the different sources of SFA, the significant changes in myristic acid (C14:0), arachidonic acid (C20:4), tyrosine, histidine, and glycine were still observed in RCT 2, suggesting that these fatty acids and amino acids were relatively robust with the different sources of SFA. Furthermore, these fatty acids and amino acids showed relatively weak discrimination abilities for identifying the participants with the hypercaloric intake of SFA. Based on these results, this study intended to examine whether their combination could elevate the

TABLE 2 | HRs and 95% CI for the association between the quartiles of the indicator and incidence of T2DM in the total, normal glycemic, prediabetes, and IR samples.

	Quartile 1	Quartile 2	Quartile 3	Quartile 4	$p_{fortrend}$
Total-sample					
Case/*N*	51/1,014	65/1,014	99/1,015	150/1,014	
Model 1	1 (Ref.)	1.21 (0.83–1.76)	1.93 (1.36–2.73)	2.93 (2.11–4.07)	<0.001
Model 2	1 (Ref.)	1.21 (0.83–1.76)	1.60 (1.13–2.28)	2.08 (1.47–2.94)	<0.001
Model 3	1 (Ref.)	1.21 (0.82–1.77)	1.60 (1.12–2.30)	2.04 (1.42–2.94)	<0.001
Normal glycemic					
Case/*N*	24/822	37/822	41/822	72/822	
Model 1	1 (Ref.)	1.41 (0.82–2.43)	2.23 (1.34–3.72)	3.07 (1.88–5.01)	<0.001
Model 2	1 (Ref.)	1.35 (0.78–2.31)	2.00 (1.20–3.35)	2.51 (1.51–4.18)	<0.001
Model 3	1 (Ref.)	1.40 (0.80–2.43)	2.10 (1.23–3.59)	2.67 (1.54–4.62)	<0.001
Pre-diabetes					
Case/*N*	30/193	42/192	52/191	67/193	
Model 1	1 (Ref.)	1.62 (1.00–2.64)	1.84 (1.15–2.94)	2.64 (1.68–4.14)	<0.001
Model 2	1 (Ref.)	1.75 (1.07–2.84)	1.88 (1.17–3.02)	2.54 (1.57–4.10)	<0.001
Model 3	1 (Ref.)	1.74 (1.06–2.84)	1.83 (1.14–2.96)	2.37 (1.44–3.91)	0.001
IR					
Case/*N*	18/253	37/253	48/253	52/253	
Model 1	1 (Ref.)	1.74 (1.00–3.04)	2.50 (1.46–4.28)	2.97 (1.76–5.01)	<0.001
Model 2	1 (Ref.)	1.71 (0.98–2.98)	2.18 (1.27–3.74)	2.48 (1.43–4.30)	0.001
Model 3	1 (Ref.)	1.59 (0.91–2.78)	2.00 (1.15–3.48)	1.95 (1.07–3.54)	0.023

In model 1, age, sex, BMI, WC, weight gain, smoke use, alcohol use, education level, family history of diabetes, energy intake, regular exercise habits, physical activity levels, and hypertension were included.

Model 2 additionally adjusted for TG, HDL-C, TC, FS glucose, 2-h glucose, and HOMA-IR based on model 1.

Model 3 additionally adjusted for serum leucine, isoleucine, and valine based on model 2.

BMI, body mass index; WC, waist circumference; TG, triglycerides; HDL-C, high-density lipoprotein cholesterol; TC, total cholesterol; FS glucose, fasting serum glucose. Normal glycemia was defined as baseline fasting serum (FS) glucose <5.5 mmol/L and 2-h glucose <7.8 mmol/L. Prediabetes was defined as baseline FS glucose >5.5 mmol/L, and/or 2-h glucose >7.8 mmol/L. IR was defined as the top quartiles of baseline HOMA-IR. Ref., reference.

accuracy of discrimination ability. Therefore, MA-TGH, as a new indicator, was developed, and it could identify the participants who were in the group of hypercaloric intake of SFA with AUC being 0.85, suggesting that this indicator based on serum fatty acids and amino acids may be more accurate than the individual fatty acids or amino acids.

These results could be supported by several studies. Consistent results from previous RCTs have documented the association between SFA intake and serum cholesterol levels (13), which were also observed in the two RCTs of this study, and it has been reported that serum myristic acid has stronger positive cholesterolemic effects than other serum fatty acids (20). Moreover, a previous observational study has shown weak but significant positive and negative association of dietary fat with serum myristic acid (20). Cell and animal studies have indicated that myristic acid has been the first long-chain endogenous SFA in the fatty acid pathways, which can be elongated to palmitic acid by *de novo* lipogenesis (21), and it is more rapidly metabolized from hepatic to circulating than are other long-chain SFA (22). For arachidonic acid, previous feeding trials have shown that a low SFA diet resulted in increased serum arachidonic acid levels (23), and a high intake of SFA prompted arachidonic acid turnover in rats (24). Meanwhile, a previous study has reported that a high-fat diet could decrease tyrosine hydroxylase mRNA expression, resulting in increased plasma tyrosine (25). For glycine, the expression of pathways of glycine catabolism in the liver and urinary excretion of acyl glycines decreased in the high-fat diet (26, 27), and previous intervention studies have shown that plasma glycine decreased after 1 week of a meat diet, in which the intervention sources were mainly used red meat (28). For histidine, an intervention study has reported that histidine increased after feeding lean meat with low fat (29). Moreover, consistent results have documented the anti-inflammatory effect of glycine and histidine in obese people (30–32).

Another important finding of this study is that MA-TGH, as an indicator of hypercaloric intake of SFA, was significantly associated with future risk of T2DM, independent of other traditional risk factors, and this association was still significant in the participants who were normal glycemic. The FFQ is a relatively valid and commonly used instrument to capture diet information in observational studies. It has been found that FFQ frequently underestimates the intake of energy, and this underestimated percentage may be greater among people with obesity or T2DM, although the association between hypercaloric intake and increased risk of T2D has been abundantly documented. The serum fatty acids and amino acids used in MA-TGH have been reported to be associated with T2DM in previous population-based studies. The EPIC study across eight European countries has documented the association between myristic acids and increased risk of T2DM (33), and tyrosine has been consistently reported to be associated with IR, decreased insulin secretion, and the development of T2DM (34, 35). A pooled analysis of 20 prospective cohorts has shown that increased arachidonic acid was associated with reduced risk of T2DM (36), and a recent study based on genetic approaches has demonstrated a protective effect of glycine on T2DM, driven by

a glycine-lowering effect of IR (37). It has also been indicated that histidine supplementation could improve IR and suppress inflammation and oxidative stress (38).

These findings of this study have important implications. A recent meta-analysis based on RCT has suggested that replacing dietary SFA with PUFA significantly lowered mortality risks of cardiovascular disease and all-cause (39); therefore, it is important to establish biomarkers that can objectively and sensitively assess the nutritional status of SFA. MA-TGH may aid in identifying individuals with excessive intake of SFA and developing targeted intervention plans for preventing the development of T2DM because the relationships of fatty acids and amino acids in MA-TGH with T2DM have been consistently confirmed in previous studies.

This study has several strengths. First, two RCTs with different doses and sources of SFA intervention were conducted, and the participants in the two RCTs were young medical students with high compliance. Second, the previous study has reported that it is difficult to modify the proportion of circulating fatty acids that are already accumulated in the body, probably leading that serum SFA did not correlate well with dietary intake of SFA (9). The participants in the two RCTs were relatively young, and therefore they may be more sensitive to the hypercaloric intake of SFA. Third, this study examined the association between the biomarker and incidence of T2DM with a relatively large OGTT sample of nutritional and metabolic analyses in this issue.

We also recognized that this study has certain limitations. First, the two RCTs in this study only included young, healthy Asian ethnic, which limits the generalizability of the findings. Compared with other ethnics, absorption and metabolic rates of carbohydrates tend to be higher, whereas that of fat tends to be lower in Asians (40). Future study is still needed to evaluate whether MA-TGH could be used for assessing the nutritional status of overeating SFA in other ethnics. Second, although the percentage of men and women was similar between the intervention group and control group after the randomization allocation, the percentage of women in the two RCTs was relatively high. Third, this study only examined the association between MA-TGH with T2DM in Asian ethnic; however, the associations of fatty acids and amino acids in the indicator with T2DM have been consistently demonstrated across different ethnicities (33–37). We would therefore expect that our observations would hold across other populations. Fourth, this study only examined the profiles of serum fatty acids but in the absence of data on intracellular values in the two RCTs. The serum profiles could be more easily used in clinical and epidemiological studies; however, fatty acids in adipose tissue may be more accurate. Fifth, in the prospective cohort, we could not exclude the possibility that the increased levels of MA-TGH were induced by other factors, such as genetic risk factors. The previous studies have identified a few gene polymorphisms for the fatty acids or amino acids used in MA-TGH (41–44). Therefore, future study is still needed to examine the interaction effects of the hypercaloric intake of SFA, levels of MA-TGH, and gene polymorphism on the development of T2DM to provide more comprehensive evidence for the association between MA-TGH and T2DM. Furthermore, we lacked information on the fatty acids and amino acids at the follow-up. Analyzing the changes in the levels of TAG-MA between baseline and follow-up might provide more compelling evidence for the association between this indicator and the risk of T2DM. Finally, this study did not control the energy intake between the intervention group and control group to be constant. It is unclear whether the indicator could reflect the intake of SFA under the condition that was not overfeeding. Future study with rigorously controlling the energy is warranted to validate the findings in this study.

In conclusion, this study developed and validated an indicator of overeating SFA based on changes in profiles of serum fatty acids and amino acids. The indicator was associated with the development of T2DM. These findings may have implications for the possible modifiable pathways to T2DM.

DATA AVAILABILITY STATEMENT

The original contributions presented in the study are included in the article/**Supplementary Material**, further inquiries can be directed to the corresponding authors.

ETHICS STATEMENT

The studies involving human participants were reviewed and approved by the Ethics Committee of Harbin Medical University. The patients/participants provided their written informed consent to participate in this study.

AUTHOR CONTRIBUTIONS

XC, XY, and WW conceived the idea. WW and RY drafted the manuscript. WJ, YC, and JX conducted the statistical analyses. WJ and TZ conducted the first feeding trial. XJ, YC, and TZ conducted the second feeding trial. TZ and WW did the amino acid and fatty acids measurements. All authors critically assessed and reviewed the manuscript.

FUNDING

This research was supported by funds from the National Key R&D Program of China (82103815 to XY), Platform construction of Heilongjiang Academy of Sciences (CZKYF2020C001) and HMU Marshal Initiative Funding (HMUMIF-21013 to WW).

ACKNOWLEDGMENTS

We thank all participants in this study for our continued cooperation and participation.

SUPPLEMENTARY MATERIAL

The Supplementary Material for this article can be found online at: https://www.frontiersin.org/articles/10.3389/fnut.2022.897375/full#supplementary-material

REFERENCES

1. Zheng Y, Ley SH, Hu FB. Global aetiology and epidemiology of type 2 diabetes mellitus and its complications. *Nat Rev Endocrinol.* (2018) 14:88–98. doi: 10.1038/nrendo.2017.151
2. Dyson PA. Saturated fat and type 2 diabetes: where do we stand. *Diabet Med.* (2016) 33:1312–4. doi: 10.1111/dme.13176
3. Svendsen K, Arnesen E, Retterstøl K. Saturated fat -a never ending story. *Food Nutr Res.* (2017) 61:1377572. doi: 10.1080/16546628.2017.1377572
4. Rosqvist F, Iggman D, Kullberg J, Cedernaes J, Johansson HE, Larsson A, et al. Overfeeding polyunsaturated and saturated fat causes distinct effects on liver and visceral fat accumulation in humans. *Diabetes.* (2014) 63:2356–68. doi: 10.2337/db13-1622
5. Luukkonen PK, Sädevirta S, Zhou Y, Kayser B, Ali A, Ahonen L, et al. Saturated fat is more metabolically harmful for the human liver than unsaturated fat or simple sugars. *Diabetes Care.* (2018) 41:1732–9. doi: 10.2337/dc18-0071
6. de Souza RJ, Mente A, Maroleanu A, Cozma AI, Ha V, Kishibe T, et al. Intake of saturated and trans unsaturated fatty acids and risk of all cause mortality, cardiovascular disease, and type 2 diabetes: systematic review and meta-analysis of observational studies. *BMJ.* (2015) 351:h3978. doi: 10.1136/bmj.h3978
7. Schwab U, Lauritzen L, Tholstrup T, Haldorssoni T, Riserus U, Uusitupa M, et al. Effect of the amount and type of dietary fat on cardiometabolic risk factors and risk of developing type 2 diabetes, cardiovascular diseases, and cancer: a systematic review. *Food Nutr Res.* (2014) 58:25145. doi: 10.3402/fnr.v58.25145
8. Arab L. Biomarkers of fat and fatty acid intake. *J Nutr.* (2003) 133:925S–32S.
9. Hodson L, Skeaff CM, Fielding BA. Fatty acid composition of adipose tissue and blood in humans and its use as a biomarker of dietary intake. *Prog Lipid Res.* (2008) 47:348–80. doi: 10.1016/j.plipres.2008.03.003
10. Mantha OL, Polakof S, Huneau JF, Mariotti F, Poupin N, Zalko D, et al. Early changes in tissue amino acid metabolism and nutrient routing in rats fed a high-fat diet: evidence from natural isotope abundances of nitrogen and carbon in tissue proteins. *Br J Nutr.* (2018) 119:981–91. doi: 10.1017/S0007114518000326
11. Lee J, Jung S, Kim N, Shin MJ, Ryu DH, Hwang GS. Myocardial metabolic alterations in mice with diet-induced atherosclerosis: linking sulfur amino acid and lipid metabolism. *Sci Rep.* (2017) 7:13597. doi: 10.1038/s41598-017-13991-z
12. Meyer JG, Softic S, Basisty N, Rardin MJ, Verdin E, Gibson BW, et al. Temporal dynamics of liver mitochondrial protein acetylation and succinylation and metabolites due to high fat diet and/or excess glucose or fructose. *PLoS One.* (2018) 13:e0208973. doi: 10.1371/journal.pone.0208973
13. Han T, Lan L, Qu R, Xu Q, Jiang R, Na L, et al. Temporal relationship between hyperuricemia and insulin resistance and its impact on future risk of hypertension. *Hypertension.* (2017) 70:703–11. doi: 10.1161/HYPERTENSIONAHA.117.09508
14. Wallace TM, Levy JC, Matthews DR. Use and abuse of HOMA modeling. *Diabetes Care.* (2004) 27:1487–95. doi: 10.2337/diacare.27.6.1487
15. Liu L, Feng R, Guo F, Li Y, Jiao J, Sun C. Targeted metabolomic analysis reveals the association between the postprandial change in palmitic acid, branched-chain amino acids and insulin resistance in young obese subjects. *Diabetes Res Clin Pract.* (2015) 108:84–93. doi: 10.1016/j.diabres.2015.01.014
16. Cui Y, Chen X, Liu L, Xie W, Wu Y, Wu Q, et al. Gas chromatography-mass spectrometry analysis of the free fatty acids in serum obtained from patients with Alzheimer's disease. *Biomed Mater Eng.* (2015) 26:S2165–77. doi: 10.3233/BME-151522
17. Hodson L, Skeaff CM, Chisholm WA. The effect of replacing dietary saturated fat with polyunsaturated or monounsaturated fat on plasma lipids in free-living young adults. *Eur J Clin Nutr.* (2001) 55:908–15. doi: 10.1038/sj.ejcn.1601234
18. Skeaff CM, Hodson L, McKenzie JE. Dietary-induced changes in fatty acid composition of human plasma, platelet, and erythrocyte lipids follow a similar time course. *J Nutr.* (2006) 136:565–9. doi: 10.1093/jn/136.3.565
19. Chisholm A, Mann J, Sutherland W, Duncan A, Skeaff M, Frampton C. Effect on lipoprotein profile of replacing butter with margarine in a low fat diet: randomised crossover study with hypercholesterolaemic subjects. *BMJ.* (1996) 312:931–4. doi: 10.1136/bmj.312.7036.931
20. Bradbury KE, Skeaff CM, Green TJ, Gray AR, Crowe FL. The serum fatty acids myristic acid and linoleic acid are better predictors of serum cholesterol concentrations when measured as molecular percentages rather than as absolute concentrations. *Am J Clin Nutr.* (2010) 91:398–405. doi: 10.3945/ajcn.2009.28159
21. Lee WN, Lim S, Bassilian S, Bergner EA, Edmond J. Fatty acid cycling in human hepatoma cells and the effects of troglitazone. *J Biol Chem.* (1998) 273:20929–34. doi: 10.1074/jbc.273.33.20929
22. Rioux V, Lemarchal P, Legrand P. Myristic acid, unlike palmitic acid, is rapidly metabolized in cultured rat hepatocytes. *J Nutr Biochem.* (2000) 11:198–207. doi: 10.1016/s0955-2863(00)00065-6
23. Garg ML, Thomson AB, Clandinin MT. Interactions of saturated, n-6 and n-3 polyunsaturated fatty acids to modulate arachidonic acid metabolism. *J Lipid Res.* (1990) 31:271–7.
24. Oliveros LB, Videla AM, Gimenez MS. Effect of dietary fat saturation on lipid metabolism, arachidonic acid turnover and peritoneal macrophage oxidative stress in mice. *Braz J Med.* (2004) 37:311–20. doi: 10.1590/s0100-879x2004000300004
25. Li Y, South T, Han M, Chen J, Wang R, Huang XF. High-fat diet decreases tyrosine hydroxylase mRNA expression irrespective of obesity susceptibility in mice. *Brain Res.* (2009) 1268:181–9. doi: 10.1016/j.brainres.2009.02.075
26. Pacana T, Cazanave S, Verdianelli A, Patel V, Min HK, Mirshahi F, et al. Dysregulated hepatic methionine metabolism drives homocysteine elevation in diet-induced nonalcoholic fatty liver disease. *PLoS One.* (2015) 10:e0136822. doi: 10.1371/journal.pone.0136822
27. Pelantová H, Bugáňová M, Holubová M, Šedivá B, Zemenová J, Sýkora D, et al. Urinary metabolomic profiling in mice with diet-induced obesity and type 2 diabetes mellitus after treatment with metformin, vildagliptin and their combination. *Mol Cell Endocrinol.* (2016) 431:88–100. doi: 10.1016/j.mce.2016.05.003
28. Altorf-van der Kuil W, Brink EJ, Boetje M, Siebelink E, Bijlsma S, Engberink MF, et al. Identification of biomarkers for intake of protein from meat, dairy products and grains: a controlled dietary intervention study. *Br J Nutr.* (2013) 110:810–22. doi: 10.1017/S0007114512005788
29. Samman S, Crossett B, Somers M, Bell KJ, Lai NT, Sullivan DR, et al. Metabolic profiling of plasma amino acids shows that histidine increases following the consumption of pork. *Diabetes Metab Syndr Obes.* (2014) 7:203–10. doi: 10.2147/DMSO.S60382
30. Hasegawa S, Ichiyama T, Sonaka I, Ohsaki A, Okada S, Wakiguchi H, et al. Cysteine, histidine and glycine exhibit anti-inflammatory effects in human coronary arterial endothelial cells. *Clin Exp Immunol.* (2012) 167:269–74. doi: 10.1111/j.1365-2249.2011.04519.x
31. Niu YC, Feng RN, Hou Y, Li K, Kang Z, Wang J, et al. Histidine and arginine are associated with inflammation and oxidative stress in obese women. *Br J Nutr.* (2012) 108:57–61. doi: 10.1017/S0007114511005289
32. Lustgarten MS, Price LL, Phillips EM, Fielding RA. Serum glycine is associated with regional body fat and insulin resistance in functionally-limited older adults. *PLoS One.* (2013) 8:e84034. doi: 10.1371/journal.pone.0084034
33. Forouhi NG, Koulman A, Sharp SJ, Imamura F, Kröger J, Schulze MB, et al. Differences in the prospective association between individual plasma phospholipid saturated fatty acids and incident type 2 diabetes: the EPIC-InterAct case-cohort study. *Lancet Diabetes Endocrinol.* (2014) 2:810–8. doi: 10.1016/S2213-8587(14)70146-9
34. Tillin T, Hughes AD, Wang Q, Würtz P, Ala-Korpela M, Sattar N, et al. Diabetes risk and amino acid profiles: cross-sectional and prospective analyses of ethnicity, amino acids and diabetes in a South Asian and European cohort from the SABRE (Southall And Brent REvisited) Study. *Diabetologia.* (2015) 58:968–79. doi: 10.1007/s00125-015-3517-8
35. Hellmuth C, Kirchberg FF, Lass N, Harder U, Peissner W, Koletzko B, et al. Tyrosine is associated with insulin resistance in longitudinal metabolomic profiling of obese children. *J Diabetes Res.* (2016) 2016:2108909. doi: 10.1155/2016/2108909
36. Wu J, Marklund M, Imamura F, Tintle N, Ardisson Korat AV, de Goede J, et al. Omega-6 fatty acid biomarkers and incident type 2 diabetes: pooled analysis of individual-level data for 39 740 adults from 20 prospective cohort studies. *Lancet Diabetes Endocrinol.* (2017) 5:965–74. doi: 10.1016/S2213-8587(17)30307-8

37. Wittemans L, Lotta LA, Oliver-Williams C, Stewart ID, Surendran P, Karthikeyan S, et al. Assessing the causal association of glycine with risk of cardio-metabolic diseases. *Nat Commun.* (2019) 10:1060. doi: 10.1038/s41467-019-08936-1
38. Feng RN, Niu YC, Sun XW, Li Q, Zhao C, Wang C, et al. Histidine supplementation improves insulin resistance through suppressed inflammation in obese women with the metabolic syndrome: a randomised controlled trial. *Diabetologia.* (2013) 56:985–94. doi: 10.1007/s00125-013-2839-7
39. Jiao J, Liu G, Shin HJ, Hu FB, Rimm EB, Rexrode KM, et al. Dietary fats and mortality among patients with type 2 diabetes: analysis in two population based cohort studies. *BMJ.* (2019) 366:l4009. doi: 10.1136/bmj.l4009
40. Wulan SN, Westerterp KR, Plasqui G. Metabolic profile before and after short-term overfeeding with a high-fat diet: a comparison between South Asian and white men. *Br J Nutr.* (2014) 111:1853–61. doi: 10.1017/S0007114514000014
41. Kim DS, Jackson AU, Li YK, Stringham HM, Kuusisto J, Kangas AJ, et al. Novel association of TM6SF2 rs58542926 genotype with increased serum tyrosine levels and decreased apoB-100 particles in Finns. *J Lipid Res.* (2017) 58:1471–81. doi: 10.1194/jlr.P076034
42. Hammouda S, Ghzaiel I, Khamlaoui W, Hammami S, Mhenni SY, Samet S, et al. Genetic variants in FADS1 and ELOVL2 increase level of arachidonic acid and the risk of Alzheimer's disease in the Tunisian population. *Prostaglandins Leukot Essent Fatty Acids.* (2020) 160:102159. doi: 10.1016/j.plefa.2020.102159
43. Yu B, Li AH, Muzny D, Veeraraghavan N, de Vries PS, Bis JC, et al. Association of rare loss-of-function alleles in HAL, serum histidine: levels and incident coronary heart disease. *Circ Cardiovasc Genet.* (2015) 8:351–5. doi: 10.1161/CIRCGENETICS.114.000697
44. Yadav AK, Sinha N, Kumar V, Bhansali A, Dutta P, Jha V. Association of CTG repeat polymorphism in carnosine dipeptidase 1 (CNDP1) gene with diabetic nephropathy in north Indians. *Indian J Med Res.* (2016) 144:32–7. doi: 10.4103/0971-5916.193280

Conflict of Interest: The authors declare that the research was conducted in the absence of any commercial or financial relationships that could be construed as a potential conflict of interest.

Publisher's Note: All claims expressed in this article are solely those of the authors and do not necessarily represent those of their affiliated organizations, or those of the publisher, the editors and the reviewers. Any product that may be evaluated in this article, or claim that may be made by its manufacturer, is not guaranteed or endorsed by the publisher.

frontiers | Frontiers in Nutrition

TYPE Original Research
PUBLISHED 18 July 2022
DOI 10.3389/fnut.2022.889407

OPEN ACCESS

EDITED BY
Elena Ibañez,
Spanish National Research Council (CSIC), Spain

REVIEWED BY
Mohammad Rizwan Khan,
King Saud University, Saudi Arabia
Jed William Fahey,
Johns Hopkins Medicine, United States

*CORRESPONDENCE
Jifang Zhang
smilehome@163.com

SPECIALTY SECTION
This article was submitted to Nutrition and Food Science Technology, a section of the journal Frontiers in Nutrition

RECEIVED 04 March 2022
ACCEPTED 27 June 2022
PUBLISHED 18 July 2022

CITATION
Mei S, He Z and Zhang J (2022) Identification and analysis of major flavor compounds in radish taproots by widely targeted metabolomics. *Front. Nutr.* 9:889407. doi: 10.3389/fnut.2022.889407

Identification and analysis of major flavor compounds in radish taproots by widely targeted metabolomics

Shiyong Mei[1,2], Zhengjin He[1,2] and Jifang Zhang[1,2]*

[1]Institute of Bast Fiber Crops, Chinese Academy of Agricultural Science, Changsha, China, [2]Center for Southern Economic Crops, Chinese Academy of Agricultural Science, Changsha, China

Radish (*Raphanus sativus* L.) is an important Brassicaceous vegetable crop that is cultivated worldwide. The taste of radish can be described as pungent, sweet, and crisp. At present, the metabolic characteristics leading to differences in radish taste remain unclear, due to the lack of large-scale detection and identification of radish metabolites. In this study, UPLC-MS/MS-based targeted metabolome analysis was performed on the taproots of eight radish landraces. We identified a total of 938 metabolites, and each landrace exhibited a specific metabolic profile, making it unique in flavor and quality. Our results show that taste differences among the taproots of different radish landraces can be explained by changes in composition and abundance of glucosinolates, polyphenols, carbohydrates, organic acids, amino acids, vitamins, and lipids. This study reveals the potential metabolic causes of variation in the taste and flavor of radish taproots.

KEYWORDS

***Raphanus sativus*, metabolite profiling, taste, taproot, landraces**

Introduction

Radish (*Raphanus sativus* L., 2n = 2x = 18) belongs to the *Brassicaceae* family and *Raphanus* genus. It is the most widely cultivated and consumed vegetable in East Asia (China, Japan, and Korea), as well as an important economic crop worldwide. Radish cultivation China has a history of more than 2000 years (1). The long-term evolution, domestication, and artificial selection led to hundreds of distinctive landraces, with variation in root sizes, shapes, colors, and flavors (2). Radish can be used for various purposes. In northern China, some green-skinned radish cultivars, with sweet and crisp flavors, are consumed as fruits (3). In southern China, the red-skinned types, with a pungent taste, are mainly used for food coloring, cosmetics, and the medical industry (4–6). The mild white-skinned types are mainly used for cooking and stewing. Some varieties with low water content and high compact texture can be used for cooking and food processing (3).

Radishes are rich in bioactive metabolites that influence its taste. In previous studies, important secondary metabolites, such as glucosinolates (GS) and flavonoids, have attracted much attention and are characteristic in some unique Chinese radish cultivars

(7–11). Different cultivars and growing conditions resulted in high variation in the profiles and content of these metabolites (8, 11, 12). In addition, fruit and vegetable flavor was greatly affected by the concentrations of carbohydrates, organic acids, and polyphenols (13–15). Studies have shown the compositions and abundance of amino acids also affected the taste (16–18). However, little information is available on the profiles of carbohydrates, amino acids, and organic acids in different radish landraces.

To date, there are few large-scale detection, identification, and quantification methods for the flavor substances in radish taproots. The reported methods mainly focus on high-performance liquid chromatography with diode-array detection (HPLC+DAD), HPLC alone or liquid chromatography-electrospray ionization-mass spectrometry (LC-ESI-MS) (19). Targeted metabolomics analysis, based on ultra-performance liquid chromatography-tandem mass spectrometry (UPLC-MS/MS), is a fast and reliable method for large-scale and comparative metabolomics studies (20).

In this study, we aimed to identify a wide range of metabolites that could contribute to taste variations among radish landraces. The UPLC-MS/MS method was performed to identify and quantify metabolites of eight radish cultivars. These metabolites included glucosinolates, phenolic acids, organic acids, lipids, vitamins, and amino acids et al. Our results provide useful data for clarifying the taste differences among radish cultivars and could further guide breeding research.

Materials and methods

Plant materials and chemicals

One double haploid (DH) line and seven advanced inbred lines of radish landraces were used in this study: Chunchangbai (CHB, DH) from Korea and Chunbulao (CBL) from Guangdong (China) with white skin and fleshed taproot, Shandongqing (SDQ) from Shandong and Jiangsuqing (JSQ) from Jiangsu (China) with green taproot flesh and green skin, Touxinhong (TXH) from Sichuan (China) with dark red skin and fleshed taproot, Nanxiang (NX) from Hubei (China) with green taproot skin and white flesh, Manshenhong (MSH) from Sichan (China) and Xuzhoulaluobo (LL) from Jiangsu (China) with light red taproot skin. CHB has a long cylindrical taproot. SDQ, JSQ, LL and TXH have an average-sized cylindrical taproot. NX, MSH and CBL have short cylindrical or oval taproots (Figure 1). All plants were grown in pots at the Institute of Best Fiber Crops at the Chinese Academy of Agricultural Sciences in December of 2020. Developed taproots (80 d after sowing) were harvested, washed with running tap water, and then cleaned with sterile water. The taproots were cut into pieces and stored at −80°C until further analysis. Each sample consisted of three replicates, and each replicate contained four individual plants.

Gradient grades of methanol, acetonitrile, and formic acid were purchased from Merck Company, Germany (www.merck-chemicals.com). The internal standard L-2-chlorophenylalanine was bought from J&K Scientific Co., Ltd (www.jkchemical.com/).

Sample preparation and extraction

The sliced radish taproots were freeze-dried in a vacuum freeze-dryer (Scientz-100F, Ningbo, China) and then ground with zirconium beads at 30 Hz for 1.5 min (MM 400, Retsch, Haan, Germany). Then, 100 mg homogenized, sieved and lyophilized powder was weighed and dissolved with 1.2 mL 70% methanol extract. The sample was vortex for 30 s every 30 min, six times in total. The mixture was extracted overnight at 4°C. After centrifugation (12,000 rpm, 10 min), the supernatant was absorbed and filtered by SCAA-104 (ANPEL, Shanghai, China) with a 0.22-μm pore size. Then, the supernatant was qualitatified by high resolution mass spectrometry AB SCIEX 6600 QTOF, and AB SciEX 4500 Q TRAP UPLC/MS/MS system.

The fresh juice of each landrace was extracted for soluble solids content measurement using a Brix refractometer (LC-DR-53B, Lichen Co., Ltd., Shanghai, China); pH measurements were recorded using a pH meter (PHS-3C, INESA Scientific Instrument Co., Ltd., Shanghai, China).

UPLC conditions

UPLC was performed on an Agilent SB-C18 column (1.8 μm, 2.1 mm*100 mm). The mobile phase consisted of solvent A (pure water with 0.1% formic acid) and solvent B (acetonitrile with 0.1% formic acid). The samples were separated *via* a solvent gradient program, starting at 95% A and 5% B, followed by a linear gradient of 5% A and 95% B over 9 min, and maintained the final composition for 1 min. A composition of 95% A, 5.0% B was adjusted within 1.10 min and kept for 2.9 min. The flow velocity was set as 0.35 ml per min. The column oven was set to 40°C. The injection volume was 4 μl. Subsequently, the effluent was connected to an ESI-triple Quadrupole Linear Ion Trap (QTRAP)-MS.

ESI-Q TRAP-MS/MS

We used an AB4500 Q TRAP UPLC/MS/MS system, equipped with linear ion trap (LIT) and triple quadrupole (QQQ) for metabolite detection. An ESI Turbo Ion-Spray interface was operated in positive and negative ion modes and controlled by Analyst 1.6.3 software (AB Scitex, Foster City, CA, USA). The ESI source operation parameters were as follows: ion source (turbo spray, 550°C, 5,500 V /−4,500 V); gas I, gas II,

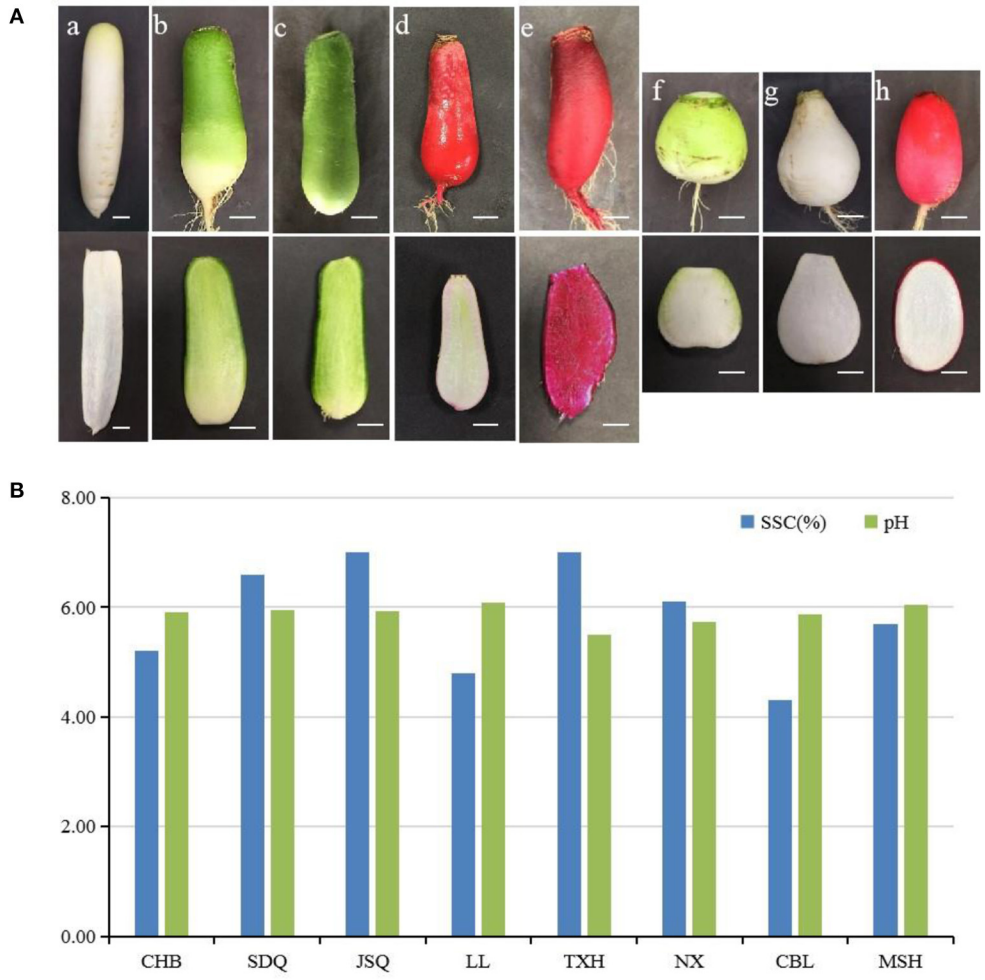

FIGURE 1
(A) Root type characteristics of eight radish landraces. **(a)**, Chunchangbai (CHB); **(b)**, Shandongqing (SDQ); **(c)**, Jiangsuqing (JSQ); **(d)**, Xuzhoulaluobo (LL); **(e)**, Touxinhong (TXH); **(f)**, Nanxiang (NX); **(g)**, Chunbulao (CBL); **(h)**, Manshenhong (MSH). Scale bar = 2 cm. **(B)** Soluble solids content (SSC) and acidity (pH) of eight radish landraces.

and curtain gas were set at 50, 60, and 25.0 psi, respectively. The collision-activated dissociation was set to "high." For QQQ and LIT modes, 10 μmol L^{-1} and 100 μmol L^{-1} polypropylene glycol solutions were used for instrument tuning and mass calibration, respectively. QQQ scans were acquired in the MRM experiments. The collision gas (nitrogen) was set to "medium." For each MRM transition, de-clustering potential (DP) and collision energy (CE) were further optimized. A specific set of MRM transitions were monitored, according to the eluted metabolites at each period.

MS data and statistical analysis

MS data acquisition and processing were conducted based on previous methods (21). Metabolites were annotated based on the self-built database MWDB (Wuhan Metware Biotechnology Co., Ltd., Wuhan, China). Metabolite identification was based on the accurate mass of metabolites, MS2 fragments, MS2 fragments isotope distribution and retention time (RT). Through the company's self-built intelligent secondary spectrum matching method, the secondary spectrum and RT of metabolites in our samples were matched intelligently with the secondary spectrum and RT of the company's database one by one. The MS tolerance and MS2 tolerance were set to 2 ppm and 5 ppm, respectively. Metabolites that did not have standard products were compared with MS2 spectra in public databases or literature. Some of the metabolites without standard secondary spectra were inferred based on experience (22).

The metabolic data were processed using multivariate statistical analysis methods, including unsupervised principal

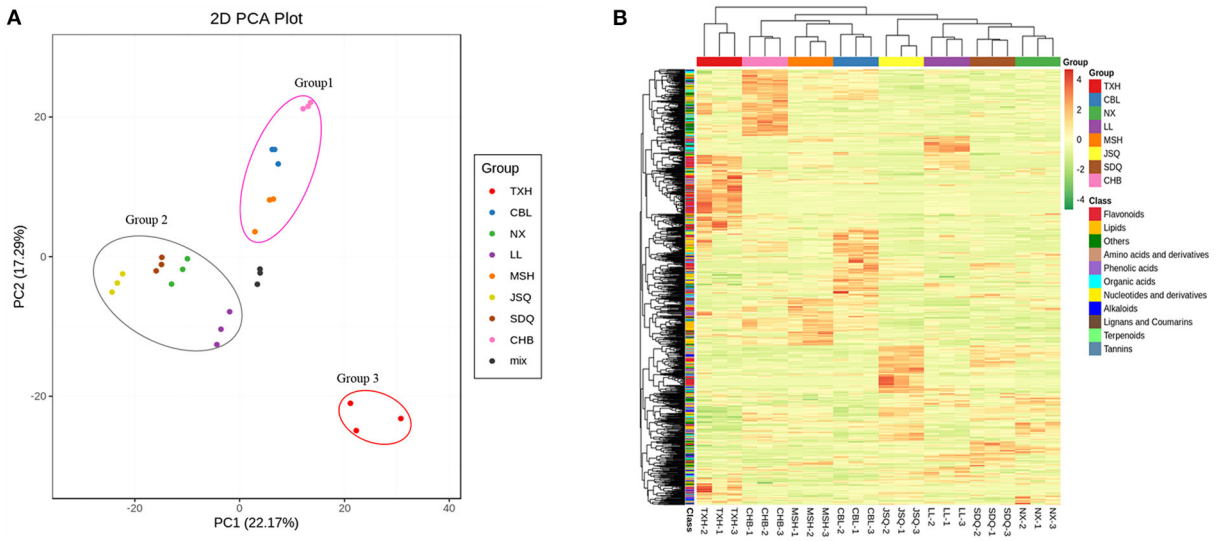

FIGURE 2
PCA **(A)** and heat map visualization **(B)** of the relative differences in the metabolite profiles among different radish landraces. The sampling groups are color-coded as follows: red, TXH; green, NX; blue, CBL; purple, LL; pink, CHB; orange, MSH; yellow, JSQ; brown, SDQ; mix, the mixture of the radish sample extracts. In the heat map, each sample is represented by a column, and each metabolite is displayed in a row. Progressive colors show the enrichment level of each metabolite from low (green) to high (red).

component analysis (PCA), supervised multiple regression orthogonal partial least squares discriminant analysis (OPLS-DA), and hierarchical clustering analysis (HCA). PCA was performed using the statistics function prcomp within R v3.5.1 (www.r-project.org). Logarithmic transformation (log2) was performed on the MS data before OPLS-DA, and the mean was centered. OPLS-DA was carried out using R package MetaboAnalystR. The p and fold change values were 0.05 and 2.0, respectively. HCA was carried out by R package pheatmap. The number of differential metabolites was illustrated by Venn diagrams among radish samples. Using the Kyoto Encyclopedia of Genes and Genomes (KEGG) database, with a p-value < 0.01, the differential metabolites between TXH and the other radish landraces were studied. All data were plotted by GraphPad Prism v6.01 (GraphPad Software Inc., La Jolla, CA, USA).

Results

Morphological and geographical taproot differences

The eight radish landraces were grown under uniform conditions. The morphology of the radish taproots, particularly the shape, color, and sizes, were obviously different (Figure 1A). The soluble solids content (SSC) of radish landraces ranged from 4.3% to 7.0%. CBL had the lowest SSC 4.30%, TXH and JSQ had the highest SSC 7.00% (Figure 1B). The pH of radish landraces ranged from 5.49 to 6.09 (Figure 1B).

Targeted metabolic profiling

To understand the taste differences among radish landraces, targeted metabolite analysis using UPLC–MS/MS was performed to identity comprehensive metabolic profiles of radish taproots. A total of 938 metabolites were identified, including 156 lipids, 87 phenolic acids, 87 organic acids, 118 amino acids, and derivatives that are likely to contribute to radish taste. Other primary and secondary metabolites were also identified (Supplementary Table S1).

Multivariate analysis revealed differences among the identified metabolite profiles

To assess the differences among the metabolite profiles of the eight radish landraces, we performed multivariate statistics. PCA was performed to clarify the internal structure of multiple variables on the 938 metabolites. The mixture of radish sample extracts was used as a quality control (QC) sample. The QC samples gathered in the same area, suggesting that they had similar metabolic profiles, and the analysis was stable and repeatable. The result showed the eight samples were divided into three different groups, indicating that each group had a relatively different metabolic profile. Group 1 included CHB, CBL, and MSH with white-fleshed taproot. Group 2 included JSQ, SDQ, NX, and LL, with green and white-fleshed taproot. Group 3 consisted of TXH with red skin and red-fleshed taproot (Figure 2A).

To remove the effects of quantity on pattern recognition, we performed a log10 transformation on the peak areas of each metabolite and conducted HCA (Figure 2B). This analysis directly reflects the differences in metabolites between and within different groups. TXH, in group 3, was rich in flavonoids and carbohydrates metabolites. CHB, in group 1, was rich in tannins, organic acids, lipids, and other metabolites. MSH was rich in phenolic acids, lipids, and tannins. CBL was rich in flavonoids, lipids, nucleotides, and derivatives. LL, in group 2, was rich in organic acids, flavonoids, amino acids, and derivatives. Thus, the results of the PCA and HCA suggest these eight landraces had distinct metabolite profiles.

Differential metabolite analysis

A pairwise comparison of the eight radish landraces was carried out to determine the metabolites that lead to differences in taste. In OPLS-DA analysis (Supplementary Figures S1A–G), CBL, CHB, JSQ, LL, MSH, NX, and SDQ were clearly separated from TXH, indicating that there are major distinctions in metabolic profiles between different landraces.

To identify differential metabolites among the eight landraces, a fold change $\geq$ 2.0 (higher) or $\leq$ 0.5 (lower) was set, as well as variables identified as important in the projection (VIP $>$ 1) scores, to select metabolites of interest. The screening results are presented as volcano plots (Supplementary Figures S2A–G) and Venn diagrams (Figures 3A–F). For landraces in group 1, there were 343 differential metabolites (148 higher and 195 lower) in CBL, compared to TXH; 346 (139 higher and 207 lower) in CHB, compared to TXH; and 328 (118 higher and 210 lower) in MSH, compared to TXH (Table 1). A total of 55 differential metabolites, including 18 flavonoids, 8 phenolic acids, 6 organic acids, and 6 saccharides and alcohols differed between the three landraces (Figures 3A,D; Supplementary Table S2).

With respect to the landraces involved in group 2, there were 421 differential metabolites (179 higher and 242 lower) in JSQ, compared to TXH; 329 (107 higher and 222 lower) in LL, compared to TXH; 362 (128 higher and 234 lower) in NX, compared to TXH; and 394 (169 higher and 225 lower) in SDQ, compared to TXH (Table 1). A total of 42 differential metabolites, including 26 flavonoids and 5 phenolic acids differed between the four landraces (Figures 3B,E; Supplementary Table S3). Furthermore, a total of 98 different metabolites were found in all eight landraces, including 59 flavonoids, 15 phenolic acids, and 6 alkaloids (Figures 3C,F; Supplementary Table S4).

The 938 differential metabolites among eight landraces were mapped to the KEGG database to obtain detailed information about the metabolic pathways (Supplementary Figures S3A-G). The enrichment analysis of identified metabolites that differ from TXH were mainly involved in flavonoid biosynthesis, phenylpropanoid biosynthesis, flavone and flavonol biosynthesis, and phenylalanine metabolism (Supplementary Table S5).

GS, organic acids, carbohydrates, polyphenols, and amino acids

In this study, we mainly focused on the classes of metabolites considered to be the major contributors of the difference in radish taproot taste. Each category of metabolite was analyzed based on the fold changes $\geq$ 2 or $\leq$ 0.5 and VIP values $>$ 1, compared with that of TXH.

Glucosinolates

GS are sulfur- and nitrogen-containing metabolites common in the order Brassicales, and their degradation products have unique health benefits, as well as pest deterrent properties (23). The content of GS has a great influence on the unique flavor of *Brassica* vegetables, such as turnip (*B. rapa*) and broccoli (*B. oleacrea*) (24, 25). GS can be classified into aliphatic, aromatic, and indole GS, according to their precursor amino acids (26). GS in the taproots significantly affect the pungent taste and quality of fresh radish (23).

In our study, a total of 38 GS was detected, including 25 aliphatic GS, 8 aromatic GS, and 5 indole GS. Based on fold changes and VIP values, the concentration of 4-phenylbutylglucosinolate was most abundant in JSQ, followed by SDQ, CBL, and LL. It was the lowest in TXH. The concentration of sulforaphane was highest in CBL, MSH, and CHB, followed by LL and SDQ. It was the lowest in TXH, NX, and JSQ. The concentration of 2-hydroxy-2-methylpropylglucosinolate was more abundant in TXH, followed by JSQ, LL, MSH, NX, and SDQ. Five kinds of GS, including1-ethyl-2-hydroxyethyl GS, 5-hexenyl GS, gexyl GS, 4-methylpentyl GS, and 3-methylpentyl GS, were most abundant in LL. Nine kinds of GS, including 3-methylbutyl GS, 3-methylsulfinylpropyl GS, 6-sinapoyl-1-thioglucoside of 4-methylthiobut-3-enyl thioglucoside, 7-(methylsulfinyl) heptyl GS, 6-methylsulfinylhexyl GS, 4-hydroxyindol-3-ylmethyl GS, 3-indolylmethyl GS, 4-hydroxy-3-indolylmethyl GS, and 2-methylbutyl GS, were most abundant in SDQ. Five kinds of GS, including 6-(p-hydroxyphenylacrylic acid)-1-GS of 4-methylsulfinyl-3-butenyl thio-glucoside, 2(R)-hydroxy-2-phenylethyl GS, sinalbin, sinigrin, and 3-phenylpropyl GS, were most abundant in CHB (Supplementary Table S6).

Organic acids

We identified 87 organic acids in radish taproots, which could explain the weak acidity (pH5.49–6.04) of radish taproots. Twelve organic acids, including 3-ureidopropionic acid,

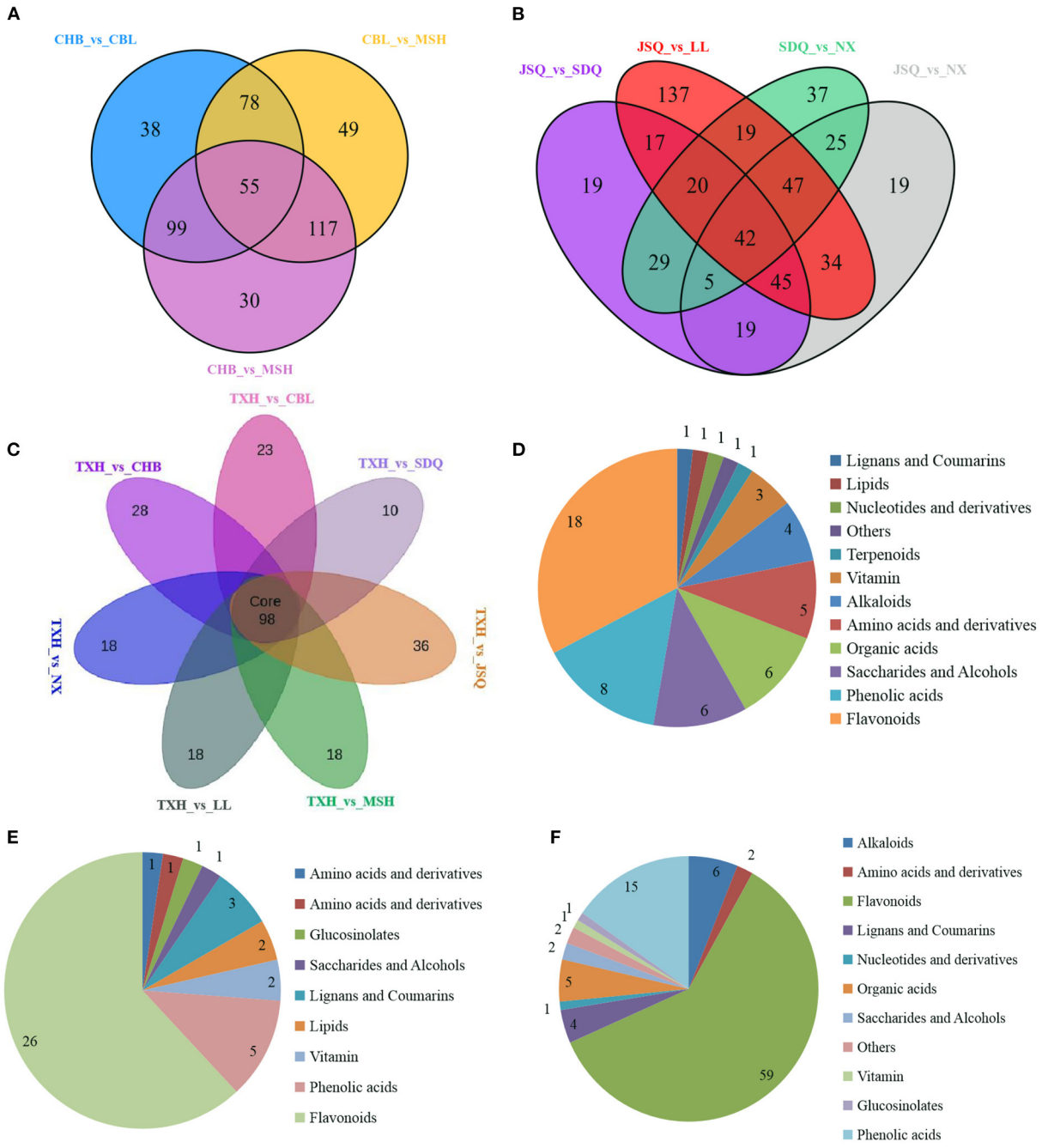

FIGURE 3
Venn diagrams display the overlapping and landrace-specific differential metabolites of group 1 landraces **(A)**, group 2 landraces **(B)** and all eight landraces **(C)**, respectively. Pie charts **(D–F)** show the biochemical categories of the differential metabolites. **(D)** shows the overlap metabolites of group 1 landraces; **(E)** represents the overlap metabolites of group 2 landraces; **(F)** displays the overlap metabolites of eight landraces.

succinic semialdehyde, abscisic acid, 2-hydroxyisocaproic acid, DL-pipecolic acid, methanesulfonic acid, phosphoenolpyruvate, piperonylic acid, L-citramalic acid, glutaric acid, 6-aminocaproic acid, and jasmonic acid were highly abundant and were more prevalent in CHB, compared with the other samples. Twelve organic acids, including 3-methylmalic acid, 2-acetyl-2-hydroxybutanoic acid, 2-propylsuccinic acid, adipic acid, suberic acid, quinic acid, pyrrole-2-carboxylic

10.3389/fnut.2022.889407

TABLE 1 Differential metabolites among the eight landraces.

Metabolite class		TXH_vs_CBL	TXH_vs_CHB	TXH_vs_JSQ	TXH_vs_LL	TXH_vs_MSH	TXH_vs_NX	TXH_vs_SDQ
Alkaloids	up	13	17	17	12	13	13	14
	down	2	8	4	5	6	5	8
Amino acids and derivatives	up	17	24	42	22	18	39	36
	down	8	13	6	5	20	3	8
Flavonoids	up	31	11	46	11	15	13	42
	down	90	95	99	93	97	104	93
Lignans and coumarins	up	12	4	5	3	12	6	5
	down	5	12	5	12	7	9	5
Lipids	up	14	17	17	7	16	7	14
	down	8	7	30	9	10	14	15
Nucleotides and derivatives	up	11	6	8	3	4	1	2
	down	8	10	13	10	11	18	13
Organic acids	up	11	21	16	22	11	13	16
	down	12	11	17	16	10	11	13
Phenolic acids	up	24	12	12	10	18	14	16
	down	28	37	33	41	27	39	39
Tannins	up	0	0	0	0	0	0	0
	down	1	1	1	1	0	0	1
Terpenoids	up	2	0	5	1	1	3	3
	down	1	3	0	0	3	2	0
Others	up	2	1	1	0	2	1	1
	down	2	2	3	2	4	3	4
Saccharides and alcohols	up	3	10	6	10	4	2	4
	down	23	2	20	15	12	17	21
Glucosinolates	up	6	11	0	4	3	9	11
	down	6	1	7	12	1	6	3
Vitamin	up	2	5	4	2	1	7	5
	down	1	5	4	1	2	3	2
Total	up	148	139	179	107	118	128	169
	down	195	207	242	222	210	234	225
	sum	343	346	421	329	328	362	394

acid, 2-methylglutaric acid, 3-hydroxyglutaric acid, methylenesuccinic acid, 2-hydroxyglutaric acid, and pimelic acid, were highly abundant in LL. 2-Hydroxyphenylacetic acid and iminodiacetic acid were most abundant in NX. Six organic acids, including 1-pyrroline-4-hydroxy-2-carboxylic acid, 5-acetamidopentanoic acid, fumaric acid, 1-aminocyclopropane-1-carboxylic acid, 6-aminocaproic acid, and aminomalonic acid, were present in high concentrations, and their concentrations were significantly higher in JSQ. 2-Picolinic acid and isocitric acid were the most abundant in SDQ. Phenylpyruvic acid, phenyllactate, 4-pentenoic acid, and tiglic acid were most abundant in MSH. 2-Hydroxy-3-phenylpropanoic acid, creatine, 2-hydroxyisocaproic acid, and 3-guanidinopropionic acid were most abundant in CBL. Fourteen organic acids, including D-lactic acid, 2-methyl-3-oxosuccinic acid, 2-hydroxyhexadecanoic acid, succinic acid, citric acid, methylmalonic acid, 4-guanidinobutyric acid, 3-hydroxybutyric acid, D-galacturonic acid, malonic acid, (-)-jasmonoyl-L-isoleucine, α-ketoglutaric acid, DL-glyceraldehyde-3-phosphate, and oxalic acid, were most abundant in TXH, compared with the other samples (Supplementary Table S7).

Carbohydrates

We identified 72 carbohydrates in radish taproots. Among these carbohydrates, D-(-)-threose, helecin, 1,6-anhydro-β-D-glucose, D-(+)-cellobiose, D(+)-melezitose, O-rhamnoside, dambonitol, D-arabinose, D-fructose, D-galactaric acid, D-galactose, D-glucose, D-mannose, D-saccharic acid, D-sorbitol, erythrose, gluconic acid, isomaltulose, L-xylose, N-acetyl-D-mannosamine, and raffinose were most abundant and enriched in TXH. Eleven carbohydrates, including 3-phospho-D-glyceric acid, D-fructose-1, 6-biphosphate, D-glucoronic acid, D-glucosamine, D-maltose, D-pinitol, D-saccharic acid, glucose-1-phosphate, N-acetyl-D-glucosamine-1-phosphate, and sedoheptulose, were more prevalent in CHB than the other landraces. 2-Dehydro-3-deoxy-L-arabinonate and D-arabinono-1,4-lactone were more abundant in LL than the other samples. 3-Methyl-1-pentanol, D-melezitose, and L-gulono-1, 4-lactone were more abundant in CBL. Turanose, lactobiose, and D-lactulose were more abundant in MSH. D-Panthenol, maltotriose and ribitol were highly abundant and had accumulated in SDQ. Sucrose-6-phosphate was more prevalent in JSQ and NX than the other samples (Supplementary Table S8).

Polyphenols

Research shows that polyphenols cause bitterness, color, and astringency in beer and other beverages (15). These compounds can be classified as hydroxycinnamic and hydroxybenzoic acid derivatives (phenolic acids), flavanols, flavanol glycosides, and prenylated flavonoids (27). Studies have shown that several phenolics, including ferulic acid, p-coumaric acid, and protocatechuic acid can cause astringency (28). Flavanol monomers, such as catechin and epicatechin, are shown to be more bitter than astringent (29, 30).

In our study, 2-hydroxycinnamic acid was most abundant in MSH and CBL, followed by CHB and SDQ. The lowest concentration was found in TXH and LL. 4-Hydroxybenzoic acid was significantly reduced in CHB, JSQ, LL, NX, and SDQ. 5-Glucosyloxy-2-hydroxybenzoic acid methyl ester was significantly more abundant in LL. 4-O-Glucosyl-4-hydroxybenzoic acid was significantly reduced in CHB, JSQ, LL, MSH, NX, and SDQ. Dihydroferulic acid, ferulic acid, and isoferulic acid were significantly reduced in LL, NX, and SDQ. p-Coumaric acid methyl ester and p-coumaric acid-4-O-glucoside were more abundant in TXH. p-Coumaric acid was most abundant in MSH, followed by CBL and CHB. The lowest concentration was found in LL. Protocatechuic acid-4-O-glucoside was significantly reduced in MSH and SDQ. Epicatechin was abundant in MSH, CBL, CHB, NX, JSQ, LL, and SDQ but absent in TXH. Catechin gallate was most abundant in MSH, followed by CBL, JSQ, and LL. Epicatechin gallate was significantly enriched in NX (Supplementary Table S9).

Amino acids

We identified 118 amino acids in the radish taproots. Among them, 34 were most abundant in JSQ, including 3-cyano-L-alanine, 5-oxo-L-proline, 5-oxoproline, cis-4-hydroxy-D-proline, cyclo (Phe-Glu), cycloleucine, DL-tryptophan, L-allo-isoleucine, L-arginine, L-arginine (hydrochloride), L-aspartic acid, L-azetidine-2-carboxylic acid, L-citrulline, L-cystine, L-glutamine, L-homomethionine, L-isoleucine, L-leucine, L-methionine, L-norleucine, L-ornithine, L-phenylalanine, L-tryptophan, L-valine, L-γ-glutamyl-L-leucine, N-acetyl-DL-phenylalanine, N-acetyl-L-tyrosine, N-alpha-acetyl-L-asparagine, nicotianamine, N-α-acetyl-L-ornithine, trans-4-hydroxy-L-proline, γ-glutamyl-L-valine, γ-glutamylmethionine and γ-glutamylphenylalanine. Seven amino acids, such as 10-formyltetrahydrofuran, 5-aminovaleric acid, L-glutamine-O-glycoside, L-homocitrulline, methiin, N-acetyl-beta-alanine and S-adenosylmethionine were highly abundant and prevalent in CHB. Seven amino acids, including 2, 6-diaminooimelic acid, histamine, L-lysine, L-tyrosine, S-methyl-L-cysteine, γ-glutamyltyrosine, and γ-L-glutamyl-S-methyl-L-cysteine were most abundant in NX. Five amino acids, including 1-methylpiperidine-2-carboxylic acid, cyclo (Ala-Gly), L-isoleucyl-L-aspartate, L-prolyl-L-leucine and N-acetyl-L-aspartic acid were most significantly enriched in CBL. Three amino acids, including L-aspartic acid-O-diglucoside, L-cysteine, and L-proline, were most abundant in SDQ. Three amino acids, including N6-acetyl-L-lysine, N-acetyl-L-phenylalanine, and trimethyllysine, were most significantly enriched in MSH. Nicotinuric acid, N-acetyl-L-threonine, S-(5'-Adenosyl)-L-methionine chloride, and γ-Glu-Cys were most abundant in LL. S-allyl-L-cysteine was most abundant in TXH (Supplementary Table S10).

Vitamin

We identified 24 vitamins in radishes. Among these vitamins, thiamine (vitamin B1) was highly abundant in CHB. Dehydroascorbic acid and pyridoxine-5'-O-glucoside were most abundant in JSQ, followed by CHB, NX, and SDQ. 4-Pyridoxic acid-O-glucoside, D-pantothenic acid, calcium pantothenate, and 4-pyridoxic acid were most abundant in NX. Biotin was the most abundant in LL (Supplementary Table S11).

Lipids

Lipids provide energy, give special flavor and taste to food, and are essential substances in human health. In this study, we identified 76 lipids. Based on fold changes and VIP values, nine lipids, including lysoPE 15:1 (2n isomer), lysoPC 17:2, lysoPC 18:1 (2n isomer), lysoPC 15:1, lysoPC 14:0, docosanoic acid, lysoPC 18:2 (2n isomer), lysoPC

18:2 and lysoPC 18:1, were most abundant in MSH. Nine lipids, including 2R-hydroxy-9Z, 12Z, 15Z-octadecatrienoic acid, 3S-hydroxy-9Z, 11E, 15Z-octadecatrienoic acid, lysoPE 16:0 (2n isomer), lysoPC 15:0, lysoPC 12:0, lysoPC 16:0, LysoPE 15:0 (2n isomer), lysoPC 15:0 (2n isomer), and 9, 12, 13-TriHOME, were most abundant in CHB. Eight lipids, including 9, 10, 11-trihydroxy-12-octadecenoic acid, 7S, 8S-DiHODE, 13-KODE, 12, 13-DHOME, (9Z, 11E)-octadecadienoic acid, 9-hydroxy-10, 12, 15-octadecatrienoic acid, and 9, 10, 13-trihydroxy-11-octadecenoic acid, were most abundant and accumulated in CBL. Eight lipids, including 1-α-linolenoyl-glycerol-2, 3-di-O-glucoside, 2-α-linolenoyl-glycerol-1-O-glucoside, 1-α-linolenoyl-glycerol-3-O-glucoside, 2-linoleoylglycerol, choline alfoscerate, linoleic acid, 1-oleoyl-Sn-glycerol, and 4-Oxo-9Z, 11Z, 13E, 15E-octadecatetraenoic acid, were most enriched in JSQ. Six lipids, including PE (oxo-11:0/16:0), 2-linoleoylglycerol-1, 3-di-O-glucoside, 2-linoleoylglycerol-1-O-glucoside, 1-linoleoylglycerol-3-O-glucoside, 1-(9Z-octadecenoyl)-2-(9-oxo-nonanoyl)-sn-glycero-3-phosphocholine and 2-aminoethylphosphonic acid, were most abundant in SDQ. 2-α-Linolenoyl-glycerol and 1-α-linolenoyl-glycerol were most abundant in NX. Ethyl 9-hydroxy-10, 12-octadecadienoic acid was most abundant in LL (Supplementary Table S12).

Discussion

Radish is an important economic crop worldwide. Previous studies on radish metabolites mainly focused on specific classes of metabolites, such as glucosinolates, anthocyanin and flavonoids (8, 11, 31–33). However, the differences in metabolic profiles of radish cultivars have not been fully understood until now. In this study, we performed a UPLC-MS/MS-based targeted metabolomic analysis to understand the differences in taste between eight representative landraces, with various shape, color, and uses. A total of 938 metabolites were identified, and more than 300 metabolites were significantly and differentially accumulated in TXH and the other landraces. Therefore, this study provides novel insights for understanding the taste differences among the taproots of different radish landraces.

Each landrace has a specific metabolic profile, making it unique in taste and different in use. TXH with red skin and red flesh, is widely used in food coloring and pigment extraction industries. In our study, 19 anthocyanins (such as pelargonidin- and cyanidin-based derivatives) were significantly abundant in TXH, which was consistent with a previous study (11). Furthermore, 21 carbohydrates and 14 organic acids were significantly enriched in TXH, which contribute to the desirable taste with slight sweet and sour flavors (Brix 7.00%, pH 5.49) (Supplementary Tables S6–12).

MSH and LL, with red taproot skin, are widely used in kimchi and cooking. In our study, 9 lipids, 4 organic acids, 3 amino acid, 3 polyphenols, 3 carbohydrates, and 3 amino acids were significantly abundant in MSH, making it distinctive from the other landraces. Twelve organic acids, 5 GS, 4 amino acids, 2 sugars, 1 lipid, and biotin were most abundant in LL, which could explain the slightly pungent taste (Brix 4.80%, pH 6.09) (Supplementary Tables S6–12).

CHB and CBL, both with white skin and white flesh, are widely used in cooking and stewing. In our study, 12 kinds of organic acids, 11 carbohydrates, 9 lipids, 7 amino acids, and 5 GS were most abundant in CHB, which contribute to its sweet and sour taste (Brix 5.20%, pH 5.91). Eight lipids and three carbohydrates were most abundant in CBL, resulting in a mild taste (Brix 4.30%, pH 5.87) (Supplementary Tables S6–12).

SDQ and JSQ with green skin and green flesh are widely used as fruits and vegetables. In our study, 9 GS, 6 lipids, 3 carbohydrates, 3 amino acids, and 2 organic acids were significantly abundant and accumulated in SDQ, which results in a strong pungent and crisp taste (Brix 6.60%, pH 5.94). Thirty-four amino acid, 8 lipids, 6 organic acids, and 2 vitamins were most abundant in JSQ, contributing to its sweet and crisp flavors (Brix 7.00%, pH 5.93) (Supplementary Tables S6–12). NX, with green-white skin and flesh, is widely used in cooking and processing. In our study, 7 amino acids, 4 vitamins, 2 lipids, and 2 organic acids were most abundant in NX, which impart a light sweet crisp taste (Brix 6.10%, pH 5.74) (Supplementary Tables S6–12).

Conclusions

In this study, UPLC-MS/MS-based metabolic analysis was performed successfully to systematically compare taste differences between the taproot of TXH and the other landraces. This work provides new insights into the differences in compositions and abundances of metabolites in radish taproot. We proposed that the difference in composition and concentrations of glucosinolates, carbohydrates, organic acids, amino acids, polyphenols, vitamins, and lipids might be the underlying causes of the differences in taste among the taproot of different radish landraces.

Data availability statement

The original contributions presented in the study are included in the article/Supplementary Material, further inquiries can be directed to the corresponding author.

Author contributions

Conceptualization, writing–original draft, and writing–review and editing: JZ and SM. Vol data analysis: ZH. All authors contributed to the article and approved the submitted version.

Funding

This work was supported by the National Key Research and Development Program of China (No. 2017YFD0101806), the Agricultural Talents Program of the Chinese Academy of Agricultural Sciences (No. CAASQNYC-KYYJ-38), the Natural Science Foundation of Hunan Province (No. 2020JJ5642), and the Central Public-interest Scientific Institution Basal Research Fund (No. 1610242021008).

Acknowledgments

We thank Wuhan Metware Biotechnology Co., Ltd (Wuhan, China) and LetPub (www.letpub.com) for its linguistic assistance during the preparation of this manuscript.

Conflict of interest

The authors declare that the research was conducted in the absence of any commercial or financial relationships that could be construed as a potential conflict of interest.

Publisher's note

Supplementary material

The Supplementary Material for this article can be found online at: https://www.frontiersin.org/articles/10.3389/fnut.2022.889407/full#supplementary-material

References

1. Li S. The origin and resources of vegetable crops in China. In: *International Symposium on Horticultural Germplasm, Cultivated and Wild, Sept 1988.* Beijing: International Academic Publishers (1989). p. 197–202.

2. Zhang X, Yue Z, Mei S, Qiu Y, Yang X, Chen X, et al. A de novo genome of a Chinese radish cultivar. *Hortic Plant J.* (2015) 1:155–64. doi: 10.16420/j.issn.2095-9885.2016-0028

3. Zhang L, Wang Q. DNA polymorphism and genetic diversity in raphanus accessions. In: *The Radish Genome*. Cham: Springer (2017). p. 71–91.

4. Giusti MM, Wrolstad RE. Characterization of red radish anthocyanins. *J Food Sci.* (1996) 61:322–6. doi: 10.1111/j.1365-2621.1996.tb14186.x

5. Giusti MM, Wrolstad RE. Radish anthocyanin extract as a natural red colorant for maraschino cherries. *J Food Sci.* (1996) 61:688–94. doi: 10.1111/j.1365-2621.1996.tb12182.x

6. Chen F, Xing C, Huo S, Cao C, Yao Q, Fang P. Red pigment content and expression of genes related to anthocyanin biosynthesis in radishes (Raphanus sativus L) with different colored flesh. *J Agric Sci.* (2016) 8:126. doi: 10.5539/jas.v8n8p126

7. Giusti M, Ghanadan H, Wrolstad R. Elucidation of the structure and conformation of red radish (*Raphanus sativus*) anthocyanins using one-and twodimensional nuclear magnetic resonance techniques. *J Agric Food Chem.* (1998) 46:4858–63. doi: 10.1021/jf980695b

8. Jing P, Zhao SJ, Ruan SY, Xie ZH, Dong Y, Yu LL. Anthocyanin and glucosinolate occurrences in the roots of Chinese red radish (Raphanus sativus L), and their stability to heat and pH. *Food Chem.* (2012) 133:1569–76. doi: 10.1016/j.foodchem.2012.02.051

9. Ishida M, Nagata M, Ohara T, Kakizaki T, Hatakeyama K. Nishio T. Small variation of glucosinolate composition in Japanese cultivars of radish (Raphanus sativus L) requires simple quantitative analysis for breeding of glucosinolate component. *Breed Sci.* (2012) 62:63–70. doi: 10.1270/jsbbs.62.63

10. Han N, Su'udi M, Kim J. The major aliphatic glucosinolate content in Korean radish during vegetative and reproductive growth. *Hortic Environ Biotechnol.* (2015) 56:152–8. doi: 10.1007/s13580-015-0100-7

11. Zhang J, Qiu X, Tan Q, Xiao Q, Mei S. A comparative metabolomics study of flavonoids in radish with different skin and flesh colors (Raphanus sativus L). *J Agric Food Chem.* (2020) 68:14463–70. doi: 10.1021/acs.jafc.0c05031

12. Schreiner M, Huyskens-Keil S, Peters P, Schonhof I, Krumbein A, Widell S. Seasonal climate effects on root colour and compounds of red radish. *J Sci Food Agric.* (2002) 82:1325–33. doi: 10.1002/jsfa.1189

13. Malundo TMM, Shewfelt RL. Scott JW. Flavor quality of fresh tomato (Lycopersicon esculentum Mill) as affected by sugar and acid levels. *Postharvest Biol Technol.* (1995) 6:103–10. doi: 10.1016/0925-5214(94)00052-T

14. Chen FX, Liu XH. Chen LS. Developmental changes in pulp organic acid concentration and activities of acid-metabolising enzymes during the fruit development of two loquat (Eriobotrya japonica Lindl) cultivars differing in fruit acidity. *Food Chem.* (2009) 114:657–64. doi: 10.1016/j.foodchem.2008.10.003

15. Collin S, Jerkovic V, Brohan M, Callemien D. Polyphenols and beer quality. In: Ramawat, KG, Mérillon, J, editors. *Natural Products: Phytochemistry, Botany and Metabolism of Alkaloids, Phenolics and Terpenes*. Springer (2013). p. 2333–2359.

16. Choi SH, Ahn JB, Kim HJ, Im NK, Kozukue N, Levin CE, et al. Changes in free amino acid, protein, and flavonoid content in Jujube (Ziziphus jujube) fruit during eight stages of growth and antioxidative and cancer cell inhibitory effects by extracts. *J Agric Food Chem.* (2012) 60:10245–55. doi: 10.1021/jf302848u

17. Zhang H, Wang ZY, Yang X, Zhao HT, Zhang YC, Dong AJ, et al. Determination of free amino acids and 18 elements in freeze-dried strawberry and blueberry fruit using an amino acid analyzer and ICP-MS with microwave digestion. *Food Chem.* (2014) 147:189–94. doi: 10.1016/j.foodchem.2013.09.118

18. Phillips SM, Fulgoni VL, Heaney RP, Nicklas TA, Slavin JL, Weaver CM. Commonly consumed protein foods contribute to nutrient intake, diet quality, and nutrient adequacy. *Am J Clin Nutr.* (2015) 101:1346S–52. doi: 10.3945/ajcn.114.084079

19. Gamba M, Asllanaj E, Raguindin PF, Glisic M, Franco OH, Minder B, et al. Nutritional and phytochemical characterization of radish (Raphanus sativus): a systematic review. *Trends Food Sci Technol.* (2021) 113:205–18. doi: 10.1016/j.tifs.2021.04.045

20. Chen W, Gong L, Guo Z, Wang W, Zhang H, Liu X, et al. A novel integrated method for large-scale detection, identification, and quantification of widely targeted metabolites: application in the study of rice metabolomics. *Mol Plant.* (2013) 6:1769–80. doi: 10.1093/mp/sst080

21. Xiao J, Gu C, He S, Zhu D, Huang Y. Zhou Q. Widely targeted metabolomics analysis reveals new biomarkers and mechanistic insights on chestnut (Castanea mollissima Bl) calcification process. *Food Res Int.* (2021) 141:110128. doi: 10.1016/j.foodres.2021.110128

22. Zhu G, Wang S, Huang Z, Zhang S, Liao Q, Zhang C, et al. Rewiring of the fruit metabolome in tomato breeding. *Cell.* (2018) 172:249–61. doi: 10.1016/j.cell.2017.12.019

23. Kakizaki T, Ishida M. Genetic profile of glucosinolate biosynthesis. In: *The Radish Genome*. Cham: Springer (2017). p. 137–150.

24. Padilla G, Cartea ME, Velasco P, de Haro A, Ordás A. Variation of glucosinolates in vegetable crops of *Brassica rapa*. *Phytochemistry.* (2007) 68:536–45. doi: 10.1016/j.phytochem.2006.11.017

25. Schonhof I, Krumbein A, Brückner B. Genotypic effects on glucosinolates and sensory properties of broccoli and cauliflower. *Food/Nahrung.* (2004) 48:25–33. doi: 10.1002/food.200300329

26. Halkier BA, Gershenzon J. Biology and biochemistry of glucosinolates. *Annu Rev Plant Biol.* (2006) 57:303–33. doi: 10.1146/annurev.arplant.57.032905.105228

27. Goiris K, Jaskula-Goiris B, Syryn E, Van Opstaele F, De Rouck G, Aerts G, et al. The flavoring potential of hop polyphenols in beer. *J Am Soc Brew Chem.* (2014) 72:135–42. doi: 10.1094/ASBCJ-2014-0327-01

28. Callemien D, Collin S. Structure, organoleptic properties, quantification methods, and stability of phenolic compounds in beer—a review. *Food Rev Int.* (2009) 26:1–84. doi: 10.1080/87559120903157954

29. Drewnowski A, Gomez-Carneros C. Bitter taste, phytonutrients, and the consumer: a review. *Am J Clin Nutr.* (2000) 72:1424–35. doi: 10.1093/ajcn/72.6.1424

30. Peleg H, Gacon K, Schlich P, Noble AC. Bitterness and astringency of flavan-3-ol monomers, dimers and trimers. *J Sci Food Agric.* (1999) 79:1123–8. doi: 10.1002/(SICI)1097-0010(199906)79:8<1123::AID-JSFA336>3.0.CO;2-D

31. Ishida M, Kakizaki T, Ohara T, Morimitsu Y. Development of a simple and rapid extraction method of glucosinolates from radish roots. *Breed Sci.* (2011) 61:208–11. doi: 10.1270/jsbbs.61.208

32. Park NI, Xu H, Li X, Jang IH, Park S, Ahn GH, et al. Anthocyanin accumulation and expression of anthocyanin biosynthetic genes in radish (*Raphanus sativus*). *J Agric Food Chem.* (2011) 59:6034–9. doi: 10.1021/jf200824c

33. Yi G, Lim S, Chae WB, Park JE, Park HR, Lee EJ, et al. Root glucosinolate profiles for screening of radish (Raphanus sativus L) genetic resources. *J Agric Food Chem.* (2016) 64:61–70. doi: 10.1021/acs.jafc.5b04575

frontiers | Frontiers in Nutrition

TYPE Original Research
PUBLISHED 22 July 2022
DOI 10.3389/fnut.2022.901944

OPEN ACCESS

EDITED BY
Cristina Garcia-Viguera,
Spanish National Research Council (CSIC), Spain

REVIEWED BY
Kemal Aganovic,
German Institute of Food Technologies, Germany
Jed William Fahey,
Johns Hopkins Medicine, United States

*CORRESPONDENCE
Luca Campone
luca.campone@unimib.it

SPECIALTY SECTION
This article was submitted to Nutrition and Food Science Technology, a section of the journal Frontiers in Nutrition

RECEIVED 22 March 2022
ACCEPTED 27 June 2022
PUBLISHED 22 July 2022

CITATION
Pagliari S, Giustra CM, Magoni C, Celano R, Fusi P, Forcella M, Sacco G, Panzeri D, Campone L and Labra M (2022) Optimization of ultrasound-assisted extraction of naturally occurring glucosinolates from by-products of *Camelina sativa* L. and their effect on human colorectal cancer cell line. *Front. Nutr.* 9:901944. doi: 10.3389/fnut.2022.901944

Optimization of ultrasound-assisted extraction of naturally occurring glucosinolates from by-products of *Camelina sativa* L. and their effect on human colorectal cancer cell line

Stefania Pagliari[1], Chiara Maria Giustra[1], Chiara Magoni[1], Rita Celano[2], Paola Fusi[1], Matilde Forcella[1], Grazia Sacco[1], Davide Panzeri[1], Luca Campone[1]* and Massimo Labra[1]

[1]Department of Biotechnology and Biosciences, University of Milano-Bicocca, Milan, Italy, [2]Department of Pharmacy, University of Salerno, Fisciano, Italy

The food waste generated by small and medium agro-industrial enterprises requires appropriate management and valorization in order to decrease environmental problems and recover high-value products, respectively. In this study, the *Camelina sativa* seed by-product was used as a source of glucosinolates. To begin, the chemical profile of the extract obtained using an international organization for standardization (ISO) procedure was determined by UPLC-HRMS/MS analysis. In addition, an extraction method based on ultrasound-assisted extraction was developed as an alternative and green method to recover glucosinolates. Main parameters that affect extraction efficiency were optimized using a response surface design. Under optimized conditions, the extract showed an improvement in extraction yield with a reduction in organic solvent amount compared to those obtained using the ISO procedure. Finally, the extract obtained with the ultrasound-assisted method was purified, tested on human colorectal cancer cell lines, and showed promising results.

KEYWORDS

***Camelina sativa* L., ultrasound-assisted extraction (USAE), experimental design optimization, human colorectal cancer cell line, recovery bioactive compounds, glucosinolates derivatives, food by-products**

Introduction

Several epidemiological studies suggest a relationship between cruciferous vegetable intake and risk of several types of cancer. Higher intakes of cruciferous vegetables (more than three servings per week) have been associated with significant reductions in the risk of lung, stomach, and colorectal cancers, and with less

consistent reductions in the risk of prostatic, endometrial, and ovarian cancers (1–4). Recent studies indicate that glucosinolates and their breakdown products including indoles and isothiocyanates have a beneficial health effect and may contribute to reduction of neurodegenerative and cardiovascular diseases when taken as part of the diet [(5–7); Le (8, 9)]. Glucosinolates (GLSs) are secondary metabolites produced by cruciferous plants. They accumulate at a high concentration in many species belonging to the Brassicaceae family. Nowadays more than 120 different glucosinolates have been identified in many plants such as mustard, cabbage, cauliflower, broccoli, and radish. The composition and concentration of GLSs have been shown to vary from one species to another and in a single variety depending on plant environment, crop conditions, age, and health (10–12). GLSs play an important role in plant protection (13, 14). In fact, these compounds remainin active unless they interact with an enzyme called myrosinase, which converts them into glucose and aglycones first and then into other molecules such as nitriles or isothiocyanates (15). The glucosinolate-myrosinase system is used as defense against the aggression of external plants, and for these reasons GLSs are also used as natural pesticide and biofumigation agents (16, 17). Different chemical and biological properties are the reason why these plant secondary metabolites attract the attention of several researchers (18). *Camelina sativa* L. is one of the plants in which GLSs are found. *C. sativa* appears to be an interesting agricultural crop because of its good oil yield with an omega-3 fatty acid content, which makes it a promising alternative source of essential fatty acids (19). *C. sativa* seed-press cake (PC) represents a co-product of a food chain particularly rich in interesting compounds such as glucosinolates, which could be used in the pharmaceutical, cosmetics, and food industries and whose valorization makes the entire supply chain environmentally and economically sustainable (19). However, in order to exploit *Camelina sativa* PC as a source of bioactive compounds, it is necessary to develop adequate extraction methods to reduce time, cost, and environmental pollution (20). Current GLS extraction methods involve several time-consuming and potentially hazardous steps. These steps are lyophilization, tissue disruption, and a long and laborious extraction protocol involving double extraction with boiling aqueous methanol.

In this study, a green extraction procedure was developed for recovery of glucosinolate compounds from by-products of *C. sativa* seeds. Initially, the international standard method ISO9167-1 (21) usually used for GLS extraction in order to obtain a reference extract characterized by ultra-pressure liquid chromatography (UPLC) coupled with a high-resolution mass spectrometry (HRMS) detector. After the chemical characterization, an extraction method based on ultrasound assisted (USA) technology using green solvents (water and ethanol) was developed. The main parameters of ultrasound-assisted solid liquid extraction (USAE) were carefully optimized using an experimental design to improve the extraction efficiency and reduce the consumption of organic solvents. Under optimized extraction conditions, the developed method demonstrated better efficiency than those obtained using the ISO procedure. Furthermore, a rapid procedure based on solid phase extraction (SPE) was applied on the USA extract to purify and concentrate glucosinolate compounds. Finally, the anticancer activity of the purified extract was measured *in vitro* on human colorectal cancer cell lines by viability assay to evaluate putative nutraceutical properties. Enriched glucosinolate fractions displayed selective cytotoxic activities against tumor cell lines but not against healthy lines and showed promising results for future studies.

Materials and methods

Standards and materials

MS-grade solvents used for UPLC analysis, acetonitrile (MeCN) water (H_2O), and formic acid (HCOOH), were provided by Romil (Cambridge, United States); analytical-grade solvents methanol (MeOH) and ethanol (EtOH) were supplied by Sigma-Aldrich (Milan, Italy). Water was purified using a Milli-Q system (Millipore, Bedford, United States). Acetic acid (Sigma-Aldrich) and ammonium hydroxide solution were provided by Sigma-Aldrich (Milan, Italy). Glucoarabinin potassium salt, glucocamelinin potassium salt, and homoglucocamelinin potassium salt were purchased from Extrasynthese (Lyon, France). Stock standard solutions (1 mg ml^{-1}) of each compound were prepared using methanol and stored at 4°C. Diluted solutions and mixtures were made in MeOH:H_2O 1:1, (v:v).

Samples

Camelina sativa PC was supplied by FlaNat Research srl (Milan, Italy). After cold oil extraction, the PC by-product was immediately finely blended using a knife mill, Grindomix GM-200 (Restek GmbH, Germany) operated at 6,000 rpm for about 30 short cycles of approximately 15 s each to prevent the samples from heating. The ground samples were sieved through a test sieve in the range of 300–600 μm to obtain a powder with homogeneous particle size distribution and stored in the dark at -80°C in polyethylene bags until analysis.

Optimization of ultrasound-assisted extraction

Extraction of GLS compounds from PC was performed by ultrasound-assisted solid liquid extraction (USAE). For

each extraction, 1 g of finely ground sample was placed in a 50-ml polypropylene tube, and an extraction solvent was added to the sample. Then, the tube was gently shaken by hands for a few seconds and immersed in an ultrasonic bath (frequency 35 kHz; power 60–120 W; Sonorex TK 52; Bandelin electronic, Berlin, Germany). During the extraction, the temperature of the water bath was continuously monitored and adjusted to maintain a constant temperature of 30°C. At the end of each extraction cycle, lasting 5 min for each, the samples were centrifuged (ALC centrifuge PK 120; Thermo Electro Corporation, San Jose, CA, United States) at 19.8 g. The supernatant was collected with a Pasteur pipette, filtered (Whatman No. 1 filter), and analyzed by UPLC-HRMS. To select the best extraction conditions, a central composite experimental design (CCD) was performed using Statgraphic Centurion XVI Version 16.1 (Rockville, MD, United States). The effect of four independent factors on extraction efficiency and the total amount of EtOH were studied through an experimental design. The range for each factor was selected by preliminary experiments. In particular, a response surface Box-Behnken design 2-factor interaction was carried out considering three variables at three different levels (low, medium, and high): solvent volume (vol) at 5, 10, and 15 ml; number of cycles (n°) 2, 3, and 4; and composition of solvent (EtOH%) 40, 60, and 80%. Four response variables were individually considered in the optimization of the extraction conditions: the extraction yield of each GLS was expressed as μg $g^{-1}$of dry matter (ug/g DM) and total ethanol used (ml). A total of 16 experiments (16 points of the factorial design, 4 center points, and 6 freedom degrees) were carried out in a randomized run. Optimal experimental conditions that independently maximized extraction efficiency and minimized the total amount of EtOH used were obtained from a fitted model. Analysis of variance (ANOVA) was conducted to evaluate the statistical significance of independent variable contributions and their first-order interactions. The experimental matrix design, with the experimental conditions of each independent variables, and the results of experimental GLS extraction yield (μg/gDM) and total EtOH used (ml) from 16 selected combinations of the independent variables, are reported in Table 1.

Purification of glucosinolates by solid-phase extraction

A solid-phase extraction procedure was developed in order to obtain an extract rich in GLSs and to perform cellular assays. Briefly, strong anion exchange (SAX) Mega Bond Elute NH_2 cartridges (1 g) were activated with methanol and equilibrated with 1% acetic acid in water. The ultrasound-assisted solid liquid extract was loaded onto an NH_3^+ cartridge and washed with 5 ml of MeOH 1% acetic acid; finally, the glucosinolate fraction was eluted with 10 ml of freshly prepared H_2O 2% NH_4OH solution. The purified extract was evaporated to dryness in a vacuum evaporator at 40°C, dissolved in water at a concentration of 1 mg ml^{-1}, and filtered with a 22-μm PES filter before cellular assays.

TABLE 1 Experimental conditions of the response surface design and experimental values of the response variables.

	Independent variables			Response variables			
Experimental condition	EtOH (%)	Volume (mL)	Cycles (n°)	Glucoarabinin (μg/gDM)	Glucocamelinin (μg/gDM)	Homoglucocamelinin (μg/gDM)	Tot EtOH (mL)
1	40	5	3	493	1047	215	6
2	60	5	2	911	1984	387	6
3	80	10	2	832	1900	380	16
4	40	10	4	264	443	178	16
5	80	5	3	981	2234	428	12
6	80	10	4	1268	2981	568	32
7	80	15	3	1417	3240	631	36
8	40	10	2	526	1181	222	8
9	60	15	2	1304	3046	562	18
10	60	10	3	1166	2722	501	18
11	60	10	3	1221	2773	510	18
12	60	10	3	1269	2855	532	18
13	40	15	3	274	408	183	18
14	60	10	3	1142	2649	490	18
15	60	5	4	1180	2553	463	12
16	60	15	4	1354	2910	601	36

Qualitative and quantitative analyzes by high-resolution mass spectrometry (HRMS)/MS analysis

Qualitative and quantitative analyzes of GLSs were carried out using an acquity UPLC system coupled with a Xevo G2-XS QT mass spectrometer (Waters Corp., Milford, MA, United States). The mass spectrometer equipped with an electrospray ion source (ESI) was used in negative and positive ionization modes to acquire full-scan MS, and spectra were recorded in the range of 50–1,000 m/z. The source parameters were as follows: electrospray capillary voltage 2 kV, source temperature 150°C, and desolvation temperature 600°C. The cone and desolvation gas flow was 20 and 900 L h^{-1}, respectively, and a scan time of 0.3 s was employed. Cone voltage was set at 70 V and source offset at 20. The mass spectrometer was calibrated with 0.5 M sodium formate, and 100 pg $\mu l^{-1}$of standard leucine-enkkephaline at m/z 554.2615 was infused with the flow of column at 5 μl min^{-1} as the lock mass and acquired for 1 s every 30 s. The total ion current (TIC) used for qualitative analysis was acquired, and an MS/MS spectrum of each compound at different collision energy was acquired and compared to reference standards on which GLS identification was performed. A quantitative analysis was performed using multiple reaction monitoring (MRM) data acquisition mode and by monitoring three characteristic fragments for each target compounds of the [M + H]-ion of glucoarabinin (506.1523 > 442.14, 248.11, and 96.96) glucocamelinin (520.1684 > 456.16, 262.12, and 96.96), and homoglucocamelinin (534.1819 > 470.18, 276.14, and 96.96) and ramping collision energy from 25 to 30 V to produce abundant product ions before detection. In order to quantify the GLS compounds in the extracts, an external standard calibration was conducted six points between 0.01 and 10 μgmL^{-1}. Each level was acquired in triplicate. An analysis of variance (ANOVA) was carried out to test the regression curves, and the linear model was found appropriate over the concentration range (R^2 values > 0.9992). Precision and intraday repeatability were also estimated in all the concentration levels with a coefficient of variation lower than 5%. The results of the quantitative analysis for each analyte were expressed as $\mu g\ g^{-1}$of dry matter (DM). The Mass Lynx software (version 4.2) was used for instrument control, data acquisition, and processing.

Cell cultures

CCD841 (ATCC® CRL-1790™) healthy human mucosa cell lines and CaCo-2 (ATCC® HTB 37™) human colorectal cancer cells were grown in an EMEM medium supplemented with heat inactivated 10% fetal bovine serum (FBS), 2 mM L-glutamine, 1% non-essential amino acids, 100 U ml^{-1}penicillin, and 100 μg ml^{-1} streptomycin. E705 (kindly provided by Fondazione IRCCS Istituto Nazionale dei Tumori, Milan, Italy) and SW480 (ATCC® CCL-228™) human colorectal cancer cells were grown in an RPMI 1640 medium supplemented with heat-inactivated 10% FBS, 2 mM L- glutamine, 100 U ml^{-1}penicillin, and 100 μg ml^{-1}streptomycin. All the cell lines were maintained at 37°C in a humidified 5% CO_2 incubator. ATCC cell lines were validated by short-tandem repeat profiles that are generated by simultaneous amplification of multiple short-tandem repeat loci and amelogenin (for gender identification). All the reagents for cell cultures were supplied by Lonza (Lonza Group, Basel, Switzerland).

Viability assay

Cell viability was investigated using an MTT-based *in vitro* toxicology assay kit (Sigma, St. Louis, MO, United States) according to the manufacturer's protocols. The different cell lines were seeded in 96-well microliter plates at a density of 1 × 10^4 cells/well, cultured in a complete medium, and treated after 24 h with 400 and 800 μg $ml^{-1}$of glucosinolate purified extract. After 48 h at 37°C, the medium was replaced with a complete medium without phenol red containing 10 μl of 5 mg ml^{-1}MTT [3-(4,5-dimethylthiazol-2-yl)-2.5-diphenyltetrazolium bromide]. After 4 h of additional incubation for CCD841 and 2 h for CRC cells lines, formazan crystals were solubilized with 10% Triton X-100 and 0.1 N HCl in isopropanol, and the absorbance was measured at 570 nm using a microplate reader. Cell viabilities were expressed as a percentage against the untreated cell lines used as controls. Two types of statistical analyzes were used using R (version 4.0.0) and GraphPad Prism 8. A general linear model (GLM) was used to evaluate the dose-dependency of the cell lines, while a 2-way ANOVA with Tukey multiple comparison test was conducted to understand differences between the lines at the same concentration of the extract. The significance threshold was set at $p = 0.05$.

Enzyme assays

To evaluate the effect of glucosinolates on enzymatic activities, CRC cell lines and healthy cell lines were seeded at 1 × 10^6 cells/100 mm dish and treated for 48 h with the extract at 400 and 800 μg ml^{-1}. The cells were rinsed with ice-cold PBS and lysed in 50 mM *Tris*-HCl (pH 7.4), 150 mM NaCl, 5 mM EDTA, 10% glycerol, and 1% NP-40 containing protease inhibitors (1 μM leupeptin, 2 μg ml^{-1}aprotinin, 1 μg ml^{-1}pepstatin, and 1 mM PMSF). Homogenates were obtained by passing the cells 5 times through a blunt 20-gauge needle fitted to a syringe and then centrifuging them at 15,000 g for 30 min at 4°C. Enzyme activities were assayed on supernatants. Glutathione S-transferase (GST) was measured as reported in

Habig (Habig et al., (22)) using 1 mM reduced glutathione (GSH) and 1 mM 1-chloro-2,4-dinitrobenzene (CDNB) as substrates in the presence of a 90-mM potassium phosphate buffer (pH 6.5),and the reaction was monitored at 340 nm. Superoxide dismutase (SOD) was measured using an indirect method according to Vance [Vance et al., (23)]. This technique is based on the ability of SOD to compete with ferricytochrome c for superoxide anions generated by the xanthine oxidase system and, thus, to inhibit the reduction of ferricytochrome c. Briefly, the protein samples were incubated with 0.01 mM ferricytochrome c in 10 mM HEPES-*Tris* (pH 7.5), 0.1 mM EDTA, 0.01 mM xanthine in 1 mM NaOH, and xanthine oxidase at a final concentration of 0.006 U/ml. Under these conditions, one unit of SOD is the amount of enzyme able to yield a 50% decrease in the rate of ferricytochrome c reduction followed at 550 nm. All the assays were performed in triplicate at 25°C with a Jasco V-550 spectrophotometer and analyzed with the Spectra Manager (version 1.33.02) software of Windows. A linear model was chosen for statistical analyzes of enzymatic assays to evaluate differences against a control set at fold = 1. The significance threshold was set at $p = 0.05$.

Results and discussion

Initially, a chemical characterization of phytochemical compounds in the Camelina seed by-product was performed by UPLC-HRMS. The full ms chromatograms are shown in **Supplementary Figure 1**, and a list of the tentatively identified phytochemicals numbered according to elution order is shown in **Supplementary Table 1**. The untarget analysis in negative ion mode allowed for identification of 11 metabolites belonging mainly to two classes, polyphenols and glucosinolates. The results of the qualitative analysis was in accordance with literature data (24–27). However, among all the compounds found in the extract, our attention was focused on glucosinolates. The analysis of chromatogram in full MS and MS/MS mode allowed for us to identify the presence of three main glucosinolates in the extract, which were assigned as glucoarabinin, glucocamelinin, and homoglucocamelinin. The identification was based on retention time and UV and MS/MS spectra and finally confirmed with commercial standards. The results of the qualitative analysis were in accordance with literature data (25, 28, 29). The individual and total GLS contents in *Camelina* sativa seeds were investigated using an international standard method (ISO 9167-1) with some slight modifications and avoiding the desulfation step. A quantitative analysis of the ISO method was carried out using a selective MRM method, and the results showed that the amount of glucoarabinin, glucocamelinin, and homoglucocamelinin was 304.3 ± 62, 403.3 ± 23, and 262.6 ± 87 $\mu g\, g^{-1}$DM, respectively.

Optimization of glucosinolate extraction

Selection of solvent composition

Given the interesting content of GLSs in the extract of *C. sativa* PC, especially considering that the matrix used is an industry by-product, we decided to develop and optimize a green extraction method based on ultrasound-assisted extraction (USAE) to improve extraction yield and reduce the

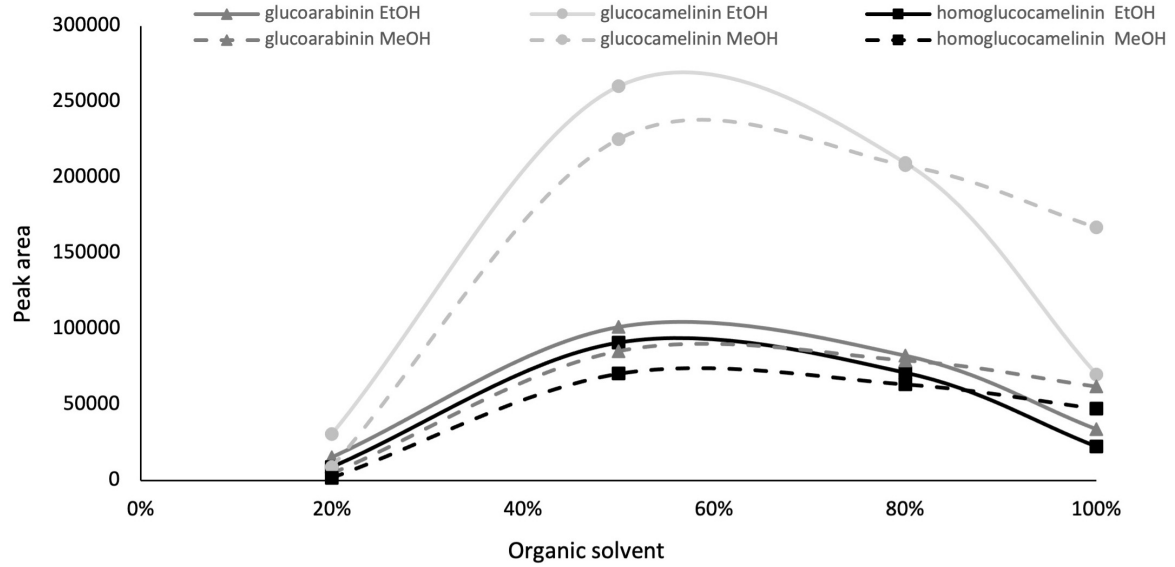

FIGURE 1
Glucosinolate peak area vs. organic solvent percentage, ethanol (solid line) and methanol (dashed line).

TABLE 2 Analysis of variance of the regression model.

	Sum of squares				Mean square			
	Glucoarabinin	**Glucocamelinin**	**Homo glucocamelinin**	**Tot EtOH**	**Glucoarabinin**	**Glucocamelinin**	**Homo glucocamelinn**	**Tot EtOH**
A: EtOH%	10801.6	66195.2	1826.8	286.8	10801.6	66195.2	1826.8	286.8
B: Volume	769.3	3988.1	293.5	836.4	769.3	3988.1	293.5	836.4
C: Cycles	303.7	749.0	83.3	187.2	303.7	749.0	83.3	187.2
A^2	7626.5	40568.0	961.2	6.8	7626.5	40568.0	961.2	6.8
B^2	31.6	4.2	4.9	5.5	31.6	4.2	4.9	5.5
C^2	66.0	539.9	10.4	5.8	66.0	539.9	10.4	5.8
AB	1073.6	6761.8	137.5	34.2	1073.6	6761.8	137.5	34.2
AC	1218.4	8271.0	135.3	20.3	1218.4	8271.0	135.3	20.3
BC	119.0	1241.9	3.5	109.2	119.0	1241.9	3.5	109.2
Lack of fit	309.1	2120.5	42.0	27.0	103.0	706.8	14.0	9.0
Pure error	97.1	224.9	9.9	0.1	32.4	75.0	3.3	0.0
Total	22415.9	130665.0	3508.2	1519.2				
R^2	98.2	98.2	98.5	98≅0.2				
Adj. R^2	95.5	95.5	96.3	95.5				

	F-value				*P*-value			
	Glucoarabinin	**Glucocamelinin**	**Homoglucocamelinin**	**Tot EtOH**	**Glucoarabinin**	**Glucocamelinin**	**Homoglucocamelinin**	**Tot EtOH**
A: EtOH%	333.6	882.9	550.8	7821.9	**0.0004**[a]	**0.0001**[a]	**0.0002**[a]	**0.0000**[a]
B: Volume	23.8	53.2	88.5	22811.1	**0.0165**[a]	**0.0053**[a]	**0.0025**[a]	**0.0000**[a]
C: Cycles	9.4	10.0	25.1	5105.8	0.0549	0.0508	**0.0153**[a]	**0.0000**[a]
A^2	235.5	541.1	289.8	184.4	**0.0006**[a]	**0.0002**[a]	**0.0004**[a]	**0.0009**[a]
B^2	1.0	0.1	1.5	150.6	0.3958	0.8273	0.3131	**0.0012**[a]
C^2	2.0	7.2	3.1	157.1	0.2486	0.0748	0.1749	**0.0011**[a]
AB	33.2	90.2	41.5	552.3	**0.0104**[a]	**0.0025**[a]	**0.0076**[a]	**0.0001**[a]
AC	37.6	110.3	40.8	2978.3	**0.0087**[a]	**0.0018**[a]	**0.0078**[a]	**0.0002**[a]
BC	3.7	16.6	1.1	245.4	0.151	**0.0268**[a]	0.3812	**0.0000**[a]
Lack of fit	3.2	9.4	4.2		0.1836	**0.0489**[a]	0.1338	**0.0004**[a]
Pure error								
Total								
R^2								
Adj. R^2								

R^2, quadratic correlation coefficient.
[a]Significant ($p < 0.05$).

10.3389/fnut.2022.901944

use of chemicals and environmental impact. As commonly reported in the literature, one of the most important parameters that affect the extraction efficiency in USAE process is the composition of the extraction solvent. For this reason, to replace methanol with a green solvent such as EtOH (generally recognized as safe) and to select a solvent composition to be used in the further experimental design, preliminary experiments were carried out by increasing from 0 to 100 the organic solvent percentage (ethanol and methanol) in water, and GLS content was monitored. The other parameters of USAE, namely, solvent volume, extraction cycle, and extraction time were kept constant at 10 ml, 2 cycles, and 5 min, respectively. The results indicate that an extraction solvent with water content higher than 80% formed a mucilaginous agglomerate that makes injection in the chromatographic system impossible. However, as shown in **Figure 1**, the quantitative trend of monitored GLSs is comparable using both methanol and ethanol. GLS content increases proportionally to the increase in organic solvent from 20 to 60%, but beyond this value it begins to decrease. Based on these results and considering that the behavior of methanol and ethanol was comparable, EtOH in the range of 40 to 80% was selected as extraction solvent in the next optimization step because of its lower environmental impact and toxicity.

Response surface design

After the preliminary experiments were carried out to select the organic solvent and its content, a response surface methodology (RSM) was used to maximize the extraction of GLSs and at the same reduce the consumption of the organic solvent. In this study, the influence of the three independent variables (solvent volume, solvent composition, and extraction cycles) on the extraction efficiency of each glucosinolate and on total EtOH consumption was simultaneously evaluated by a Box-Behnken 2 factor interaction design. GLS contents ($\mu g g^{-1}$DM) were considered as response variable to be maximized and total consumption of EtOH (ml) as variable to be minimized considering that reduction of the organic solvent has a positive influence on the cost of the analysis and on environmental impact. **Table 1** reports the total volume of EtOH used and the amount of glucosinolates for each run provided by the CCD used as a response variable. The statistical parameters of the experimental design are summarized in **Table 2**.

Based on the results, the model showed a high correlation ($R^2 \cong 98\%$), indicating a slight variance of the data and a good prediction of the model with respect to all the considered response variables. Two independent variables, percentage of EtOH and its volume, had a significant influence on both GLS extraction and volume of total EtOH ($p < 0.05$) while the extraction cycles had a significant influence only on the extraction efficiency of homoglucocamelinin and on the volume of EtOH. Moreover, the quadratic effect of multiple parameters as well as the interaction among many parameters was statistically significant ($p < 0.05$) for the response variables considered (**Table 2**). As shown in the desirability plot (**Figure 2**), the volume of the extraction solvent linearly influences the desired effect; in fact, by increasing the extraction volume from 5 to 15 ml, there is an increase in desirability. Regarding the percentage of EtOH, the desirable effect increases proportionally to the increase in organic solvent from 40 to ≅70%, but beyond this value it begins to decrease. This result was also in agreement with those obtained in our preliminary results. Finally, the optimized conditions to maximize the extraction of glucosinolate compounds and at same time reduce the consumption of organic solvents were calculated as EtOH 65%, cycles 2, and solvent volume 5 ml. After selecting the optimized extraction conditions to evaluate the improvement

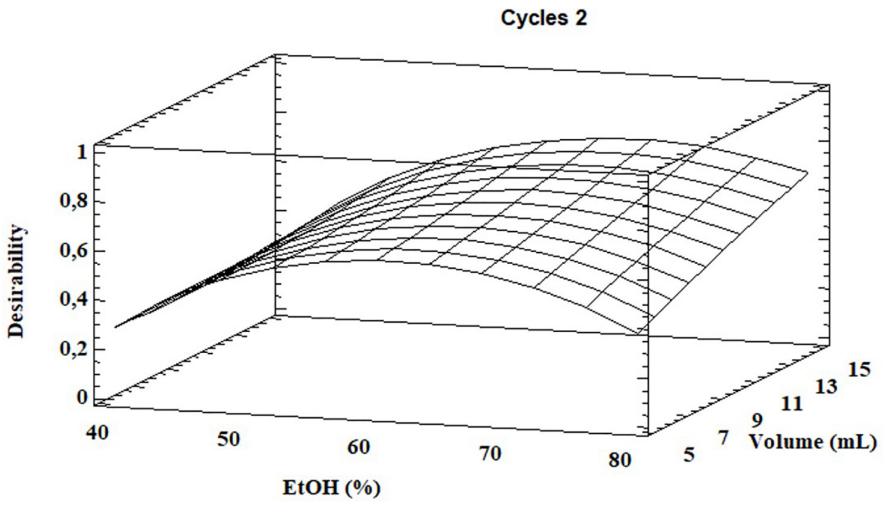

FIGURE 2
Desirability plot for total glucosinolate extraction as functions of ethanol percentage and total solvent volume.

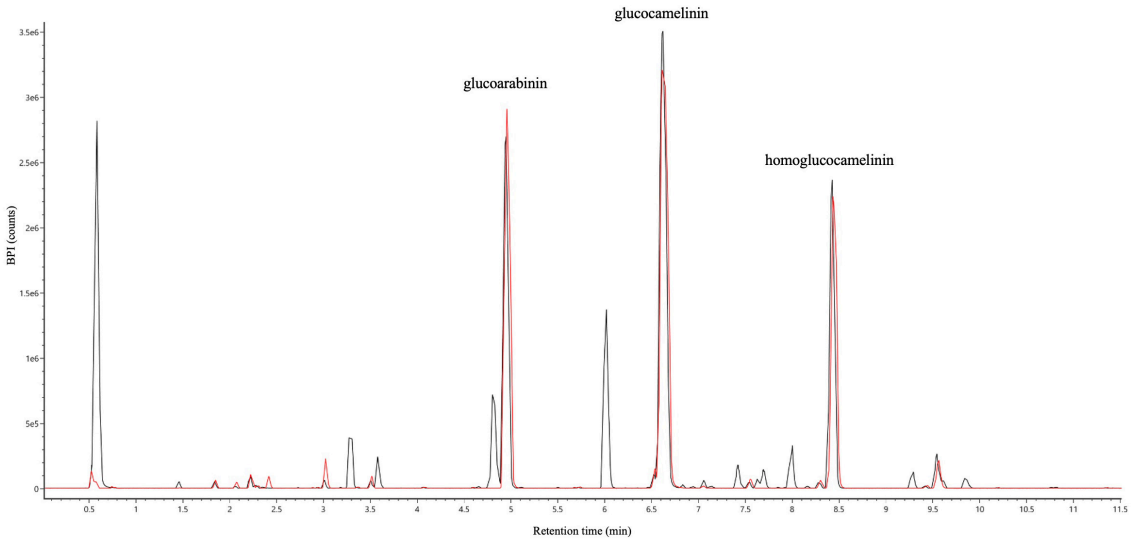

FIGURE 3
UHPLC full MS chromatograms of ultrasound-assisted solid liquid extraction (USAE) under optimized conditions before (black line) and after (red line) purification by solid phase extraction (SPE).

in extraction efficiency, these results have been comparted with those obtained using the ISO method. A quantitative analysis of the three glucosinolates was carried out by UPLC-HRMS using the external standard method. The calibration curve of glucosinolates in the concentration range of.1–10 μg ml^{-1} were used to quantify their content in both extracts. The external standard calibration curves for all the analytes provided good linearity within the investigated concentration range with correlation coefficients (R^2) ranging from 9993 and 9998. The quantitative analysis of the extract obtained by using USAE shows that the content of glucoarabinin, glucocamelinin, and homoglucocamelinin were 1,525.6 ± 53, 3,544.6 ± 209, and 615.5 ± 68 μg g^{-1}DM, respectively. This result highlights a huge increase in extraction efficiency for all target compounds, in particular, the recovery of glucoarabinin, glucocamelinin, and homoglucocamelinin increased by 501, 878 and 234%, respectively. These results can be explained by the increased chemical stability of glucosinolates under the milder extraction conditions of the developed USAE method, compared to the ISO procedure which uses methanol at 75°C as extraction solvent. These conditions can cause thermal degradation of glucosinolates as highlighted by some authors (30–33).

Purification of glucosinolates

Given the high content of GLSs in *Camelina sativa* PC, we decided to develop an efficient protocol based on solid phase extraction (SPE) to obtain a purified extract and test cell activity while preventing other compounds from interfering with results. USA extract 140 mg of was diluted in 10 ml H_2O and 1% HCOOH and loaded into an SPE column. After the loading, a washing solution using 10 ml H_2O and 1% HCOOH was passed through the SPE cartridge to remove non-retained compounds, while the GLSs were eluted using 10 ml of H_2O and 2% NH_4OH.

Both wash and elution fractions were collected, and each one was analyzed by UPLC-HRMS-DAD to detect the presence of GLSs and verify the purity of the SPE extracts. The results of HRMS chromatographic profiling of elution fractions, crude extract, and reference standard compounds are shown in Figure 3. The chromatographic analysis suggests that the developed SPE procedure allowed to selectively purify the GLSs, avoiding losses of compounds of interest in the washing

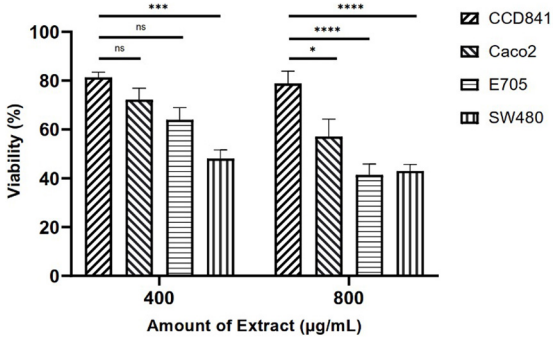

FIGURE 4
MTT viability assays on four cell lines treated with *Camelina sativa* extracts at two concentrations by 2-way analysis of variance (ANOVA) statistical analysis (ns, not significant, * = $p < 0.05$, ***$p < 0.001$, and ****$p < 0.0001$).

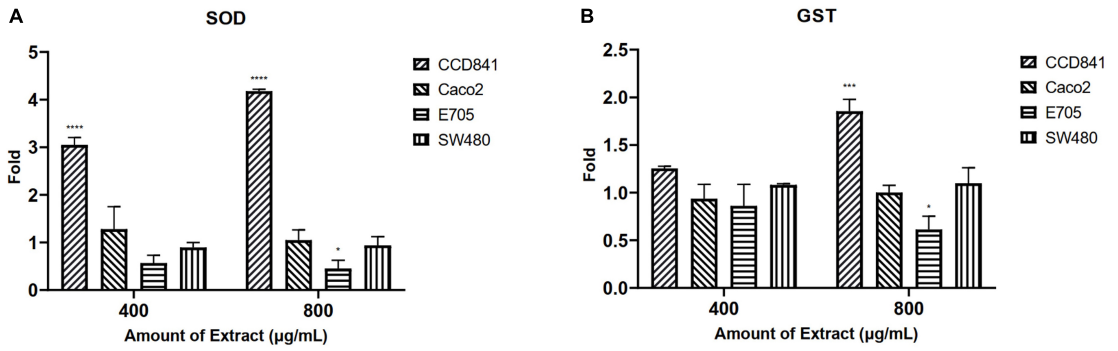

FIGURE 5
Fold increase in **(A)** superoxide dismutase (SOD) and **(B)** glutathione S-transferase (GST) activity after 48 h of treatment. The statistical analysis used a linear model against a fold control equal to 1 (*$p < 0.05$, ***$p < 0.001$, and ****$p < 0.0001$).

step. In general, the results show that USAE coupled with the SPE procedure allow to obtain a high purity of GLS molecules from *Camelina sativa* PC. An overall balance in the extraction, isolation, and purification processes suggests that approximately 800 mg of purified GLS extract can be recovered from 10 g of PC used.

Antiproliferative effect of purified glucosinolate extract

Initially, screening was performed to define the concentrations of purified extract to be used in MTT viability tests. Among the concentrations tested in the range of 100 to 1,000 µg ml^{-1}, the experimental results suggested to select a concentration range of 400–800 µg ml^{-1} for further experiments. Four different cell lines were selected to perform MTT assays and evaluate cell viability after a 48-h treatment through mitochondrial activity. The cell lines chosen were healthy colorectal mucosa CCD841 cell lines and three colorectal cancer cell lines with peculiar mutations or behaviors. In particular, CaCo-2 and E705 show no hyperactivating mutations in the KRAS, NRAS, BRAF, and PIK3CA genes, with the E705 cell line carrying a silent mutation in the PIK3CA gene, whereas SW480 carries a hyperactivating mutation in exon 2 of the KRAS gene. The Caco-2 and SW480 cell lines do not respond to cetuximab, a MoAbs against EGFR, while the E705 cell line is sensitive to cetuximab (34). A general linear model analysis on MTT assays demonstrated that the purified extract had a significantly dose-dependent antiproliferative effect on the three tumor cell lines ($p < 0.001$), and that no significant effect ($p > 0.07$) on the healthy cell lines was found, demonstrating specific selectivity against the tumor cell lines. The 2-way ANOVA analysis (**Figure 4**) using the healthy cell lines as control showed a strong effect at the 800 mg ml^{-1} concentration on the E705 and SW480 cells, where the viability dropped to 40%. Subsequently, to clarify the possible mechanisms involved, two enzymes involved in reactive oxygen species (ROS) detoxification, superoxide dismutase (SOD), and glutathione S-transferase (GST) were assayed. SOD converts the superoxide radical ($O_2^{\cdot -}$) into hydrogen peroxide (H_2O_2), while GST is an enzyme that transfers glutathione to xenobiotic substrates. We hypothesize that the extract acts as a stressor element by increasing oxidative metabolism. Upon extract addition, the healthy cells respond physiologically by increasing the activity of the enzymes, but the tumor cell lines do not. **Figure 5** shows the increase in both enzymes' activity: at the highest extract concentration, SOD is increased by 4-fold ($p < 0.05$) and GST by 2-fold ($p < 0.05$) in healthy CCD841 cells. Caco-2 and SW480 maintain the basal level of these enzymes after treatment with both extract concentrations ($p > 0.05$). E705 shows an opposite behavior: the activity of the two enzymes is decreased by 0.5 fold already at 400 µg $ml^{-1}$of extract for SOD ($p < 0.05$) and 800 µg $ml^{-1}$for GST ($p < 0.05$).

Conclusions

For the first time, a green methodology based on the use of the USAE method with green solvents has been developed to obtain glucosinolates with high purity from *Camelina sativa* seed by-product. The effect of extraction parameters on GLS content in the raw extract and the reduction of organic solvent were optimized using an experimental design. The volume of the solvent and the percentage of ethanol show the main effect on the selected response variables. Under optimized conditions, the procedure allowed for enormous recovery of compounds compared to the ISO method. Based on our results, approximately 800 mg of enriched GLS extract can be obtained from 10 g of *Camelina sativa* PC subjected to USA extraction followed by SPE purification. The purified extract, rich in glucoarabinin, glucocamelinin, and homoglucocamelinin, showed an interesting chemopreventive action against different colorectal cancer cell lines without

affecting the healthy cell lines. However, the exact mechanism of action of the purified extract on the tumor cell lines needs further studies to be clarified with a view to developing new sustainable treatments for patients with cancer refractory to conventional chemotherapy. Moreover, the glucosinolate extract can increase the activity of two of the most important enzymes involved in cell defense against oxidative stress, SOD and glutathione S-transferase, thus showing antioxidative properties, which could be exploited in cancer and oxidative stress prevention. The developed method can be considered a suitable green protocol to obtain nutraceutical products with interesting and promising anticancer activities from a natural and cheap food by-product.

Data availability statement

The original contributions presented in this study are included in the article/**Supplementary Material**, further inquiries can be directed to the corresponding author.

Author contributions

ML and LC: conceptualization. SP, DP, RC, and LC: data curation. SP, CG, and RC: formal analysis. SP, CM, MF, and GS: investigation. LM and LC: supervision. LC, PF, and LM: writing – original draft. All authors contributed to the article and approved the submitted version.

Funding

This research was funded by Food Social Sensor Network (FOOD NET), (grant number: 2251551, POR FESR 2014–2020) and supported by the Italian Ministry of University and Research (MIUR) through grant "Dipartimenti di Eccellenza 2017" to University of Milano Bicocca, Department of Biotechnology and Biosciences. The funder had no role in study design, data collection and analysis, decision to publish, or preparation of the manuscript.

Acknowledgments

The authors are grateful to Sara Rizzo for her English language support.

Conflict of interest

The authors declare that the research was conducted in the absence of any commercial or financial relationships that could be construed as a potential conflict of interest.

Publisher's note

Supplementary material

The Supplementary Material for this article can be found online at: https://www.frontiersin.org/articles/10.3389/fnut.2022.901944/full#supplementary-material

References

1. Verhoeven DT, Goldbohm RA, van Poppel G, Verhagen H, van den Brandt PA. Epidemiological studies on brassica vegetables and cancer risk. *Cancer Epidemiol Prevent Biomark.* (1996) 5:733–48.

2. Higdon JV, Delage B, Williams DE, Dashwood RH. Cruciferous vegetables and human cancer risk: epidemiologic evidence and mechanistic basis. *Pharmacol Res.* (2007) 55:224–36. doi: 10.1016/j.phrs.2007.01.009

3. Gründemann C, Huber R. Chemoprevention with isothiocyanates–From bench to bedside. *Cancer Lett.* (2018) 414:26–33. doi: 10.1016/j.canlet.2017.10.033

4. Johnson IT. Cruciferous vegetables and risk of cancers of the gastrointestinal tract. *Mol Nutrit Food Res.* (2018) 62:1701000. doi: /10.1002/mnfr.201701000

5. Traka M, Mithen R. Glucosinolates, isothiocyanates and human health. *Phytochem Rev.* (2009) 8:269–82. doi: 10.1007/s11101-008-9103-7

6. Vig AP, Rampala G, Thind TS, Arora S. Bio-protective effects of glucosinolates–A review. *LWT Food Sci Technol.* (2009) 42:1561–72. doi: 10.1016/j.lwt.2009.05.023

7. Traka MH. Health benefits of glucosinolates. *Adv Botanic Res.* (2016) 80:247–79. doi: 10.1016/bs.abr.2016.06.004

8. Ma L, Liu G, Zong G, Sampson L, Hu FB, Willett WC, et al. Intake of glucosinolates and risk of coronary heart disease in three large prospective cohorts of US men and women. *Clin Epidemiol.* (2018) 10:749. doi: 10.2147/CLEP.S164497

9. Kamal RM, Abdull Razis AF, Mohd Sukri NS, Perimal EK, Ahmad H, Patrick R, et al. Beneficial health effects of glucosinolates-derived isothiocyanates on cardiovascular and neurodegenerative diseases. *Molecules.* (2022) 27:624. doi: 10.3390/molecules27030624

10. Fahey JW, Zalcmann AT, Talalay P. The chemical diversity and distribution of glucosinolates and isothiocyanates among plants. *Phytochemistry.* (2001) 56:5–51. doi: 10.1016/S0031-9422(00)00316-2

11. Mithen R, Bennett R, Marquez J. Glucosinolate biochemical diversity and innovation in the Brassicales. *Phytochemistry.* (2010) 71:2074–86. doi: 10.1016/j.phytochem.2010.09.017

12. Bhandari SR, Jo JS, Lee JG. Comparison of glucosinolate profiles in different tissues of nine Brassica crops. *Molecules.* (2015) 20:15827–41. doi: 10.3390/molecules200915827

13. Redovnikoviæ IR, GliveticT, Delonga K, Furac. Glucosinolates and their potential role in plant. *Periodicum Biologor.* (2008) 110:297–309.

14. Bohinc T, Smiljana GB, Dean B, Stanislav T. Glucosinolates in plant protection strategies: a review. *Arch Biol Sci.* (2012) 64:821–8. doi: 10.2298/ABS1203821B

15. Li N, Wu X, Zhuang W, Wu C, Rao Z, Du L, et al. Cruciferous vegetable and isothiocyanate intake and multiple health outcomes. *Food Chem.* (2021) 375:131816. doi: 10.1016/j.foodchem.2021.131816

16. Holst B, Williamson G. A critical review of the bioavailability of glucosinolates and related compounds. *Nat Prod Rep.* (2004) 21:425–47. doi: 10.1039/b204039p

17. Ziedan E-SH. A review of the efficacy of biofumigation agents in the control of soil-borne plant diseases. *J Plant Protect Res.* (2022) 62:2.

18. Brown PD, Morra MJ. Glucosinolate-containing plant tissues as bioherbicides. *J Agricult Food Chem.* (1995) 43:3070–4. doi: 10.1021/jf00060a015

19. Zubr J. Oil-seed crop: camelina sativa. *Industr Crops Prod.* (1997) 6:113–9. doi: 10.1016/S0926-6690(96)00203-8

20. Pagano I, Campone L, Celano R, Piccinelli AL, Rastrelli L. Green non-conventional techniques for the extraction of polyphenols from agricultural food by-products: a review. *J Chromatogr A.* (2021) 1651:462295. doi: 10.1016/j.chroma.2021.462295

21. Norm ISO. Rapeseed-determination of glucosinolates content-Part 1: method using high-performance liquid chromatography. *ISO.* (1992) 9167:1–9.

22. Habig WH, Pabst MJ, Jakoby WB. Glutathione S-transferases: the first enzymatic step in mercapturic acid formation. *J Biol Chem.* (1974) 249:7130–9. doi: 10.1016/S0021-9258(19)42083-8

23. Vance PG, Keele BB Jr., Rajagopalan KV. Superoxide dismutase from Streptococcus mutans: isolation and characterization of two forms of the enzyme. *J Biol Chem.* (1972) 247:4782–6. doi: 10.1016/S0021-9258(19)44979-X

24. Terpinc P, Polak T, Makuc D, Ulrih NP, Abramovic H. The occurrence and characterisation of phenolic compounds in Camelina sativa seed, cake and oil. *Food Chem.* (2012) 131:580–9. doi: 10.1016/j.foodchem.2011.09.033

25. Berhow MA, Polat U, Glinski JA, Vaughn SF, Isbell T, et al. Optimized analysis and quantification of glucosinolates from Camelina sativa seeds by reverse-phase liquid chromatography. *Industr Crops Prod.* (2013) 43:119–25. doi: 10.1016/j.indcrop.2012.07.018

26. Quéro A, Molinié R, Mathiron D, Thiombiano B, Fontaine JX, et al. Metabolite profiling of developing Camelina sativa seeds. *Metabolomics.* (2016) 12:1–14. doi: 10.1007/s11306-016-1135-1

27. Rahman MJ, de Camargo AC, Shahidi F. Phenolic profiles and antioxidant activity of defatted camelina and sophia seeds. *Food Chem.* (2018) 240:917–25. doi: 10.1016/j.foodchem.2017.07.098

28. Schuster A, Friedt W. Glucosinolate content and composition as parameters of quality of Camelina seed. *Industr Crops Prod.* (1998) 7:297–302. doi: 10.1016/S0926-6690(97)00061-7

29. Russo R, Reggiani R. Antinutritive compounds in twelve Camelina sativa genotypes. *Am J Plant Sci.* (2012) 3:1408–12. doi: 10.4236/ajps.2012.310170

30. MacLeod AJ, Panesar SS, Gil V. Thermal degradation of glucosinolates. *Phytochemistry.* (1981) 20:977–80. doi: 10.1016/0031-9422(81)83011-7

31. Oerlemans K, Barrett DM, Suades CB, Verkerk R, Dekker M. Thermal degradation of glucosinolates in red cabbage. *Food Chem.* (2006) 95:19–29. doi: 10.1016/j.foodchem.2004.12.013

32. Hanschen FS, Rohn S, Mewis I, Schreiner M, Kroh LW. Influence of the chemical structure on the thermal degradation of the glucosinolates in broccoli sprouts. *Food Chem.* (2012) 130:1–8. doi: 10.1021/jf302744y

33. Mao X, Zhao X, Huyan Z, Liu T, Yu X. Relationship of glucosinolate thermal degradation and roasted rapeseed oil volatile odor. *J Agricult Food Chem.* (2019) 67:11187–97. doi: 10.1021/acs.jafc.9b04952

34. Bovio F, Epistolio S, Mozzi A, Monti E, Fusi P, Forcella M, et al. Role of NEU3 overexpression in the prediction of efficacy of EGFR-targeted therapies in colon cancer cell lines. *Int J Mol Sci.* (2020) 21:8805. doi: 10.3390/ijms21228805

frontiers | Frontiers in Nutrition

TYPE Original Research
PUBLISHED 29 August 2022
DOI 10.3389/fnut.2022.928805

OPEN ACCESS

EDITED BY
Alberto Valdés,
Spanish National Research Council (CSIC), Spain

REVIEWED BY
Carlos L. Cespedes-Acuña,
University of Bio Bio Chillan Chile, Chile
Ya-Fang Shang,
Hefei University of Technology, China

*CORRESPONDENCE
Ji-dao Du
djdbynd@163.com

SPECIALTY SECTION
This article was submitted to Nutrition and Food Science Technology, a section of the journal Frontiers in Nutrition

RECEIVED 26 April 2022
ACCEPTED 22 July 2022
PUBLISHED 29 August 2022

CITATION
Zhang Q, Zheng G, Wang Q, Zhu J, Zhou Z, Zhou W, Xu J, Sun H, Zhong J, Gu Y, Yin Z, Du Y-l and Du J-d (2022) Molecular mechanisms of flavonoid accumulation in germinating common bean (*Phaseolus vulgaris*) under salt stress. *Front. Nutr.* 9:928805. doi: 10.3389/fnut.2022.928805

Molecular mechanisms of flavonoid accumulation in germinating common bean (*Phaseolus vulgaris*) under salt stress

Qi Zhang[1], Guangyue Zheng[1], Qi Wang[1], Jixing Zhu[1], Zhiheng Zhou[1], Wenshuo Zhou[1], Junjie Xu[1], Haoyue Sun[2], Jingwen Zhong[1], Yanhua Gu[1], Zhengong Yin[3], Yan-li Du[1] and Ji-dao Du[1,4]*

[1]Legume Crop Laboratory, Agricultural College, Heilongjiang Bayi Agricultural University, Daqing, China, [2]Qiqihar Branch of Heilongjiang Academy of Agricultural Sciences, Qiqihar, China, [3]Crop Resources Institute of Heilongjiang Academy of Agricultural Sciences, Harbin, China, [4]National Cereals Technology Engineering Research Center, Daqing, China

Flavonoids are important secondary metabolites, active biomolecules in germinating beans, and have prominent applications in food and medicine due to their antioxidant effects. Rutin is a plant flavonoid with a wide biological activity range. In this study, flavonoid (rutin) accumulation and its related molecular mechanisms in germinating common bean (*Phaseolus vulgaris*) were observed at different time points (0–120 h) under salt stress (NaCl). The rutin content increased from germination onset until 96 h, after which a reducing trend was observed. Metabolome analysis showed that salt stress alters flavonoid content by regulating phenylpropanoid (ko00940) and flavonoid (ko00941) biosynthesis pathways, as well as their enzyme activities, including cinnamyl-alcohol dehydrogenase (CAD), peroxidase (POD), chalcone isomerase (CHI), and flavonol synthase (FLS). The RNA-seq and quantitative real-time PCR (qRT-PCR) analyses also showed that these two pathways were linked to changes in flavonoid content following salt treatment. These results reveal that salt stress effectively enhanced rutin content accumulation in germinating beans, hence it could be employed to enhance the functional quality of germinating common beans.

KEYWORDS

flavonoids (rutin) content, common bean, germinating, salt stress, mechanism, phenylpropanoid biosynthesis, flavonoid biosynthesis

Introduction

The common bean (*Phaseolus vulgaris* L.) is an annual legume crop that has been cultivated in temperate and semitropical regions for ∼8,000 years (1). Common beans constitute an essential part of the human diet not only because of their protein-rich seed but also because they contain active phytochemicals, which are beneficial for health (2), including proteases, galacto-oligosaccharides, phytic acid, and flavonoids (3).

Flavonoids are an abundant and biologically active family of natural plant products that offer a range of health benefits (4). For instance, several flavonoids have anticancer functions, both *in vitro* and *in vivo* (5, 6). Some of the reported mechanisms by which flavonoids exert their anticancer functions include (1) preventing new cancer cell development, (2) restraining carcinogens that turn into activation sites, and (3) preventing compound metabolism and reducing their toxicity (7). Recently, with the ever-growing food quality concerns, the international market has shown a growing interest in flavonoid production, with high demand and a growing compound rate of 16.5%.

Plants are the most common material used for flavonoid extraction (7). These flavonoids have a C6–C3–C6 carbon skeleton with two phenyl aromatic rings, along with a heterocyclic ring (8). Flavonoids can be split into several subclasses according to basic skeleton substitution and B-ring attachment, such as chalcones, stilbenes, aurones, flavanones, flavones, isoflavones, phlobaphenes, dihydroflavonols, flavonols, leucoanthocyanidins, proanthocyanidins, and anthocyanins (9, 10). Rutin ($C_{27}H_{30}O_{16}$) is a relatively large and representative flavonoid in leguminous crops (11–13), which could also be used as a representative flavonoid for studying plant nutrition (14). In plants, certain flavonoids, including rutin, have been proven to play an important role in plant growth, development, hormone signaling, facilitating pollen–tube germination, plant–microorganism interactions, and biotic and abiotic stresses (15, 16).

Legumes are potential raw materials used for producing flavonoids for nutritional and dietary applications (4). However, abiotic stress (e.g., drought, salt, and cold) can affect the flavonoid biosynthetic pathway by regulating flavonoid transport and the expression and accumulation of related proteins, finally affecting the flavonoid content in plants (17). Previous studies have shown that salt stress significantly inhibits the germination of legume crops (including *Lathyrus sativus*, *Vicia sativa*, *Vigna radiata*, and *Vigna unguiculata*) but increases the flavonoid content in their seeds (18). Besides, another study reported significant differences in the flavonoid content and anti-inflammatory effects of soybean when seeds were germinated under different abiotic stress treatments (19). It has also been reported that abiotic stress could increase the content of total phenolic compounds and total flavonoids in soybean (*Glycine max*) and mung bean (*V. radiata*) sprouts (19, 20). Therefore, the regulation of flavonoid biosynthesis is considered an important regulatory mechanism of legume crops in response to salt stress (18). In another study, Gu et al. (21) demonstrated that moderate drought stress treatment could increase flavonoid content in plants. From a nutritional viewpoint, it could be concluded that exposing plants to appropriate stress treatment is an effective strategy for increasing the flavonoid content in food. However, few studies have reported the correlation between germinating common beans and flavonoids. This study determined the accumulation of rutin (used as the representative flavonoid in the common bean) in different common bean tissues at different germination stages under salt stress. Furthermore, the effect and mechanism of salt stress on total flavonoid accumulation in common bean sprouts were evaluated through metabolome and transcriptome analysis. The results presented herein provide a theoretical basis and new insights for improving the flavonoid content of common bean sprouts.

Materials and methods

Common bean materials and treatments

A local common bean cultivar (Longjiang Black Yun) was used as testing material, and its seeds were provided by the National Coarse Cereals Technology Engineering Research Center (Heilongjiang, China). The seeds were surface-sterilized with sodium hypochlorite (NaClO) and washed three times with distilled water. Germination was done in a germination box (BSC-250, Boxun, Shanghai, China) at a constant temperature of 25°C without light. Salt stress was simulated using 70 mmol/L NaCl (22) and was added at different times, as illustrated in Supplementary Table 1. The seeds were exposed to salt stress for 0, 24, 48, 72, 96, and 120 h for sprouting, and the germinating common beans were sampled to measure the rutin content. Different tissues with the highest flavonoid content in the germinating common beans were isolated since they were most suitable for further research. Flavonoid extraction was done using the method described by Liu et al. (23), while the rutin content was determined using HPLC (AB SCIEX, shimadzuLc-20A, MA, USA) from the Customs Quality Inspection Center (Dalian, Liaoning, China), using rutin ($C_{27}H_{30}O_{16}$) (SR8250, Solarbio, Beijing, China) as the reference (24–26). The standard rutin curve is shown in Supplementary Figure 1.

Metabolome and transcriptome analysis

Bean sprouts, without cotyledons, in the 3d+S treatment were taken at three time points (3d+S-0h, 3d+S-12h, and 3d+S-24h) and used as test samples for metabolome and transcriptome analysis, with three biological replicates at each time point. The hours (0, 12, and 24 h) represent the time salt stress was introduced at 3 days. The broadly targeted metabolome was determined using the UPLC-ESI-MS/MS system (Nexera X2, SHIMADZU, Japan) and ESI-Q TRAP-MS/MS (4500 QTRAP, Applied Biosystems, USA) from Matwell Biotechnology Company (Wuhan, China) (Supplementary Figure 2). The HPLC conditions included liquid-phase chromatographic column (Waters ACQUITY UPLC HSS T3 C18 1.8 μm, 2.1 mm * 100 mm), mobile phase (phase A was ultrapure water with 0.04% acetic acid while phase B was acetonitrile with 0.04% acetic acid), flow rate (0.35 ml/min), column temperature (40°C), and injection volume (4 μl). The mass spectrometry conditions included an electrospray ionization temperature of 550°C, a mass spectrometer voltage of 5,500 V, and a curtain gas pressure of 30 psi. Each ion pair in a triple quadrupole was scanned according to the optimized declustering potential and collision energy (27). The reagents (including methanol, acetonitrile, and ethanol) were bought from Merck (Darmstadt, Germany), while the standards were bought from Sigma (Sigma-Aldrich, Shanghai, China). The blank reagent sample was run during the detection process in order to clean the detection residue. The qualitative analysis of metabolites in samples was based on the MetWare database, so the isotopic and repeating signals (including K^+, Na^+, and NH_4^+) were removed. The metabolite identification method was based on a self-built database, including standard products and experimental samples. The secondary mass spectrometry data were collected based on the mass spectrometry MIM-EPI mode, and the unique Q1 (molecular ion), Q3 (characteristic fragment ion), RT (chromatographic retention time), DP (declustering potential), and CE (collision energy) of each metabolite were constructed by combining with manual analysis of the spectrum. Subsequently, the experimental samples were quantitatively detected using the multiple reaction monitoring (MRM) mode, which could eliminate nontarget ion interference and increase the accuracy and reproducibility of the quantification (27). After screening, the Analyst 1.6.3 software was used to process the mass spectrometry data, and the MultiQuant software to open the sample off-machine mass spectrometry file to integrate and calibrate the chromatographic peaks. The peak area of each chromatographic peak represents the relative content of the corresponding substance. The quality control (QC) in this study was used with mixed samples and internal standards (L-2-chlorophenylalanine, CAS: 103616-89-3) using the processing method applied for the samples. During the instrumental analysis, a QC sample was inserted into every 10 detection and analysis samples to monitor the repeatability of the analysis process. Fold change (FC) and VIP value analysis were used to find differentially altered metabolites (DAMs), and the screening conditions for DAMs were VIP $\geq$ 1 and FC $\geq$ 2 or FC $\leq$ 0.5 (28). The Kyoto Encyclopedia of Genes and Genomes (KEGG) database was used to annotate the information from the DAMs (29), with the *p*-value set to <0.05.

Also, the bean sprouts without cotyledons at three time points (3d+S-0h, 3d+S-12h, and 3d+S-24h) were used as transcriptome samples with three biological replicates at each time point. The transcriptome of samples was determined using HiSeq X Ten (Illumina, CA, USA) from the Biomarker Company (Beijing, China), and the transcriptome data were analyzed on the BMKCloud platform. The TopHat2 software (30) was used for sequence alignment of clean reads with a reference genome, while fragments per kilobase of transcript per million fragments mapped was used to measure the transcript or gene expression levels (31). The FC and false discovery rate (FDR) were calculated to determine the differentially expressed genes (DEGs). The value of FC was the average value in each group, which was calculated by merging three biological replicates in one treatment. The screening conditions for DEGs were FC $\geq$ 2 and FDR $<$ 0.01 (28). The KEGG database was used to annotate the information from the DEGs (29), with the *p*-value set to <0.05.

Physiology and qRT-PCR analysis

Enzyme activities, including cinnamyl-alcohol dehydrogenase (CAD) (32), peroxidase (POD) (33), chalcone isomerase (CHI) (34), and flavonol synthase (FLS) (35), in the enriched pathways were determined with an ELISA Kit (Michy, Suzhou, China), and data were acquired using a microplate reader (SpectraMax® 190, Molecular Devices, CA, USA). The data were then analyzed using ANOVA at a significance level of $p < 0.05$ on the SPSS19.0 platform.

The RNA of each sample was extracted with the *Trelief*™ RNA Pure Plant Kit (TSP412, Tsingke, China), and a NanoDrop (OneC, Thermo, USA) was used to detect quality and concentration. Quality RNA was reverse-transcribed into cDNA with the *Evo M-MLV* RT Premix (Accurate-Biotechnology, AG11706, Hunan, China). Primers of DEGs enriched in CAD (*Phvul.002G144800* and *Phvul.003G029500*), POD (*Phvul.001G143300*, *Phvul.007G008400* and *Phvul.008G249900*), and FLS (*Phvul.003G216600*) were designed using Primer Premier 5.0, while *Pvactin-11* was selected as the reference gene; the primer sequences are shown in Supplementary Table 2. The qRT-PCR program was conducted on a Light Cycler 480II (Roche Diagnostics, Switzerland), using a Hieff UNICON® Universal qPCR SYBR Green Master Mix (Yeason, 11184ES03, Shanghai, China). Subsequently, the relative gene expression level was computed using the $2^{-\Delta Ct}$ method (36).

Results

The rutin content in germinating common bean

The rutin content of common beans without germination was significantly lower (1.99 mg/ml; $p < 0.05$) at different germination times compared to common beans with germination. The rutin content of common bean sprouts at different germinating times increased with time and peaked at 96 h, after which a reducing trend was observed. Compared with other germination times, the periods from 72 to 120 h were more suitable for germinating bean sprouts due to the rutin content, while 96 h could be considered optimal (Figure 1A). Bean sprouts at 96 h were divided into two parts for the determination of flavonoid content (Figure 1B);

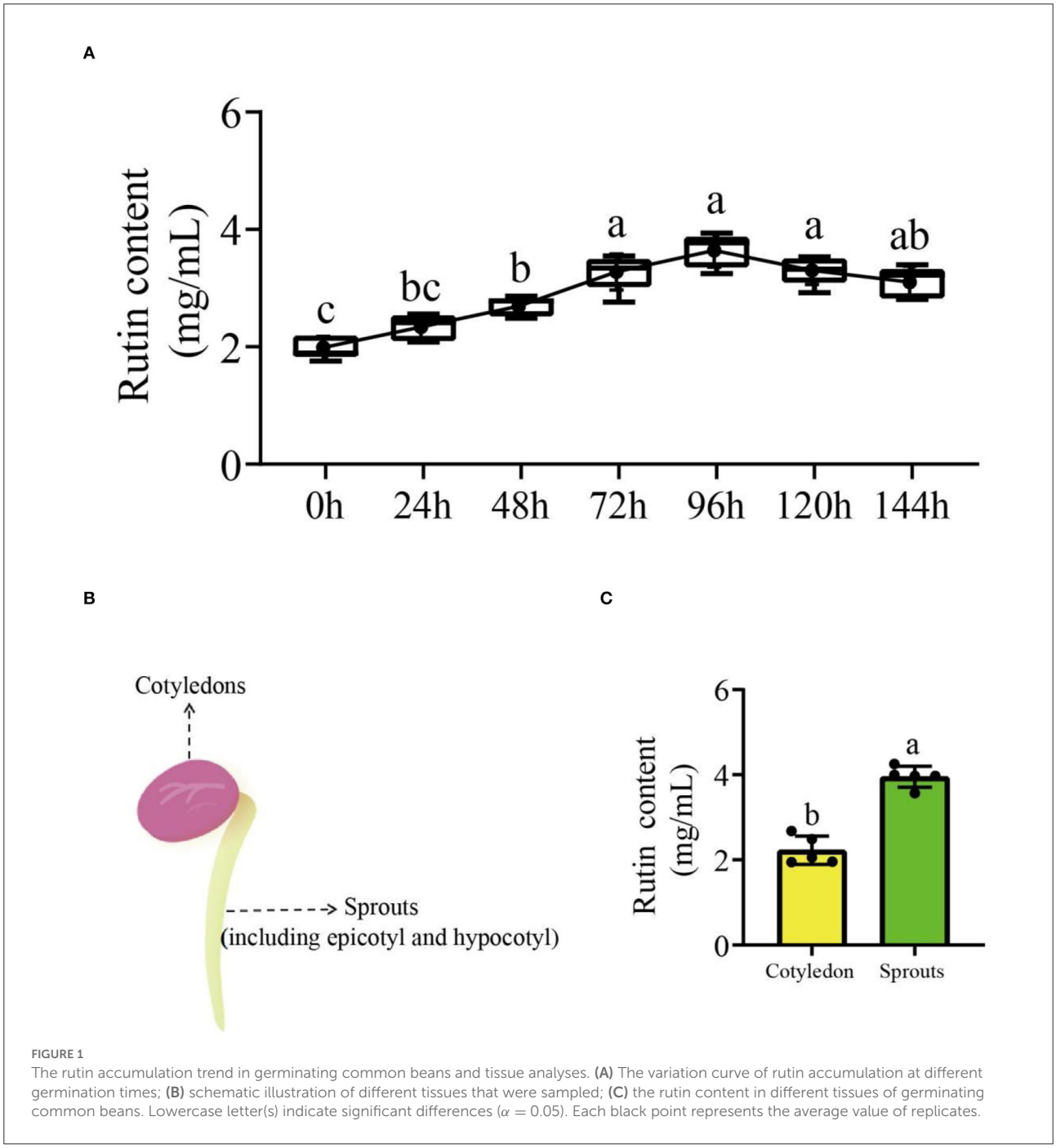

FIGURE 1
The rutin accumulation trend in germinating common beans and tissue analyses. **(A)** The variation curve of rutin accumulation at different germination times; **(B)** schematic illustration of different tissues that were sampled; **(C)** the rutin content in different tissues of germinating common beans. Lowercase letter(s) indicate significant differences ($\alpha = 0.05$). Each black point represents the average value of replicates.

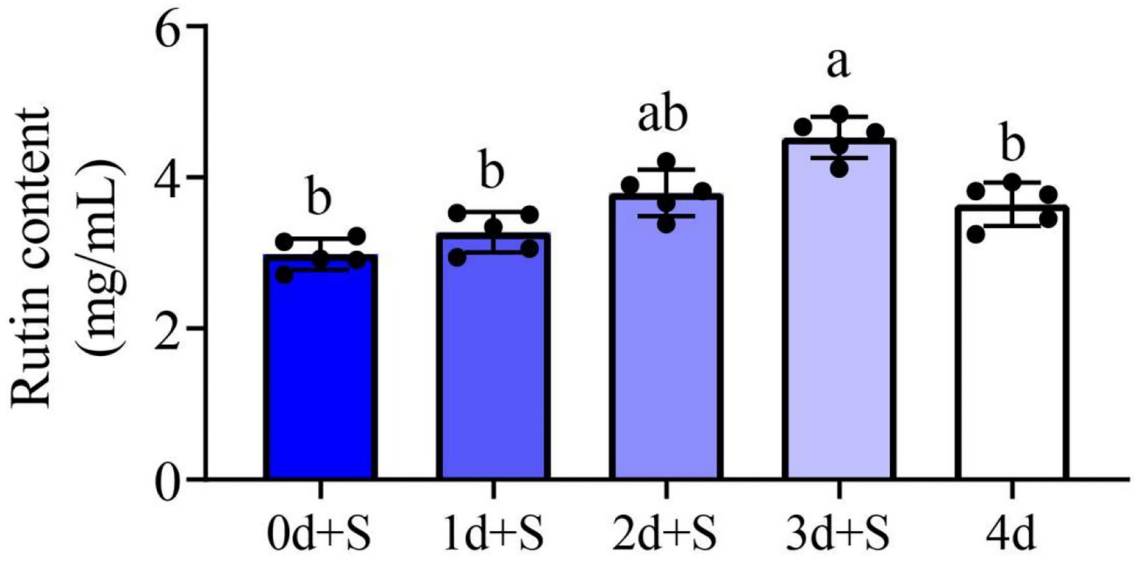

FIGURE 2
The rutin content in different treatments. Different columns represent different treatments, and dark to light color represents the salt addition time from long to short. Lowercase letter(s) indicate significant differences ($\alpha = 0.05$). Each black point represents the average value of replicates.

cotyledons and sprouts (including epicotyl and hypocotyl). Sprouts had a significantly ($p < 0.05$) higher rutin content than cotyledons (Figure 1C). The rutin content in different tissues revealed that sprouts are a suitable target tissue for further research.

Effects of salt stress on rutin content

The rutin contents under different salt exposure times were determined in this study. The result revealed differences in rutin content accumulation at different periods of salt addition. Compared to the treatment without salt (4 days), the rutin content of 2d+S and 3d+S treatments increased, while that of treatments 0d+S and 1d+S decreased (Figure 2). Short-term salt stress, thus, accelerated rutin content accumulation more than long-term stress, and the 3d+S treatment could be used as an optimal treatment to study the mechanism of rutin content accumulation.

Metabolome and transcriptome analysis

The study added a time point (12 h) to enhance broad target metabolome accuracy, with three time points (3d+S-0h, 3d+S-12h, and 3d+S-24h) in the 3d+S treatment, and each time point had three biological replicates. The raw data were uploaded to the Zenodo database (doi.org/10.5281/zenodo.6820497). A total of 732 metabolites were detected; the detailed information, including Q1, Q3, Rt, molecular weight, and ionization model, is shown in Supplementary Table 3. The overlay analysis of the QC-TIC diagram and the sample multipeak detection of MRM analysis diagram (Figure 3) showed that the data had good reproducibility and reliability, hence they could be used for further analysis.

In the comparison of 3d+S-0h vs. 3d+S-24h, 86 DAMs were increased while 55 were decreased (Supplementary Table 4). In the comparison of 3d+S-0h vs. 3d+S-12h, 62 DAMs were increased, while 63 were decreased (Supplementary Table 5 and Table 1). In this study, the DAMs in 3d+S-0h vs. 3d+S-24h and 3d+S-0h vs. 3d+S-12h had been combined together for analysis. A total of 189 DAMs were obtained after removing 77 duplicate DAMs, while 68 DAMs were associated with flavonoids after removing 36 duplicate flavonoid DAMs. In these, 68 DAMs were associated with flavonoids, five types of flavonoids (i.e., flavone, flavonol, flavonoid, flavanone, and isoflavone) had different expression levels (Figure 4), and each compound tested by HPLC-MS is listed in Supplementary Table 6. Rutin made up one DAM metabolome, and its content increased significantly. The KEGG enrichment was analyzed for two comparisons. In 3d+S-0h vs. 3d+S-12h, eight pathways had a p-value <0.05 and could thus be used as enrichment pathways (Table 2). In 3d+S-0h vs. 3d+S-24h, five pathways had a p-value <0.05

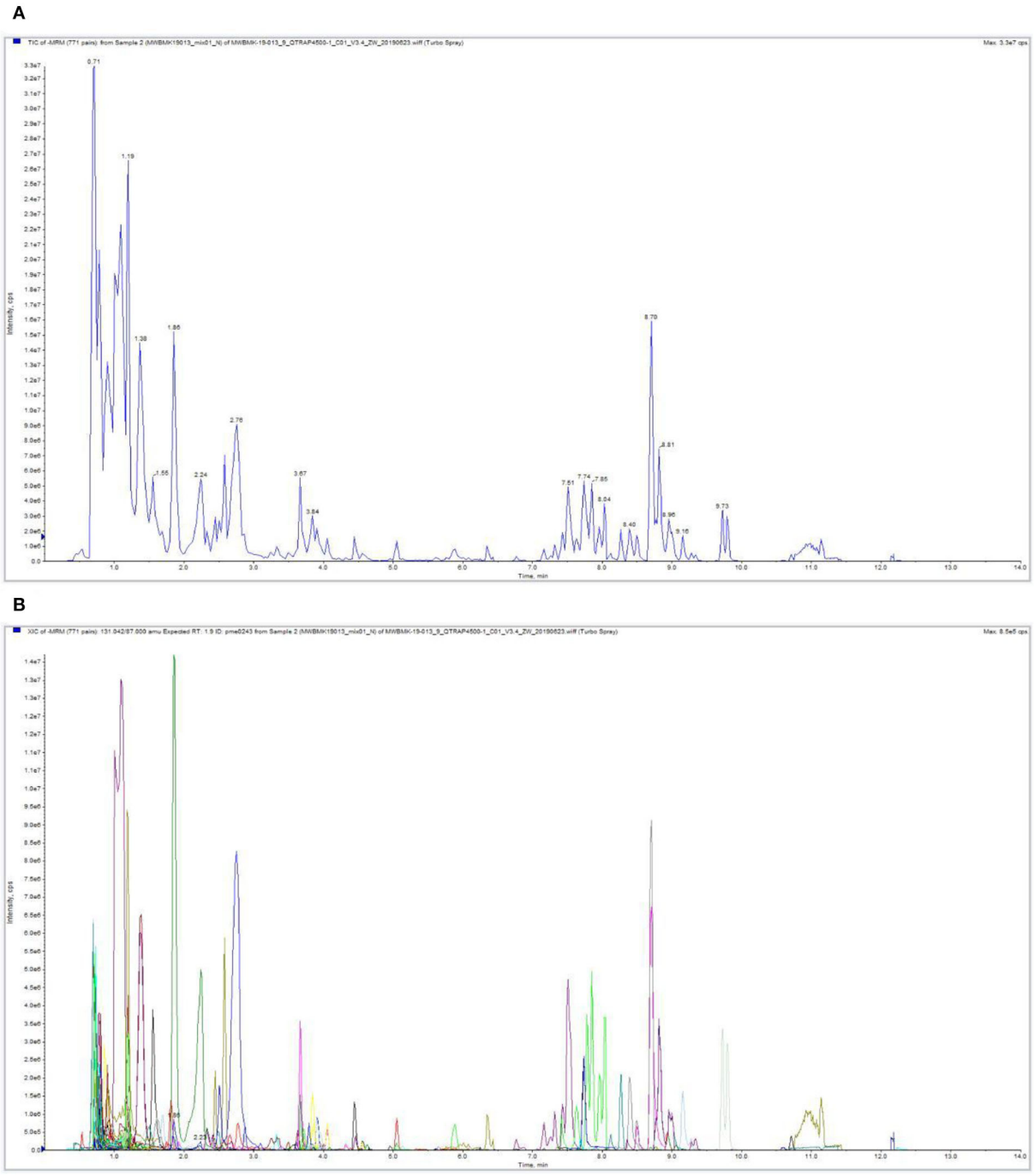

FIGURE 3
The overlay analysis of the QC-TIC and multipeak detection in MRM analysis of the metabolome. **(A)** The ion current of one sample, as revealed by mass spectrometry detection. **(B)** A multipeak detection plot of the metabolites in the multiple reaction monitoring mode.

and could thus be used as enrichment pathways (Table 3). Four candidate pathways were found in the metabolomics analysis, namely, phenylpropanoid biosynthesis (ko00940), flavonoid biosynthesis (ko00941), flavone and flavonol biosynthesis (ko00944), and biosynthesis of secondary metabolites (ko01110).

The samples of three time points, i.e., 3d+S-0h, 3d+S-12h, and 3d+S-24h in the 3d+S treatment, were used for RNA-seq. The data quality was sufficient for follow-up analysis (Supplementary Table 7) and data were uploaded to the NCBI database (PRJNA746732) (Supplementary Table 8). In the comparisons of 3d+S-0h vs. 3d+S-12h, and 3d+S-0h vs. 3d+S-24h, a total of 1,230 and 1,450 DEGs were found, of which 812 and 904 DEGs were upregulated, respectively, and 418 and 546 were downregulated, respectively (Table 4). All DEGs were analyzed in KEGG enrichment, respectively. A total of 16 pathways were enriched in 3d+S-0h vs. 3d+S-12h (Table 5), while 13 pathways were enriched in 3d+S-0h vs. 3d+S-24h (Table 6). In the transcriptome analysis of 3d+S-0h vs. 3d+S-12h, and 3d+S-0h vs. 3d+S-24h, seven candidate pathways were found. From the combined metabolome and transcriptome results of enriched KEGG pathways, phenylpropanoid biosynthesis (ko00940) and flavonoid biosynthesis (ko00941) responded to salt stress by accumulating flavonoids.

TABLE 1 The number of differentially altered metabolites (DAMs).

Groups	Total DAMs	Up DAMs	Down DAMs
3d+S-0h *vs.* 3d+S-12h	141	86	55
3d+S-0h *vs.* 3d+S-24h	125	62	63

Analysis and verification of pathway mechanisms

The mechanisms of pathways enriched under salt stress are presented in Figure 5. Phenylpropanoid biosynthesis was the upstream pathway in which the metabolites, such as caffeate, scopoletin, sinapic acid, and sinapyl alcohol, were differentially expressed and directly affected the downstream pathway (flavonoid biosynthesis). Also, DEGs were enriched in some enzymes, including 4-coumarate-CoA ligase (4CL), caffeoyl-CoA o-methyltransferase, CAD, and POD. The flavonoid biosynthetic pathway was also enriched as the downstream pathway of phenylpropanoid biosynthesis, and the DEGs were enriched in some enzymes, such as FLS, CHI, and dihydroflavonol-4-reductase. A heatmap of DAMs (such as rutin, cosmosiin, luteolin, garbanzol, and quercetin) showed a significant change in the flavonoid biosynthesis pathway. Analysis of these two pathways revealed that the phenylpropanoid and flavonoid biosynthesis pathways could be crucial in salt stress response by promoting flavonoid accumulation.

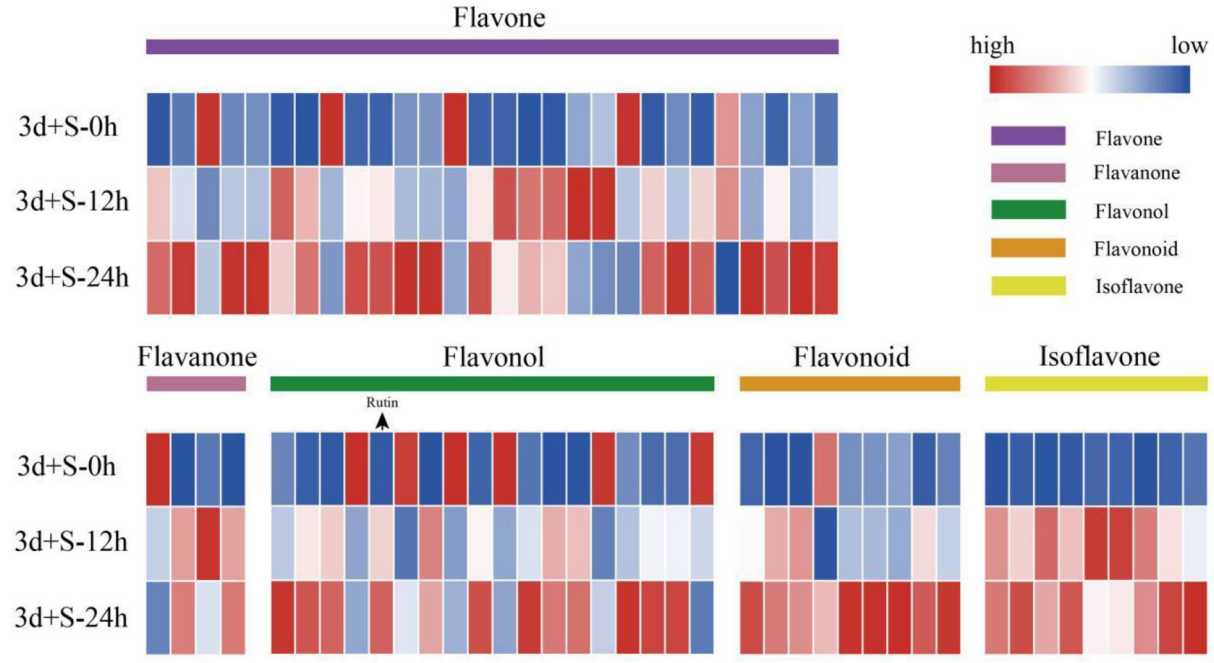

FIGURE 4
The heatmap of differentially altered metabolites associated with flavonoids. Different colored modules on the heatmap represent different types of flavonoids, while the order from top to bottom is 3d+S-0h, 3d+S-12h, and 3d+S-24h. Blue to red color represents expression from low to high.

10.3389/fnut.2022.928805

TABLE 2 The enriched pathways of differentially altered metabolites (DAMs) compared 3d+S-0h vs. 3d+S-12h in KEGG analysis.

No.	Ko ID	KEGG pathway	P-value	DAMs
1	Ko00944	Flavone and flavonol biosynthesis	0.000	pmb0605; pme0199; pme0197; pme3211; pme1622; pme0089
2	Ko00941	Flavonoid biosynthesis	0.001	pme0199; pmf0108; pme0089; pme1521; pme3461; pme1201
3	Ko00945	Stilbenoid, diarylheptanoid and gingerol biosynthesis	0.015	pme1458
4	Ko00940	Phenylpropanoid biosynthesis	0.018	pme3125; pme0030; pma0149; pme3305
5	Ko01110	Biosynthesis of secondary metabolites	0.021	pme0199; pme3261; pme0030; pme3125; pme2555; pmf0558; pme1622; pme3266; pme0089; pme1521; pme1692; pme1201; pme0197; pmf0248; pme3211; pme1002; pme1458; pme3233; pme0026; pmb0449; pme3305
6	Ko00965	Betalain biosynthesis	0.027	pme0030
7	Ko00230	Purine metabolism	0.027	pme1119; pme0193; pme1692; pmb0514; pmb2684; pme2555; pmd0023
8	Ko00910	Nitrogen metabolism	0.033	pme0193

TABLE 3 The enriched pathways of differentially altered metabolites (DAMs) compared 3d+S-0h vs. 3d+S-24h in KEGG analysis.

No.	Ko ID	KEGG pathway	P-value	DAMs
1	Ko00944	Flavone and flavonol biosynthesis	0.000	pme0374; pme1622; pme3211; pme0197
2	Ko00941	Flavonoid biosynthesis	0.000	pme1201; pmf0345; pme3509; pme1521; pmf0108
3	Ko01110	Biosynthesis of secondary metabolites	0.001	pme1695; pme2801; pme2993; pme0006; pmf0558; pme0303; pme3266; pme3125; pme2122; pme3305; pme0197; pme1622; pme0355; pmf0117; pme2155; pme1201; pmf0345; pme3252; pme1841; pme3233; pme1521; pme3211; pme3261; pme0013; pme3553
4	Ko00940	Phenylpropanoid biosynthesis	0.003	pme0303; pmb0242; pme2993; pma0149; pme3125; pme1695; pme3305
5	Ko00943	Isoflavonoid biosynthesis	0.028	pme3233; pme3509; pme3208; pme3252; pme0355; pmf0117; pme3266; pme3261

TABLE 4 The number of differentially expressed genes (DEGs).

Groups	Total DEGs	Up DEGs	Down DEGs
3d+S-0h *vs* 3d+S-12h	1230	812	418
3d+S-0h *vs* 3d+S-24h	1450	904	546

Herein, enzyme activity analysis in DEG-enriched points and qRT-PCR analysis was also done. Four enzyme activities that were DEG-enriched were tested. The results showed that salt stress significantly changed the activities of CAD, POD, CHI, and FLS (Figure 6). Besides, the DEGs heatmap showed that DEGs' expression associated with the enzymes differed significantly following salt exposure. Also, six different DEGs in these two pathways, which were enriched in CAD (*Phvul.002G144800* and *Phvul.003G029500*), POD (*Phvul.001G143300*, *Phvul.007G008400* and *Phvul.008G249900*), and FLS (*Phvul.003G216600*), were selected for qRT-PCR analysis while their expression and functional analysis are shown in Supplementary Table 9. The results showed that the values of $|\log_2(\text{FoldChange})|$ expression were all >1 (Figure 7), suggesting that these six genes had a significant expression change at the transcriptional level. Metabolome and transcriptome results revealed that phenylpropanoid and flavonoid biosynthesis responded to salt stress by promoting flavonoid accumulation.

TABLE 5 The enriched pathways of differentially expressed genes (DEGs) compared 3d+S-0h vs. 3d+S-12h in KEGG analysis.

No.	Ko ID	KEGG pathway	*P*-value
1	Ko00195	Photosynthesis	0.000
2	Ko00196	Photosynthesis—antenna proteins	0.000
3	Ko00904	Diterpenoid biosynthesis	0.000
4	Ko00360	Phenylalanine metabolism	0.000
5	Ko00940	Phenylpropanoid biosynthesis	0.000
6	Ko00710	Carbon fixation in photosynthetic organisms	0.001
7	Ko00730	Thiamine metabolism	0.008
8	Ko00330	Arginine and proline metabolism	0.009
9	Ko00860	Porphyrin and chlorophyll metabolism	0.012
10	Ko00380	Tryptophan metabolism	0.015
11	Ko00290	Valine, leucine and isoleucine biosynthesis	0.016
12	Ko00908	Zeatin biosynthesis	0.022
13	Ko00906	Carotenoid biosynthesis	0.026
14	Ko00280	Valine, leucine and isoleucine degradation	0.030
15	Ko01220	Degradation of aromatic compounds	0.033
16	Ko00591	Linoleic acid metabolism	0.047

TABLE 6 The enriched pathways of differentially expressed genes (DEGs) compared 3d+S-0h vs. 3d+S-24h in KEGG analysis.

No.	Ko ID	KEGG pathway	*P*-value
1	Ko00195	Photosynthesis	0.000
2	Ko04712	Circadian rhythm—plant	0.000
3	Ko00196	Photosynthesis—antenna proteins	0.000
4	Ko04075	Plant hormone signal transduction	0.000
5	Ko00360	Phenylalanine metabolism	0.000
6	Ko00941	Flavonoid biosynthesis	0.001
7	Ko00904	Diterpenoid biosynthesis	0.001
8	Ko00940	Phenylpropanoid biosynthesis	0.004
9	Ko00906	Carotenoid biosynthesis	0.008
10	Ko00710	Carbon fixation in photosynthetic organisms	0.014
11	Ko00905	Brassinosteroid biosynthesis	0.043
12	Ko00350	Tyrosine metabolism	0.044
13	Ko02010	ABC transporters	0.046

Discussion

Flavonoid trends in germinating common beans

Seed germination is the beginning of most plant life cycles. When seeds (including legumes) begin to germinate, they break dormancy and restore physiological function, which induces metabolism and produces secondary metabolites and other nutrients (37). Rutin is often used as a flavonoid standard in botanical research (26, 38–40) because of its high content in legumes (41, 42). Similarly, the metabolome analysis conducted in this study revealed that germinating common beans have high levels of rutin. Here, the rutin content in germinating common beans initially increased, which illustrates that the beans were activated from hibernation and produced flavonoids (43). The rutin content then decreased after 96 h, which might be related to tissue differentiation after plant germination (44). Other nutrients in germinating beans also show similar trends; for instance, the γ-aminobutyric acid (GABA) content in germinating adzuki beans (*Vigna angularis*) showed increasing and decreasing, of which the highest content was at 48 h (37). The polyphenol content in germinating mung beans (*V. radiata*) also showed similar trends, and day 3 was the best time because it had the highest polyphenol content (45). Similarly, Lu and Guo (46) demonstrated that the vitamin C content of beans was at the highest level on day 3 and also showed an increasing and decreasing trend. Flavonoids (represented by rutin in this study) are important intermediates in plants' physiological metabolism, and their content also changes significantly during seed germination (47). Although secondary metabolites show these trends, the time elapsed for the levels to peak varies among species. This phenomenon might be because different nutrient types have different accumulation mechanisms, while different genotypes, or even different legume species, could also affect optimal times. In this study, rutin levels peaked at 96 h, which could be used as the optimal germination time.

Short-term salt stress promotes rutin accumulation

Abiotic stress could influence grain quality and composition in crops (48) and significantly affect the flavonoid content in plants because flavonoids are an important regulator of plant responses to abiotic stress (49). As common abiotic stress, salt stress is important and accelerates the accumulation of certain plant metabolites (50, 51). Several studies have

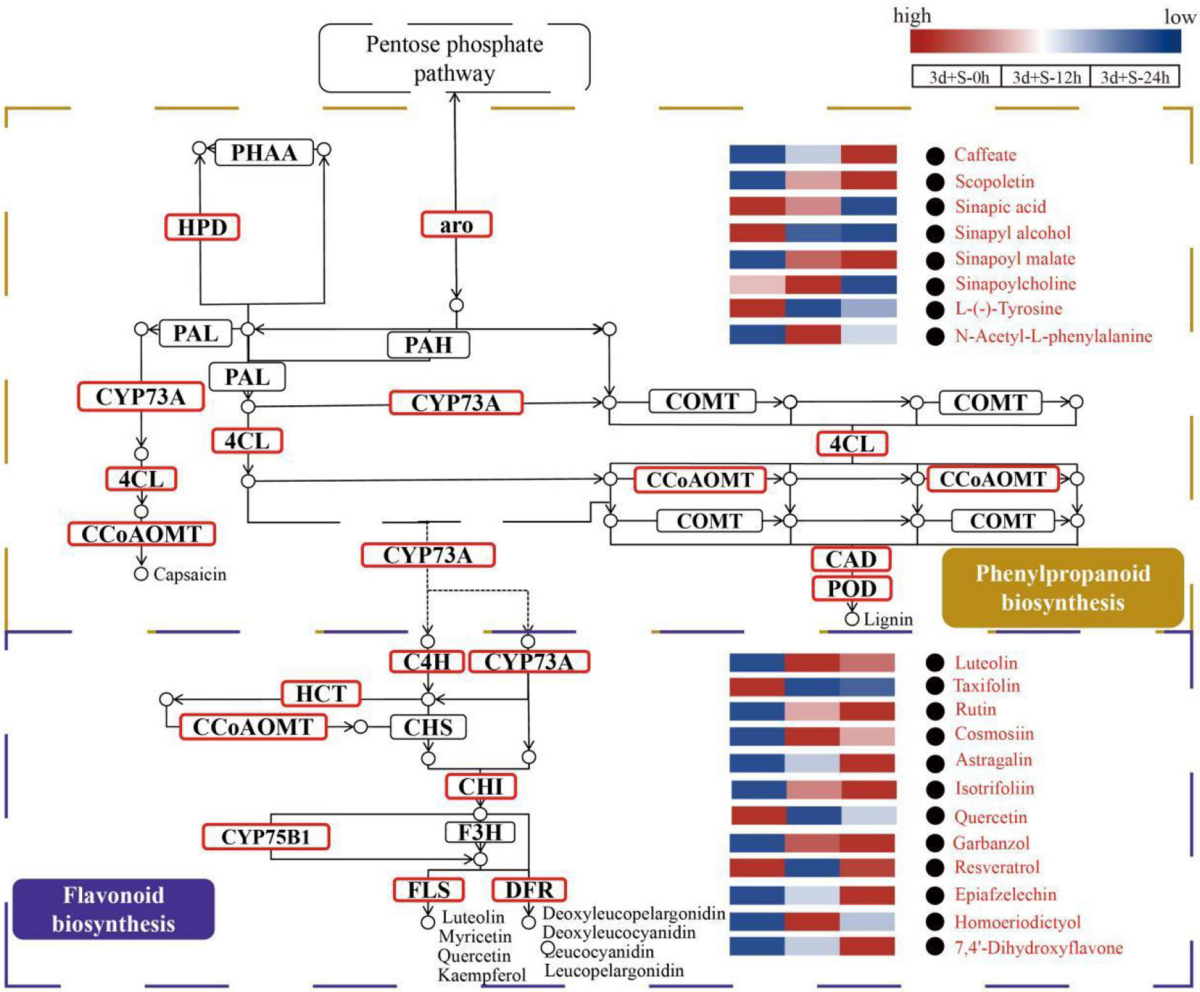

FIGURE 5
The enriched pathways analyzed by metabolomics and transcriptomics. The brown box represents the phenylpropanoid biosynthesis pathway, while the purple box represents the flavonoid biosynthesis pathway. The modules with red borders are differentially expressed genes (DEGs) enriched modules, while the red words with black circles are differentially altered metabolites (DAMs). Blue to red color represents expression from low to high.

demonstrated that 70 mmol/L NaCl is the appropriate salt concentration for inducing salinity stress in the common bean (22, 52). Rutin is an important class of secondary metabolites widely found in plants and contributes to plant growth and development (16). Previous studies demonstrated that rutin content increases under stress, especially abiotic stress (42, 52, 53). Numerous studies found that flavonoids, including rutin, significantly accumulate under abiotic stress in many plant species, including *Arabidopsis*, maize (54), tomato (55), and green tea (56). However, flavonoids, including rutin, are stressful substances, and prolonged stress does not necessarily enable continued flavonoid accumulation (57). The antioxidant levels in soybean during drought showed an alternating increasing and decreasing trend, suggesting that short-term drought could rapidly enhance antioxidant intensities, while long-term droughts might cause plants to gradually adapt to these stresses and stop enhancement (58). Also, plant antioxidant enzyme activities showed a similar trend under abiotic stress, which revealed that short-term stress could increase plants' secondary metabolite production, while secondary metabolites under long-term stress might return to a lower level (59). In contrast, stress might inhibit plant germination and reduce flavonoid accumulation. The salt-tolerant common bean germinated better than the salt-sensitive variety, while oxidase enzyme activities of salt-sensitive variety produced insignificant differences at the sprouting stage, limiting plant growth and vitality (52). Here, short-term salt stress was more conducive to rutin accumulation in germinating

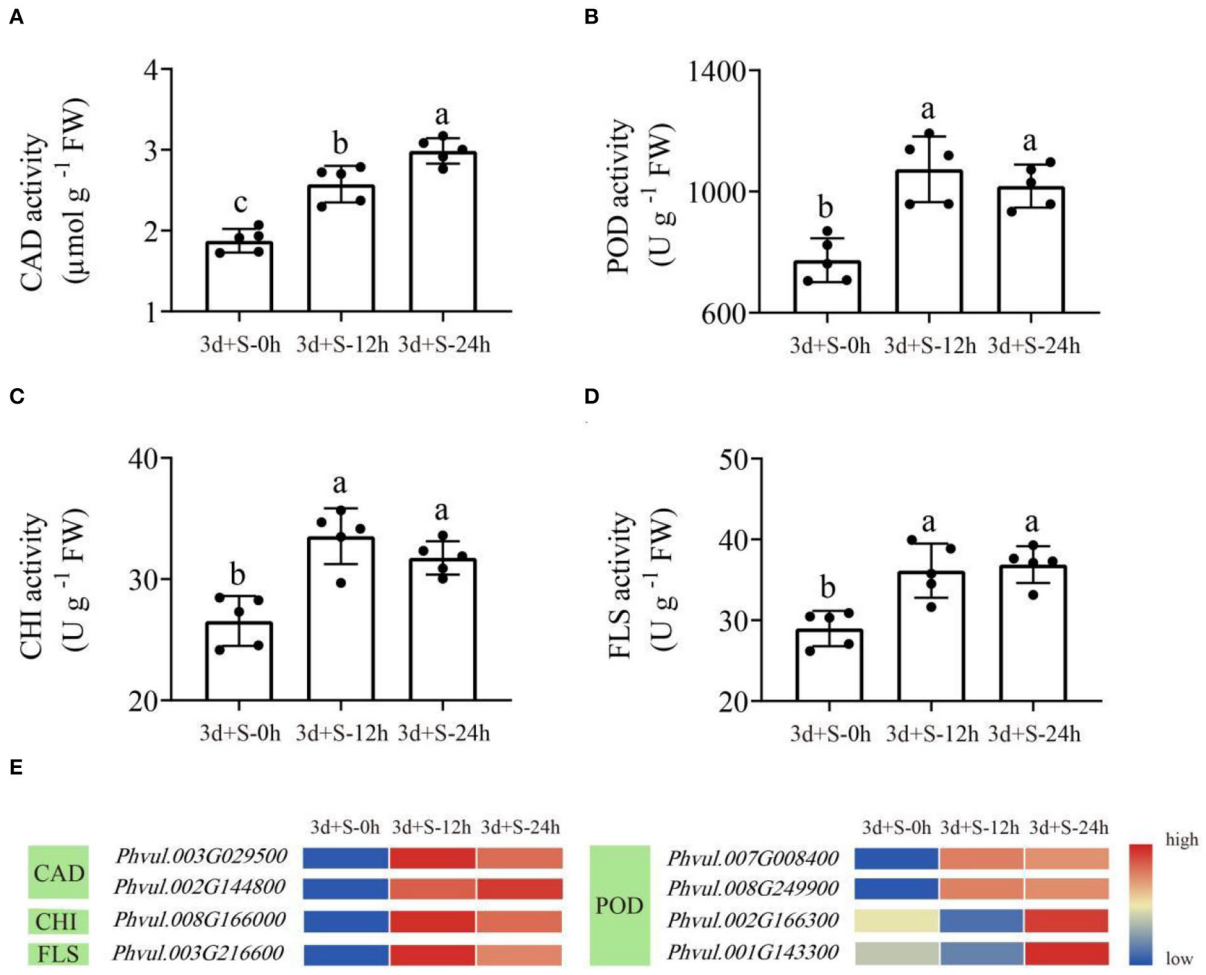

FIGURE 6
The enzyme activities in the enriched pathways at three time points. Lowercase letter(s) indicate significant differences ($\alpha = 0.05$). Each black point represents the average value of replicates. **(A)** CAD activity; **(B)** POD activity; **(C)** CHI activity; **(D)** FLS activity; **(E)** the heatmap of differentially expressed genes (DEGs) enriched in these four enzymes. Blue to red color represents low to high expression.

common beans, and 3d+S could be used to study the mechanism of rutin accumulation under salt stress.

The mechanism of flavonoid (rutin) accumulation under salt stress

In this study, phenylpropanoid and flavonoid biosynthesis were the two pathways that responded to salt stress and promoted flavonoid accumulation. Interestingly, phenylpropanoid biosynthesis was studied by a botanist researching the effects of abiotic stress on plant growth (60). Furthermore, phenylpropanoid biosynthesis is the pathway by which most flavonoids are produced, while enzyme activities in the phenylpropanoid biosynthetic pathway could alter the flavonoid accumulation rate (16). A key enzyme in phenylpropanoid metabolism is 4CL, which responds to abiotic stress, and the *4CL* genes have a function in regulating resilience (61). CAD is the final enzyme-catalyzed step in the phenylpropanoid biosynthesis pathway, and CAD activity is affected by salt stress, thus affecting the flavonoid accumulation rate (62). POD is a large family of plant-specific oxidoreductases, and POD activity can change significantly under salt stress (63).

As the downstream pathway of phenylpropanoid biosynthesis, flavonoid biosynthesis is an important pathway for flavonoid accumulation (16). Some enzymes in the flavonoid metabolic pathway, such as CHI and FLS, have also been implicated in flavonoid accumulation and abiotic stress response (64). CHI catalyzes the conversion of bicyclic chalcone into tricyclic (2S)-flavanone and is linked to salt stress (65). FLS

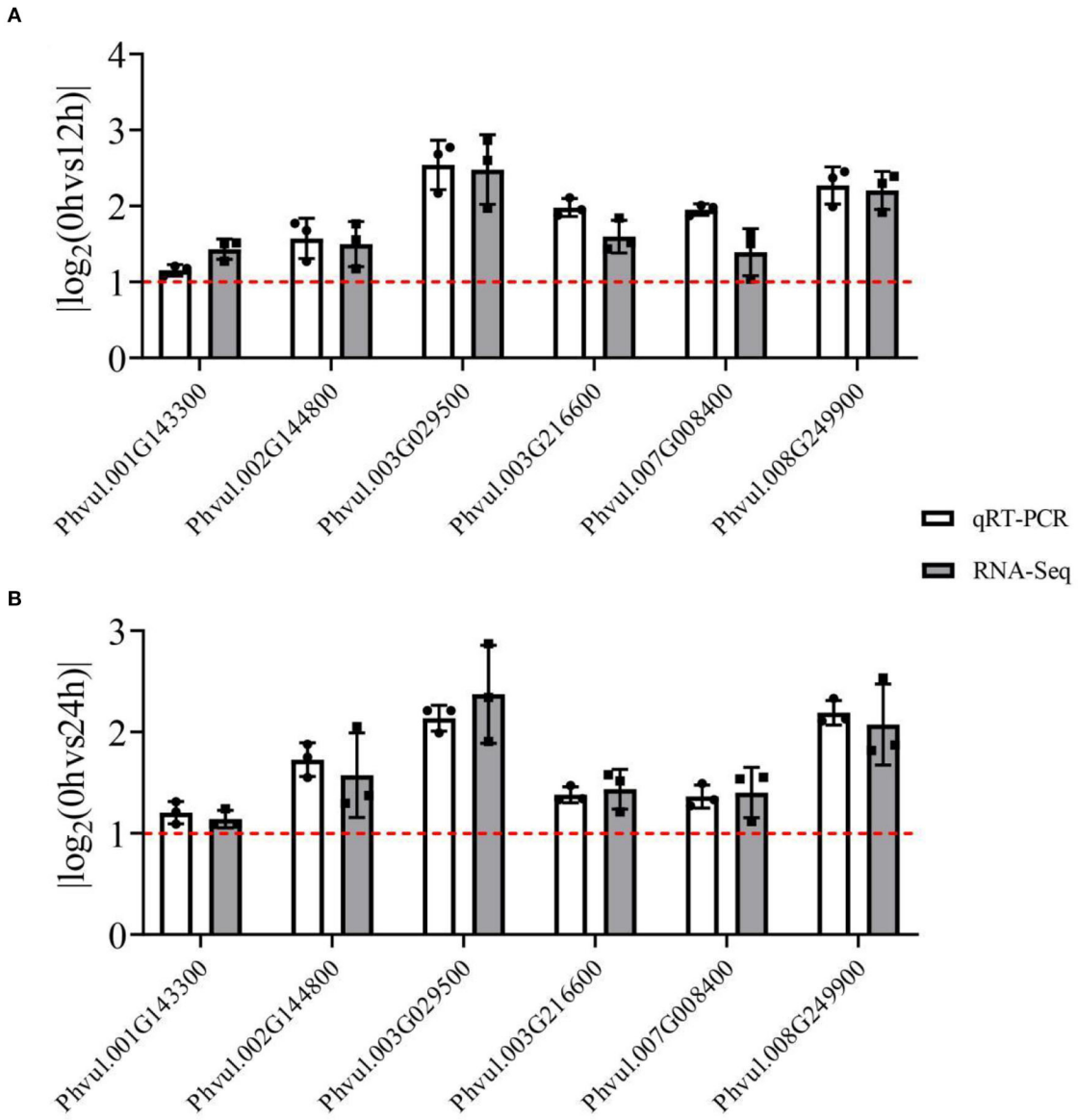

FIGURE 7
The qRT-PCR analysis of RNA-seq results of six differentially expressed genes (DEGs) from enriched pathways. The white grids represent the qRT-PCR results, while the gray grids represent the RNA-seq results. The red line represents the value of the |log2(FoldChange)|; a value >1 indicates that the genes were DEGs. Each black point represents the average value of replicates. **(A)** The |log2(FoldChange)| value of 3d+S-0h vs. 3d+S-12h; **(B)** the |log2(FoldChange)| value of 3d+S-0h vs. 3d+S-24h.

mediates the oxidation of dihydroflavonol to flavonol, while *FLS* gene upregulated and increased flavonoid content under salt stress (66). In this study, enzyme activities and expression levels were determined. The results revealed that salt stress affected the expression level of genes in the phenylpropanoid and flavonoid biosynthesis pathways and influenced the activities of CAD, POD, CHI, and FLS, which might be linked to flavonoid accumulation (Figure 8).

Conclusion

In this study, rutin accumulation trends in germinating common beans were researched, and 96 h was the most suitable germination time because the sprouts had the highest rutin content. Sprouts (including epicotyls and hypocotyls) had more rutin content than cotyledons, hence they could be used as a target research tissue. Short-term salt treatment was

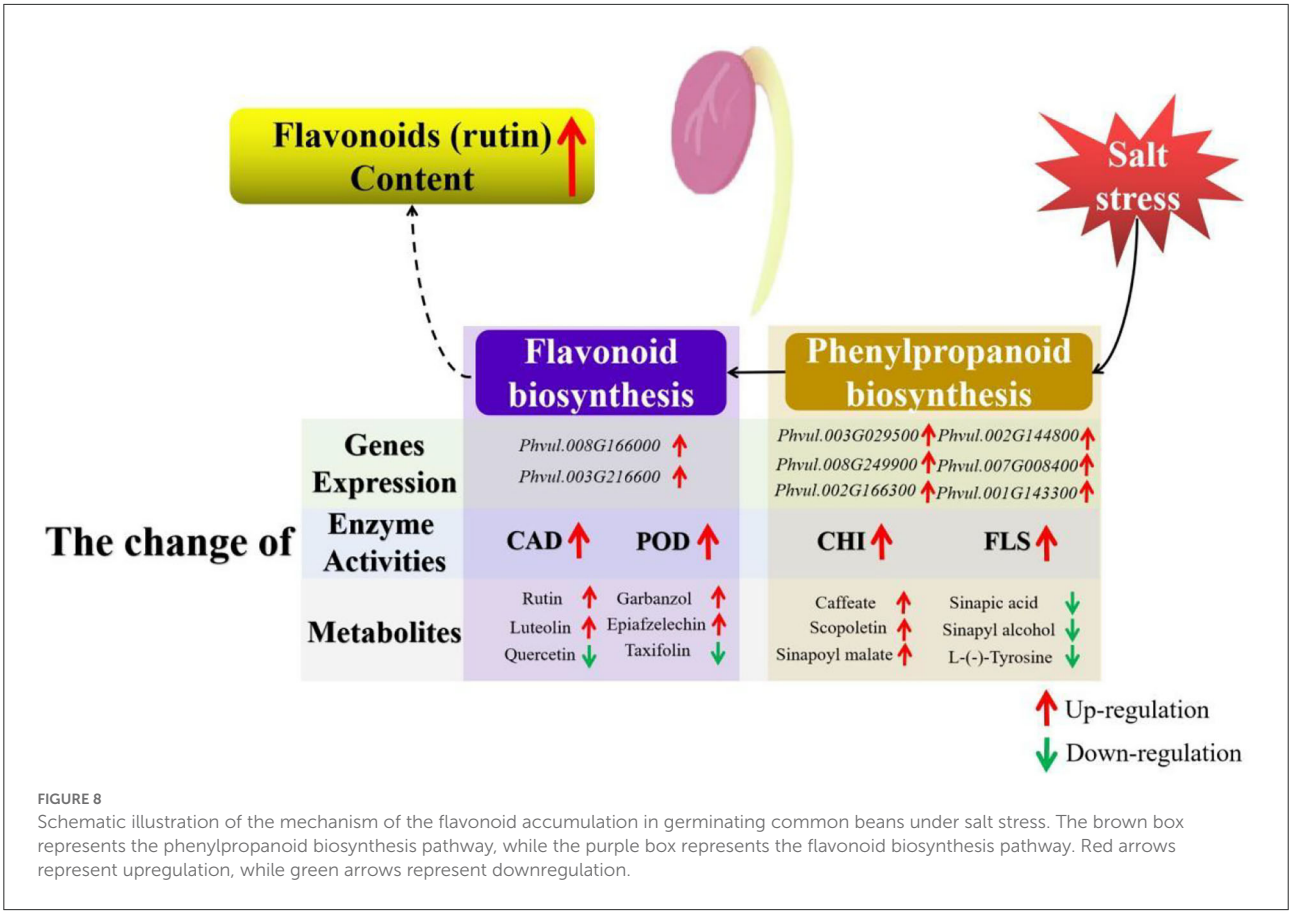

FIGURE 8
Schematic illustration of the mechanism of the flavonoid accumulation in germinating common beans under salt stress. The brown box represents the phenylpropanoid biosynthesis pathway, while the purple box represents the flavonoid biosynthesis pathway. Red arrows represent upregulation, while green arrows represent downregulation.

more favorable for flavonoid accumulation than long-term salt treatment. Furthermore, metabolome and transcriptome analysis during short-term salt treatment revealed that phenylpropanoid and flavonoid biosynthesis are the enriched pathways that respond to salt stress and promote flavonoid accumulation. This study provides a rationale for germinating common beans and gives a new insight into the molecular mechanism of flavonoid accumulation in common beans under salt stress.

Data availability statement

The transcriptome raw data was deposited to NCBI database, accession number PRJNA746732. The metabolome raw data was deposited to Zenodo database: doi.org/10.5281/zenodo.6820497.

Author contributions

QZ: data curation and writing original draft. HS, GZ, JixZ, and ZZ: data curation. WZ, QW, and JinZ: conceptualization and methodology. JX and YG: software. Y-lD: formal data analysis and preparation of materials. QZ, ZY, and Y-lD: methodology and revised the manuscript. J-dD: data curation and funding acquisition. All authors contributed to the article and approved the submitted version.

Funding

This study was financially supported by the National Key Research and Development Program (2020YFD1001402), the Research Project of Heilongjiang Bayi Agricultural University (XDB2011-02), and Special Funds from the Central Finance to Support the Development of Local Universities. The funding organizations had no role in experimental design, data collection, analysis, and interpretation of data or writing of the manuscript.

Conflict of interest

The authors declare that the research was conducted in the absence of any commercial or financial relationships that could be construed as a potential conflict of interest.

Publisher's note

Supplementary material

The Supplementary Material for this article can be found online at: https://www.frontiersin.org/articles/10.3389/fnut.2022.928805/full#supplementary-material

SUPPLEMENTARY FIGURE 1
The standard reference rutin curve.

SUPPLEMENTARY FIGURE 2
The proof of metabolome test.

SUPPLEMENTARY TABLE 1
Detailed information on the different treatments.

SUPPLEMENTARY TABLE 2
The qRT-PCR primers for differentially expressed genes (DEGs).

SUPPLEMENTARY TABLE 3
The detailed information of the metabolome analysis in this study.

SUPPLEMENTARY TABLE 4
The detailed information of differentially altered metabolites (DAMs) in the comparison of 3d+S-0h vs. 3d+S-24h.

SUPPLEMENTARY TABLE 5
The detailed information of differentially altered metabolites (DAMs) in the comparison of 3d+S-0h vs. 3d+S-12h.

SUPPLEMENTARY TABLE 6
The order of each compound expression in the five flavonoid kinds analyzed by metabolomics of differentially altered metabolites (DAMs) in the comparison of 3d+S-0h vs. 3d+S-12h or 3d+S-0h vs. 3d+S-24h.

SUPPLEMENTARY TABLE 7
The quality of the transcriptome results.

SUPPLEMENTARY TABLE 8
Transcriptome information uploaded to the NCBI database.

SUPPLEMENTARY TABLE 9
The expression and functional analysis of differentially expressed genes (DEGs) in qRT-PCR analysis.

References

1. Ganesan K, Xu B. Polyphenol-rich dry common beans (phaseolus vulgaris l.) and their health benefits. *Int J Mol Sci.* (2017) 18:2331. doi: 10.3390/ijms181123313

2. McDougall GJ. Phenolic-enriched foods: sources and processing for enhanced health benefits. *Proc Nutr Soc.* (2017) 2:163–71. doi: 10.1017/S0029665116000835

3. Díaz-Batalla L, Widholm JM, Fahey GC, Castaño-Tostado E, Paredes-López O. Chemical components with health implications in wild and cultivated mexican common bean seeds (*Phaseolus Vulgaris L.*). *J Agric Food Chem.* (2006) 6:2045–52. doi: 10.1021/jf051706l

4. Sajid M, Channakesavula CN, Stone SR, Kaur P. Synthetic Biology Towards Improved Flavonoid Pharmacokinetics. *Biomolecules.* (2021) 5. doi: 10.3390/biom11050754

5. Sudhakaran M, Sardesai S, Doseff AI. Flavonoids: new frontier for immuno-regulation and breast cancer control. *Antioxidants (Basel).* (2019) 4. doi: 10.3390/antiox8040103

6. Ye Q, Liu K, Shen Q, Li Q, Hao J, Han F, et al. Reversal of multidrug resistance in cancer by multi-functional flavonoids. *Front Oncol.* (2019) 487. doi: 10.3389/fonc.2019.00487

7. Amawi H, Ashby CR, Tiwari AK. Cancer Chemoprevention through Dietary Flavonoids: what's Limiting? *Chin J Cancer.* (2017) 1:50. doi: 10.1186/s40880-017-0217-4

8. Nabavi SM, Šamec D, Tomczyk M, Milella L, Russo D, Habtemariam S, et al. Flavonoid biosynthetic pathways in plants: versatile targets for metabolic engineering. *Biotechnol Adv.* (2020) 38:107316. doi: 10.1016/j.biotechadv.2018.11.005

9. Winkel-Shirley B. Flavonoid biosynthesis. A colorful model for genetics, biochemistry, cell biology, and biotechnology. *Plant Physiol.* (2001) 2:485–93. doi: 10.1104/pp.126.2.485

10. Sasaki N, Nakayama T. Achievements and perspectives in biochemistry concerning anthocyanin modification for blue flower coloration. *Plant Cell Physiol.* (2015) 1:28–40. doi: 10.1093/pcp/pcu097

11. Nakamura K, Koyama M, Ishida R, Kitahara T, Nakajima T, Aoyama T. Characterization of bioactive agents in five types of marketed sprouts and comparison of their antihypertensive, antihyperlipidemic, and antidiabetic effects in fructose-loaded SHRs. *J Food Sci Technol.* (2016) 53:581–90. doi: 10.1007/s13197-015-2048-0

12. Sritongtae B, Sangsukiam T, Morgan MR, Duangmal K. Effect of acid pretreatment and the germination period on the composition and antioxidant activity of rice bean (Vigna umbellata). *Food Chem.* (2017) 227:280–8. doi: 10.1016/j.foodchem.2017.01.103

13. Johnson JB, Skylas DJ, Mani JS, Xiang J, Walsh KB, Naiker M. Phenolic profiles of ten australian faba bean varieties. *Molecules.* (2021) 26:4642. doi: 10.3390/molecules26154642

14. Tsurunaga Y, Takahashi T, Katsube T, Kudo A, Kuramitsu O, Ishiwata M, Matsumoto S. Effects of UV-B irradiation on the levels of anthocyanin, rutin and radical scavenging activity of buckwheat sprouts. *Food Chem.* (2013) 141:552–6. doi: 10.1016/j.foodchem.2013.03.032

15. Taylor LP, Grotewold E. Flavonoids as developmental regulators. *Curr Opin Plant Biol.* (2005) 3:317–23. doi: 10.1016/j.pbi.2005.03.005

16. Liu W, Feng Y, Yu S, Fan Z, Li X, Li J, et al. The flavonoid biosynthesis network in plants. *Int J Mol Sci.* (2021) 23. doi: 10.3390/ijms222312824

17. Li Q, Yu HM, Meng XF, Lin JS, Li YJ, Hou BK, et al. Ectopic expression of glycosyltransferase Ugt76e11 increases flavonoid accumulation and enhances abiotic stress tolerance in arabidopsis. *Plant Biol (Stuttg).* (2018) 1:10–9. doi: 10.1111/plb.12627

18. Tlahig S, Bellani L, Karmous I, Barbieri F, Loumerem M, Muccifora S, et al. Response to salinity in legume species: an insight on the effects of salt stress during seed germination and seedling growth. *Chem Biodivers.* (2021) 4:e2000917. doi: 10.1002/cbdv.202000917

19. Eum HL, Park Y, Yi TG, Lee JW, Ha KS, Choi IY, et al. Effect of germination environment on the biochemical compounds and anti-inflammatory properties of soybean cultivars. *PLoS ONE.* (2020) 4:e0232159. doi: 10.1371/journal.pone.0232159

20. Guo X, Li T, Tang K, Liu RH. Effect of Germination on Phytochemical Profiles and Antioxidant Activity of Mung Bean Sprouts (Vigna Radiata). *J Agric Food Chem.* (2012) 44:11050–5. doi: 10.1021/jf304443u

21. Gu H, Wang Y, Xie H, Qiu C, Zhang S, Xiao J, et al. Drought stress triggers proteomic changes involving lignin, flavonoids and fatty acids in tea plants. *Sci Rep.* (2020) 1:15504. doi: 10.1038/s41598-020-72596-1

22. Zhang Q, Geng J, Du Y, Zhao Q, Zhang W, Fang Q, et al. Heat shock transcription factor (hsf) gene family in common bean (phaseolus vulgaris): genome-wide identification, phylogeny, evolutionary expansion and expression analyses at the sprout stage under abiotic stress. *BMC Plant Biol.* (2022) 1:33. doi: 10.1186/s12870-021-03417-4

23. Liu J, Li C, Ding G, Quan W. Artificial intelligence assisted ultrasonic extraction of total flavonoids from rosa sterilis. *Molecules*. (2021) 26:3835. doi: 10.3390/molecules26133835

24. Lou H, Yuan H, Yamazaki Y, Sasaki T, Oka S. Alkaloids and flavonoids from peanut skins. *Planta Med.* (2001) 67:345–9. doi: 10.1055/s-2001-14319

25. Rolim A, Maciel CP, Kaneko TM, Consiglieri VO, Salgado-Santos IM, Velasco MV. Validation assay for total flavonoids, as rutin equivalents, from Trichilia catigua Adr. Juss (Meliaceae) and Ptychopetalum olacoides Bentham (Olacaceae) commercial extract. *J AOAC Int.* (2005) 88:1015–9.

26. Rolim A, Oishi T, Maciel CP, Zague V, Pinto CA, Kaneko TM, et al. Total flavonoids quantification from O/W emulsion with extract of Brazilian plants. *Int J Pharm.* (2006) 308:107–14. doi: 10.1016/j.ijpharm.2005.10.031

27. Chen W, Gong L, Guo Z, Wang W, Zhang H, Liu X, et al. A novel integrated method for large-scale detection, identification, and quantification of widely targeted metabolites: application in the study of rice metabolomics. *Mol Plant.* (2013) 6:1769–80. doi: 10.1093/mp/sst080

28. Scholz M, Selbig J. Visualization and analysis of molecular data. *Methods Mol Biol.* (2007) 87–104. doi: 10.1007/978-1-59745-244-1_6

29. Wixon J, Kell D. The Kyoto Encyclopedia of Genes and Genomes—Kegg. *Yeast.* (2000) 1:48–55. doi: 10.1155/2000/981362

30. Kim D, Pertea G, Trapnell C, Pimentel H, Kelley R, Salzberg SL, et al. Tophat2: accurate alignment of transcriptomes in the presence of insertions, deletions and gene fusions. *Genome Biol.* (2013) 4:R36. doi: 10.1186/gb-2013-14-4-r36

31. Florea L, Song L, Salzberg SL. Thousands of exon skipping events differentiate among splicing patterns in sixteen human tissues. (2013) F1000Res: 188. doi: 10.12688/f1000research.2-188.v1

32. Goffner D, Joffroy I, Grima-Pettenati J, Halpin C, Knight ME, Schuch W, et al. Purification and characterization of isoforms of cinnamyl alcohol dehydrogenase from eucalyptus xylem. *Planta.* (1992) 1:48–53. doi: 10.1007/BF01160711

33. Doerge DR, Divi RL, Churchwell MI. Identification of the colored guaiacol oxidation product produced by peroxidases. *Anal Biochem.* (1997) 1:10–7. doi: 10.1006/abio.1997.2191

34. Lister CE, Lancaster JE, Walker JR. Developmental changes in enzymes of flavonoid biosynthesis in the skins of red and green apple cultivars. *J Sci Food Agric.* (1996). doi: 10.1002/(SICI)1097-0010(199607)71:3<313::AID-JSFA586>3.0.CO;2-N

35. Hrazdina G, Weeden NF. Enzymatic control of anthocyanin expression in the flowers of pea (Pisum Sativum) mutants. *Biochem Genet.* (1986) 3–4:309–17. doi: 10.1007/BF00502797

36. Livak KJ, Schmittgen TD. Analysis of relative gene expression data using real-time quantitative pcr and the 2(-Delta Delta C(T)) Method. *Methods.* (2001) 4:402–8. doi: 10.1006/meth.2001.1262

37. Jiang X, Xu Q, Zhang A, Liu Y, Zhao L, Gu L, et al. Optimization of Γ-aminobutyric acid (gaba) accumulation in germinating adzuki beans (vigna angularis) by vacuum treatment and monosodium glutamate, and the molecular mechanisms. *Front Nutr.* (2021) 693862. doi: 10.3389/fnut.2021.693862

38. Rice-Evans CA, Miller NJ, Paganga G. Structure-antioxidant activity relationships of flavonoids and phenolic acids. *Free Radic Biol Med.* (1996) 20:933–56. doi: 10.1016/0891-5849(95)02227-9

39. Janjua NK, Siddiqa A, Yaqub A, Sabahat S, Qureshi R, ul Haque S. Spectrophotometric analysis of flavonoid-DNA binding interactions at physiological conditions. *Spectrochim Acta A Mol Biomol Spectrosc.* (2009) 74:1135–7. doi: 10.1016/j.saa.2009.09.0225

40. Yang Y, Zhao Y, Zuo X, Wang Y. Determination of total flavonoids for paris polyphylla var. yunnanensis in different geographical origins using uv and ft-ir spectroscopy. *J AOAC Int.* (2019) 2:457–64. doi: 10.5740/jaoacint.18-0188

41. Kan L, Nie S, Hu J, Wang S, Cui SW, Li Y, et al. Nutrients, phytochemicals and antioxidant activities of 26 kidney bean cultivars. *Food Chem Toxicol.* (2017) PtB:47–77. doi: 10.1016/j.fct.2016.09.007

42. Xu C, Wei L, Huang S, Yang C, Wang Y, Yuan H, et al. Drought resistance in qingke involves a reprogramming of the phenylpropanoid pathway and udp-glucosyltransferase regulation of abiotic stress tolerance targeting flavonoid biosynthesis. *J Agric Food Chem.* (2021) 13:3992–4005. doi: 10.1021/acs.jafc.0c07810

43. Kayembe N, Jansen V. Germination as a processing technique for soybeans in small-scale farming. *S Afr J Anim Sci.* (2013) 2:167–73. doi: 10.4314/sajas.v43i2.7

44. Yang R, Yin Y, Guo L, Han Y, Gu Z. Sequence analysis of diamine oxidase gene from fava bean and its expression related to Γ-aminobutyric acid accumulation in seeds germinating under hypoxia-nacl stress. *J Sci Food Agric.* (2014) 8:1585–91. doi: 10.1002/jsfa.6461

45. Kapravelou G, Martínez R, Perazzoli G, Sánchez González C, Llopis J, Cantarero S, et al. Germination improves the polyphenolic profile and functional value of mung bean (*Vigna radiata* L.). *Antioxidants (Basel).* (2020) 9:746. doi: 10.3390/antiox9080746

46. Lu Y, Guo X. The effect of light in vitamin c metabolism regulation and accumulation in mung bean (*Vigna Radiata*) germination. *Plant Foods Hum Nutr.* (2020) 1:24–9. doi: 10.1007/s11130-019-00787-x

47. Yiming Z, Hong W, Linlin C, Xiaoli Z, Wen T, Xinli S, et al. Evolution of nutrient ingredients in tartary buckwheat seeds during germination. *Food Chem.* (2015) 244–8. doi: 10.1016/j.foodchem.2015.03.115

48. Farooq M, Hussain M, Usman M, Farooq S, Alghamdi SS, Siddique KHM, et al. Impact of abiotic stresses on grain composition and quality in food legumes. *J Agric Food Chem.* (2018) 34:8887–97. doi: 10.1021/acs.jafc.8b02924

49. Nakabayashi R, Saito K. Integrated metabolomics for abiotic stress responses in plants. *Curr Opin Plant Biol.* (2015) 10–6. doi: 10.1016/j.pbi.2015.01.003

50. Borsai O, Hassan MA, Negruier C, Raigón MD, Boscaiu M, Sestra RE, et al. Responses to salt stress in portulaca: Insight into its tolerance mechanisms. *Plants (Basel).* (2020) 9:1660. doi: 10.3390/plants9121660

51. Genzel F, Dicke MD, Junker-Frohn LV, Neuwohner A, Thiele B, Putz A, et al. Impact of moderate cold and salt stress on the accumulation of antioxidant flavonoids in the leaves of two capsicum cultivars. *J Agric Food Chem.* (2021) 69:6431–43. doi: 10.1021/acs.jafc.1c00908

52. Zhang Q, Li M, Xia CY, Zhang WJ, Yin ZG, Zhang YL, et al. Transcriptome-based analysis of salt-related genes during the sprout stage of common bean (*Phaseolus Vulgaris*) under salt stress conditions. *Biotechnol Biotechnol Equip.* (2021) 1:1086–98. doi: 10.1080/13102818.2021.1954091

53. Röhlen-Schmittgen S, Ellenberger J, Groher T, Hunsche M. Boosting leaf contents of rutin and solanesol in bio-waste of Solanum lycopersicum. *Plant Physiol Biochem.* (2020) 155:888–97. doi: 10.1016/j.plaphy.2020.08.035

54. Qin L, Sun L, Wei L, Yuan J, Kong F, Zhang Y, et al. Maize Sro1e represses anthocyanin synthesis through regulating the mbw complex in response to abiotic stress. *Plant J.* (2021) 4:1010–25. doi: 10.1111/tpj.15083

55. Atkinson NJ, Dew TP, Orfila C, Urwin PE. Influence of combined biotic and abiotic stress on nutritional quality parameters in tomato (*Solanum lycopersicum*). *J Agric Food Chem.* (2011) 17:9673–82. doi: 10.1021/jf202081t

56. Prasanth MI, Sivamaruthi BS, Chaiyasut C, Tencomnao T. A review of the role of green tea (*Camellia sinensis*) in antiphotoaging, stress resistance, neuroprotection, and autophagy. *Nutrients.* (2019) 11:474. doi: 10.3390/nu11020474

57. Nakabayashi R, Mori T, Saito K. Alternation of flavonoid accumulation under drought stress in arabidopsis thaliana. *Plant Signal Behav.* (2014) 8:e29518. doi: 10.4161/psb.29518

58. Easwar Rao D, Viswanatha Chaitanya K. Changes in the Antioxidant Intensities of Seven Different Soybean (*Glycine Max* (L) Merr) Cultivars During Drought. *J Food Biochem.* (2020) 2:e.(13118). doi: 10.1111/jfbc.13118

59. Du Y, Zhao Q, Chen L, Yao X, Zhang H, Wu J, et al. Effect of drought stress during soybean R2-R6 growth stages on sucrose metabolism in leaf and seed. *Int J Mol Sci.* (2020) 21:618. doi: 10.3390/ijms21020618

60. Cao L, Jin X, Zhang Y, Zhang M, Wang Y. Transcriptomic and metabolomic profiling of melatonin treated soybean (*Glycine Max* L.) under drought stress during grain filling period through regulation of secondary metabolite biosynthesis pathways. *PLoS ONE.* (2020) 10:e0239701. doi: 10.1371/journal.pone.0239701

61. Khakdan F, Nasiri J, Ranjbar M, Alizadeh H. Water deficit stress fluctuates expression profiles of 4cl, C3h, comt, cvomt and eomt genes involved in the biosynthetic pathway of volatile phenylpropanoids alongside accumulation of methylchavicol and methyleugenol in different iranian cultivars of Basil. *J Plant Physiol.* (2017) 74–83. doi: 10.1016/j.jplph.2017.07.012

62. Moura JC, Bonine CA, de Oliveira Fernandes Viana J, Dornelas MC, Mazzafera P. Abiotic and biotic stresses and changes in the lignin content and composition in plants. *J Integr Plant Biol.* (2010) 4:360–76. doi: 10.1111/j.1744-7909.2010.00892.x

63. Zhu JK. Salt and drought stress signal transduction in plants. *Annu Rev Plant Biol.* (2002) 247–73. doi: 10.1146/annurev.arplant.53.091401.143329

64. Zuk M, Szperlik J, Hnitecka A, Szopa J. Temporal biosynthesis of flavone constituents in flax growth stages. *Plant Physiol Biochem.* (2019) 234–45. doi: 10.1016/j.plaphy.2019.07.009

65. Wang H, Hu T, Huang J, Lu X, Huang B, Zheng Y, et al. The expression of millettia pinnata chalcone isomerase in saccharomyces cerevisiae salt-sensitive mutants enhances salt-tolerance. *Int J Mol Sci.* (2013) 5:8775–86. doi: 10.3390/ijms14058775

66. Xu N, Liu S, Lu Z, Pang S, Wang L, Wang L, et al. Gene expression profiles and flavonoid accumulation during salt stress in ginkgo biloba seedlings. *Plants (Basel).* (2020) 9:1162. doi: 10.3390/plants9091162

frontiers | Frontiers in Nutrition

TYPE Brief Research Report
PUBLISHED 26 September 2022
DOI 10.3389/fnut.2022.928074

OPEN ACCESS

EDITED BY
Alberto Valdés,
Spanish National Research Council (CSIC), Spain

REVIEWED BY
Vuyo Mavumengwana,
South African Medical Research Council, South Africa
Wei Ye,
Sanming Academy of Agricultural Science, China
Jen-Tsung Chen,
National University of Kaohsiung, Taiwan
Rajiv Gandhi Gopalsamy,
Federal University of Sergipe, Brazil

*CORRESPONDENCE
Yingdan Yuan
yyd@yzu.edu.cn

SPECIALTY SECTION
This article was submitted to Nutrition and Food Science Technology, a section of the journal Frontiers in Nutrition

RECEIVED 25 April 2022
ACCEPTED 06 September 2022
PUBLISHED 26 September 2022

CITATION
Yuan Y, Zuo J, Zhang H, Zu M and Liu S (2022) Analysis of the different growth years accumulation of flavonoids in *Dendrobium moniliforme* (L.) Sw. by the integration of metabolomic and transcriptomic approaches. *Front. Nutr.* 9:928074. doi: 10.3389/fnut.2022.928074

Analysis of the different growth years accumulation of flavonoids in *Dendrobium moniliforme* (L.) Sw. by the integration of metabolomic and transcriptomic approaches

Yingdan Yuan*, Jiajia Zuo, Hanyue Zhang, Mengting Zu and Sian Liu

College of Horticulture and Plant Protection, Yangzhou University, Yangzhou, China

Dendrobium moniliforme (L.) Sw. is a valuable herbal crop, and flavonoids are primarily distributed as active ingredients in the stem, but the composition and synthesis mechanisms of flavonoids in different growth years are not clear. The accumulation of flavonoids in *D. moniliforme* from four different years was investigated, using a combined metabolomics and transcriptomics approach in this study. The phenylpropanoid and flavonoid biosynthetic pathways were significantly enriched in the Kyoto Encyclopedia of Genes and Genomes (KEGG) enrichment analysis of differentially expressed genes (DEGs) and differentially accumulated metabolites (DAMs). The widely targeted metabolomics technique revealed a total of 173 kinds of flavonoid metabolites. The metabolomics data confirmed the trend of total flavonoids (TF) content in stems of *D. moniliforme*, with chalcone, naringenin, eriodictyol, dihydroquercetin, and other flavonoids considerably up-accumulating in the third year. Twenty DEGs were detected that regulate flavonoid synthesis and the expression of these genes in different growth years was verified using real-time quantitative PCR (qRT-PCR). Furthermore, a comprehensive regulatory network was built for flavonoid biosynthesis and it was discovered that there is one *FLS* gene, one *CCR* gene and two MYB transcription factors (TFs) with a high connection with flavonoid biosynthesis by weighted gene co-expression network analysis (WGCNA). In this study, the correlation between genes involved in flavonoid biosynthesis and metabolites was revealed, and a new regulatory mechanism related to flavonoid biosynthesis in *D. moniliforme* was proposed. These results provide an important reference for the farmers involved in the cultivation of *D. moniliforme*.

KEYWORDS

***Dendrobium moniliforme*, transcriptome, metabolome, flavonoids, different growth years**

Introduction

Dendrobium is an epiphytic orchid whose stems are commonly used for the generation of nutritional beverages and food raw material (1). It has the effects of nourishing the kidney, hydrating the lung, benefitting the stomach; therefore, it is a type of plant with high development and utilization value (2). In the past, *Dendrobium moniliforme* (L.) Sw. was commonly employed as an attractive plant (3). The distribution of wild *D. moniliforme* is mainly in tropical and subtropical regions of Asia, such as China, Japan, South Korea, and Myanmar (4). In recent years, many studies have revealed that *D. moniliforme* also has medicinal value, including anti-inflammatory and antioxidant properties (5). Many studies have demonstrated that *D. moniliforme* includes a wide range of beneficial secondary metabolites, such as alkaloids (6) and flavonoids (7). The flavonoids in *D. moniliforme* are an important part of its pharmacological activity and an important index for evaluating *D. moniliforme* quality. Flavonoids are important secondary metabolites in plants, which have been proven to exert healthy functions in the human body and to have significant pharmacological effects such as anti-inflammatory, immunosuppressive, and antioxidant (8). Researchers discovered that the amount and composition of flavonoids change between species according to factors such as habitat, growth stage, and tissues (9). Therefore, due to the diversity of flavonoids and the complex laws of their distribution in different plants, it is significant to explore the flavonoid composition and biosynthetic pathways of *D. moniliforme* for different growth years.

As perennial plants, the content of medicinal components in *Dendrobium* spp. varies with the year of harvesting. Therefore, the active components in medicinal plants of different growth years should be evaluated in order to obtain high quality and optimal benefits of the herbs. At present, the most studies on the harvesting period of *Dendrobium* are reported on *D. officinale*, *D. huoshanense* and *D. nobile*; however there are few reports on *D. moniliforme* (10). People have greatly overlooked the potential of *D. moniliforme* as a medicinal plant. In summary, in this study, the *D. moniliforme* stems were used as the research object, and the transcriptome combined with the metabolome was analyzed so as to select the key genes that might affect the flavonoid synthesis in *D. moniliforme*. Some DEGs involved in flavonoid synthesis were also selected for real-time quantitative PCR (qRT-PCR) to prove the reliability of transcriptome data and further analysis. In addition, weighted gene co-expression network analysis (WGCNA) was used to obtain modules with high correlation of flavonoids, and screened the key genes involved in flavonoid biosynthesis. The data obtained in this study will provide important information for future research on the accumulation of flavonoids in *D. moniliforme* and provide a theoretical basis for determining the ideal harvesting year of *D. moniliforme*.

Materials and methods

Plant materials and determination of total flavonoids and alkaloids

Dendrobium moniliforme (L.) Sw. were cultivated artificially and gathered in the greenhouse of Anhui Tongjisheng Biotechnology Co., Ltd. In terms of culture conditions, the samples were consistent with previous research (11). The stems of *D. moniliforme* were collected from 1-year-old (Stem length: 17.35 ± 3.87 cm; stem diameter: 1.98 ± 0.54 cm), 2-year-old (Stem length: 22.47 ± 2.59 cm; stem diameter: 2.33 ± 0.48 cm), 3-year-old (Stem length: 27.7 ± 6.92 cm; stem diameter: 2.67 ± 0.52 cm), and 4-year-old (Stem length: 30.45 ± 3.58 cm; stem diameter: 3.64 ± 1.32 cm) plants, respectively, as the research object (**Supplementary Figure 1**). We removed the leaves and partial roots from the stems to get the clean stems. To extract ribonucleic acid (RNA) and metabolites, all materials were frozen in liquid nitrogen at -80°C. To determine the total alkaloids (TA) and total flavonoids (TF), all materials were washed and dried. Furthermore, in this study, all experiments were carried out in three biological replicates.

TF and TA were extracted and measured using a plant flavonoid kit and a plant alkaloid kit (Suzhou Comin Biotechnology Co., Ltd., Suzhou, China), respectively.

Widely targeted metabolomics profiling

The frozen samples (systematic samples maintained in a temperature of -80°C) were crushed with a zirconia head at 30 Hz for 15 min using a blender mill (MM 400, Retsch). The powder was then weighed and extracted overnight at 4°C with 1.0 mL of 70% aqueous methanol. The supernatant was collected and filtered (microporous membrane filters with pore sizes of 0.22 μm) before LC-ESI-MS/MS analysis after centrifugation at 10,000 g for 10 min. An LC-ESI-MS/MS system was used to examine the sample extracts (HPLC: Shim-pack UFLC Shimadzu CBM30A system[1]; MS: Applied Biosystems 6500 Q TRAP).[2] Qualitative and quantitative mass spectrometry analysis of metabolites in samples was based on the KEGG compound database, the MetWare database (MWDB), and multiple reaction monitoring (MRM). Metabolite identification is based on the accurate mass of metabolites, MS2 fragments, MS2 fragment isotope distribution and retention time (RT). The secondary spectrum and RT of the Metware company's database are intelligently matched one by one, and the MS tolerance

1 www.shimadzu.com.cn/
2 www.appliedbiosystems.cn/

and MS2 tolerance are set to 20 and 20 ppm, respectively. For each treatment group, three biological replicates were examined individually. The samples were evaluated using Yang's methods under the following HPLC conditions (12).

Principal component analysis (PCA) was used to investigate the specific accumulation of *D. moniliforme* metabolites in different growth years using R.[3] The data were normalized, and all samples were examined using a cluster heatmap, which was then generated. The following conditions were used to screen differentially accumulated metabolites (DAMs): foldchange ≥ 2 and foldchange ≤ 0.5, VIP ≥ 1, and the up and down regulation of differential metabolites was compared between different comparison groups. The mean values of the relative content of the differential metabolites in each group were standardized by z-score and then subjected to K-means clustering analysis to analyze trends in the relative content of metabolites in distinct subgroups.

Ribonucleic acid extraction, Illumina sequencing, and differentially expressed genes analysis

According to the manufacturer's instructions, total RNA of *D. moniliforme* was extracted using the OmniPlantRNA kit (CWBIO, China), mRNA libraries of each sample were constructed, and the libraries were sequenced using Illumina platform. RNA extraction, library construction and sequencing were carried out as described by Yang's method (12). Using the HISAT2 software, the filtered reads were mapped to the reference genome (13).[4] As a measure of transcription or gene expression, fragments per kilobase of transcript per million mapped reads (FPKM) were utilized. The DESeq2 was used to find differentially expressed genes (DEGs) (14), and the filter condition was $|\log2(\text{fold change})| > 1$, with p-value < 0.05. TopGO and clusterprofiler were used to enrich all DEGs in Gene Ontology (GO) and the Kyoto Encyclopedia of Genes and Genomes (KEGG) to better understand the function and critical pathway of DEGs.

Gene co-expression network construction

WGCNA was conducted by using R software package. Before constructing the network, the RNA sequencing data was examined to eliminate low-quality genes and low-quality samples. Then, the Pearson correlation coefficients of all DEGs were calculated and the appropriate soft threshold ß was automatically selected (15). The Pearson result weighted by ß exponent was transformed into adjacency matrix (16). Then, the adjacency matrix was transformed into topological overlap (TOM) matrix and TOM was used to demonstrate the similarity expression of genes. Finally, hierarchical clustering method is used to generate a hierarchical clustering tree of DEGs, and similar modules are combined (17). Hub genes are commonly used for highly connected genes, which have a high level of connectivity in the co-expression module. Depending on the size of the module, the top 20 genes with the strongest connection have been designated as hub genes, and genes were further examined in these modules. Cytoscape (v.3.6.1) was used to build and visualize a network of gene-gene interactions.

Integration analysis of transcriptome and metabolome

According to the metabolite content and gene expression value in the stem of *D. moniliforme* at different growth years, the DEGs and the DAMs of flavonoid biosynthesis pathway in each comparison group were analyzed. First, pathway analysis was used to analyze the DEGs and DAMs related to flavonoid biosynthesis. Moreover, in order to better understand the relationship between transcriptome and metabolome, DEGs and DAMs were mapped to the KEGG pathway database to obtain their common pathway information.

Real-time quantitative PCR validation

Eleven DEGs were screened for qRT-PCR using specific primers designed by Oligo7 software. **Supplementary Table 1** lists the primers that were used in this study. qRT-PCR was performed on the ABI 7500 Real-time PCR system (Applied Biosystems) according to the manufacturer's instructions. $2^{-\Delta\Delta CT}$ method was used for relative quantitative analysis of the data, and the internal reference gene was *Actin* (18). Three replicates were analyzed for each sample to ensure reproducibility and reliability (**Supplementary Figure 2**).

Statistical analysis

The differences between multiple groups were analyzed using a one-way ANOVA followed by Duncan's multiple comparisons test. The experimental data were expressed as the mean ± standard deviation, p-values less than 0.05 were regarded as statistically significant. SPSS 22.0 software was used for statistical analysis and GraphPad Prism 8.0 software was used for drawing. In this study, all experiments were conducted in three biological replicates.

3 www.r-project.org

4 https://www.ncbi.nlm.nih.gov/genome/69090

Results

Measurement of total flavonoid and alkaloid contents in *Dendrobium moniliforme*

In order to determine the accumulation of flavonoids and alkaloids in the stems of *D. moniliforme* in different years, their contents in different growth years were measured. In general, the contents of flavonoids were very variable at different growth stages. As seen in the **Figure 1**, the flavonoid content increased from 1Dm to 3Dm, peaked at 3Dm then dropped in the fourth year. The highest flavonoid in the stem of *D. moniliforme* was 11.13 $mg{\cdot}g^{-1}$ DW and the lowest 3.35 $mg{\cdot}g^{-1}$ DW (**Figure 1**). The flavonoid content of 2-year-old, 3-year-old, and 4-year-old *D. moniliforme* was significantly different from that of 1-year-old *D. moniliforme*. The trend of the content of alkaloids in stems of *D. moniliforme* in four different growth years was similar to that of the contents of flavonoids. The alkaloid content increased in the first 3 years, reached the maximum value of 0.61 $mg{\cdot}g^{-1}$ DW in the third year, and decreased in the fourth year (**Figure 1**). They are all significantly higher than that in the first year. The results suggested that the third year of *D. moniliforme* growth could be an essential stage of accumulation of flavonoids and alkaloids.

Metabolite profiling of different growth years of *Dendrobium moniliforme*

In order to explore the metabolic changes during the different growth years of *D. moniliforme*, metabolic analysis on the stems of *D. moniliforme* with four growth years was carried out by using widely targeted metabolomics. 767 metabolites were identified from 1Dm, 2Dm, 3Dm and 4Dm, indicating that the spectrum of *D. moniliforme* metabolites was diverse in different growth years. **Supplementary Tables 2–7** listed all the metabolites identified in all samples. PCA was used to evaluate 12 samples in order to gain a preliminary understanding of the overall metabolic difference. The analytical results show that there are significant differences between each group, but no significant differences within the group (**Supplementary Figure 3A**). The biological repeats were all gathered together, indicating that the metabolomic data is highly reliable. The heatmap results revealed that flavonoids accumulated at a high level in 3 and 4Dm (**Supplementary Figure 3B**). The maximum expression of organic acid was found in 2Dm, compared with the samples of other years. Furthermore, lipids, amino acids and derivatives, alkaloids, nucleotides and derivatives, quinones and terpenoids were more abundant in 2Dm and 4Dm than in 1Dm and 3Dm.

A K-means cluster analysis was performed on 366 metabolites in four developmental stages. The nine figures showed obvious cluster changes of metabolites, and the change trend is shown in **Supplementary Figure 3C**. Furthermore, these 366 metabolites contained 63 flavonoids. Notably, 61.9% of TF were found in Clusters 4, Cluster 7 and Cluster 8. Interestingly, in the metabolite expression trends of these three clusters, the levels of expression of metabolites in 3 and 4Dm were higher than in 1 and 2Dm. A total of 480 DAMs were identified (**Supplementary Figure 3D**). The most up-accumulated DAMs were found in 1Dm vs. 4Dm, the least up-accumulated DAMs were found in 3Dm vs. 4Dm. While 2Dm vs. 3Dm had the most down-regulated DAMs, 3Dm vs. 4Dm had the least down-regulated DAMs. According to **Supplementary Figure 3D**, the highest number of DAMs was found in 1 and 2Dm, while the lowest number of DAMs was found in 3Dm vs. 4Dm. In **Supplementary Figure 4**, the top 10 up-accumulated and down-accumulated metabolites with significant differences were listed.

Ribonucleic acid sequencing and identification of differentially expressed genes

The RNA-Seq data were submitted to NCBI with accession number PRJNA776418. Transcriptome analysis was used to identify DEGs in stems to better understand the molecular basis of *D. moniliforme*. The DEGs among different comparison groups of *D. moniliforme* can be seen using the volcano figure (**Supplementary Figure 5**). There were 3,734 DEGs in six comparison groups (1Dm vs. 2Dm, 1Dm vs. 3Dm, 1Dm vs. 4Dm, 2Dm vs. 3Dm, 2Dm vs. 4Dm, 3Dm vs. 4Dm) using $|\ \mathrm{Log_2FC}| > 1$ and p-value < 0.05 as screening criterion. The largest number of DEGs were discovered in 2Dm vs. 3Dm (2,183). The lowest amount of DEGs were found in 3Dm vs. 4Dm (228).

Gene ontology and Kyoto encyclopedia of genes and genomes enrichment of differentially expressed genes

The functions of the DEGs were categorized according to the classification of the GO database. As shown in **Supplementary Figure 6**, "Biosynthetic processes" was the most enriched subcategory in the biological process (BP) category, followed by "Metabolic processes." The most enriched subcategories in the molecular function (MF) category were "Transferase activity" and "Transporter activity." DEGs are typically found in "Membranes" and "Cell walls" in the cell component (CC) category.

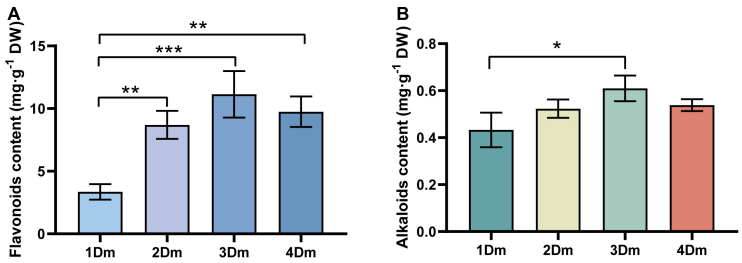

FIGURE 1
Determination of total flavonoids and alkaloids in the stem of *D. moniliforme*. **(A)** Content of total flavonoids in stems of *D. moniliforme* with different growth years; **(B)** contents of total alkaloids in stems of *D. moniliforme* with different growth years. The asterisk "*" indicates statistical differences in the same indicator between different growth years by a *t*-test, with a significant difference of $p < 0.05$ (*$p < 0.05$, **$p < 0.01$, ***$p < 0.001$). Error bars represent standard deviations ($n = 3$).

To understand the biological functions of DEGs, the transcriptome sequencing data were blasted to the KEGG database (**Supplementary Figure 7**). Among the top 20 enriched pathways, the largest proportion of DEGs was located in the "Metabolism pathway," while "Environmental information processing," and "Organismal systems" were in the second and third place. Among them, "Phenylpropanoid biosynthesis" and "Starch and sucrose metabolism" were significantly enriched in all comparison groups, except for 3Dm vs. 4Dm. "Fructose and mannose metabolism" was significantly enriched in both the 1Dm vs. 3Dm and 2Dm vs. 4Dm. In both 1Dm vs. 3Dm and 3Dm vs. 4Dm, "Tropane, piperidine and pyridine alkaloid biosynthesis" were remarkably enriched. In **Supplementary Figure 8**, the top 20 KEGG pathways are listed.

KEGG enrichment analysis showed that many DEGs are associated with metabolic pathways. Secondary metabolism-related pathways are important in medicinal plants. In this study, secondary metabolism-related DEGs in 1Dm vs. 2Dm, 1Dm vs. 3Dm, 2Dm vs. 4Dm, 3Dm vs. 4Dm, and 3Dm vs. 4Dm were classified as 34, 49, 47, 56, 57, and 11 secondary-metabolic KEGG pathways. Among them, 56, 57, and 11 ts. In this study, meivatives, quiee gene was e appropriate soft threshold ractfour growth years of *D. moniliforme*.

Identified metabolites and genes involved in flavonoid biosynthesis pathway

As shown in **Figure 2**, there have been identified a total of 20 DEGs involving the flavonoid biosynthetic pathway. Overall, the levels of expression of two *CHS* genes (*LOC110105249*, *LOC110105073*), one *F3'H* gene (*LOC110096779*), one *FLS* gene (*LOC1100114984*), and one OMT gene (*LOC110101682*) were higher in 3Dm or 4Dm than in 1 and 2Dm. However, the expression of some genes upstream of the flavonoid biosynthetic pathway was higher in 1 and 2Dm than in 3Dm or 4Dm, such as *PAL*, *4CL* and *C4H*. In order to verify the reliability of transcriptomic results, 17 DEGs involved in flavonoid biosynthesis were further selected for qRT-PCR analysis. qRT-PCR results were basically consistent with RNA-seq results, indicating the validity of RNA-seq results (**Supplementary Figure 2G**).

There have been identified a total of 34 DAMs related to the flavonoid biosynthetic pathway. The DAMs content revealed diverse trends of expression each year, but most metabolites were most expressive at 3 and 4Dm, except keampferol, dihydrokaempferol and flavones. In addition, keampferol was more expressed in 1 and 3Dm than 2 and 4Dm, while dihydrokaempferol was exactly the opposite of keampferol; that is, it was more expressed in 2 and 4Dm than 1 and 3Dm.

Gene co-expression network analysis

To investigate the gene regulatory network of flavonoid synthesis in *D. moniliforme* stems, co-expression analysis and network construction for 3,734 DEGs were performed. The analysis yielded nine different modules (black, blue, brown, green, gray, pink, red, turquoise and yellow) in a dendrogram, where modules are clusters of highly correlated genes that are co-expressed within the same module (**Figure 3A**). To detect the interactions between gene models, network heatmap for co-expression modules was performed. The heatmap of the co-expression network is in red, indicating high DEG co-expression within the module and low co-expression outside the module (**Figure 3B**). The modules associated with TF, TA, and different growth years (Year) were identified from the above modules (**Figure 3C**). The results showed that four modules were highly correlated with TF, TA, and Year, including yellow, brown, turquoise and black gene modules, while the rest of the modules were less correlated with TF, TA, and Year. Among them, turquoise and black gene modules were significantly positively correlated with Year, and yellow and brown gene modules were significantly negatively correlated with Year.

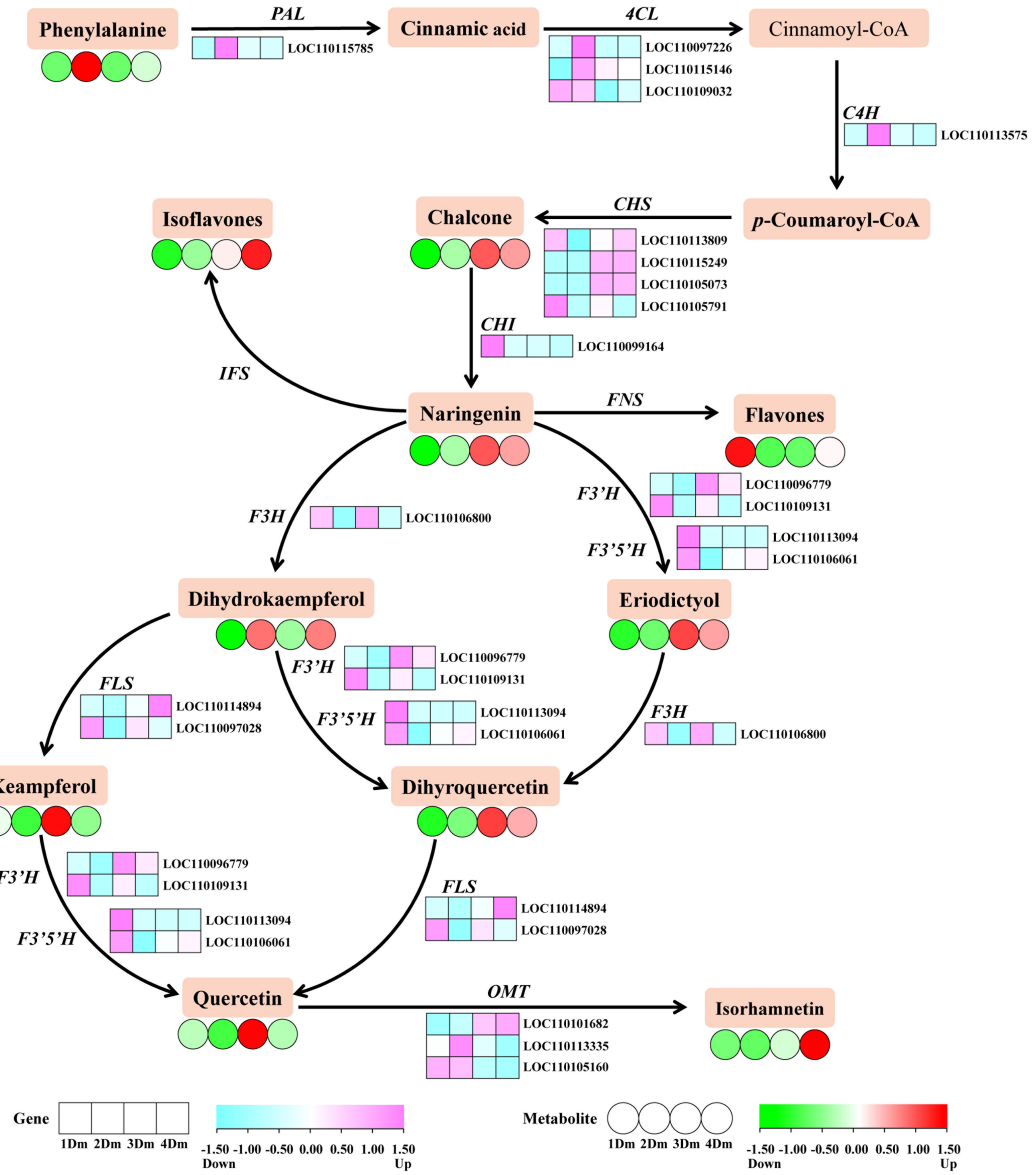

FIGURE 2
The flavonoids biosynthetic pathway of *D. moniliforme*. The heatmap shows the expression patterns of DEGs and DAMs during flavonoid biosynthesis. The rectangles represent the expression changes of DEGs and the circles represent the expression changes of DAMs. The color scale indicates the relative amounts of DEGs and DAMs. Darker colors indicate higher expression. Pink represents up-regulated DEGs, and blue represents down-regulated DEGs. Red represents up-regulated DAMs and green represents down-regulated DAMs. Key enzyme gene abbreviation: C4H, cinnamate 4-hydroxylase; PAL, phenylalanine ammonia lyase; 4CL, 4-coumarate: CoA ligase; CHS, chalcone synthase; CHI, chalcone isomerase; F3H, flavonoid 3-hydroxylase; F3'H, flavonoid 3'-hydroxylase; FLS, flavonol synthase; IFS: isoflavone synthase; FNS, flavone synthase; OMT, O-methyltransferase.

In the co-expression networks, hub genes are highly co-expressed with other genes and play important roles in key pathways. 20 hub genes were identified in each of the yellow, brown, turquoise, and black modules (**Figures 3D–G**), and these hub genes were highly connected. In **Supplementary Figure 9**, a heatmap of the expression of hub genes in the four modules was performed. In both turquoise and black modules, hub genes had high expression in 3Dm and 4Dm. The expression of hub genes in the yellow and brown modules was higher in 1Dm and 2Dm than in 3Dm and 4Dm. Overall, this result was generally consistent with the variation of flavonoid and alkaloid contents in *D. moniliforme*. In-depth analysis revealed that the black module identified one *FLS* gene (*LOC110114894*) involved in flavonoid biosynthesis, which had strong connectivity with other hub genes, which further indicated that *FLS* genes are key genes in flavonoid biosynthesis.

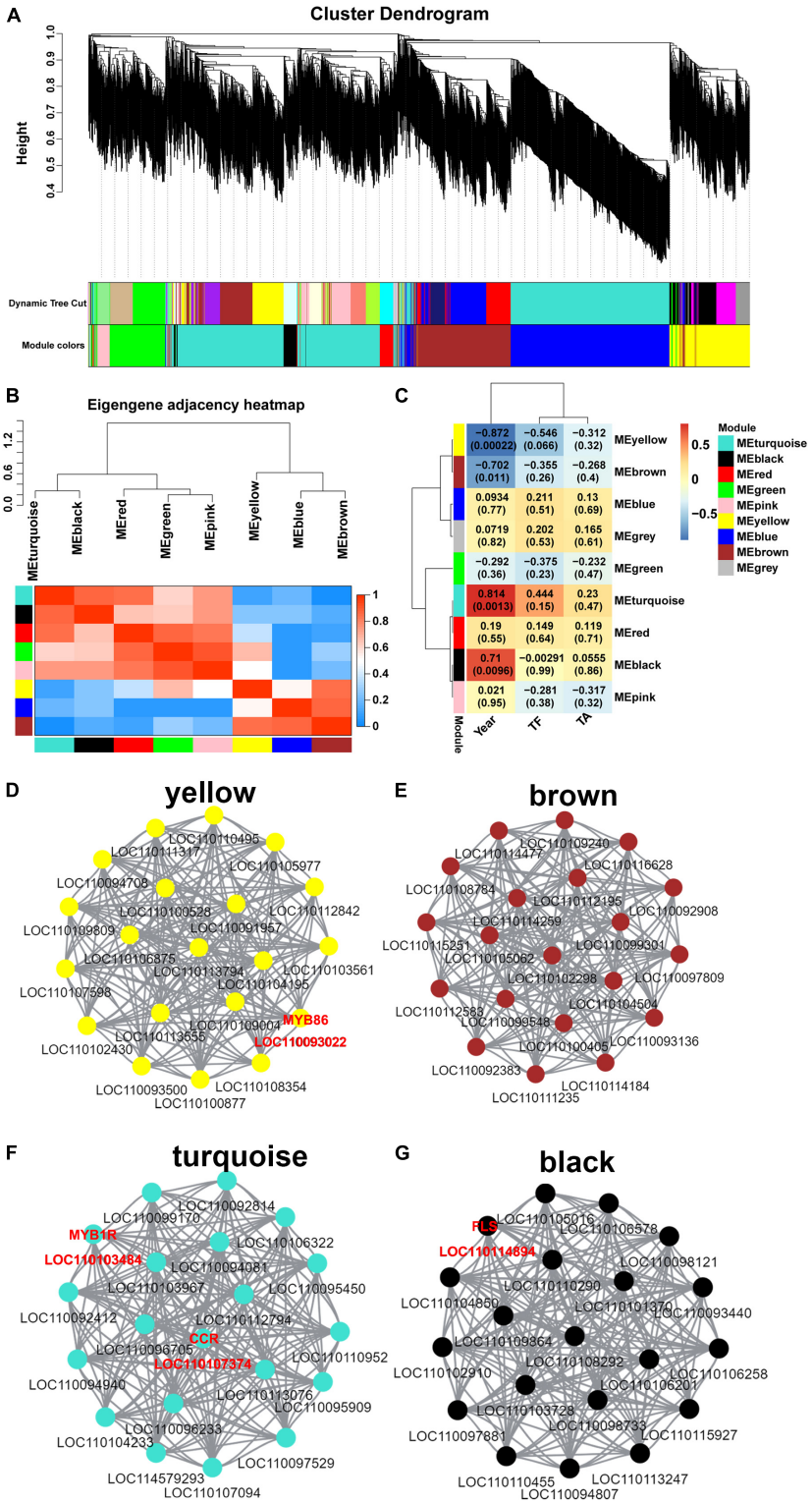

FIGURE 3
Weighted gene co-expression network of *D. moniliforme*. **(A)** Clustering dendrogram of DEGs, with dissimilarity based on the topological overlap, together with assigned module colors. The clustered branches represent different modules, and each line represents one DEG. **(B)** The heatmap of connectivity of eigengenes. **(C)** Module-trait associations. Each row corresponds to a module characteristic gene (eigengene), and each column corresponds to a trait. Each cell contains a corresponding correlation coefficient and *p*-value. **(D–G)** *D. moniliforme* transcriptome co-expression network diagram: **(D)** Yellow module; **(E)** brown module; **(F)** turquoise module; **(G)** black module.

In yellow and turquoise modules, two MYB transcription factors (TFs) (*LOC110103484* and *LOC110093022*) regulating flavonoid synthesis were found. In addition, in the turquoise module, a key enzyme *cinnamoyl-CoA reductase* (*CCR*, *LOC110107374*) involved in lignin synthesis was identified.

Integrated metabolomic and transcriptomic analysis

To assess the relationship between transcriptome and metabolome, the KEGG pathway enrichment results were integrated (**Figure 4**). KEGG pathways were classified into 5 categories, including Cellular Processes, Environmental Information Processing, Genetic Information Processing, Human Diseases, Metabolism, and Organismal Systems. Among them, the Metabolism class has the most genes. The results showed a high enrichment of metabolism-related pathways in all comparison groups, such as, "Flavonoid biosynthesis," "Phenylpropanoid biosynthesis," "Fructose and mannose metabolism," "Tropane, piperidine and pyridine alkaloid biosynthesis" and "Starch and sucrose metabolism." Among them, "Flavonoid biosynthesis" and "Phenylpropanoid biosynthesis," which are involved in flavonoid synthesis, were significantly enriched in 1Dm vs. 2Dm, 1Dm vs. 3Dm, 1Dm vs. 4Dm, 2Dm vs. 3Dm, 2Dm vs. 4Dm (**Figure 4**). The "Fructose and mannose metabolism" and "Starch and sucrose metabolism" pathways involved in polysaccharide synthesis were significantly enriched in 1Dm vs. 4Dm, 1Dm vs. 3Dm, 2Dm vs. 3Dm, 2Dm vs. 4Dm. The "Tropane, piperidine and pyridine alkaloid biosynthesis" pathways involved in alkaloid synthesis were significantly enriched in 1Dm vs. 3Dm and 3Dm vs. 4Dm. These are all related to the synthesis of important medicinal components of *D. moniliforme*. Moreover, based on the metabolite results, it is known that flavonoid compounds were significantly higher in 3Dm and 4Dm. Meanwhile, the transcriptome results showed a more significant effect of phenylpropanoid biosynthesis in each comparison group, while the phenylpropanoid pathway is upstream of the flavonoid pathway. In summary, both DAMs and DEGs were significantly correlated with the flavonoid synthesis pathway.

Discussion

The differential metabolites of the stems of *D. moniliforme* at four growth years were detected. A total of 480 DAMs were identified, including 107 types of flavonoid metabolites, mainly flavonoids and flavonols. It is worth noting that 3Dm and 4Dm have much higher expression levels of key flavonoids, such as eriodictyol, kaempferol, quercetin, and isorhamnetin than 1Dm and 2Dm. These metabolites have been reported to have antioxidant (19), anti-inflammatory (20), prevention and treatment of cardiovascular diseases (21), anti-tumor (22), kidney protection (23) and other medicinal properties. Compared with those of our previous studies, the numbers of species of flavonoids metabolites in *D. moniliforme* were fewer than those in *D. huoshanense* (24). The accumulation pattern of flavonoids was different in different species of *Dendrobium*. In *D. huoshanense*, flavonoids showed a tendency of accumulation, and the content of flavonoids was the highest in stems of 4-year-old, whereas in *D. moniliforme*, the content of flavonoids was the highest in 3-year-old stems, but decreased in 4-year-old stems. Meanwhile, the content of flavonoids in stems of 3-year-old *D. moniliforme* was 11.13 $mg \cdot g^{-1}$ DW, which was higher than that in stems of 4-year-old *D. huoshanense* (8.94 $mg \cdot g^{-1}$ DW). Therefore, *D. moniliforme* is more suitable as an antioxidant to scavenge free radicals in the human body than *D. huoshanense*. Meanwhile, the best effect was obtained from 3-year-old *D. moniliforme*. The results of this experiment illustrate the great potential of *D. moniliforme* as a food and cosmetic ingredient.

With the advancement of sequencing technology and the growing volume of transcriptome data, WGCNA analysis allows for the quick and efficient identification of genes or TFs associated with specific traits. In this study, the WGCNA was used to screen out a *FLS* gene (*LOC110114894*) that is highly correlated with flavonoid accumulation, regulates the biosynthesis of flavonoids, and influences the production of related secondary metabolites including kaempferol and quercetin. This is consistent with the results of previous studies with findings on the transcriptional regulation of *FLS* genes in species such as *Vitis vinifera* (25), *Camellia nitidissima* (26), and *Scutellaria baicalensis* (27), which also found that FLS is a key enzyme in the flavonol biosynthesis pathway, significantly correlated with total flavonol content, and its high expression promoted the accumulation of flavonols (28). This gene was also found in the transcriptome of *D. huoshanense*. The results of transcriptome sequencing and qRT-PCR results showed that the expression level of *FLS* in *D. moniliforme* was higher than that in *D. huoshanense*. Therefore, we hypothesized that the expression level of *FLS* affected the biosynthesis level of flavonoids in *Dendrobium*.

MYB transcription factors (TFs) are of great interest because of their importance in repressing or activating the transcription of genes related to the biosynthesis of anthocyanins, proanthocyanidins, flavonols, and other flavonoid biosynthesis in plants (29). In this study, one *MYB1R* (*LOC110103484*) and one *MYB86* (*LOC110093022*) were identified as hub genes, indicating that they play an important role in regulating flavonoid metabolism. In tobacco, *Arabidopsis* and other plants, MYB1R has been reported as transcriptional repressors of anthocyanin biosynthesis (30, 31). In our study, overexpression of MYB1R was hypothesized as one of the reasons for

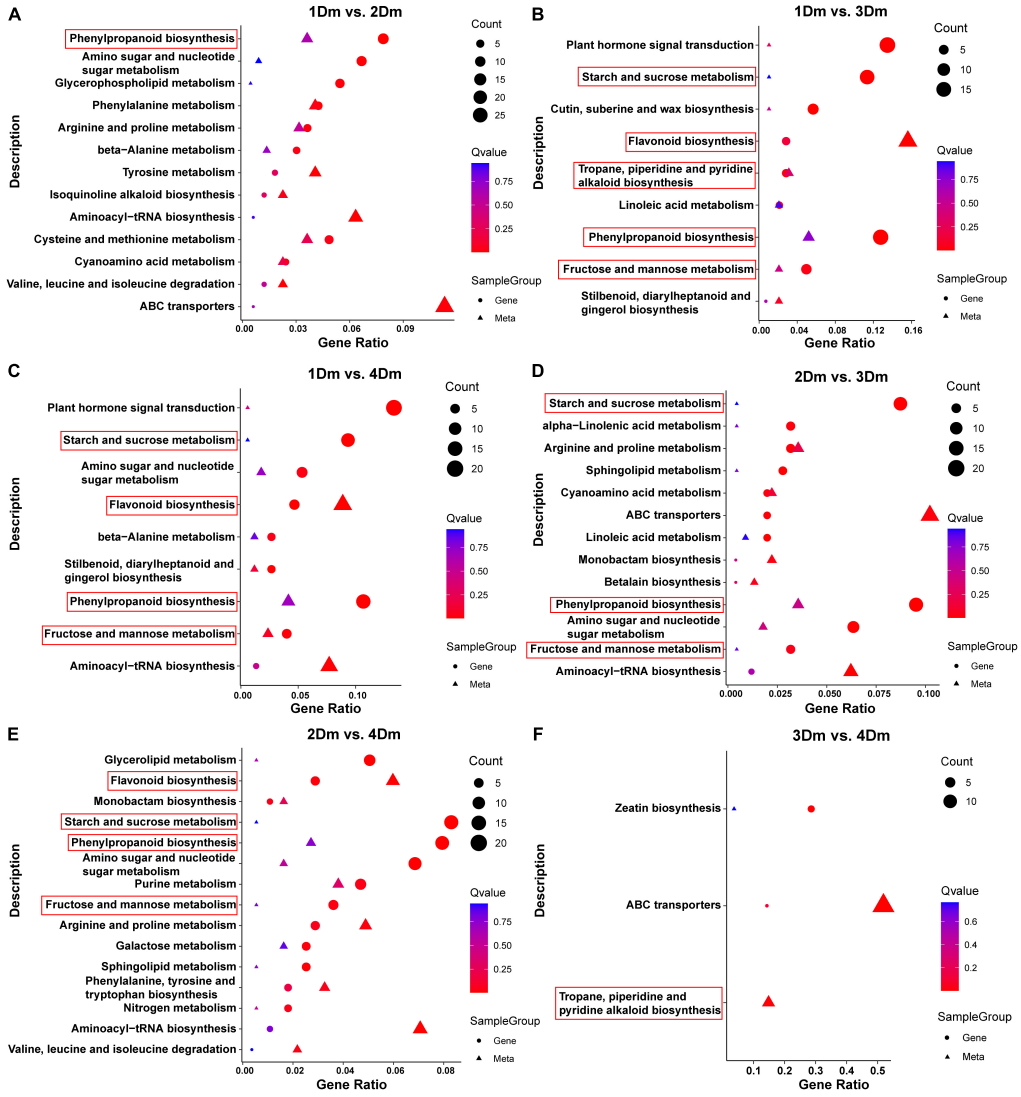

FIGURE 4
Scatterplot of KEGG pathway enrichment for transcriptome and metabolome. The circles indicate genes and the triangles indicate metabolites. The horizontal axis is the gene ratio and the vertical axis is the pathway terms. The larger the point, the greater the number of DEGs or DAMs involved. The pathways related to flavonoid, polysaccharide and alkaloid biosynthesis are marked with red boxes. **(A)** 1Dm vs. 2Dm; **(B)** 1Dm vs. 3Dm; **(C)** 1Dm vs. 4Dm; **(D)** 2Dm vs. 3Dm; **(E)** 2Dm vs. 4Dm; **(F)** 3Dm vs. 4Dm.

the deficiency of anthocyanins. Furthermore, MYB86 was found to be up-regulated in the first and second years, while down-regulated in the third and fourth years. Gao et al. found that MYB86 was up-regulated during initial fruit development, which may promote the accumulation of anthocyanin, and this may explain the up-regulation of MYB86 in the first and second years (32). It was found that cinnamoyl-CoA reductase (CCR) is the entry point of phenylpropanoid pathway into lignin pathway (33). In this study, a key enzyme involved in lignin synthesis, *CCR* (*LOC110107374*), in the turquoise module was identified, suggesting that lignin plays a key regulatory role in the synthesis of flavonoids. This has been confirmed in *Arabidopsis*, tobacco, peach and other plants (34–36).

Also, a regulatory network for flavonoid biosynthesis in *D. moniliforme* stems was built to visualize the role of flavonoid synthesis genes in the pathway (**Figure 2**). The synthesis of flavonoids starts from the phenylpropanoid metabolic pathway, which is one of the most well-studied secondary metabolic pathways (37). The phenylpropanoid metabolic pathway contains enzymes such as PAL, C4H, and 4CL, which catalyze the conversion of phenylalanine to coumaroyl-CoA (38). **Figure 2** shows that genes *PAL, C4H, and 4CL* were significantly up-regulated in *D. moniliforme* in first and second years; meanwhile, lignin in the downstream

pathway was not found. Numerous studies have shown that MYBs play an significant regulatory function in the synthesis of lignin and flavonoids (39). Zhang et al. found that most R2R3-MYB contribute to flavonoid synthesis at the expense of repressing lignin synthesis (40). A large number of MYB TFs were found in the transcriptome data. So, these MYB TFs were speculated to inhibit the production of lignin and affect the expression of genes like *PAL, C4H, and 4CL* in different growth years of *D. moniliforme*.

Conclusion

In summary, this study revealed the changes of flavonoids and related genes in different growth years, and constructs a regulatory network of flavonoid synthesis. The results showed that *FLS* occupies an important position in the biosynthesis of flavonoids. Also, the biosynthetic pathway of flavonoids is influenced by lignin biosynthesis, and a decrease in lignin biosynthesis may provide more substrates for flavonoids. MYB TFs also have a regulatory role in the flavonoid biosynthesis pathway. Transcriptomic and metabolomic data showed a gradual increase in flavonoids in the stems of *D. moniliforme* with increasing growth years. Considering factors such as time and cost, the best harvesting period for *D. moniliforme* is the third year. This study provides important data for farmers and processors involved in the *D. moniliforme* cultivation industry and provides new theory and evidence for determining the optimal harvesting period for *D. moniliforme*.

Data availability statement

The datasets presented in this study can be found in online repositories. The names of the repository/repositories and accession number(s) can be found in the article/**Supplementary material**.

Author contributions

YY: conception and design of the research, drafting the manuscript, and revision of manuscript for important intellectual content. JZ: acquisition of data, analysis and interpretation of data, drafting the manuscript, and revision of manuscript for important intellectual content. HZ: acquisition of data. MZ: statistical analysis. SL: conception and design of the research. All authors contributed to the article and approved the submitted version.

Funding

This project was funded by the Natural Science Foundation of Jiangsu Province, China (Grant No. BK20210800) and the Priority Academic Program Development of Jiangsu Higher Education Institutions (PAPD).

Conflict of interest

The authors declare that the research was conducted in the absence of any commercial or financial relationships that could be construed as a potential conflict of interest.

Publisher's note

All claims expressed in this article are solely those of the authors and do not necessarily represent those of their affiliated organizations, or those of the publisher, the editors and the reviewers. Any product that may be evaluated in this article, or claim that may be made by its manufacturer, is not guaranteed or endorsed by the publisher.

Supplementary material

The Supplementary Material for this article can be found online at: https://www.frontiersin.org/articles/10.3389/fnut.2022.928074/full#supplementary-material

SUPPLEMENTARY FIGURE 1
Plant size of *Dendrobium moniliforme* from four different years.

SUPPLEMENTARY FIGURE 2
Verification of the expression patterns of RNA-seq results using qRT-PCR.

SUPPLEMENTARY FIGURE 3
Metabolomic analysis of *D. moniliforme* with different growth years. **(A)** PCA analysis of metabolomic data. **(B)** Heatmap of all metabolites detected in *D. moniliforme*. **(C)** K-means cluster analysis. **(D)** The number of up and down regulated differential metabolites in different groups. 1, 2, 3, and 4Dm represent the four growth stages of *D. moniliforme*: 1Dm represents the first year of growth; 2Dm represents the second year of growth; 3Dm represents the third year of growth; 4Dm represents the fourth year of growth.

SUPPLEMENTARY FIGURE 4
Top 10 up-accumulated and down-accumulated metabolites with significant differences. The metabolites marked in red are flavonoid metabolites. **(A)** 1Dm vs. 2Dm; **(B)** 1Dm vs. 3Dm; **(C)** 1Dm vs. 4Dm; **(D)** 2Dm vs. 3Dm; **(E)** 2Dm vs. 4Dm; **(F)** 3Dm vs. 4Dm.

SUPPLEMENTARY FIGURE 5
Differentially expressed genes (DEGs) in different comparisons. The red dots mean significantly up-regulated genes and the blue dots represent significantly down-regulated genes. The gray dots represent non-DEGs. **(A)** 1Dm vs. 2Dm volcano; **(B)** 1Dm vs. 3Dm volcano; **(C)** 1Dm vs. 4Dm volcano; **(D)** 2Dm vs. 3Dm volcano; **(E)** 2Dm vs. 4Dm volcano; **(F)** 3Dm vs. 4Dm volcano.

SUPPLEMENTARY FIGURE 6
GO enrichment circle diagram. The outermost circle indicates the GO term, and different colors represent different subcategories; the second circle indicates the number and *P*-value of that GO term. The more genes the longer the bar, the smaller the value the redder the color; the third circle indicates the number of up- and down-regulated genes of the GO term, red indicates up-regulation and green indicates down-regulation. The fourth circle indicates the Rich Factor value of each classification. **(A)** 1Dm vs. 2Dm volcano; **(B)** 1Dm vs. 3Dm; **(C)** 1Dm vs. 4Dm; **(D)** 2Dm vs. 3Dm; **(E)** 2Dm vs. 4Dm; **(F)** 3Dm vs. 4Dm.

SUPPLEMENTARY FIGURE 7
KEGG pathway enrichment bubble diagram. The bubble diagram shows the top 20 KEGG enrichment pathways. Each bubble represents a different pathway. The bubble color represents the KEGG category and the bubble size represents the number of DEGs. The smaller the *p*-value of the enriched pathway, the more significant it is. **(A)** 1Dm vs. 2Dm; **(B)** 1Dm vs. 3Dm; **(C)** 1Dm vs. 4Dm; **(D)** 2Dm vs. 3Dm; **(E)** 2Dm vs. 4Dm; **(F)** 3Dm vs. 4Dm.

SUPPLEMENTARY FIGURE 8
Top 20 KEGG pathways. **(A)** 1Dm vs. 2Dm; **(B)** 1Dm vs. 3Dm; **(C)** 1Dm vs. 4Dm; **(D)** 2Dm vs. 3Dm; **(E)** 2Dm vs. 4Dm; **(F)** 3Dm vs. 4Dm.

SUPPLEMENTARY FIGURE 9
The heatmap of the expression of hub genes in four modules. **(A)** yellow module; **(B)** brown module; **(C)** turquoise module; **(D)** black module.

SUPPLEMENTARY TABLE 1
Gene IDs and primers used in the quantitative real-time PCR (qRT-PCR) experiments.

SUPPLEMENTARY TABLES 2–7
The complete list of identified metabolites.

References

1. Meng Q, Fan H, Chen F, Xiao T, Zhang L. Preparation and characterization of *Dendrobium officinale* powders through superfine grinding. *J Sci Food Agric.* (2018) 98:1906–13. doi: 10.1002/jsfa.8672

2. Cheng J, Dang P-P, Zhao Z, Yuan L-C, Zhou Z-H, Wolf D, et al. An assessment of the Chinese medicinal *Dendrobium* industry: supply, demand and sustainability. *J Ethnopharmacol.* (2019) 229:81–8. doi: 10.1016/j.jep.2018.09.001

3. Shah S, Shrestha R, Maharjan S, Selosse M-A, Pant B. Isolation and characterization of plant growth-promoting endophytic fungi from the roots of *Dendrobium moniliforme*. *Plants.* (2019) 8:5. doi: 10.3390/plants8010005

4. Ye M, Hou B, Luo J, Yan W, Liu W, Ding X. Genetic diversity and conservation of the endangered herb *Dendrobium moniliforme* based on amplified fragment length polymorphism markers. *Sci Hortic.* (2015) 189:51–8. doi: 10.1016/j.scienta.2015.03.035

5. Teixeira da Silva JA, Ng TB. The medicinal and pharmaceutical importance of *Dendrobium* species. *Appl Microbiol Biotechnol.* (2017) 101:2227–39. doi: 10.1007/s00253-017-8169-9

6. Liu W-H, Hua Y-F, Zhan Z-J. Moniline, a new alkaloid from *Dendrobium moniliforme*. *J Chem Res.* (2019) 2007:317–8. doi: 10.3184/030823407x218048

7. Whang SS, Um WS, Song I-J, Lim PO, Choi K, Park K-W, et al. Molecular analysis of anthocyanin biosynthetic genes and control of flower coloration by flavonoid 3',5'-hydroxylase (F3'5'H) in *Dendrobium moniliforme*. *J Plant Biol.* (2011) 54:209–18. doi: 10.1007/s12374-011-9158-7

8. Tsai PJ, Huang WC, Hsieh MC, Sung PJ, Kuo YH, Wu WH. Flavones isolated from *Scutellariae* radix suppress *Propionibacterium* acnes-induced cytokine production in vitro and in vivo. *Molecules.* (2015) 21:E15. doi: 10.3390/molecules21010015

9. Liu J, Hefni ME, Witthoft CM. Characterization of flavonoid compounds in common Swedish berry species. *Foods.* (2020) 9:358. doi: 10.3390/foods9030358

10. Yan S, Zhao T, Zhang X, Xing J, Yadong H, Chun Z. Comparison of polysaccharide and dendrobine content in Hejiang *Dendrobium* nobile at different harvesting time. *China Pharmacy.* (2018) 29:73–7.

11. Yuan Y, Zhang B, Tang X, Zhang J, Lin J. Comparative transcriptome analysis of different *Dendrobium* species reveals active ingredients-related genes and pathways. *Int J Mol Sci.* (2020) 21:861. doi: 10.3390/ijms21030861

12. Yang B, He S, Liu Y, Liu B, Ju Y, Kang D, et al. Transcriptomics integrated with metabolomics reveals the effect of regulated deficit irrigation on anthocyanin biosynthesis in cabernet sauvignon grape berries. *Food Chem.* (2020) 314:126170. doi: 10.1016/j.foodchem.2020.126170

13. Kim D, Langmead B, Salzberg SL. HISAT: a fast spliced aligner with low memory requirements. *Nat Methods.* (2015) 12:357–60. doi: 10.1038/nmeth.3317

14. Love MI, Huber W, Anders S. Moderated estimation of fold change and dispersion for RNA-seq data with DESeq2. *Genome Biol.* (2014) 15:550. doi: 10.1186/s13059-014-0550-8

15. Feng T, Li K, Zheng P, Wang Y, Lv Y, Shen L, et al. Weighted gene coexpression network analysis identified MicroRNA coexpression modules and related pathways in type 2 diabetes mellitus. *Oxid Med Cell Longev.* (2019) 2019:9567641. doi: 10.1155/2019/9567641

16. Yip AM, Horvath S. Gene network interconnectedness and the generalized topological overlap measure. *BMC Bioinformatics.* (2007) 8:22. doi: 10.1186/1471-2105-8-22

17. Li A, Horvath S. Network neighborhood analysis with the multi-node topological overlap measure. *Bioinformatics.* (2007) 23:222–31. doi: 10.1093/bioinformatics/btl581

18. Li H, Yao W, Fu Y, Li S, Guo Q. De novo assembly and discovery of genes that are involved in drought tolerance in Tibetan Sophora moorcroftiana. *PLoS One.* (2015) 10:e111054. doi: 10.1371/journal.pone.0111054

19. Rossato MF, Trevisan G, Walker CI, Klafke JZ, de Oliveira AP, Villarinho JG, et al. Eriodictyol: a flavonoid antagonist of the TRPV1 receptor with antioxidant activity. *Biochem Pharmacol.* (2011) 81:544–51. doi: 10.1016/j.bcp.2010.11.004

20. Lee JK. Anti-inflammatory effects of eriodictyol in lipopolysaccharide-stimulated raw 264.7 murine macrophages. *Arch Pharm Res.* (2011) 34:671–9. doi: 10.1007/s12272-011-0418-3

21. Zhang N, Pei F, Wei H, Zhang T, Yang C, Ma G, et al. Isorhamnetin protects rat ventricular myocytes from ischemia and reperfusion injury. *Exp Toxicol Pathol.* (2011) 63:33–8. doi: 10.1016/j.etp.2009.09.005

22. Wang JL, Quan Q, Ji R, Guo XY, Zhang JM, Li X, et al. Isorhamnetin suppresses PANC-1 pancreatic cancer cell proliferation through S phase arrest. *Biomed Pharmacother.* (2018) 108:925–33. doi: 10.1016/j.biopha.2018.09.105

23. Yamaguchi M, Hamamoto R, Uchiyama S, Ishiyama K. Effects of flavonoid on calcium content in femoral tissue culture and parathyroid hormone-stimulated osteoclastogenesis in bone marrow culture in vitro. *Mol Cell Biochem.* (2007) 303:83–8. doi: 10.1007/s11010-007-9458-x

24. Yuan Y, Zuo J, Zhang H, Li R, Yu M, Liu S. Integration of transcriptome and metabolome provides new insights to flavonoids biosynthesis in *Dendrobium huoshanense*. *Front Plant Sci.* (2022) 13:850090. doi: 10.3389/fpls.2022.850090

25. Fang F, Tang K, Huang W-D. Changes of flavonol synthase and flavonol contents during grape berry development. *Eur Food Res Technol.* (2013) 237:529–40. doi: 10.1007/s00217-013-2020-z

26. Zhou XW, Fan ZQ, Chen Y, Zhu YL, Li JY, Yin HF. Functional analyses of a flavonol synthase-like gene from *Camellia nitidissima* reveal its roles in flavonoid metabolism during floral pigmentation. *J Biosci.* (2013) 38:593–604. doi: 10.1007/s12038-013-9339-2

27. Kim YB, Kim K, Kim Y, Tuan PA, Kim HH, Cho JW, et al. Cloning and characterization of a flavonol synthase gene from *Scutellaria baicalensis*. *Sci World J.* (2014) 2014:980740. doi: 10.1155/2014/980740

28. Duan Y, Eduardo Melo Santiago F, Rodrigues Dos Reis A, de Figueiredo MA, Zhou S, Thannhauser TW, et al. Genotypic variation of flavonols and antioxidant capacity in broccoli. *Food Chem.* (2021) 338:127997. doi: 10.1016/j.foodchem.2020.127997

29. Nabavi SM, Šamec D, Tomczyk M, Milella L, Russo D, Habtemariam S, et al. Flavonoid biosynthetic pathways in plants: versatile targets for metabolic engineering. *Biotechnol Adv.* (2020) 38:107316. doi: 10.1016/j.biotechadv.2018.11.005

30. Zhu H-F, Fitzsimmons K, Khandelwal A, Kranz RG. CPC, a single-repeat R3 MYB, is a negative regulator of anthocyanin biosynthesis in *Arabidopsis*. *Mol Plant.* (2009) 2:790–802. doi: 10.1093/mp/ssp030

31. Nakatsuka T, Yamada E, Saito M, Fujita K, Nishihara M. Heterologous expression of gentian MYB1R transcription factors suppresses anthocyanin pigmentation in tobacco flowers. *Plant Cell Rep.* (2013) 32:1925–37. doi: 10.1007/s00299-013-1504-4

32. Gao X, Wang L, Zhang H, Zhu B, Lv G, Xiao J. Transcriptome analysis and identification of genes associated with floral transition and fruit development in rabbiteye blueberry (*Vaccinium ashei*). *PLoS One.* (2021) 16:e0259119. doi: 10.1371/journal.pone.0259119

33. Yin N, Li B, Liu X, Liang Y, Lian J, Xue Y, et al. Two types of cinnamoyl-CoA reductase function divergently in accumulation of lignins, flavonoids and glucosinolates and enhance lodging resistance in *Brassica napus*. *Crop J.* (2021) 10:647–60. doi: 10.1016/j.cj.2021.10.002

34. Shi J, Yan X, Sun T, Shen Y, Shi Q, Wang W, et al. Homeostatic regulation of flavonoid and lignin biosynthesis in phenylpropanoid pathway of transgenic tobacco. *Gene.* (2022) 809:146017. doi: 10.1016/j.gene.2021.146017

35. Besseau S, Hoffmann L, Geoffroy P, Lapierre C, Pollet B, Legrand M. Flavonoid accumulation in *Arabidopsis* repressed in lignin synthesis affects auxin transport and plant growth. *Plant Cell.* (2007) 19:148–62. doi: 10.1105/tpc.106.044495

36. Dardick CD, Callahan AM, Chiozzotto R, Schaffer RJ, Piagnani MC, Scorza R. Stone formation in peach fruit exhibits spatial coordination of the lignin and flavonoid pathways and similarity to *Arabidopsis* dehiscence. *BMC Biol.* (2010) 8:13. doi: 10.1186/1741-7007-8-13

37. Fraser CM, Chapple C. The phenylpropanoid pathway in *Arabidopsis*. *Arabidopsis Book.* (2011) 9:e0152. doi: 10.1199/tab.0152

38. Moldovan B, David L. Bioactive flavonoids from *Cornus mas* L. fruits. *Mini Rev Org Chem.* (2017) 14:489–95. doi: 10.2174/1573398X13666170426102809

39. Zhu L, Shan H, Chen S, Jiang J, Gu C, Zhou G, et al. The heterologous expression of the chrysanthemum R2R3-MYB transcription factor CmMYB1 alters lignin composition and represses flavonoid synthesis in *Arabidopsis thaliana*. *PLoS One.* (2013) 8:e65680. doi: 10.1371/journal.pone.0065680

40. Zhang S, Yang J, Li H, Chiang VL, Fu Y. Cooperative regulation of flavonoid and lignin biosynthesis in plants. *Crit Rev Plant Sci.* (2021) 40:109–26. doi: 10.1080/07352689.2021.1898083

frontiers | Frontiers in Nutrition

TYPE Review
PUBLISHED 13 October 2022
DOI 10.3389/fnut.2022.941527

OPEN ACCESS

EDITED BY
Elena Ibañez,
Institute of Food Science Research (CSIC), Spain

REVIEWED BY
Khalid Gul,
National Institute of Technology Rourkela, India
J. Mendiola,
Spanish National Research Council (CSIC), Spain

*CORRESPONDENCE
Li Han
hanliyx@163.com
Dingkun Zhang
zhangdingkun@cdutcm.edu.cn
Zhenfeng Wu
zfwu527@163.com

†These authors have contributed equally to this work

SPECIALTY SECTION
This article was submitted to Nutrition and Food Science Technology, a section of the journal Frontiers in Nutrition

RECEIVED 11 May 2022
ACCEPTED 23 September 2022
PUBLISHED 13 October 2022

CITATION
Deng X, Huang H, Huang S, Yang M, Wu J, Ci Z, He Y, Wu Z, Han L and Zhang D (2022) Insight into the incredible effects of microwave heating: Driving changes in the structure, properties and functions of macromolecular nutrients in novel food. *Front. Nutr.* 9:941527. doi: 10.3389/fnut.2022.941527

Insight into the incredible effects of microwave heating: Driving changes in the structure, properties and functions of macromolecular nutrients in novel food

Xuan Deng[1†], Haozhou Huang[1†], Shengjie Huang[1], Ming Yang[2,3], Jing Wu[4], Zhimin Ci[1], Yanan He[1], Zhenfeng Wu[2,3]*, Li Han[1]* and Dingkun Zhang[1]*

[1]State Key Laboratory of Southwestern Chinese Medicine Resources, Pharmacy School, Chengdu University of Traditional Chinese Medicine, Chengdu, China, [2]Key Laboratory of Modern Preparation of Chinese Medicine, Ministry of Education, Jiangxi University of Traditional Chinese Medicine, Nanchang, China, [3]State Key Laboratory of Innovation Medicine and High Efficiency and Energy Saving Pharmaceutical Equipment, Jiangxi University of Traditional Chinese Medicine, Nanchang, China, [4]Xinqi Microwave Co., Ltd., Guiyang, China

Microwave heating technology performs the characteristics of fast heating, high efficiency, green energy saving and easy control, which makes it deeply penetrate into the food industry and home cooking. It has the potential to alter the appearance and flavor of food, enhance nutrient absorption, and speed up the transformation of active components, which provides an opportunity for the development of innovation foods. However, the change of food driven by microwave heating are very complex, which often occurs beyond people's cognition and blocks the development of new food. It is thus necessary to explore the transformation mechanism and influence factors from the perspectives of microwave technology and food nutrient diversity. This manuscript focuses on the nutritional macromolecules in food, such as starch, lipid and protein, and systematically analyzes the change rule of structure, properties and function under microwave heating. Then, the flavor, health benefits, potential safety risks and bidirectional allergenicity associated with microwave heating are fully discussed. In addition, the development of new functional foods for health needs and future market based on microwave technology is also prospected. It aims to break the scientific fog of microwave technology and provide theoretical support for food science to understand the change law, control the change process and use the change results.

KEYWORDS

microwave heating, innovation foods, nutritional macromolecules, flavor, safety risks

Introduction

The microwave technology was first employed in the food business in the 1970s, and it is most widely used for thawing and drying foods. With the development of microwave technology, it began to be utilized in the puffing, sterilization and alteration of foods. The advent of microwave puffing method offers an opportunity to create an expanded snack product, which can change the food texture, and better preserve the nutrients and rich flavor. In 1976, Pillsbwry company of the United States introduced microwave popcorn for the first time, and then microwave foods such as potato chips, cakes, noodles, etc. appeared on the market in the mid to late 1990s. These foods have the characteristics of fast heating speed, low oil content, high product quality, uniform heating and environmental protection. Based on the above advantages, it is now very popular in daily life. However, different views believe that microwave heating will destroy the nutrients in the food and produce unknown substances, which also have potential health risks. For this purpose, this paper summarizes the effects of microwave on macromolecule nutrients (starch, lipid and protein) in food, in order to answer whether microwave heating has a negative effect on food nutrition, and to provide a comprehensive overview of the most recent research findings in order to provide a theoretical foundation for promoting microwave use in the food industry.

Starch

Carbohydrate-rich foods and root vegetables, such as rice, wheat, corn, and yams, are examples of starchy foods. Microwave heating affects the vibration of groups in starch molecules through both thermal and non-thermal effects. The temperature effect affects the vibration intensity of polar groups in starch molecules, whereas the non-thermal effect primarily affects the vibration intensity of skeleton modes like the glucoside bond and pyran ring, as well as skeleton groups like C-O and C-O-H (1, 2). Microwave stimulates the development of free radicals at the C1 and C6 locations in starch molecules, as well as the structural modification of C1 free radicals, resulting in the production of more free radicals (3). Furthermore, the microwave sensitivity of different starch molecules varies, owing to differences in starch crystal structure and amylose concentration (4). Due to the heat resilience of amylopectin, which creates the waxy starch, waxy corn starch is less impacted by microwave heating (5). However, the features of microwaves that promote slow starch digestion are tightly related to microwave power and starch moisture: The fundamental reason for the creation of resistant starch is starch recombination generated by high-power microwaves, and the higher the water content in a given range, the higher the gelatinization degree and swelling power, and the higher the digestibility.

Structure

The starch system is a polycrystalline one. The crystallization area and amorphous area, the two main components of starch, alternate to form the semicrystalline area, which then alternates with the amorphous lamella to form starch particles. The structure of starch granules is shown in Figure 1. Microwave heating changes the polycrystalline structure of starch, mostly from ordered to disordered, and hence affects crystallinity, surface morphology, and other significant aspects. Microwave treatment, on the other hand, reduces the conversion of starch structure from ordered to disordered as compared to traditional heating. Amylopectin is the semi-crystalline portion of starch, and its molecular structure is the most important component in determining starch's physical qualities (6). Amylopectin degradation can be separated into two stages and is aided by microwave heating (7). The major degradation occurred in internal chain (amorphous region) at the first stage, the external chain (crystalline region) mostly destroyed at the second stage (6). The external chains (A chain) and short B chain of amylopectin are twirled into a double helix and exist in the crystalline domain, which affects the crystallinity. The inner chain is primarily seen in amorphous lamellae. The amorphous structure is primarily made up of amylose. Microwave treatment causes starch to transform from an ordered to a disordered structure, however the microwave's thermal and non-thermal actions have different impacts on starch structure. The rapid heating effect causes the double helix structure of amylopectin molecules to become more closely arranged in the crystalline layer, compressing the amorphous layer, whereas the non-thermal effect can protect the amorphous layer from the damage caused by rapid heating by causing irregular lamellar structure alternation (2). As a result of the combined action of microwave's fast heating effect and non-thermal effect, the influence of microwave on the ordered and disordered structure of starch is somewhere between conventional slow heating and fast heating. For example, following microwave heating, the content of amorphous structure of potato starch rose by 29% compared to the original starch, while the quantity of double helix structure reduced by 22%, both of which were between the fast and slow heating samples.

The change in starch crystallinity crystallization type reflects the influence of microwave on starch crystal structure. In general, microwave heating lowers the crystallinity of starch, as shown in Table 1. After microwave heating, the relative crystallinity of white sorghum, maize, and other starches, for example, was seen to decrease (above 300 W). However, because of the thick structure, waxy corn starch crystallinity remained intact following microwave treatment (5). Natural

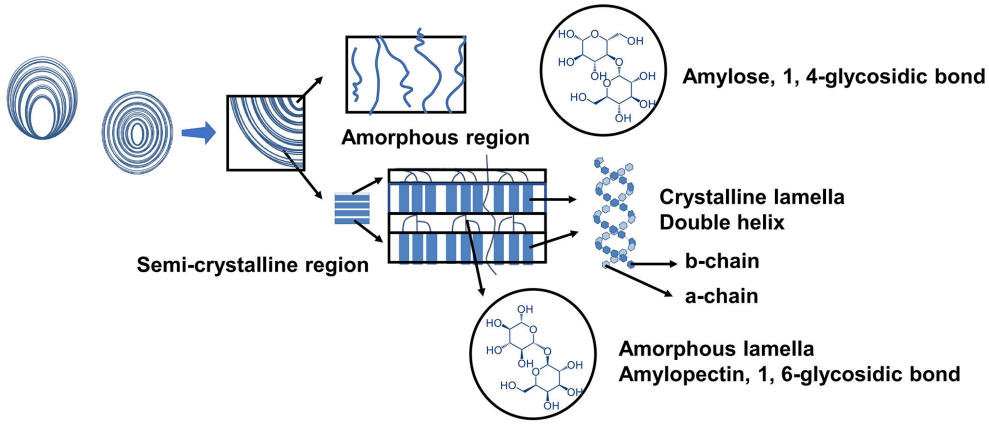

FIGURE 1
The structure of starch granule.

TABLE 1 Effect of microwave treatment on starch crystallinity in food.

Food species	Relative crystallinity (%) (natural starch)	Relative crystallinity (%) (microwave starch)	References
Maize	19.58	2.91	(6)
White sorghum	25.88	18.08	(8)
Chinese chestnut	23.52	20.11	(9)
Wheat	36.81	27.53	(10)
Cassava	28.1	18.47	(11)
Potato	29.09	26.25	(12)

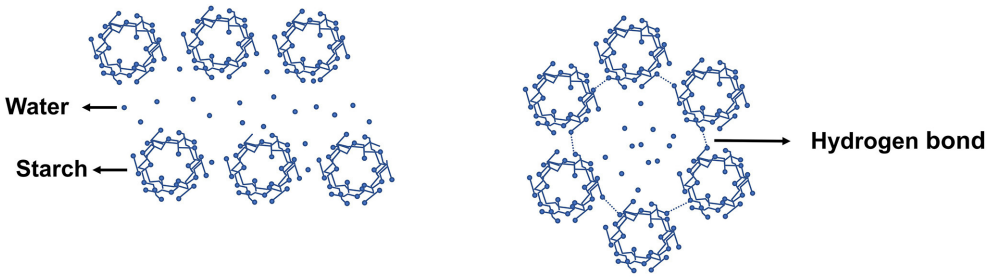

FIGURE 2
Crystal pattern of natural starch (type-A on the **left** and Type-B on the **right**).

starch crystallinity varies with plant kinds from various sources, however there are primarily four types (A, B, C and V-type). The majority of the change generated by microwave heating is from type-B to type-A, shown in Figure 2. Microwave heating, for example, transformed the crystallinity pattern of potato and Canna edulis Ker starch from type-B to type-A (13, 14), as shown in Figure 3. However, after using an optimized microwave-enzymatic hydrolysis process (800 W, 90 S), the crystal structure of potato starch changed from type-B to type-C (16). Because type-C is the intermediate state of continuous change from type-A to type-B, which can be transformed in some special methods or under predetermined conditions, and can also be regarded as a mixture of type-A and type-B, this change also conforms to the general change law of transformation from type-B to type-A.

The existence of a significant number of intermolecular and intramolecular hydrogen bonds is strongly related to the structure stability of natural starch, and microwave heating can impact them primarily by modifying the water distribution and dynamic process in the granules (9, 17). The thermal stability

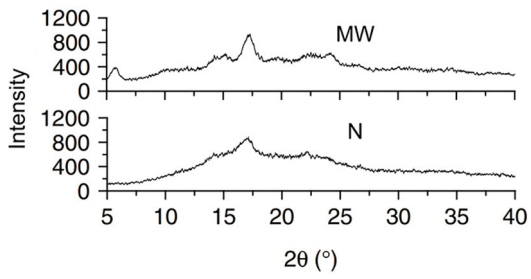

FIGURE 3
X-ray diffraction (XRD) of Indian horse chestnut starch granules. N, native; MW, microwaved (15).

of starch before gelatinization is determined by the quick heating action of microwaves, which can impede the breaking of hydrogen bonds between starch and water molecules, altering the macroscopic physical and chemical properties of starch (18). However, the vibrating motion of the polar molecules, on the other hand, promotes the breaking of hydrogen bonds, and the effect is generally stronger than the microwave's quick heating effect (19). Microwave's non-thermal effects on starch are limited to microcosmic features such molecule polarization, skeleton compactness, and water distribution in multilayer structures.

Because microwave treatment alters the structure and crystallinity of starch, it also alters the surface morphology and properties of the starch, such as viscosity, gelatinization, swelling force, oxidation resistance, and digestibility.

Starch grain morphology

Microwave treatment can degrade the integrity of starch particles, increasing the number of concave or folds on their surface, shown in Figures 4, 5. Because the weakest section of the particle breaks when it absorbs water and expands to a certain level, the internal starch polymer flows out of the fractured part and separates the particle shell, causing the surface to fold. For example, after microwave heating, there were many depressions or folds appeared on the starch grains surface of cassava and chestnut (9). At the same time, microwave heating causes the polarization cross characteristic of starch granules to vanish. The polarizing cross in the granules is caused by the radial arrangement of amylose and amylopectin. The difference in density and refractive index of crystal and amorphous structure reveals anisotropy when viewed with a microscope under polarized light, demonstrating birefringent phenomena. Because the vibrational motion of the polar water molecules breaks the lamellar arrangement during the microwave heating process, the particles' birefringent vanishes altogether (21, 22). The polarized cross of potato and white sorghum, for example, vanished following microwave treatment (23, 24).

Properties

Viscosity

When heated, starch becomes more viscous. The hydrogen connections between the starch molecules in crystalline region and the starch molecules in amorphous region are broken when water molecules enter during heating. The starch-protein interaction vanishes, and the double helix straightens to generate a separation state, destroying the amylopectin crystal structure. This causes amylose with a tiny structure to exudate from the particles, resulting in increased viscosity and transparency. After microwave heating, for example, there were apparent aggregation and bonding behaviors between starch particles of chestnut and lotus seed (16).

However, the dissolved viscosity of microwave-processed starch food (dry, puffed) is frequently lower than that of conventional dry food. The starch viscosity with this treatment decreases after a period of increase, and the peak viscosity is lower than the final viscosity of untreated starch, as shown in Table 2. This is related to the degradation of starch particle structure and a decrease in relative crystallinity, which prevents starch from absorbing or binding water (16). Microwave may also encourage the creation of a double helix structure of the long chain segment of amylopectin or build a compound with other dietary components such as lipid and protein to prevent starch from expanding. At the same time, it was shown that as microwave treatment progresses, intermolecular and intramolecular hydrogen bonds in starch increase, implying enhanced starch association, reduced amylose exudation, and lower viscosity (26, 27).

Furthermore, the apparent viscosity of microwave-treated starch decreases with increasing shear rate and exhibits shear thinning behavior, which is linked to the progressive orientation of molecules in the flow direction and the breaking of hydrogen bonds formed in the amylopectin-amylopectin-water structure during shear (28, 29). After microwave treatment, the viscosity of starch is lowered, reducing the taste unpleasantness caused by high viscosity of food. Furthermore, the starch hardness is improved, making microwave method more suitable for the production of biscuits and other chewable foods that require a specific amount of hardness.

Expansion force

The interaction between the starch chains in amorphous domains and starch chains in crystalline region could be reflected by the value of swelling power, which depends on properties of amylose and amylopectin such as the molecular weight, relative content, branch length and degree of branching.

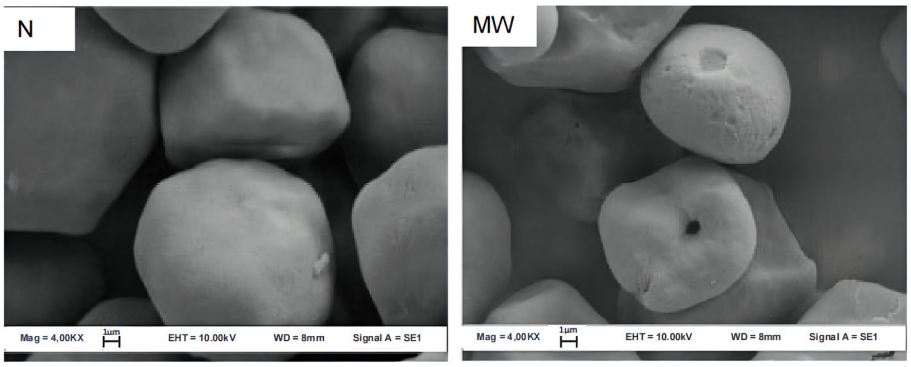

FIGURE 4
Scanning electron micrographs (SEM) of maize starch granules. N, native; MW, microwaved (20).

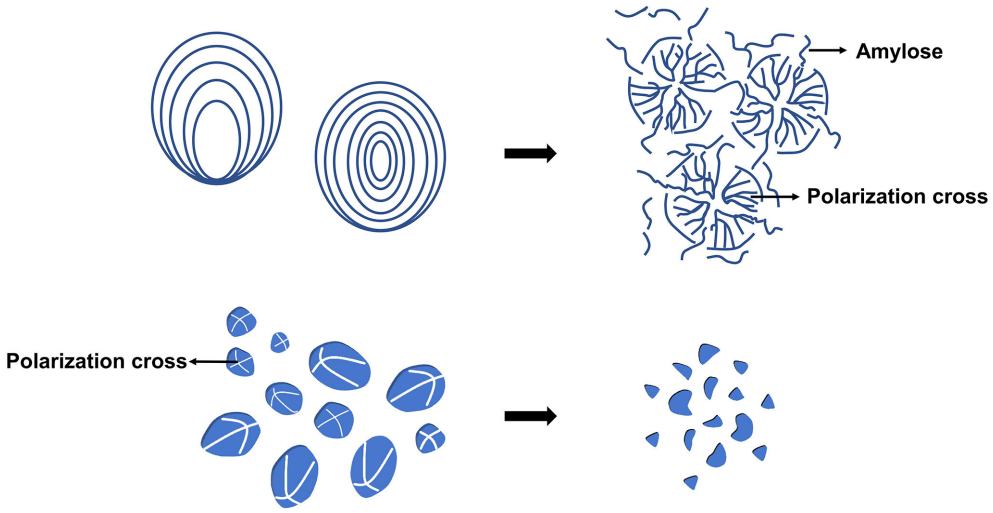

FIGURE 5
Morphological changes of starch grains treated by microwave.

Under conventional heating, the expansion force of starch will increase with the increase of heating temperature, but microwave heating can inhibit expansion by increasing contacts between amylose and amylopectin molecules, preventing water molecules from entering the inner region and reducing amylose dissolution (30). Because amylose works as a diluent, a high concentration of amylose or binding molecules will limit the expansion (31). At the same time, physical interactions between food's key components are common. These interactions may encourage the formation of V-type starch-lipid complexes or terpolymer starch-lipid-protein complexes with bigger molecular and weight structures from starch, lipids, and proteins, shown in Figure 6. These compounds can also prevent water molecules from entering the starch, reducing its swelling potential (32, 33). Aside from that, changes in other food elements throughout the microwave cooking process will have an indirect impact on expansibility. For example, in late microwave processing, protein forms a rigid gel network (34, 35). Furthermore, during microwave heating, the molecular vibration and rapid increase in temperature will cause the particles to rupture and form a polymer film covering the surface of the particles, preventing expansion. Simultaneously, because granule hydration does not keep up with granule expansion, the resulting stress induces granule rupture (26). When microwave heating was employed to treat wheat starch dispersions, for example, the grains fractured due to a lack of gelatinization expansion (22).

Gelatinization

When starch is heated, it absorbs water, swells, and disperses throughout the solution, forming an extremely thick paste

TABLE 2 Effect of microwave treatment on starch viscosity in food.

Food species	Viscosity (Pa·s) (natural starch)	Viscosity (Pa·s) (microwave starch)	References
Cassava	1.9343	0.85433	(11)
Potato	8.2292	2.1250	(16)
Maize	302.7	200.2	(6)
Millet	785.3	448.6	(25)
Indian horse chestnut	3.540	1.689	(14)

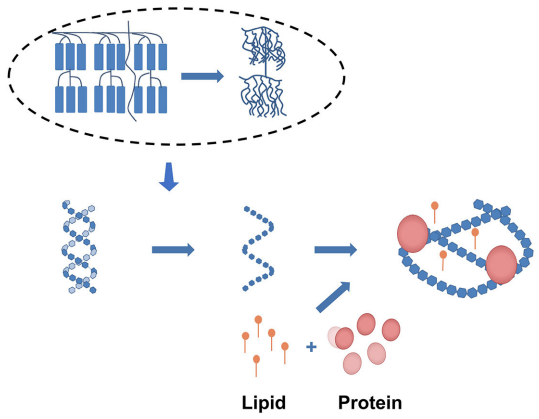

FIGURE 6
Starch forms a complex with proteins and lipids.

known as starch gelatinization. Gelatinization is defined as the breakdown of hydrogen bonds, the loss of association, and the separation of the double helix when water is introduced into starch grains. The starch molecules are then distributed in water, resulting in a hydrophilic colloid solution.

The gelatinization mechanism and rheological properties of starch can be affected by microwave treatment. Two crucial parameters in the gelatinization process are gelatinization temperature and gelatinization enthalpy. The lowest temperature necessary for starch gelatinization is the gelatinization temperature. And, to some extent, the gelatinization enthalpy can reflect the energy needed to separate the double helices structures (13). Microwave gelatinization is often characterized by an increase in gelatinization temperature and a decrease in gelatinization enthalpy (ΔH). Corn, Chinese chestnut starch and other starches, for example, increased in gelatinization temperature while ΔH dropped under microwave treatment, as shown in Table 3. Microwave causes starch molecules to reorganize, resulting in tighter crystal regions, delaying the commencement of starch gelatinization. At the same time, as the microwave expansion force and amylose dissolution diminish, the starch gelatinization decreases. Microwave-treated lotus seed starch, for example, had a tight crystal zone structure and reduced amylose dissolution, altering the rheological properties of starch paste (38). Reduced starch gelatinization can improve food tensile strength and formability, as well as boost product crispness and strength. Microwave pizzas from the American Peel business and microwave pre-fried items from the Nichirei firm, such as Kelekai and Tianbuluo, for example, are both more crisp.

In addition, compared with the conventional heating treatment, which only leads to the gelatinization of the particle surface, microwave treatment will completely destroy them, because the microwave energy will affect the water molecules existing in the crystalline area of starch particles and enhance the cracking (39).

Oxidation resistance

Microwave-treated starch exhibits a greater DPPH free radical scavenging activity. One of the explanations is the lowering of free radical reactivity caused by the synthesis of new double bonds during starch breakdown. The phenolic compounds, on the other hand, may take precedence over the starch oxidation reaction. Microwave heat treatment can help to free bound phenolic chemicals in materials and increase phenolic exposure. The DPPH clearance of chestnut starch, for example, increased from 18.89 to 29.02 percent (14). The increased antioxidant activity of starch serves to lower the degree of oxidation of lipids and other dietary components, preventing peroxide damage to the body.

Digestibility

Heat treatment improves the digestibility of starch in general. Because heating leads to wide cracks and deep cavities on the granule surface, which facilitates access for the starch hydrolyzing enzymes to starch chains and accelerates the digester process (25). However microwave treatment can diminish the digestibility of starch, causing it to have slow digesting properties, as seen in rice and lotus seeds, which compared with conventional heating, have both increased their resistant starch (RS) and slow digestibility starch (SDS) (40).

The process by which the microwave slows the pace of starch digestion can be explained in two ways. On the one hand, after microwave heating, amylopectin degrades to create additional

TABLE 3 Effect of microwave treatment on starch gelatinization parameters in food.

Food species	Gelatinization temperature (°C)	ΔH(J/g)	References
Maize	10.69↑	3.1↓	(6)
Chinese chestnut	2.79↑	2.49↓	(9)
Barley	12.7↑	2.8↓	(36)
Indian horse chestnut	20.18↑	1.4↓	(14)
Peanut	11↑	2.3↓	(37)
Millet	7.83↑	5.78↓	(25)

amylose and forms an amylopectin-polyphenol complex with polyphenols in the system, resulting in a high-amylose, heat-resistant, and slow-digesting product. To lotus seed, for example, could produce a heat-stable slowly digestible high-amylose maize starch by adding certain amount of tea polyphenols (26). At the same time, an increase in amylose molecular weight can cause glucan chains to recombine and form an organized semi-crystalline region structure, slowing digestion. High-power microwave treatment, compared to typical cooking storage, enhances the molecular sequence and cyclical amorphous crystal structure, according to studies. This alteration encourages the creation of amyloid chain domains with a medium density accumulation and delayed digestion (41). In conclusion, the sluggish digestion of starch is caused by the breakdown of amylopectin and the creation of high amylose. After microwave treatment, the amylose and RS contents of potatoes increased to 35.06 and 27.09%, respectively (42). These are also the reasons why waxy and low-amylose rice's starch hydrolysis in life is often faster and more complete than intermediate- and high-amylose rice's.

Microwave-induced reductions in starch digestibility, on the other hand, can be related to changes in starch's multistage structure during digestion. Not only does digestion hydrolyze the starch matrix, resulting in porous substrates and a reduction in polycrystalline and nanoscale order, but it also reorganizes the starch chain, resulting in a crystalline transition from untreated starch type-A to type-B and the formation of new molecular structures. As a result, matrix hydrolysis and molecular recombination, which occur simultaneously during the process, play a major role in starch digestion. Unlike normal starch, the microwave processed starch's polycrystalline component is preferentially digested (43). However, when compared to starch treated with ordinary heating, microwave-treated starch has a higher molecular recombination ability during digestion, resulting in slower digestion. Conversion from type-B to type-A+B (type-C) can also enhance the concentration of RS while decreasing digestibility by increasing crystallization area and resistance to enzymatic hydrolysis (27, 44).

After microwave heating, the content of resistant and slow digestible starch increases, and it is not enzymatically hydrolyzed in the small intestine, but it can be fermented with volatile fatty acids. As a result, it can lower the body's glycemic index and weight, making it ideal for diabetics and beauty enthusiasts.

It is not difficult to find that the particle shape, crystallinity, rheological behavior, gelatinization temperature, enthalpy and digestibility of starch all depend on the starch type and its moisture content, microwave treatment time, treatment temperature and absorbed microwave energy. Therefore, future research should systematically focus on the physical, chemical and structural changes of different kinds of starch under microwave treatment under different parameters, so as to better understand the specific changes related to the parameters of starch during microwave heating, which will be more helpful to predict the overall behavior of starch on this microwave processing, and help design and improve the processing of starch and starch products and the quality of final products.

Lipids

Daily high fat food is mainly the food with high oil content and fried, including peanut, fatty meat, animal viscera, butter products and so on. Because lipids have a low specific heat and heat up quickly, they are particularly vulnerable to microwave heating. Microwave heating, on the other hand, has a lower impact on oil than traditional heating. The polar molecules content in the oil is lower, but it is the main heating under microwave, because microwave heating can convert mechanical energy generated by asymmetric vibrations of polar molecules into heat energy. To minimize lipid oxidation, microwave energy can also inactivate lipoxygenase and eliminate hydrogen peroxide. Microwave treatment, for example, lowered the oxidation rate of rice bran oil when compared to traditional heating (45).

Structure

Microwave heating will trigger lipids oxidation, leading to lipid polymerization and thermal oxidative decomposition. However, compared with conventional heating, microwave has a lower degree of lipid oxidation, because on the one hand, heating

will accelerate oxidation, and on the other hand, microwave can enhance the antioxidant capacity of lipids and delay oxidation. Microwave-treated vegetable oils, in general, produce hydrogen peroxide and secondary oxidation products quickly. Because lipid secondary metabolites can harm the body, lipid oxidation should be prevented as much as possible during food processing. Furthermore, lipolysis, which might result in a rise in acid, is a significant alteration in lipid during microwave heating. Lipolysis, lipid polymerization, and heat oxidative breakdown will all have an impact on lipid composition and characteristics.

Lipid composition

Fats and lipoids are two types of lipids. Because lipolysis and lipid oxidation are common, the total content of lipids, as well as the contents of fats and lipoids, are all reduced following microwave treatment, while the quantity of fatty acids is increased and the composition of fatty acids changes, the oxidation process of polyunsaturated fatty acids is shown in Figure 7. The content of crude fat and phospholipid in trichosanthis seed, for example, dropped after microwave treatment, whereas the content of free fatty acids increased (46).

Temperature, oxygen, the unsaturated fatty acid ratio, and other factors influence lipids loss during microwave therapy. Because of the high temperatures and copious oxygen involved in heating, baked foods lose substantially more phospholipids than microwaved foods. Phosphatidylcholine (PC), phosphatidylethanolamine (PE), phosphatidic acid (PA), and sphingomyelin (SM), which are abundant in polyunsaturated fatty acids, were more affected by microwave than other components in black egg yolk (47). In addition, other factors, such as water evaporation from the treatment process, also affect lipids content, because lipids oozes out when water evaporates. For example, the lipids loss of hot air drying fish was more serious than that of microwave drying fish (48).

Microwave treatment of free fatty acids in food can increase their content and change their composition. Monounsaturated fatty acids (MUFA) and polyunsaturated fatty acids (PUFA) proportions decrease, whereas saturated fatty acids (SFA) and trans fatty acids (TFA) proportions increase. The rapid oxidation of lipids and the loss of water in the microwave process, which fatty acids spread and exchange between fat and water, causes this occurrence. The retention rate of unsaturated fatty acids is higher when compared to standard cooking and drying methods such as baking and air drying (49). Buckwheat and other foods arfter microwave, for example, had a larger PUFA proportion than that after conventional heating, although they had lower total lipids content, SFAs, MUFAs, and PUFAs under microwave, as shown in Table 4 (51).

Furthermore, the content of unsaturated fatty acids influences microwave heating rate, with the larger the content, the faster the heating rate. Sunflower oil, for example, which has a larger proportion of unsaturated fatty acids, heats up faster, whereas peanut oil, which has a lesser content, heats up more slowly (53).

Acid value and peroxide value

The acid value and peroxide value of lipids in microwave foods have a significant impact on food safety. The more fat is oxidized, the more chemicals like aldehydes, ketones, and acids are generated, causing more cell damage. Cells can be damaged by partial oxidation products of lipids, SFA, hydroperoxides, and malondialdehyde, however, MUFA and PUFA can protect cells (54).

The content of fatty acid grows as lipids decompose, and the acid value of the oil increases as the microwave intensity and time increase, but the pace of growth is sluggish. On the other hand, the peroxide value follows a zigzag pattern of increasing-decreasing-increasing. Because of their instability, peroxide, the main result of lipid oxidation, is transitory. When lipids are heated in the microwave, they oxidize and breakdown to create peroxide, which is quickly degraded into oxidized secondary products as the temperature rises. The peroxide value tends to rise when the rate of peroxide generation exceeds the rate of peroxide decomposition; otherwise, it tends to fall. Furthermore, as the heating temperature and duration increase, the acid value of fatty foods increases, and the degree of influence is related to the unsaturated degree of oil. For example, following microwave heating, the acid value of tea seed oil increased and was related to temperature and heating duration. Meanwhile, the peroxide value rose first, then fell, and the larger the microwave power, the shorter the time it took to reach its maximum value (55).

Because of the quick disintegration of the primary product hydroperoxide, various subsequent products can represent the oxidation degree of lipids in addition to acid and peroxide values. Microwave heating usually further degrades lipids *via* fission, dehydration, and the generation of free radicals, resulting in hydrocarbons, ketones, and aldehydes, among other things. Malondialdehyde is a common secondary product of lipid oxidation, and its synthesis is influenced by the temperature, power, and duration of microwave heating. The concentration of malondialdehyde increases initially and subsequently drops during microwave heating, which is related to its volatility (56).

Although the acid value and peroxide value of dietary lipids will invariably rise as a result of microwave processing, but compared with conventional heating, the acid value and peroxide value are lower, and we can reduce the degree of lipid oxidation by controlling temperature, power, time, water and other factors. Food treated with a short time microwave, for example, had much lower carbonyl value and trans-fatty acid level than food treated with a long time microwave (57).

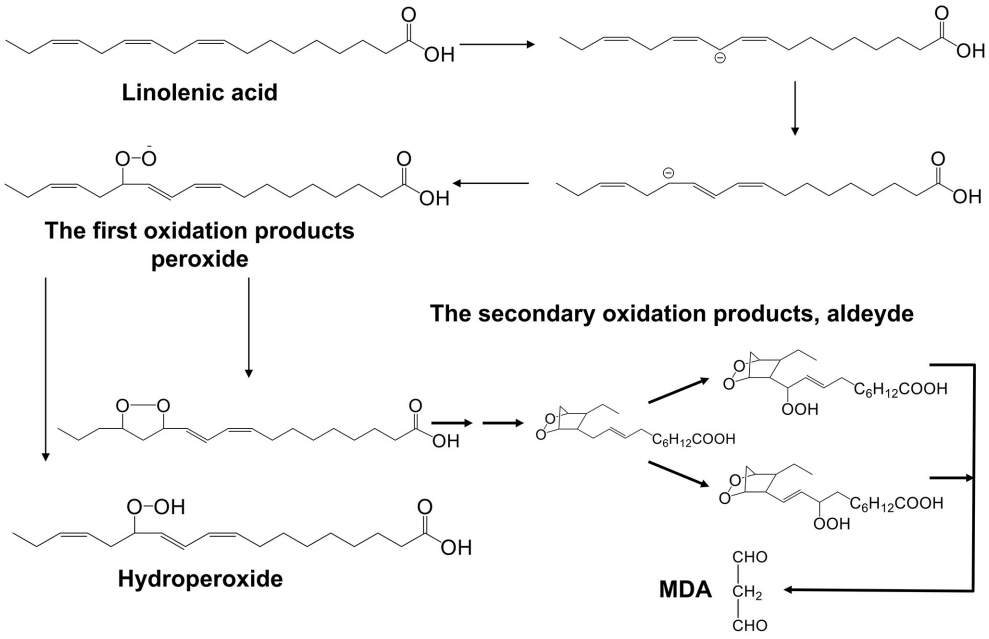

FIGURE 7
Oxidation process of polyunsaturated fatty acids (taking linolenic acid as an example).

TABLE 4 Effect of microwave treatment on lipid composition in food.

Food species	Conventional heating		Microwave heating		References
	MUNA/SFA	PUFA/SFA	MUNA/SFA	PUFA/SFA	
Hamburgers	0.023↓	0.01↓	0.381↑	0.009↓	(50)
Buckwheat	0.05↓	0.025↓	0.03↓	0.024↓	(51)
Grass carp	0.172↓	0.302↑	0.114↓	0.353↑	(52)

Lipid oxidation

Microwave heating boosts lipid antioxidant capability and lowers lipid peroxidation. The following are the three main mechanisms: Microwave heating, for starters, can produce antioxidant active molecules to take part in the reaction of free radicals prior to the lipids. The other option is to lower the amount of reaction catalyst needed by improving metal chelating capacity. Third, by decreasing the action of oxidase, it can prevent the enzymatic oxidation of lipids.

To begin with, microwave heating promotes the formation of antioxidant active components in oil, such as carotenoids, phenolic compounds, and other chemicals. This is because microwave heating causes intense movement of polar molecules, which breaks the cellular structure of the food matrix and allows digestion enzymes to enter. The extraction rate then increases as the biological accessibility of these components improves (58). Microwaves also cause the protein's phenolic binding sites to be disrupted, allowing additional phenol to be released. These active chemicals take part in the reaction of free radicals before they react with lipids, removing free radicals and preventing lipid oxidation (59). At the same time, vitamin E has been associated to free radical disruption events and the formation of antioxidant dimers, and the retention rate of water-soluble and thermally unstable vitamins, such as vitamin E, is higher after microwave cooking than after conventional heating (60, 61). For example, after microwave processing, the total phenol content of trichosanthes seed oil increased, resulting in improved antioxidant capacity (46). Although the phenolic compounds of rice bran treated by microwave decreased slightly, the antioxidant capacity was still increased due to the enhanced extraction effect of carotenoid and chlorophyll (45).

Microwaves also increase lipid oxidation indirectly by changing the protein characteristics of foods. It can, for example, accelerate the Maillard reaction, boost proteins' metal chelating ability, and inhibit the activity of lipid oxidase. The lipoxygenase activity of trichosanthis seed oil, for example, was reduced by 90.30% after microwave heating (46). Apart from that, a minor

amount of amino acid derivatives was discovered in the fat of the bran after microwave cooking, which could be Maillard reaction products and could be used as antioxidants to preserve oil from oxidation (45).

Microwave pretreatment and crushing is currently employed in the oil processing sector because it not only improves oil extraction rates, but also boosts oil oxidation resistance, reducing the impact of oil oxidation on flavor and safety.

Protein

Protein is the building block of life and one of the most important nutrients for the human body. Microwave heating, in contrast to traditional heating, uses a combination of thermal and non-thermal effects to alter complicated protein structures by disrupting intramolecular interactions. These alterations will then have an impact on the characteristics of proteins.

Structure

By creating free radicals and larger or smaller molecules during microwave heating, electric and electromagnetic fields can cause conformational changes in proteins, damaging the primary, secondary, tertiary, and quaternary structures of proteins, the secondary structure and intramolecular forces of proteins is shown in Figure 8. Compared with conventional heating, microwave can accelerate the unfolding of proteins. Under high-powered microwave heating, the protein disulfide link breaks, exposing the hydrophobic core residue to the solvent, and the protein depolymerizes. The percentage of ordered and disordered structure will shift during this process, primarily from ordered to disordered. Because the hydrogen connection between carbonyl (C=O) and amino (-NH2) contributes to the stability, the α-helix has a regular ordered structure, and the more of it there is, the more stable the protein's secondary structure is (62, 63). The following are the structural alterations in proteins caused by microwave treatment: Random coil rises, α-helix decreases, β-sheet and β-turns increase first and subsequently decrease. In other word, the α-helix changes to β-sheet and β-turns throughout this procedure, while the β-chain changes to random coil (64). A possible mechanism is proposed: the various effects of microwave synergistically weaken the previously intra-molecular and inter-molecular forces including hydrogen bonding, disulfide bonding, and hydrophobic interactions, which led to the formation a new structure by the rearrangement of the molecular forces (65). For example, under microwave heating treatment of lotus seed and pigeon bean flour, the ordered structure of protein decreases and the disordered structure increases, as shown in Table 5.

However, during the treatment procedure, microwave may cause glucan glycosylation, which is aided by protein. The effect of the microwave on the secondary structure of the protein will be reduced, and only the tertiary structure will be affected. Because high quantities of dextran crowd the system and produce steric hindrance, which prevents excessive denaturation. For example, after the Maillard reaction was triggered by microwave, no substantial modifications in the secondary structure of rice protein were identified (67). Furthermore, the Maillard process was discovered to transform the protein structure from disorder to order to some extent. In the microwave-induced Maillard reaction of rice residue protein, for example, the α-helix increased while the β-sheet and β-turns decreased (74).

Microwave treatment can alter the structure of proteins, which can affect properties such as hydrophobicity, digestibility, emulsification, foaming, gel resistance, oxidation, and allergenicity. Also affected is the Maillard process between protein and decreasing sugar, shown in Figure 9. For example, a high β-sheet and α-helix ratio causes digestive enzymes in the gastrointestinal tract to be less accessible, resulting in poorer protein value and utilization.

Properties

Hydrophobicity

Protein hydrophobicity rises when heated with high-powered microwaves. At the same time, compared with conventional heating, a higher degree of hydrophobicity can be obtained (75). This is because when polar protein molecules collide, free radicals are produced, causing disulfide bonds to dissolve and sulfhydryl groups to form. Protein hydrophobicity increases as the total sulfhydryl group content increases (76). The majority of hydrophobic residues are found in the interior of protein's structural structure (4, 77). As the structure unfolds during microwave treatment, more non-polar amino acids are exposed on the surface, increasing the hydrophobicity (76). At the same time, the repulsion of more homogeneous charges on the protein surface will limit molecule aggregation, reduce particle size, and increase the stability of the solution due to the increased Zeta potential of microwave protein solution. The degree of enrollment of hydrophobic groups decreases at this period, but surface hydrophobicity rises (78). The protein water solubility of soybean meal, for example, reduced from 94.4 to 48.1% following microwave treatment, whereas the disulfide bond content increased by 42% (79).

However, after a period of microwave heating, protein hydrophobicity decreases rather than increases. On the one hand, this is because certain sulfhydryl can be converted to disulfide bonds with the help of active free radicals, resulting in a reduction in overall sulfhydryl group content and hydrophobicity. In the presence of oxygen, the sulfur group becomes more reactive, and the distance between the groups shrinks, making disulfide bonds easier to form (80).

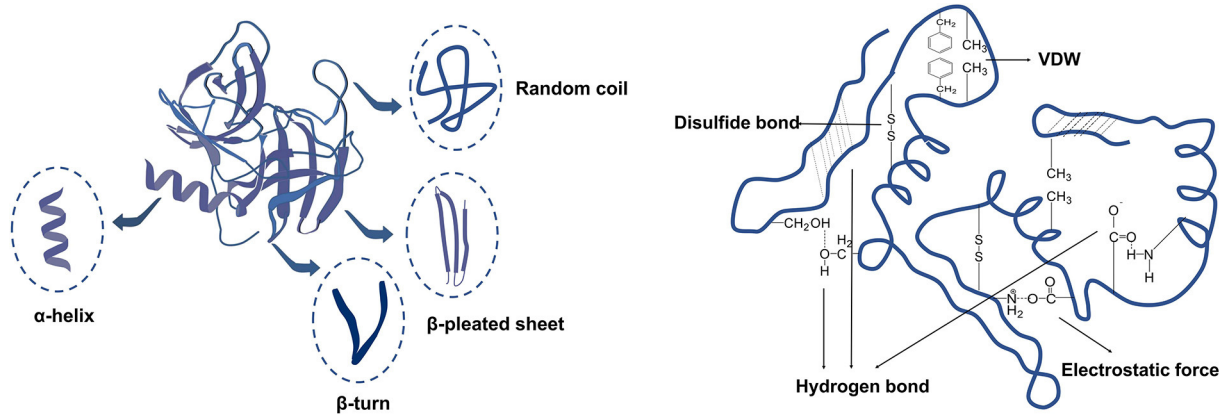

FIGURE 8
Secondary structure and intramolecular forces of proteins.

TABLE 5 Effect of microwave treatment on protein structure in food.

Species	α-helix (%)	β-sheet (%)	β-turn (%)	Random coils (%)	References
Lotus seed	20.59↓	7.36↓	9.46↑	18.49↑	(66)
Myofibril	22.5↓	9↑	4.2↑	4.9↑	(1)
Rice	0.5↑	3.5↓	0.2↓	1.6↑	(67)
Barley grains	0.003↓	0.014↓			(68)
Fiber	8.71↑	5.8↓	11.58↓	10.55↑	(69)
Peanut flour	2.7↓	1.4↑		4.3↑	(70)
Soybean	4.8↑	9.49↓	3.8↑	0.89↑	(71)
Quinoa	1.5↓	0.7↑	0.3↓	1.3↑	(72)
Pigeon pea	3↓	5↓	2↑	5↑	(73)

The hydrophobic residues, on the other hand, are prone to aggregation when microwaved at high power or over long periods of time (81). For example, as microwave power and time were increased, the surface hydrophobicity of beef proteins increased at first, then reduced slightly (13).

After microwave heating, the hydrophobicity of protein increases and the interaction with low polar solvents becomes stronger, so it is more suitable for cake ingredients, salad seasonings and other oil-based ingredients. Protein hydrophobicity also has an impact on its antioxidant, foaming, gelation, and oil absorption abilities, and these properties are linked to the appearance and flavor of food. As a result, in the food processing process, careful attention should be paid to the time and power of microwave treatment to avoid excessive protein denaturation and aggregation caused by excessive power and heating time, excessive protein denaturation and aggregation will alter the hydrophobic properties and cause the final product's appearance and flavor to differ from expectations.

Digestibility

The digestibility of protein can be improved by microwave treatment. One of the most important reasons is that microwaves can alter enzyme function, resulting in increased protein-protease interaction. Microwaves alter enzyme activity in four main ways. (1) Microwave treatment inhibits thermally unstable enzymes due to heat denaturation (82). (2) Due to molecular rearrangement and protein unfolding, microwave may render specific protein locations more vulnerable to enzymatic hydrolysis. (3) The microwave-treated protein sample's reduced particle size can provide greater surface area and expose more cleavage sites for digesting protease activity. (4) After microwave treatment, a protein with a high Zeta potential developed, which helped to stabilize the protein suspension and prevent protein aggregation in water, increasing the number of exposed particular sites and the likelihood of protein-protease interaction (73). For example, after microwave heating, the protein of lotus seed unfolded, exposing more cleavage sites and increasing the degree of hydrolysis (6).

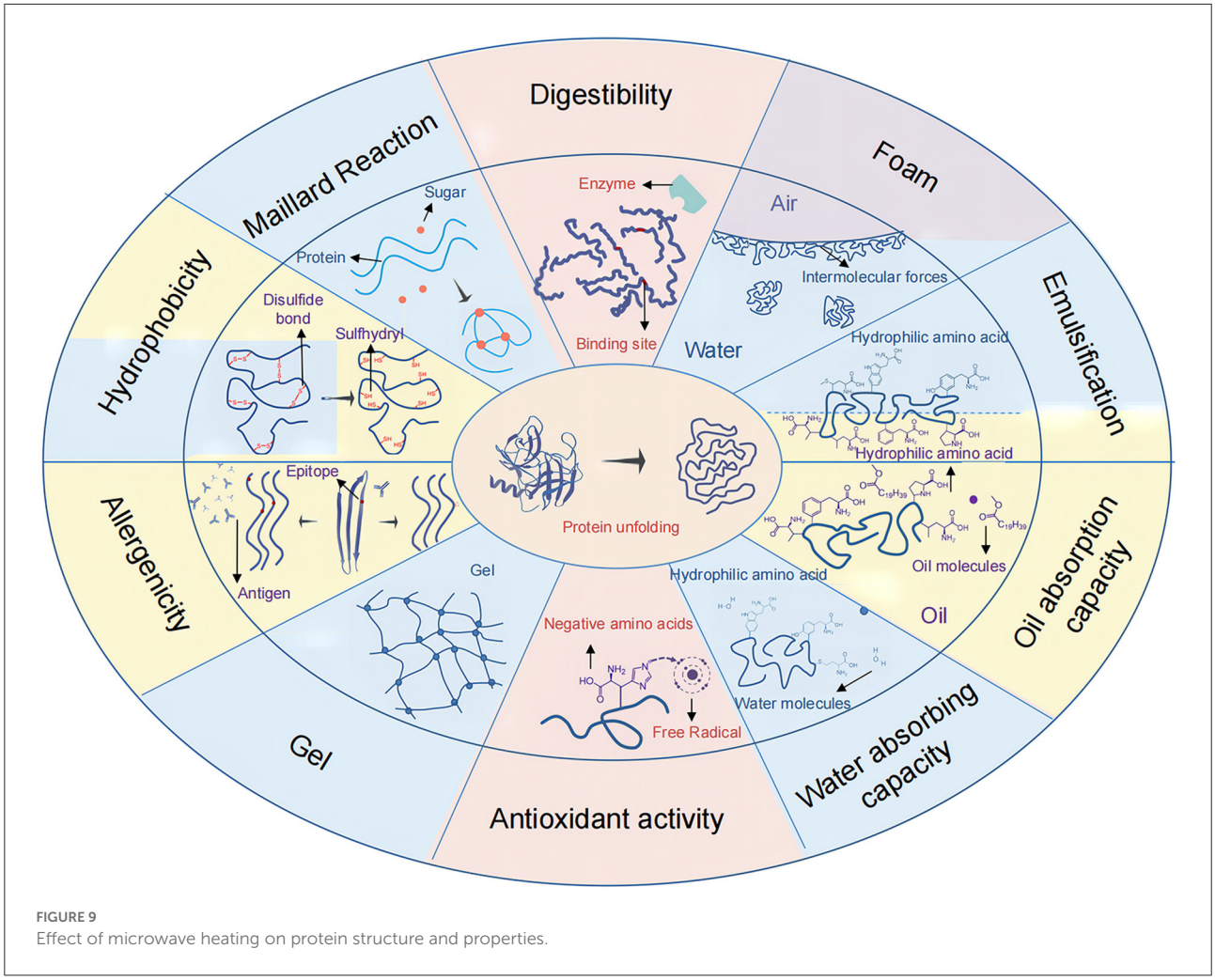

FIGURE 9
Effect of microwave heating on protein structure and properties.

Protein unfolding and exposure to the enzyme reaction can also be caused by conventional heating. However, conventional hydrolysis takes longer to achieve the same degree of hydrolysis as microwave. This is because microwave non-thermal coupling can promote the breaking of non-covalent bonds in protein molecules, speeding up protein unfolding. Protein hydrolysis is best above 70°C, according to some studies, but protease is inactivated at this temperature, so it must be kept below 65°C. The final enzymatic hydrolysis result demonstrates that microwave heating with both thermal and non-thermal effects is clearly better to traditional heating using a conduction heat source (83).

However, as the microwave temperature, time, and power are increased, the digestibility of the protein decreases, because the increased heat treatment leads in complete denaturation of proteins. Then, through hydrophobic and electrostatic interactions, cross-linking reactions take place between proteins, transforming them into larger molecular weight aggregates, an insoluble three-dimensional network. Protein endonuclease will be more difficult to access as a result (84). This phenomenon is less likely to occur in microwave than in traditional heating because microwave's non-thermal effects contribute to appropriate denaturation of protein with modest aggregate extent. In general, non-thermal coupling can encourage protein molecules to break their non-covalent interactions, whereas a significant thermal influence can cause protein refolding or aggregation (4). Furthermore, the Maillard reaction has an inhibitory effect on proteolytic enzymes and can reduce digestibility through a mechanism similar to cross-linking aggregation between proteins (85). For example, milk protein began to aggregate after an 8 min microwave treatment, and the degree of hydrolysis and digestibility both decreased (86).

Antioxidant activity

Microwave treatment can enhance the antioxidant ability of protein, which is related to the fact that microwave can promote protein hydrolysis to produce more active peptides

and enhance the metal chelating ability of protein. At present, it has been confirmed by experiments that compared with the unprocessed protein, the total antioxidant capacity (TAC) of hydrolysates of fish protein and shrimp protein after microwave treatment showed an increasing trend (87, 88). At the same time, compared with conventional heating, microwave protein has a higher DPPH value (75).

After protein hydrolysis, active peptides having antioxidant activity are generated. They can combine with free radicals to generate more stable products, as well as provide an extra source of protons and electrons for oxidation processes to keep the REDOX potential high (89). Microwave speeds up the hydrolysis of proteins into peptides, allowing more reactive species and electron-dense peptide bonds to reach the functional side of the chain (90). Microwave treatment can also cleave peptides into smaller molecular weight peptides, which have stronger antioxidant properties and are easier to permeate the intestinal barrier to perform biological functions (91).

The electrons, hydrogen-bonding characteristics, and position of the amino acids, as well as the steric properties of the amino acid residues at the C- and N-termini, all affect the antioxidant activity of peptides. Hydrophobic amino acids (Leu, Val, and Phe), hydrophilic and basic amino acids (His, Pro, and Lys), and aromatic amino acids (Phe and Tyr) all contribute to the improvement of antioxidant activity in the peptide sequence (92). Microwaves can increase the antioxidant activity of peptides by exposing hydrophobic residues and some polar charged amino acids to the peptide's terminal.

Furthermore, the ability of proteins to chelate metals has an impact on their antioxidant activity. Metal ion chelating (MIC) activity is attributed to peptides containing sulfhydryl amino acids, which can bind heavy metals and diminish their pro-oxidant action. Protein rearranges and releases the encrypted Sulfur peptide to grab metal ions during microwave treatment, resulting in improved MIC capacity (88, 93). The Salvia hispanica protein, for example, have higher MIC activity than conventional heating (75). However, several investigations indicated that when the protein was microwaved again during the enzymatic hydrolysis step, no increase in metal chelation was detected. This is because when microwave time, temperature, and power increase, protein reaggregation occurs and enzymatic proteolysis is prevented, resulting in a decrease in active peptide release (57, 94). Finally, some of the products of the Maillard process generated by microwaves have antioxidant characteristics.

Microwave-induced alterations in protein antioxidant capacity have an indirect effect on lipid oxidation, as some proteins can act as antioxidants after being microwaved. Metal chelation, for example, can help non-absorbed proteins contribute to the free radical scavenging mechanism of lipid antioxidant activity. Microwave protein's antioxidant properties can significantly reduce nutrient loss caused by oxidation of other substances in meals, as well as prevent damage caused by peroxidation.

Maillard reaction

Microwave treatment can increase the occurrence of food Maillard reaction (89). Because the active sites of Maillard reaction are mostly located in the internal regions of protein structures, and the extension microwave heating time exposes these sites. At the same time, under the high-power microwave treatment, the protein expands, which increases the probability of effective collision between it and sugar molecules, enhancing the Maillard reaction (95). For example, the activation energy of RP-dextran Maillard reaction of rice protein treated by microwave was lower than that of conventional heating (67). The Maillard reaction products can improve flavor, some can increase the antioxidant capacity and reduce the damage caused by peroxide to the body, but there are also some reaction products that are carcinogenic and harmful to the body's health. Moreover, the Maillard reaction process is complicated and there are many influencing factors. Therefore, at present, microwave-induced Maillard reaction still has uncontrollability and uncertainty of product properties. It is vital to undertake in-depth research on the microwave-induced Maillard reaction's reaction process and products if we wish to employ it to improve particular food features. At the same time, some of the negative effects of the Maillard reaction make it important to prevent this type of reaction from occurring in the processing process, which limits the use of microwave heating technology. However, we may explore decreasing the heating time, lowering the power, or adjusting some internal food parameters (starting moisture content and pH value), as well as adding some compounds (mercaptan compounds) to the pretreatment materials to reduce the incidence of Maillard reaction.

Allergenicity

Antigenicity of proteins is induced by the presence of epitopes, which are particular sequences in allergen proteins that, when recognized by the immune system, elicit allergic reactions. One reason microwave treatment reduces allergenicity is that it causes protein aggregation and structural changes, which prevent epitopes from being targeted. The other is that microwaves can reduce natural protein immune responses by destroying particular allergen epitopes through enzymatic hydrolysis. Microwave treatment can disrupt disulfide links in proteins, lowering their stability and making allergens more susceptible to enzyme breakdown, shown in Figure 10A. Although the raw protein has several protease digestive sites, the aggregated structure makes potential cleavage sites unavailable until the protein is denatured. Microwave decreases allergenicity by increasing the accessibility of sequence epitope proteases (87). For example, after microwave treatment, the antigenicity

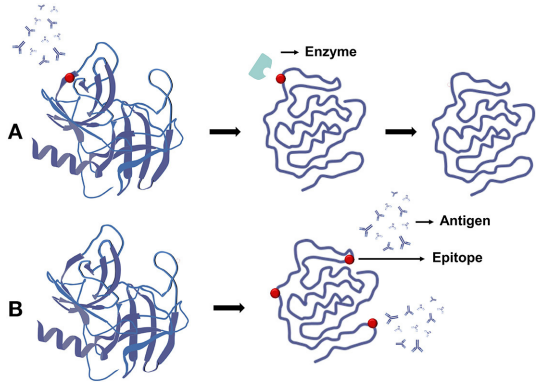

FIGURE 10
Effect of microwave on protein allergenicity. **(A)** Microwave promotes the degradation of protein epitopes and reduces allergenicity. **(B)** Microwave promotes the generation of new antigenic determinants and increases allergenicity.

of gliadin, a proline protein linked to celiac disease in patients with gluten intolerance, was dramatically reduced (96). The hypersensitivity of prawn myosin also disappeared after microwave treatment (87). However, after microwave heating (500 W, 1–3 min), the allergenicity of tree nut proteins such as almond, cashew, and walnut remained unchanged (97). The reason for this is that the corresponding epitopes in allergenic proteins were not responsive to microwave heating, even when heated for a long time or at a high temperature.

Microwaves, on the other hand, may increase allergenicity. Because the unpredictability of the protein structure is unfolding, new binding sites may open up. Microwaves, in other words, induce denaturation of natural allergens, which causes proteins to develop new epitopes or make previously hidden epitopes available (crypt antigens), shown in Figure 10B. Microwave-treated peanuts and milk, for example, were shown to be more allergic in one study (98, 99).

The key aspect determining the bidirectional regulation of protein allergenicity by microwave is the type of meal. However, because there have been few studies on the subject, it is impossible to say which foods are less allergic and which are more allergenic after being microwaved. To avoid the occurrence of user allergy, special attention should be paid to the change in food allergenicity when using the microwave to process food. Furthermore, foods whose allergenicity has been shown to increase after being microwaved should be avoided being microwaved.

Water absorption and oil absorption capacity

Protein's propensity to absorb water and oil impacts not only the taste and flavor of food, but also the characteristics of other elements in food, such as the degree of gelatinization of starch. Microwave heating, according to studies, alters a protein's ability to absorb water and oil, owing to a change in protein structure. Protein depolymerization may expose more polar and non-polar amino acids, boosting the protein's interaction with water or oil molecules and so promoting water and oil absorption.

Water absorption capacity (WAC) is related to the presence of polar amino acids at primary cites of the protein-water interface. The uncoiling of hydrophilic domains of protein and the exposure of more polar amino acids after microwave treatment can lead to an increase in water absorption. Because of the accelerated expansion of protein, microwave protein can obtain higher water absorption capacity than conventional heating (100). For example, after microwave treatment, the WAC of red bean, potato etc. increased, as shown in Table 6. Because of the varying hydrophilic structures, the effect of microwave on the WAC of different proteins varies. Furthermore, once a certain level of water absorption capacity has been achieved, it is no longer increased. The ingested water will be released as the protein denatures and unfolds, and then promptly absorbed by carbohydrates and fiber from grains and legumes. The degree of gelatinization of starch will be affected by this moisture, which dictates the final texture and size of baked goods.

Oil absorptivity (OBC) is an important functional characteristic as it is essential to improve mouth feel and flavor retention. Microwave heating can increase the strength of protein binding oil molecules because more non-polar side chains are exposed during this process, increasing oil absorption by binding the hydro-carbon chains of lipids (100). In general, as the microwave treatment period is increased, the ability of the protein to bind oil increases initially, then decreases. Protein reaggregation and a decrease in hydrophobic and non-polar amino acids are to blame for the dip. When red bean, wheat, and melanin wheat flour were heated in the microwave, for example, OBC grew at first, then reduced. At the same time, due to the variability of protein oil solubility, the oil absorption capacity of proteins varies.

Emulsification

Proteins' ability to diffuse over the oil-water interface and interconnect with water and hydrophilic amino acids, as well as oil and hydrophobic amino acids, is referred to as emulsifying capacity. Because the emulsion can change the food system to make it the ideal food, its development and stability during processing is critical. Protein emulsification is generated by the interaction of water and oil with the protein. The creation of these chemicals is beneficial to the food system and has an impact on the final product's flavor and texture. Microwave heating can cause the protein to unfold, exposing the hydrophobic unit. The unfolded protein then interacts with nonpolar solvents, preventing oil droplets from flocculating and improving the emulsion's overall stability. For example,

TABLE 6 Effect of microwave treatment on water absorption and oil absorption capacity of protein in food.

Species	WAC (ml)	OAC (ml)	References
Rice bran	0.2↓	0.1↑	(100)
Red bean flour	0.889↑	0.308↑	(101)
Wheat flour	1.173↓	0.419↑	(101)
Haleem wheat flour	0.139↑	0.02↓	(101)
Indian horse chestnut	3.88↑		(14)
Potato	3.62↑	0.078↓	(12)
Lotus seed	69.8↑		(4)

microwave vacuum treatment (50–100 W mV) enhanced the stability of emulsion flocculation and paste of lotus seed protein isolate (LSPIs) (63).

Gel

During microwave heating, the protein conformational changes and subsequent intermolecular interaction are usually followed by stiffening and thickening of the pre-formed gel through thiol-disulfide exchange reactions (100). On the one hand, microwave treatment's high temperature may hasten the oxidation of protein sulfhydryl groups and increase disulfide bond content (80). Proteins then cross-link to form dense protein networks, which improves the gel's properties. Microwaves, on the other hand, increase exposure to the reactive phenol and mercaptan groups required to produce protein gels, which are normally embedded in natural proteins' dense structure (71). For example, acid gels formed with microwave treated casein solutions were harder and had a more compact microstructure compared to those made with heated caseins (51). In general, two types of protein gels are distinguished. When proteins with a high level of non-polar amino acid residues undergo a denaturation treatment, random aggregation rapidly takes place and an opaque coagulum-type gel is formed that usually contains covalent cross-links. Such protein denaturation and subsequent aggregation is irreversible. Proteins with fewer non-polar residues upon denaturation tend to engage in intermolecular interactions more gradually which results in ordered translucent gels. Here, upon removal of the denaturing conditions, proteins may to a degree refold. In a word, after microwave processing, enhanced protein gelation can increase food transparency and modify the taste and appearance of the final product.

Foam

Some scattered proteins and peptides have typical amphiphilic architectures that reduce surface tension and facilitate interface formation and foaming at the water-air interface. Because proteins and their hydrolysates quickly diffuse into the air-water interface and partially unfold to form a thin film with viscosity and flexibility, they are ideal foaming agents. Foaming capacity depends on the diffusion of protein at the air-water interface by unfolding its structure, while foaming stability is dependent on the formation of a thick cohesive layer around the air bubble (100). Partial enzymatic hydrolysis usually can improve foaming properties. The number of hydrophobic amino acids and substrates exposed to the surface of a protein molecule is directly proportional to its foaming capacity. Microwave-induced increases in hydrophobic amino acids increase protein viscosity and drive the formation of multilayer sticky protein films at the bubble interface, resulting in anti-coalescence. A thick membrane can limit the flow of proteins out of the membrane while also keeping the bubbles stable. Microwave-treated rainbow trout skeletal protein hydrolysates, for example, foamed better than enzymatic proteins (7). Rice bran protein treated by microwave had better foaming property than conventional heating (100). Many meals, such as cake, bread, and ice cream, require the foaming qualities of protein in daily life. The change of mechanical properties and the increase of gel properties after microwave processing can increase the transparency of food and change the taste and appearance of the final product, such as konjak, tofu and noodles. On the other side, it produces a more flexible and edible food packaging material. The quality of protein gelatin produced *via* microwave processing, however, remains uncontrolled. Microwave inhomogeneity can induce faults in the gel matrix, and too much power can cause the protein to expand too quickly, faster than the rate of polymerization, resulting in a rough gel network.

Composition of amino acids

The total content of amino acids falls with microwave cooking, however the content of essential amino acids somewhat increases. Different types of amino acids have different variations in the microwave heating process. Because of heat intolerance or the Maillard reaction, the majority of hydrophobic and sulfur-containing amino acids increase,

TABLE 7 Changes of different amino acid contents in food after microwave heating.

Food species	Changes in amino acid content	References
Lentils	Leucine goes up and valine stays the same	(102)
Soy milk	Lysine, tryptophan and cysteine decreased	(103)
Buckwheat	Serine, proline, leucine and phenylalanine increased, methionine and tyrosine did not change significantly, but some sensitive amino acids, such as histidine, are reduced	(51)
Sunflower	Proline, aspartic acid, threonine, valine, isoleucine and lysine increased	(104)
Fish fillet	Lysine, valine, alanine and leucine increased slightly, aspartate, threonine and cysteine changed little, but histidine decreased	(52)
Rice	Glutamic acid, glycine, alanine, phenylalanine, valine, lysine, methionine, leucine, isoleucine increased, serine changed little, Aspartic acid, arginine, cysteine, but Aspartic acid arginine cysteine histidine and tyrosine decreased	(74)
Milk protein concentrate	Cysteine, valine, phenylalanine and tyrosine increased, while alanine, leucine and proline decreased	(86)

while a small number of amino acids, such as histidine and lysine, decrease. Aside from that, cysteine's contents don't alter significantly due to its heat resistance. Of course, the variation trends of the same amino acid in different foods are different, which could be connected to food type and microwave processing settings. In order to minimize the massive loss of heat-resistant amino acid components caused by long-term heating, special attention should be paid to the temperature, power, and duration in the microwave processing process for meals containing a large number of heat-resistant amino acids. The changes of different amino acid contents in food after microwave heating are shown in Table 7.

The influence of microwave on flavor, nutrients and security

Flavor

Alcohols, ketones, hydrocarbons, lipids, organic acids, heterocyclic compounds, free amino acids, and other components in food alter the flavor of the dish. Aldehydes, for example, have a volatile and greasy fragrance (105). Pelargonic aldehyde smells like roses (106). Sweet amino acids include glycine, alanine, serine, threonine, and proline, while bitter amino acids include methionine, leucine, isoleucine, histidine, arginine, and phenylalanine (84).

The synthesis and adsorption of taste compounds are the key reasons for the improvement of flavor in food cooked in the microwave. On the one hand, taste compounds can be produced through the microwave-promoted Maillard process, lipid oxidative degradation, and protein hydrolysis. Alcohols and organic acids, for example, are produced *via* oxidative lipid degradation. The Maillard process produces pyrrole, pyrazine, and sulfur compounds (107). Microwave, on the other hand, changes the structure of proteins and increases the number of binding sites that react with volatile chemicals, boosting taste adsorption (1, 108). Microwave cooking has been shown to improve protein adsorption to ketone flavor compounds by increasing the concentration of sulfhydryl groups, which can react with the ketone and produce disulfide (109). Microwave protein has a better binding affinity to ketone taste chemicals than conventional water cooking heating which just affects the surface hydrophobicity (1). The umami flavor of mushrooms can be enhanced by increasing the concentration of aspartic acid and glutamic acid in the microwave. It also decreased the content of organic acids in the product to reduce astringency. Although the amount of mannitol, fructose, and trehalose in the solution was lowered, the retention rate was higher than with ordinary heating (110). Furthermore some undesirable flavors can also be reduce by cross-linking (111). Microwave heating, on the other hand, should be avoided to take a long time or a high power. Because protein aggregation can cause the sulfhydryl to become buried inside the protein, reducing its ability to bind to flavor compounds (112, 113).

Nutrients

Small molecular components, minerals, and vitamins are the main nutrients in food, in addition to protein, carbohydrates, and lipids. Although the effect of microwave cooking on vitamins varies, it often outperforms traditional cooking methods like as boiling. Due to the water avoidance and shortening of treatment time in this process, microwave treatment can prevent the loss of vitamins A and C owing to water and reduce the thermal degradation of vitamins B1 and B6 (114). Microwave cooking, for example, had a retention rate of carotene that was 1.31–1.83 times higher than conventional water cooking (115). The most easily degraded form of vitamin E is α-tocopherol, but microwave-induced total disintegration of plant cell walls could improve α-tocopherol extractability and hence increase its amount. Cooking fresh broccoli, Swiss

chard, mallow, daisies, Perilla leaves, spinach, and zucchini in the microwave, for example, resulted in a considerable rise in α-tocopherol (60). Some oxidases, which can be activated by plant tissue damage induced by cutting or mixing, may be involved in the effect of microwave on vitamin E levels. Microwave heat treatment can inactivate natural oxidases, enhancing vitamin E retention. Because of vitamin K's thermal stability, microwave heating has no effect on it. Microwaves can also preserve the mineral content of food. The quantities of Na, K, and P in raw trout, for example, increased considerably following microwave heating (7).

Security

It's been a common misconception that microwaved food might cause carcinogens. According to studies, microwave heating not only prevents the formation of heterocyclic amines and other carcinogens, but also regulate the allergenicity of proteins, reduce the accumulation of saturated fatty acids and trans fatty acids, which lowers the risk of allergic reactions and cardiovascular illnesses. Heterocyclic amines (HCAS) are mutagenic, carcinogenic, and cardiotoxic chemicals formed when protein amino acids are pyrolyzed during food preparation (116). Microwave can inhibit the production of heterocyclic amines, which may be related to its effect on the amino acid composition of protein and the improvement of the antioxidant capacity of some components. First of all, microwave can regulate the composition of amino acids in food proteins, and proline and other essential amino acids have been proven to reduce the production of heterocyclic amines by inhibiting the production of heterocyclic amine intermediates or precursors, forming adducts with heterocyclic amines and heterocyclic amine intermediates (117). Secondly, microwave improves the antioxidation of some food ingredients, which can prevent the free radical chain reaction that produces heterocyclic amine, hence lowering the production of heterocyclic amine (118). Finally, the temperature and duration are the most important variables in the production of dioxins, heterocyclic amines, and other chemicals. Foods high in fat can easily produce these compounds through prolonged high-temperature cooking. Therefore, Therefore, one of the factors contributing to the reduction of heterocyclic amines is the microwave's short-time and low-temperature cooking features. For example, Microwave pretreatment of fried beef pie could reduce fat, water, and HCAS precursors, compared with conventional heating (119).

In addition, microwaves help prevent food from becoming contaminated with microorganisms. Aflatoxin in naturally contaminated peanuts can be efficiently destroyed by microwave baking in the range of 32–40%. Beverage items frequently mildew and contain high amounts of bacteria, and is unsuitable for sterilizing at high temperatures (120). Given these considerations, using microwave technology for sterilizing at a low temperature and quick speed is an excellent solution, since it not only kills all types of bacteria in the drink but also prevents mildew throughout the storage process.

Conclusion

In this manuscript, we have found that microwave heating can change the structure and specific qualities of starch, lipid, and protein in food, making it an excellent food to meet the new needs of markets. For particular properties: (1) For the puffy products with toughness and brittleness: Microwave can improve the gel property of protein and reduce the viscosity, expansion, and gelatinization of starch to meet these goals. (2) For products that need foam, such as cake, bread and ice cream: Microwave can help produce the desired results. (3) For the low sugar products that diabetics and dieters require: Microwave can increase the resistant starch content to reach these targets. (4) For the easily oxidized products: Microwave can increase the antioxidant activity of some components and reduce body damage caused by peroxidation. (5) For emulsified products: Microwave can increase the stability of emulsified food and prevent the flocculation of ingredients. (6) For persons who have specific amino acid requirements: The microwave can boost the quantity of certain specific amino acids in food. (7) For allergy sufferers: Microwave can reduce the allergenicity of their meals. At the same time, there are no safety concerns with microwave-processed foods, and more flavor and small molecular nutrients such as vitamins and minerals have been preserved. These evidences demonstrate that the microwave can replace traditional food processing processes.

However, microwave heating is still insufficient, such as (1) The complex composition of the foods influences the final qualities of foods during microwave treatment. Some foods will become more allergic after being microwaved. Therefore, due to the unknown nature of food, it is necessary to carry out strict process screening before processing. (2) When the microwave process parameters do not match the food, the quality of the finished product will be completely different from the expected. As a result, while utilizing microwaves for food processing, we must consider the meal's composition, heating power, time, temperature, etc. In this way, it can play its greatest advantage in food processing. Furthermore, the majority of available research focuses on the effect of microwaves on single food components, with few investigations involving numerous components at the same time. However, it is not difficult to deduce from this paper that if you want to fully exploit the performance advantages of various food Components, you must select appropriate microwave parameters based on the requirements of target products and the change law of component properties, but different components have different or even opposite microwave parameter requirements. High microwave power, for example,

promotes the synthesis of resistant starch but not protein digestibility, foaming, emulsification, or food flavor. At the same time, there are interactions among food components that impact the structure, properties, and functions of food in an indirect manner. As a result, in future related study, it will be important to take into account all of the different components in food and find the most appropriate processing procedure. It can also be regarded to affect the final nutritional qualities, structure, and texture of food by adding some components based on the interaction of starch, fat, and protein under microwave conditions.

Author contributions

XD, HH, and YH contributed to conception and design of the study. XD and HH wrote the first draft of the manuscript. SH wrote sections of the manuscript. JW, ZC, and MY reviewed the manuscript. LH, DZ, and ZW reviewed and supervised the manuscript. All authors contributed to manuscript revision, read, and approved the submitted version.

Funding

This work was supported by grants from the National Natural Science Foundation of China (82173991, 81760716, and 81960718), Open Project of Key Laboratory of Modern Preparation of Chinese Medicine (TCM-201904), Open Project of State key Laboratory of Innovation Medicine and High Efficiency and Energy Saving Pharmaceutical Equipment in Jiangxi University of Traditional Chinese Medicine (GZSYS202003), and National Interdisciplinary Innovation Team of Traditional Chinese Medicine (ZYYCXTD-D-202209).

Conflict of interest

Author JW was employed by Xinqi Microwave Co., Ltd.

The remaining authors declare that the research was conducted in the absence of any commercial or financial relationships that could be construed as a potential conflict of interest.

Publisher's note

References

1. Han Z, Cai M-j, Cheng J-h, Sun D-W. Effects of constant power microwave on the adsorption behaviour of myofibril protein to aldehyde flavour compounds. *Food Chem.* (2021) 336:127728. doi: 10.1016/j.foodchem.2020.127728

2. Han Z, Li Y, Luo D-H, Zhao Q, Cheng J-H, Wang J-H. Structural variations of rice starch affected by constant power microwave treatment. *Food Chem.* (2021) 359:129887. doi: 10.1016/j.foodchem.2021.129887

3. Yi-xiao L, Da-ming F, Li-yun W, Hui-zhang L, Jian-xin Z, Z. Hao, et al. Growth and annihilation of microwave-induced free radicals in rice starch. *Food Sci.* (2014) 35:114—7. doi: 10.7506/spkx1002-6630-201413021

4. Zheng Y, Li Z, Zhang C, Zheng B, Tian Y. Effects of microwave-vacuum pre-treatment with different power levels on the structural and emulsifying properties of lotus seed protein isolates. *Food Chem.* (2020) 311:125932. doi: 10.1016/j.foodchem.2019.125932

5. Lewandowicz G, Jankowski T, Fornal J. Effect of microwave radiation on physico-chemical properties and structure of cereal starches. *Carbohydr Polym.* (2000) 42:193–9. doi: 10.1016/S0144-8617(99)00155-1

6. Yang Q, Qi L, Luo Z, Kong X, Xiao Z, Wang P, et al. Effect of microwave irradiation on internal molecular structure and physical properties of waxy maize starch. *Food Hydrocoll.* (2017) 69:473–82. doi: 10.1016/j.foodhyd.2017.03.011

7. Asghari L, Zeynali F, Sahari MA. Effects of boiling, deep-frying, and microwave treatment on the proximate composition of rainbow trout fillets: changes in fatty acids, total protein, and minerals. *J Appl Ichthyol.* (2013) 29:847–53. doi: 10.1111/jai.12212

8. Jianan L, Lei Y, Ting W, Shuaifei L, Weixu W. Effect of microwave treatment on physicochemical properties of white sorghum starch. *Food Science.* (2017) 38:186–90. doi: 10.7506/spkx1002-6630-201705030

9. Li S, Duan C, Liu C. Effect of microwave on the structure and physicochemical properties of Chestnut Starch. *J Chin Cereals Oils Assoc.* (2020) 35:31–5+49. Available online at: https://kns.cnki.net/kcms/detail/11.2864.TS.20200120.0949.024.html

10. Zhao K, Saleh ASM Li B, Wu H, Liu Y, Zhang G, et al. Effects of conventional and microwave pretreatment acetylation on structural and physicochemical properties of wheat starch. *Int J Food Sci Technol.* (2018) 53:2515–24. doi: 10.1111/ijfs.13845

11. Colman TAD, Demiate IM, Schnitzler E. The effect of microwave radiation on some thermal, rheological and structural properties of cassava starch. *J Therm Anal Calorim.* (2014) 115:2245–52. doi: 10.1007/s10973-012-2866-5

12. Kumar Y, Singh L, Sharanagat VS, Patel A, Kumar K. Effect of microwave treatment (low power and varying time) on potato starch: microstructure, thermo-functional, pasting and rheological properties. *Int J Biol Macromol.* (2020) 155:27–35. doi: 10.1016/j.ijbiomac.2020.03.174

13. Lewandowicz G, Fornal J, Walkowski A. Effect of microwave radiation on physico-chemical properties and structure of potato and tapioca starches. *Carbohydr Polym.* (1997) 34:213–20. doi: 10.1016/S0144-8617(97)00091-X

14. Shah U, Gani A, Ashwar BA, Shah A, Wani IA, Masoodi FA. Effect of infrared and microwave radiations on properties of Indian Horse Chestnut starch. *Int J Biol Macromol.* (2016) 84:166–73. doi: 10.1016/j.ijbiomac.2015.12.020

15. Zhang J, Wang Z-W, Shi X-M. Effect of microwave heat/moisture treatment on physicochemical properties of Canna edulis Ker starch. *J Sci Food Agric.* (2009) 89:653–64. doi: 10.1002/jsfa.3497

16. Huan H, Shaofan W, Min L, Yumei H. Effect of microwave-enzymatic hydrolysis on structure and physicochemical properties of potato starch. *Food Sci Technol.* (2019) 44:308–15. doi: 10.13684/j.cnki.spkj.2019.01.053

17. Haixin S, Liping F, Airong W, Xiaoli W. Variations in structure and properties of cassava starch after microwave irradiation. *Food Science.* (2015) 36:68–74. doi: 10.1016/j.tifs.2014.01.008

18. Kohyama K, Sasaki T. Differential scanning calorimetry and a model calculation of starches annealed at 20 and 50°C. *Carbohydr Polym.* (2006) 63:82–8. doi: 10.1016/j.carbpol.2005.08.004

19. Fan D, Ma S, Wang L, Zhao H, Zhao J, Zhang H, et al. 1H NMR studies of starch–water interactions during microwave heating. *Carbohydr Polym.* (2013) 97:406–12. doi: 10.1016/j.carbpol.2013.05.021

20. Luo Z, He X, Fu X, Luo F, Gao Q. Effect of microwave radiation on the physicochemical properties of normal maize, waxy maize and amylomaize V starches. *Starch Stärke.* (2006) 58:468–74. doi: 10.1002/star.200600498

21. Palav T, Seetharaman K. Mechanism of starch gelatinization and polymer leaching during microwave heating. *Carbohydr Polym.* (2006) 65:364–70. doi: 10.1016/j.carbpol.2006.01.024

22. Palav T, Seetharaman K. Impact of microwave heating on the physico-chemical properties of a starch–water model system. *Carbohydr Polym.* (2007) 67:596–604. doi: 10.1016/j.carbpol.2006.07.006

23. Zhu J, Li L, Chen L, Li X. Study on supramolecular structural changes of ultrasonic treated potato starch granules. *Food Hydrocoll.* (2012) 29:116–22. doi: 10.1016/j.foodhyd.2012.02.004

24. Shen H, Fan D, Huang L, Gao Y, Lian H, Zhao J, et al. Effects of microwaves on molecular arrangements in potato starch. *RSC Adv.* (2017) 7:14348–53. doi: 10.1039/C6RA28048J

25. Li Y, Hu A, Wang X, Zheng J. Physicochemical and in vitro digestion of millet starch: effect of moisture content in microwave. *Int J Biol Macromol.* (2019) 134:308–15. doi: 10.1016/j.ijbiomac.2019.05.046

26. Zhao B, Sun S, Lin H, Chen L, Qin S, Wu W, et al. Physicochemical properties and digestion of the lotus seed starch-green tea polyphenol complex under ultrasound-microwave synergistic interaction. *Ultrason Sonochem.* (2019) 52:50–61. doi: 10.1016/j.ultsonch.2018.11.001

27. O'Brien S, Wang Y-J. Susceptibility of annealed starches to hydrolysis by α-amylase and glucoamylase. *Carbohydr Polym.* (2008) 72:597–607. doi: 10.1016/j.carbpol.2007.09.032

28. Moreira R, Chenlo F, Torres MD, Glazer J. Rheological properties of gelatinized chestnut starch dispersions: effect of concentration and temperature. *J Food Eng.* (2012) 112:94–9. doi: 10.1016/j.jfoodeng.2012.03.021

29. Sha-sha Y, Yan-li X, Jin-shui W. The advance of the microwave on starch character's effect. *Food Sci Technol.* (2011) 36:242–243+247. doi: 10.13684/j.cnki.spkj.2011.07.075

30. Xu J, Zhou C-w, Wang R-z, Yang L, Du S-s, Wang F-p, et al. Lipase-coupling esterification of starch with octenyl succinic anhydride. *Carbohydr Polym.* (2012) 87:2137–44. doi: 10.1016/j.carbpol.2011.10.035

31. Guo Y, Diao M, Tu K, Cao X, Li J, Xu H. Pasting properties of stored rice with ascorbic acid before or after storage. *Int J Food Prop.* (2017) 20:S2969–79. doi: 10.1080/10942912.2017.1389953

32. Jaisut D, Prachayawarakorn S, Varanyanond W, Tungtrakul P, Soponronnarit S. Accelerated aging of jasmine brown rice by high-temperature fluidization technique. *Food Res Int.* (2009) 42:674–81. doi: 10.1016/j.foodres.2009.02.011

33. Wang L, Zhang C, Chen Z, Wang X, Wang K, Li Y, et al. Effect of annealing on the physico-chemical properties of rice starch and the quality of rice noodles. *J Cereal Sci.* (2018) 84:125–31. doi: 10.1016/j.jcs.2018.10.004

34. Guo Y, Cai W, Tu K, Wang S, Zhu X. Key proteins causing changes in pasting properties of rice during aging. *Cereal Chem.* (2015) 92:384–8. doi: 10.1094/CCHEM-05-14-0104-R

35. Tananuwong K, Malila Y. Changes in physicochemical properties of organic hulled rice during storage under different conditions. *Food Chem.* (2011) 125:179–85. doi: 10.1016/j.foodchem.2010.08.057

36. Emami S, Perera A, Meda V, Tyler RT. Effect of microwave treatment on starch digestibility and physico-chemical properties of three barley types. *Food Bioprocess Technol.* (2012) 5:2266–74. doi: 10.1007/s11947-011-0688-2

37. Oyeyinka SA, Umaru E, Olatunde SJ, Joseph JK. Effect of short microwave heating time on physicochemical and functional properties of Bambara groundnut starch. *Food Biosci.* (2019) 28:36–41. doi: 10.1016/j.fbio.2019.01.005

38. Bin-yan C, Ze-bin G, Li-bing X, Shuai Z, Bao-dong Z, Shao-xiao Z. Effect of physical and chemical properties of lotus seed starch by microwave treatment. *Modern Food Sci Technol.* (2015) 31:213–9. doi: 10.13982/j.mfst.1673-9078.2015.3.036

39. Kärkkäinen J, Lappalainen K, Joensuu P, Lajunen M, HPLC-ELSD. analysis of six starch species heat-dispersed in [BMIM]Cl ionic liquid. *Carbohydr Polym.* (2011) 84:509–16. doi: 10.1016/j.carbpol.2010.12.011

40. Li J, Han W, Xu J, Xiong S, Zhao S. Comparison of morphological changes and *in vitro* starch digestibility of rice cooked by microwave and conductive heating. *Starch Stärke.* (2014) 66:549–57. doi: 10.1002/star.201300208

41. Li N, Cai Z, Guo Y, Xu T, Qiao D, Zhang B, et al. Hierarchical structure and slowly digestible features of rice starch following microwave cooking with storage. *Food Chem.* (2019) 295:475–83. doi: 10.1016/j.foodchem.2019.05.151

42. Li Y-D, Xu T-C, Xiao J-X, Zong A-Z, Qiu B, Jia m, et al. Efficacy of potato resistant starch prepared by microwave–toughening treatment. *Carbohydr Polym.* (2018) 192:299–307. doi: 10.1016/j.carbpol.2018.03.076

43. Li N, Wang L, Zhao S, Qiao D, Jia C, Niu M, et al. An insight into starch slowly digestible features enhanced by microwave treatment. *Food Hydrocoll.* (2020) 103:105690. doi: 10.1016/j.foodhyd.2020.105690

44. Chung H-J, Liu Q, Hoover R. Impact of annealing and heat-moisture treatment on rapidly digestible, slowly digestible and resistant starch levels in native and gelatinized corn, pea and lentil starches. *Carbohydr Polym.* (2009) 75:436–47. doi: 10.1016/j.carbpol.2008.08.006

45. Qing-bo W, Cong-ping T, Lei Z, Bo C. The microwave heating process optimization for improving grain stability. *J Qilu Univ Technol.* (2014) 28:6—10.

46. Ma S, Zheng C, Guo P, Huang F. Effects of microwave pretreatment on raw materials, oil and meal quality of Trichosanthes seed. *J Chin Cereals Oils Assoc.* (2019) 32:22–5. doi: 10.3969/j.issn.1008-9578.2019.11.007

47. Wen-cai H, Shuai Y, Zu-ming C. Effect of microwave cooking method on lipid changes of silky fowl's egg yolk. *Modern Food Sci Technol.* (2019) 35:223–9. doi: 10.13982/j.mfst.1673-9078.2019.6.029

48. Duan Z-h, Jiang L-n, Wang J-l, Yu X-y, Wang T. Drying and quality characteristics of tilapia fish fillets dried with hot air-microwave heating. *Food Bioprod Process.* (2011) 89:472–6. doi: 10.1016/j.fbp.2010.11.005

49. Xu X, Li J, Fan Y, Deng Z. Effects of cooking methods on fatty acid composition in intramuscular fat of pork. *J Chin Inst Food Sci Technol.* (2020) 20:196–203. doi: 10.16429/j.1009-7848.2020.05.025

50. Rodriguez-Estrada MT, Penazzi G, Caboni MF, Bertacco G, Lercker G. Effect of different cooking methods on some lipid and protein components of hamburgers. *Meat Sci.* (1997) 45:365–75. doi: 10.1016/S0309-1740(96)00123-4

51. Deng Y, Padilla-Zakour O, Zhao Y, Tao S. Influences of high hydrostatic pressure, microwave heating, and boiling on chemical compositions, antinutritional factors, fatty acids, *in vitro* protein digestibility, and microstructure of buckwheat. *Food Bioprocess Technol.* (2015) 8:2235–45. doi: 10.1007/s11947-015-1578-9

52. Wu T, Mao L. Influences of hot air drying and microwave drying on nutritional and odorous properties of grass carp (Ctenopharyngodon idellus) fillets. *Food Chem.* (2008) 110:647–53. doi: 10.1016/j.foodchem.2008.02.058

53. Yan J-a, Zhu L, Yu W, Yang H, Liu X, Gao C, et al. Effects of microwave heating on edible oil quality and fatty acid composition. *J Chin Cereals Oils Assoc.* (2020) 35:110–5. Available online at: http://kns.cnki.net/kcms/detail/11.2864

54. Xu X. *Effect of Different Processing Methods on Lipid in Pork*. Nanchang: Nanchang University (2018).

55. Wu X, Huang A, Zhou S, Cheng Z, Li L. Effect of microwave heating on quality of camellia oil. *J Chin Cereals Oils Assoc.* (2009) 24:74–6.

56. Farhoosh R, Moosavi SMR. Evaluating the performance of peroxide and conjugated diene values in monitoring quality of used frying oils. *J Agric Sci Technol.* (2009) 11:173–9.

57. Zhao W, Yang R, Tang Y, Zhang W, Hua X. Investigation of the protein–protein aggregation of egg white proteins under pulsed electric fields. *J Agric Food Chem.* (2009) 57:3571–7. doi: 10.1021/jf803900f

58. Thakkar SK, Huo T, Maziya-Dixon B, Failla ML. Impact of style of processing on retention and bioaccessibility of β-carotene in Cassava (Manihot esculanta, Crantz). *J Agric FOOD Chem.* (2009) 57:1344–8. doi: 10.1021/jf803053d

59. Zhang Y, Yang L, Zu Y, Chen X, Wang F, Liu F. Oxidative stability of sunflower oil supplemented with carnosic acid compared with synthetic antioxidants during accelerated storage. *Food Chem.* (2010) 118:656–62. doi: 10.1016/j.foodchem.2009.05.038

60. Lee J, Yang J, Choi Y, Lee K. Effect of different cooking methods on vitamin contents and true retention in selected vegetables. *FASEB J.* (2016) 30:680.3.

61. Zhou Q. Anti-lipid oxidation of vitamin E by supercritical extraction under microwave condition. *J Chin Cereals Oils Assoc.* (2006) 04:101–5. doi: 10.3321/j.issn:1003-0174.2006.04.022

62. Cao H, Jiao X, Fan D, Huang J, Zhao J, Yan B, et al. Microwave irradiation promotes aggregation behavior of myosin through conformation changes. *Food Hydrocoll.* (2019) 96:11–9. doi: 10.1016/j.foodhyd.2019.05.002

63. Li X, Liu T, Song L, Zhang H, Li L, Gao X. Influence of high-molecular-weight glutenin subunit composition at Glu-A1 and Glu-D1 loci on secondary and micro structures of gluten in wheat (*Triticum aestivum* L). *Food Chem.* (2016) 213:728–34. doi: 10.1016/j.foodchem.2016.07.043

64. Cao M, Cao A, Wang J, Cai L, Regenstein J, Ruan Y, et al. Effect of magnetic nanoparticles plus microwave or far-infrared thawing on protein conformation changes and moisture migration of red seabream (Pagrus Major) fillets. *Food Chem.* (2018) 266:498–507. doi: 10.1016/j.foodchem.2018.06.057

65. Zhu Y, Vanga SK, Wang J, Raghavan V. Effects of ultrasonic and microwave processing on avidin assay and secondary structures of egg white protein. *Food Bioprocess Technol.* (2018) 11:1974–84. doi: 10.1007/s11947-018-2158-6

66. Gohi BF, Du J, Zeng HY, Cao XJ, Zou KM. Microwave pretreatment and enzymolysis optimization of the lotus seed. *Bioengineering.* (2019) 6:28. doi: 10.3390/bioengineering6020028

67. Cheng Y-H, Mu D-C, Jiao Y, Xu Z, Chen M-L. Microwave-assisted maillard reaction between rice protein and dextran induces structural changes and functional improvements. *J Cereal Sci.* (2021) 97:103134. doi: 10.1016/j.jcs.2020.103134

68. Yan X, Khan NA, Zhang F, Yang L, Yu P. Microwave irradiation induced changes in protein molecular structures of barley grains: relationship to changes in protein chemical profile, protein subfractions, and digestion in dairy cows. *J Agric Food Chem.* (2014) 62:6546–55. doi: 10.1021/jf501024j

69. Liu C, Ma X. Study on the mechanism of microwave modified wheat protein fiber to improve its mechanical properties. *J Cereal Sci.* (2016) 70:99–107. doi: 10.1016/j.jcs.2016.05.018

70. Ochoa-Rivas A, Nava-Valdez Y, Serna-Saldívar SO, Chuck-Hernández C. Microwave and ultrasound to enhance protein extraction from peanut flour under alkaline conditions: effects in yield and functional properties of protein isolates. *Food Bioprocess Technol.* (2017) 10:543–55. doi: 10.1007/s11947-016-1838-3

71. Mu D, Li H, Li X, Zhu J, Qiao M, Wu X, et al. Enhancing laccase-induced soybean protein isolates gel properties by microwave pretreatment. *J Food Process Preserv.* (2020) 44:e14386. doi: 10.1111/jfpp.14386

72. Wang L, Dong J-l, Zhu Y-y, Shen R-l, Wu L-g, Zhang K-y. Effects of microwave heating, steaming, boiling and baking on the structure and functional properties of quinoa (*Chenopodium quinoa* Willd) protein isolates. *Int J Food Sci Technol.* (2021) 56:709–20. doi: 10.1111/ijfs.14706

73. Sun X, Ohanenye IC, Ahmed T, Udenigwe CC. Microwave treatment increased protein digestibility of pigeon pea (*Cajanus cajan*) flour: elucidation of underlying mechanisms. *Food Chem.* (2020) 329:127196. doi: 10.1016/j.foodchem.2020.127196

74. Meng X, Li T, Song T, Chen C, Venkitasamy C, Pan Z, et al. Solubility, structural properties, and immunomodulatory activities of rice dreg protein modified with sodium alginate under microwave heating. *Food Sci Nutr.* (2019) 7:2556–64. doi: 10.1002/fsn3.1105

75. Urbizo-Reyes U, San Martin-González MF, Garcia-Bravo J, López Malo Vigil A, Liceaga AM. Physicochemical characteristics of chia seed (*Salvia hispanica*) protein hydrolysates produced using ultrasonication followed by microwave-assisted hydrolysis. *Food Hydrocoll.* (2019) 97:105187. doi: 10.1016/j.foodhyd.2019.105187

76. Lou X, Yang Q, Sun Y, Pan D, Cao J. The effect of microwave on the interaction of flavour compounds with G-actin from grass carp (*Catenopharyngodon idella*). *J Sci Food Agric.* (2017) 97:3917–22. doi: 10.1002/jsfa.8325

77. Zeng H-Y, Cai L-H, Cai X-L, Wang Y-J, Li Y-Q. Amino acid profiles and quality from lotus seed proteins. *J Sci Food Agric.* (2013) 93:1070–5. doi: 10.1002/jsfa.5848

78. Baokun Q, Yang L, Zhongjiang W, Xiaonan S, Lianzhou J. Relationship between surface hydrophobicity and zeta potential as well as particle size distribution of soybean protein isolates from different varieties. *Food Sci.* (2017) 38:114–8. doi: 10.7506/spkx1002-6630-201703019

79. Mizutani Y, Shibata M, Yamada S, Nambu Y, Hirotsuka M, Matsumura Y. Effects of heat treatment under low moisture conditions on the protein and oil in soybean seeds. *Food Chem.* (2019) 275:577–84. doi: 10.1016/j.foodchem.2018.09.139

80. Wei S, Yang Y, Feng X, Li S, Zhou L, Wang J, et al. Structures and properties of chicken myofibrillar protein gel induced by microwave heating. *Int J Food Sci Technol.* (2020) 55:2691–9. doi: 10.1111/ijfs.14522

81. de la Hoz A, Díaz-Ortiz Á, Moreno A. Microwaves in organic synthesis. Thermal and non-thermal microwave effects. *Chem Soc Rev.* (2005) 34:164–78. doi: 10.1039/B411438H

82. Habinshuti I, Mu T-H, Zhang M. Ultrasound microwave-assisted enzymatic production and characterisation of antioxidant peptides from sweet potato protein. *Ultrason Sonochem.* (2020) 69:105262. doi: 10.1016/j.ultsonch.2020.105262

83. El Mecherfi KE, Curet S, Lupi R, Larré C, Rouaud O, Choiset Y, et al. Combined microwave processing and enzymatic proteolysis of bovine whey proteins: the impact on bovine β-lactoglobulin allergenicity. *J Food Sci Technol.* (2019) 56:177–86. doi: 10.1007/s13197-018-3471-9

84. Sun Q, Zhang M, Mujumdar AS. Recent developments of artificial intelligence in drying of fresh food: a review. *Crit Rev Food Sci Nutr.* (2019) 59:2258–75. doi: 10.1080/10408398.2018.1446900

85. Hafez YS, Mohamed AI, Hewedy FM, Singh G. Effects of microwave heating on solubility, digestibility and metabolism of soy protein. *J Food Sci.* (1985) 50:415–7. doi: 10.1111/j.1365-2621.1985.tb13415.x

86. Uluko H, Zhang S, Liu L, Tsakama M, Lu J, Lv J. Effects of thermal, microwave, and ultrasound pretreatments on antioxidative capacity of enzymatic milk protein concentrate hydrolysates. *J Funct Foods.* (2015) 18:1138–46. doi: 10.1016/j.jff.2014.11.024

87. Dong X, Wang J, Raghavan V. Impact of microwave processing on the secondary structure, *in-vitro* protein digestibility and allergenicity of shrimp (Litopenaeus vannamei) proteins. *Food Chem.* (2021) 337:127811. doi: 10.1016/j.foodchem.2020.127811

88. Farvin KS, Andersen LL, Nielsen HH, Jacobsen C, Jakobsen G, Johansson I, et al. Antioxidant activity of Cod (Gadus morhua) protein hydrolysates: In vitro assays and evaluation in 5% fish oil-in-water emulsion. *Food Chem.* (2014) 149:326–34. doi: 10.1016/j.foodchem.2013.03.075

89. Sadeghi AA, Shawrang P. Effects of microwave irradiation on ruminal protein degradation and intestinal digestibility of cottonseed meal. *Livest Sci.* (2007) 106:176–81. doi: 10.1016/j.livsci.2006.08.006

90. Udenigwe CC, Aluko RE. Chemometric analysis of the amino acid requirements of antioxidant food protein hydrolysates. *Int J Mol Sci.* (2011) 12, 3148–61. doi: 10.3390/ijms12053148

91. Sae-leaw T, Benjakul S. Lipase from liver of seabass (Lates calcarifer): characteristics and the use for defatting of fish skin. *Food Chem.* (2018) 240:9–15. doi: 10.1016/j.foodchem.2017.07.089

92. Wiriyaphan C, Xiao H, Decker EA. Yongsawatdigul J. Chemical and cellular antioxidative properties of threadfin bream (Nemipterus spp) surimi byproduct hydrolysates fractionated by ultrafiltration. *Food Chem.* (2015) 167:7–15. doi: 10.1016/j.foodchem.2014.06.077

93. Binsi PK, Viji P, Panda SK, Mathew S, Zynudheen AA, Ravishankar CN. Characterisation of hydrolysates prepared from engraved catfish (Nemapteryx caelata) roe by serial hydrolysis. *J Food Sci Technol.* (2016) 53:158–70. doi: 10.1007/s13197-015-1998-6

94. Uluko H, Zhang S, Liu L, Chen J, Sun Y, Su Y, et al. Effects of microwave and ultrasound pretreatments on enzymolysis of milk protein concentrate with different enzymes. *Int J Food Sci Technol.* (2013) 48:2250–7. doi: 10.1111/ijfs.12211

95. Guan J-J, Zhang T-B, Hui M, Yin H-C, Qiu A-Y, Liu X-Y. Mechanism of microwave-accelerated soy protein isolate–saccharide graft reactions. *Food Res Int.* (2011) 44:2647–54. doi: 10.1016/j.foodres.2011.05.015

96. Lamacchia C, Landriscina L, D'Agnello P. Changes in wheat kernel proteins induced by microwave treatment. *Food Chem.* (2016) 197:634–40. doi: 10.1016/j.foodchem.2015.11.016

97. Su M, Venkatachalam M, Teuber SS, Roux KH, Sathe SK. Impact of γ-irradiation and thermal processing on the antigenicity of almond, cashew nut and walnut proteins. *J Sci Food Agric.* (2004) 84:1119–25. doi: 10.1002/jsfa.1748

98. Taheri-Kafrani A, Gaudin J-C, Rabesona H, Nioi C, Agarwal D, Drouet M, et al. Effects of heating and glycation of β-lactoglobulin on its recognition by IgE of sera from cow milk allergy patients. *J Agric Food Chem.* (2009) 57:4974–82. doi: 10.1021/jf804038t

99. Vanga SK, Singh A, Kalkan F, Gariepy Y, Orsat V, Raghavan V. Effect of thermal and high electric fields on secondary structure of peanut protein. *Int J Food Prop.* (2016) 19:1259–71. doi: 10.1080/10942912.2015.1071841

100. Khan SH, Butt MS, Sharif MK, Sameen A, Mumtaz S, Sultan MT. Functional properties of protein isolates extracted from stabilized rice bran by microwave, dry heat, and parboiling. *J Agric Food Chem.* (2011) 59:2416–20. doi: 10.1021/jf104177x

101. Ashraf S, Saeed G, Saeed S, And S, Ali R. Impact of microwave treatment on the functionality of cereals and legumes. *Int J Agric Biol.* (2012) 14:356–70.

102. Hefnawy TH. Effect of processing methods on nutritional composition and anti-nutritional factors in lentils (Lens culinaris). *Ann Agric Sci.* (2011) 56:57–61. doi: 10.1016/j.aoas.2011.07.001

103. Vagadia BH, Vanga SK, Singh A, Gariepy Y, Raghavan V. Comparison of conventional and microwave treatment on soymilk for inactivation of trypsin inhibitors and *in vitro* protein digestibility. *Foods.* (2018) 7:6. doi: 10.3390/foods7010006

104. New CY, Thung TY, Premarathne KJK, Russly AR, Abdulkarim SM, Son R. Microwave oven safety: a food safety consumer survey in Malaysia. *Food Control.* (2017) 80:420–7. doi: 10.1016/j.foodcont.2017.05.024

105. Arkus KAJ, Cahoon EB, Jez JM. Mechanistic analysis of wheat chlorophyllase. *Arch Biochem Biophys.* (2005) 438:146–55. doi: 10.1016/j.abb.2005.04.019

106. Jiang N, Xu B, Zhao L, Huang M, Zhou G. Effects of high-temperature–short time (HTST) drying process on proteolysis, lipid oxidation and sensory attributes of Chinese dry-cured chicken. *CyTA J Food.* (2016) 14:440–8. doi: 10.1080/19476337.2015.1124291

107. Cao W. ed. The development and application of microwave heating. *BoD-Books on Demand.* (2012) 2:17–44. doi: 10.5772/2619

108. Lv T, Wang Y, Pan D, Cao J, Zhang X, Sun Y, et al. Effect of trypsin treatments on the structure and binding capacity of volatile compounds of myosin. *Food Chem.* (2017) 214:710–6. doi: 10.1016/j.foodchem.2016.07.115

109. Martel A, Chewchanwuttiwong S, Dujardin G, Brown E. Low temperature syntheses of thioketals from enol ethers and carbonyl compounds. *Tetrahedron Lett.* (2003) 44:1491–4. doi: 10.1016/S0040-4039(02)02855-1

110. Tian Y, Zhao Y, Huang J, Zeng H, Zheng B. Effects of different drying methods on the product quality and volatile compounds of whole shiitake mushrooms. *Food Chem.* (2016) 197:714–22. doi: 10.1016/j.foodchem.2015.11.029

111. Wang CH, Damodaran S. Thermal gelation of globular proteins: weight-average molecular weight dependence of gel strength. *J Agric Food Chem.* (1990) 38:1157–64. doi: 10.1021/jf00095a001

112. Du X, Sun Y, Pan D, Wang Y, Ou C, Cao J. Change of the structure and the digestibility of myofibrillar proteins in Nanjing dry-cured duck during processing. *J Sci Food Agric.* (2018) 98:3140–7. doi: 10.1002/jsfa.8815

113. Han Z, Cai M-j, Cheng J-H, Sun D-W. Effects of electric fields and electromagnetic wave on food protein structure and functionality: a review. *Trends Food Sci Technol.* (2018) 75:1–9. doi: 10.1016/j.tifs.2018.02.017

114. Bowers JA, Fryer BA, Engler PP. Vitamin B6 in Turkey breast muscle cooked in microwave and conventional ovens. *Poult Sci.* (1974) 53:844–6. doi: 10.3382/ps.0530844

115. Schnepf M, Driskell J. Sensory attributes and nutrient retention in selected vegetables prepared by conventional and microwave methods. *J Food Qual.* (1994) 17:87–99. doi: 10.1111/j.1745-4557.1994.tb00135.x

116. Hoffman CJ, Zabik ME. Effects of microwave cooking/reheating on nutrients and food systems: a review of recent studies. *J Am Diet Assoc.* (1985) 85:922–6. doi: 10.1016/S0002-8223(21)03737-8

117. Tong-Tong W, Zi-Xuan W, Min W, Tian-Long H, Deng-Yong L. Research progress on the effects of exogenous substances on the formation of heterocyclic amines. *J Food Saf Qual.* (2022) 13:2535–42. doi: 10.19812/j.cnki.jfsq11-5956/ts.2022.08.025

118. Liu D, Zhou R, Wang Y, Chen D, Liu R, Wang F, et al. Research progress on formation mechanism and control technology of hazards in fried and roasted foods. *Sci Technol Food Ind.* (2021) 42:405–12. doi: 10.13386/j.issn1002-0306.2020080046

119. Nader CJ, Spencer LK, Weller RA. Mutagen production during pan-broiling compared with microwave irradiation of beef. *Cancer Lett.* (1981) 13:147–51. doi: 10.1016/0304-3835(81)90141-5

120. Guo W. Discussion on the safety and application of microwave technology. *Mech Elect Inf.* (2017) 1−6+33. doi: 10.19514/j.cnki.cn32-1628/tm.2017.05.001

frontiers | Frontiers in Nutrition

TYPE Original Research
PUBLISHED 09 November 2022
DOI 10.3389/fnut.2022.884381

OPEN ACCESS

EDITED BY
Alberto Valdés,
Spanish National Research Council (CSIC), Spain

REVIEWED BY
Marta Laranjo,
University of Evora, Portugal
Mehanathan Muthamilarasan,
University of Hyderabad, India
Saloni Sharma,
National Agri-Food Biotechnology Institute, India

*CORRESPONDENCE
Mahalingam Govindaraj
m.govindaraj@cgiar.org
Nepolean Thirunavukkarasu
nepolean@millets.res.in

SPECIALTY SECTION
This article was submitted to Nutrition and Food Science Technology, a section of the journal Frontiers in Nutrition

RECEIVED 26 February 2022
ACCEPTED 14 October 2022
PUBLISHED 09 November 2022

CITATION
Goud CA, Satturu V, Malipatil R, Viswanath A, Semalaiyappan J, Kudapa H, Rathod S, Rathore A, Govindaraj M and Thirunavukkarasu N (2022) Identification of iron and zinc responsive genes in pearl millet using genome-wide RNA-sequencing approach.
Front. Nutr. 9:884381.
doi: 10.3389/fnut.2022.884381

Identification of iron and zinc responsive genes in pearl millet using genome-wide RNA-sequencing approach

Chengeshpur Anjali Goud[1], Vanisri Satturu[1], Renuka Malipatil[2], Aswini Viswanath[2], Janani Semalaiyappan[2], Himabindu Kudapa[3], Santosha Rathod[4], Abhishek Rathore[3,5], Mahalingam Govindaraj[3,6]* and Nepolean Thirunavukkarasu[2]*

[1]Institute of Biotechnology, Professor Jayashankar Telangana State Agricultural University, Hyderabad, India, [2]Genomics and Molecular Breeding Lab, ICAR-Indian Institute of Millets Research, Hyderabad, India, [3]International Crops Research Institute for the Semi-Arid Tropics (ICRISAT), Hyderabad, India, [4]Agricultural Statistics, ICAR-Indian Institute of Rice Research, Hyderabad, India, [5]Excellence in Breeding Platform, The International Maize and Wheat Improvement Center (CIMMYT), Texcoco, Mexico, [6]HarvestPlus, Alliance of Bioversity International and the International Center for Tropical Agriculture (CIAT), Cali, Colombia

Pearl millet (*Pennisetum glaucum* L.), an important source of iron (Fe) and zinc (Zn) for millions of families in dryland tropics, helps in eradicating micronutrient malnutrition. The crop is rich in Fe and Zn, therefore, identification of the key genes operating the mineral pathways is an important step to accelerate the development of biofortified cultivars. In a first-of-its-kind experiment, leaf and root samples of a pearl millet inbred ICMB 1505 were exposed to combinations of Fe and Zn stress conditions using the hydroponics method, and a whole-genome transcriptome assay was carried out to characterize the differentially expressed genes (DEGs) and pathways. A total of 37,093 DEGs under different combinations of stress conditions were identified, of which, 7,023 and 9,996 DEGs were reported in the leaf and root stress treatments, respectively. Among the 10,194 unique DEGs, 8,605 were annotated to cellular, biological, and molecular functions and 458 DEGs were assigned to 39 pathways. The results revealed the expression of major genes related to the mugineic acid pathway, phytohormones, chlorophyll biosynthesis, photosynthesis, and carbohydrate metabolism during Fe and Zn stress. The cross-talks between the Fe and Zn provided information on their dual and opposite regulation of key uptake and transporter genes under Fe and Zn deficiency. SNP haplotypes in rice, maize, sorghum, and foxtail millet as well as in Arabidopsis using pearl millet Fe and Zn responsive genes could be used for designing the markers in staple crops. Our results will assist in

10.3389/fnut.2022.884381

developing Fe and Zn-efficient pearl millet varieties in biofortification breeding programs and precision delivery mechanisms to ameliorate malnutrition in South Asia and Sub-Saharan Africa.

KEYWORDS

malnutrition, biofortification, iron, zinc, genes, transcriptome

Introduction

Pearl millet is a high-energy cereal with high protein, and high dietary fiber (1), free of gluten (2) with higher amounts of iron (Fe) and zinc (Zn) accounting for up to 40%. It is the economical source of micronutrients for poor people, who suffer from micronutrient deficiencies (3). Owing to breeding for yield and yield-contributing traits over the decades, less emphasis has been given to breeding nutritional traits (4, 5). This signifies the importance of improving the essential grain micronutrients (Fe and Zn) in future pearl millet varieties besides core breeding traits.

Malnutrition refers to the inadequate nutrient supply and/or inefficient uptake resulting from an imbalance of essential nutrients in the regular diet of an individual or population. Globally, 144 million children under 5 years are stunted and 45% of child deaths are associated with malnutrition.[1] Worldwide, non-pregnant women (33%), pregnant women (40%), and children (42%) are reported with Fe deficiency (see text footnote 1) resulting in low body weight of the child, and maternal mortality affecting both mother and infants (6). Fe deficiency causes improper functioning of the immune system, and poor health, and may reduce the working capacity of a person (7). Zn deficiency causes stunted growth, and improper neural development, and is highly susceptible to disease attack. It is reported to be a major cause of respiratory infections leading to high infant mortality (8).

Compared to sorghum (26–60 mg kg^{-1} Fe and 21–57 mg kg^{-1} Zn) (9), maize (18.9–47.6 mg kg^{-1} Fe and 5.4–30.8 mg kg^{-1} Zn) (10), and foxtail millet (36.9–75.1 mg kg^{-1} Fe and 45.4–57.1 mg kg^{-1} Zn) (11), the pearl millet possesses high grain Fe (30–140 mg kg^{-1}) and Zn (20–90 mg kg^{-1}) contents in the germplasm (5, 12). So, pearl millet has gained importance concerning available wider genetic variability for Fe and Zn contents in germplasm and its ability to grow in harsh environmental conditions (13). Several studies reported a positive correlation between the densities of Fe and Zn, which helps in the selection of both Fe and Zn micronutrients simultaneously (14), and are assumed to be involved or connected in physiological mechanisms for their uptake and translocation into the seed (15, 16). To combat the micronutrient-based hidden hunger, biofortification would be an efficient and cost-effective method (3) to enhance the nutrient contents of crops through breeding techniques (17). Pearl millet was one of the crops included in the Biofortification Challenge Program (BCP), a micronutrient project in 2002 under the HarvestPlus program of the CGIAR for decreasing Fe and Zn deficiencies (18). To date, HarvestPlus supported the pearl millet biofortification program at ICRISAT for the development of several high Fe and Zn lines and cultivars in association with NARS (5).

Understanding the functional genomics of Fe and Zn homeostasis and their uptake and transport mechanism will assist in the biofortification of Fe and Zn content in crops. Transcriptomic studies on functional characterization of differentially expressed genes (DEGs) and their dynamic role in Fe and Zn uptake in deficiency, which helps in genetic biofortification of Fe and Zn, have been carried out in rice (19), maize (20), Arabidopsis (21), and several other crops. The above studies reported the importance of genes related to the mugineic acid (MA) pathway, plant hormones, and carbohydrate metabolism in nutrient uptake and the negative effect on photosynthesis-related genes under deficient conditions.

So far, there has been no research carried out on pearl millet to understand the functional mechanisms of Fe and Zn homeostasis through a genome-wide transcriptome approach although the crop is known for its rich iron and zinc content. Hence, this study was constituted to understand the gene expression of pearl millet shoot and root under Fe and Zn stress through the RNA-Seq approach to identify the DEGs, and gene regulatory networks under mineral stress conditions and identify the genes involved in Fe and Zn homeostasis.

Materials and methods

Experiment material and growth conditions

Seeds of the biofortified pearl millet inbred ICMB 1505 (a high Fe inbred with 110 ppm Fe and 55 ppm Zn) using 1% sodium hypochlorite solution were surface sterilized for 5 min

1 http://www.wmo.int

and rinsed 5–6 times with MilliQ water. The seeds were placed on the germination sheets soaked with MilliQ water and allowed to germinate in the darkroom at 25°C temperature.

Three nutrient stress treatments (+Fe−Zn, −Fe+Zn, and −Fe−Zn) and one control (+Fe+Zn) solutions were prepared to understand the stress response of the root and leaf. The control nutrient solution (+Fe+Zn) contained 0.7 mM K_2SO_4, 0.1 mM KCL, 2.0 mM Ca $(NO_3)_2$, 0.1 mM KH_2PO_4, 10 μM H_3BO_3, 0.5 mM $MgSO_4$, 0.5 μM $MnSO_4$, 0.2 μM $CuSO_4$, 0.5 μM $ZnSO_4$, 0.05 μM Na_2MoO_4, and 0.1 mM Fe (III)-EDTA. The pH of the solution was adjusted by adding a 1 N HCL solution to 5.5. In −Fe+Zn and +Fe−Zn treatments, the Fe (III)-EDTA and $ZnSO_4$ were not added respectively in the control solution. While in −Fe−Zn treatment both Fe (III)-EDTA and $ZnSO_4$ were not added in the control solution (Table 1).

Customized 96-well PCR plates with holes at the bottom side were used for supporting the seedlings for the effective harvesting of roots and leaves after the treatment period. After placing the germinated seedlings in the PCR plates with roots emerging out on the bottom side, the plates were left floating in the treatment solutions containing trays. Each tray was accommodated with three plates, indicating three replicates per treatment. Three to four days later, seedlings (nearly 40 per tray) were transferred to the respective treatment and were maintained for 12 days (20).

RNA-sequencing

Total RNA was extracted from the replicated leaf and root samples of control (+Fe+Zn) and stress treatments (−Fe−Zn, −Fe+Zn, and+Fe−Zn) using QIAGEN RNeasy Plant Mini Kit. Genomic DNA contamination was removed with RNase-Free DNase (QIAGEN). The purity of RNA, i.e., RNA degradation and DNA contamination were checked by agarose gel electrophoresis. The Total RNA was quality checked using RNA 6000 Nano Kit (Agilent Technologies, USA) on 2100 Bioanalyzer (Agilent Technologies, USA), with a minimum RNA Integrity Number (RIN) value of 7. RNA concentrations were determined with a NanoDrop ND-8000 spectrophotometer (Nano-Drop Technologies; THERMO Scientific, Wilmington, DE, USA). Poly(A) messenger RNA (mRNA) was purified from the total RNA using oligo-dT attached magnetic beads, to capture for polyA tails, using two rounds of purification. The RNA was fragmented into 200–500 bp fragments during the second elution of poly-A RNA using an ultrasonicator. The Superscript-II reverse transcriptase (Life Technologies, Inc.) and random primers were used to copy the cleaved RNA fragments into first-strand cDNA. After second-strand cDNA synthesis, fragments were end-repaired and A-tailed, and indexed adapters were ligated. The purified products enriched with PCR were used to generate the final cDNA library. RNA-Seq libraries for all samples were prepared using NEBNext UltraII RNA library preparation kit for Illumina; Cat. no. E7770 (New England Biolabs), according to manufacturers recommended protocol. The tagged cDNA libraries were used for 2 × 150-bp paired-end sequencing by pooling them in equal ratios onto a single lane of the Illumina HiSeq4000. Sequencing was done by 2× 150 bp paired-end chemistry of Illumina HiSeq 4000 using generated Illumina clusters loaded onto Illumina Flow Cell.

The quality of the raw reads obtained by sequencing was checked by the FASTQC online tool. The Trimmomatic tool was used for filtering low-quality reads and adaptor sequences (22) followed by assessing the data with the FASTQC. Finally, the obtained clean reads were aligned to the pearl millet reference genome (23) using hisat2 (24) to reconstruct the transcriptome and perfectly aligned sequences were considered for further analysis. The alignments were converted to a sorted bam format using Samtools (25).

Differential gene expression and pathway enrichment analysis

The sequence reads per each genomic feature were measured with featureCounts (26).[2] DESeq2 R Package was used in determining the gene expression differences between control and treatments (27). The combined features for each combination of control and treatment sample data were fed to R package DESeq (27) to measure the DEGs. DEGs were selected based on fold-change (FC) and FDR-corrected $p < 0.05$ and classified as upregulated (≥+1.5 FC) or downregulated (≤−1.5 FC). The identified DEG sequences were further

2 http://subread.sourceforge.net

TABLE 1 Details of the nutrient stress treatments given to the seedlings of the pearl millet inbred ICMB 1505.

S. No.	Treatment	Nutrient solution details	Stress level
1	Control (+Fe+Zn)	Presence of both Fe (III)-EDTA and ZnSO4	No stress
2	Treatment (+Fe−Zn)	Presence of Fe (III)-EDTA and the absence of ZnSO4	Zn stress
3	Treatment (−Fe+Zn)	Absence of Fe (III)-EDTA and presence of ZnSO4	Fe stress
4	Treatment (−Fe−Zn)	Absence of both Fe (III)-EDTA and ZnSO4	Fe and Zn stress

Blast (28) and compared with the Viridiplantae protein sequence from the UniProt database to assign the associated annotations. With the known gene ontology (GO) terms from the annotations, the Cytoscape plugin Bingo was used to make the metabolic pathway.

Validation of RNA-sequencing data by real-time PCR

To check the accuracy of transcriptomic analysis, data validation by qRT-PCR was carried out. The 17 selected DEGs were chosen for validation (**Supplementary Figure 1**) and the cDNA was synthesized from the extracted RNA from the samples. Normalization of all the cDNA samples was done to equalize the concentrations of all the samples. Primers were designed for the chosen DEGs using Primer3plus software (**Supplementary Table 1**). To normalize the data, the actin gene (*PgActin*) of pearl millet was used as a reference gene. The ΔΔCT method was used for the calculation of the relative gene expression of targeted genes (29).

Identification of gene orthologs

The top 68 Fe and Zn homeostasis pathway-related genes identified in pearl millet through RNA-Seq were BLAST searched against the genomes of *Arabidopsis* spp., maize, rice, sorghum, and foxtail millet to identify the orthologs. All the hits with at least 70% similarity were considered significant. The orthologous relationships between pearl millet and the other five crop species were visualized in the circos plots using the ClicO FS tool (30). The orthologs of a gene were aligned using Bioedit sequence alignment editor software version 7.2.5 for the identification of haplotypes (31).

Results

RNA-sequencing

Twenty-four leaf and root samples of Fe and Zn stress-induced pearl millet inbred ICMB 1505 were subjected to genome-wide transcriptome sequencing using a paired-end method with three biological replicates. A total of 841 million reads accounting for 39 GB of data was generated. After trimming the low-quality reads, a total of 753 million reads were aligned to the reference genome. Ultimately, of the 562 million high-quality successfully mapped reads, over 78.57% were observed to be uniquely mapped reads and 21.10% were multiple mapped reads (**Table 2**).

Identification of differentially expressed genes

A total of 37,093 DEGs were identified in control vs. stress conditions of leaf, root, and leaf-root comparisons after adjusting the *p*-value (<0.05) and $\log_2$ fold change value (>1.5-upregulated, <-1.5-downregulated). In leaf comparisons, more DEGs (2,418) were identified in the Fe-deficient condition and few DEGs (105) were observed in both nutrient-deficient conditions (−Fe−Zn) when compared to the Zn-deficient leaf (**Figure 1A**). In root comparisons, a high number of DEGs (3,737) was differentially expressed in −Fe−Zn treatment when compared to −Fe treatment whereas a low number (345) was observed in Fe-deficient root (**Figure 1B**). In leaf-root comparisons, the high number of DEGs (6,366) was recorded in −Fe−Zn root treatment over −Fe leaf, and a low number of DEGs (629) were found in −Fe leaf compared to −Zn root treatment (**Figure 1C**). The 10,194 unique DEGs identified from all comparisons were further analyzed for gene ontology studies, of which 9,981 DEGs were annotated and the remaining were unannotated besides showing a higher level of expression under stress conditions (**Supplementary Figure 2**).

Gene ontology and pathway enrichment

The GO terms were assigned to the identified DEGs, of which 8,605 sequences were annotated to cellular, biological, and molecular functions. A total of 5,352 genes were annotated for 406 cellular components, 6,764 genes for 1,223 molecular functions, and 4,327 genes for the 1,475 biological process (**Supplementary Figures 3A,B**). Besides GO terms, KEGG (Kyoto Encyclopedia of Genes and Genomes) was used to assign biological pathways to the identified DEGs. A total of 458 DEGs were assigned to 39 pathways (**Supplementary Figure 3C**), of which carotenoid biosynthesis, hormone biosynthesis, isoprenoid biosynthesis, and porphyrin-containing compound metabolism pathways were root-specific. The DEGs expressed in the leaf treatments were identified to be involved in 22 pathways, of which the tRNA modification pathway was specific to leaf tissue.

Differentially expressed genes in leaf

A total of 2,418 DEGs were expressed in Fe-deficient conditions, 1,596 DEGs in −Zn, and 1,753 DEGs under combined nutrient stress (−Fe−Zn) when compared to control (+Fe+Zn). More than 1,000 genes were commonly expressed across all stress treatments (−Fe, −Zn, and −Fe−Zn) wherein 213, 939, and 298 DEGs were unique to −Zn, −Fe, and

TABLE 2 Total and mapped reads obtained from different treatments of Fe and Zn stresses in leaf and root samples of pearl millet through RNA-Seq analysis.

Sample ID	Tissue	Treatment	Raw reads	Filtered reads	Alignment reads	Alignment rate (%)	Unique mapped reads	Unique mapped reads (%)	Multiple mapped reads	Multiple mapped reads (%)
T1	Leaf	+Fe+Zn	36795692	32809362	28250596	86.11	19327977	68.42	8922619	31.58
T2	Root	+Fe+Zn	33824036	30018012	26174715	87.2	20404340	77.95	5778409	22.08
T3	Leaf	+Fe+Zn	41783596	37190222	31715264	85.28	24260737	76.5	4370771	13.78
T4	Root	+Fe+Zn	33948826	30712570	25190307	82.02	17980023	71.38	3155284	12.53
T5	Leaf	+Fe+Zn	40559716	35966150	31266122	86.93	20995588	67.15	2463312	7.88
T6	Root	+Fe+Zn	33906822	31641708	17895047	56.56	13224359	73.9	2949473	16.48
T7	Leaf	+Fe−Zn	34095324	31130340	24504705	78.72	18437836	75.24	3367225	13.74
T8	Root	+Fe−Zn	22642636	19698618	16691728	84.74	12241161	73.34	2066750	12.38
T9	Leaf	+Fe−Zn	39145306	35702360	23984228	67.18	18646736	77.75	4559974	19.01
T10	Root	+Fe−Zn	33953090	30666148	18742678	61.12	16972046	90.55	8567585	45.71
T11	Leaf	+Fe−Zn	37231716	31305440	23893854	76.32	17922925	75.01	2553549	10.69
T12	Root	+Fe−Zn	33841022	31614084	23138671	73.19	16478780	71.22	2517123	10.88
T13	Leaf	−Fe+Zn	33404644	29522426	23177557	78.51	19867827	85.72	6307947	27.22
T14	Root	−Fe+Zn	33961006	31053560	20648235	66.49	16650136	80.64	5594728	27.1
T15	Leaf	−Fe+Zn	33948012	31072284	19925667	64.13	16928586	84.96	5555340	27.88
T16	Root	−Fe+Zn	33301490	29389602	22936316	78.04	19842220	86.51	7438655	32.43
T17	Leaf	−Fe+Zn	33545702	31478028	25591969	81.3	24330975	95.07	5149769	20.12
T18	Root	−Fe+Zn	33873046	31054986	13156922	42.37	11230946	85.36	3915141	29.76
T19	Leaf	−Fe−Zn	33873386	30979330	20625017	66.58	16974699	82.3	5071939	24.59
T20	Root	−Fe−Zn	33365282	29965330	25839367	86.23	20623662	79.81	6554304	25.37
T21	Leaf	−Fe−Zn	36237904	30243802	10899044	36.04	9526648	87.41	3628364	33.29
T22	Root	−Fe−Zn	33656568	29609644	22437717	75.78	17337974	77.27	3499404	15.6
T23	Leaf	−Fe−Zn	33199966	30775425	29449912	95.69	26748778	86.92	10222785	33.22
T24	Root	−Fe−Zn	46935698	40922628	35931492	87.8	24712599	68.78	4391710	12.22

−Fe−Zn treatments, respectively (Figure 1D). Among the genes involved in Fe and Zn uptake, *O-methyltransferases* were >7 times upregulated in all the leaf treatments (−Fe, −Zn, −Fe−Zn) when compared to control (+Fe+Zn). *Heavy metal ATPase* (HMA), *plasma membrane ATPase*, *putative ABC transporter B family member*, *ABC transporter G family member*, *calcium-transporting ATPase,* H^+-ATPase domain-containing members gene transcripts related to metal ion transport were induced several folds, wherein, *magnesium transporter* was downregulated (1.75-fold) in all the leaf treatments. Fe storage protein, *ferritin,* and *solute protein family 40* were nearly twofold downregulated in −Fe and −Fe−Zn leaf. *Zinc-induced facilitator* (ZIF) like protein and a gene involved in Fe ion homeostasis were >1.78 times induced in −Fe condition while the *potassium transporter* gene was 2.22 times upregulated under −Fe condition. *Zinc transporter 5* was highly downregulated in −Fe leaf (−2.67) when compared to −Fe−Zn (−1.61) whereas *vacuolar cation/proton exchanger* was highly upregulated in −Fe−Zn leaf (2.15) when compared to −Fe leaf (1.89). *Mugineic-acid 3-dioxygenase* (IDS2) gene was fourfold upregulated in the presence of Fe and was 1.68-fold downregulated in the absence of Fe in the leaf. The protein involved in the Zn transmembrane transporter activity was 2.88 times upregulated in the presence of Zn (Supplementary Table 2).

The enzymes, *sucrose synthase* (twofold) and *starch synthases* (fivefold) involved in the carbohydrate biosynthesis process and alcohol dehydrogenase enzyme (>3.60-fold) were upregulated in all the leaf treatments. *Photosystem II CP47 reaction center* and *ATP synthase* were >3-fold upregulated under Fe deficiency (−Fe, −Fe−Zn). *RUBISCO,* an enzyme involved in photosynthetic processes was twofold upregulated, wherein *carbonic anhydrase* (−1.89) was downregulated in Fe-deficient condition (Supplementary Table 3). The glycolysis-associated enzymes, *glyceraldehyde-3-phosphate dehydrogenase* (>2.45), *phosphoglycerate mutase* (>4.44), *pyrophosphate-fructose 6-phosphate* (>2.35), ATP-dependent *6-phosphofructokinase* (>3.37), were upregulated in all the leaf treatments (−Fe, −Zn, −Fe−Zn). Additionally, *succinate dehydrogenase* (2.83), *phosphoenolpyruvate carboxylase* (PEPC 2.07) enzymes involved in the TCA cycle, and photorespiration process was induced in −Fe condition (Supplementary Table 4).

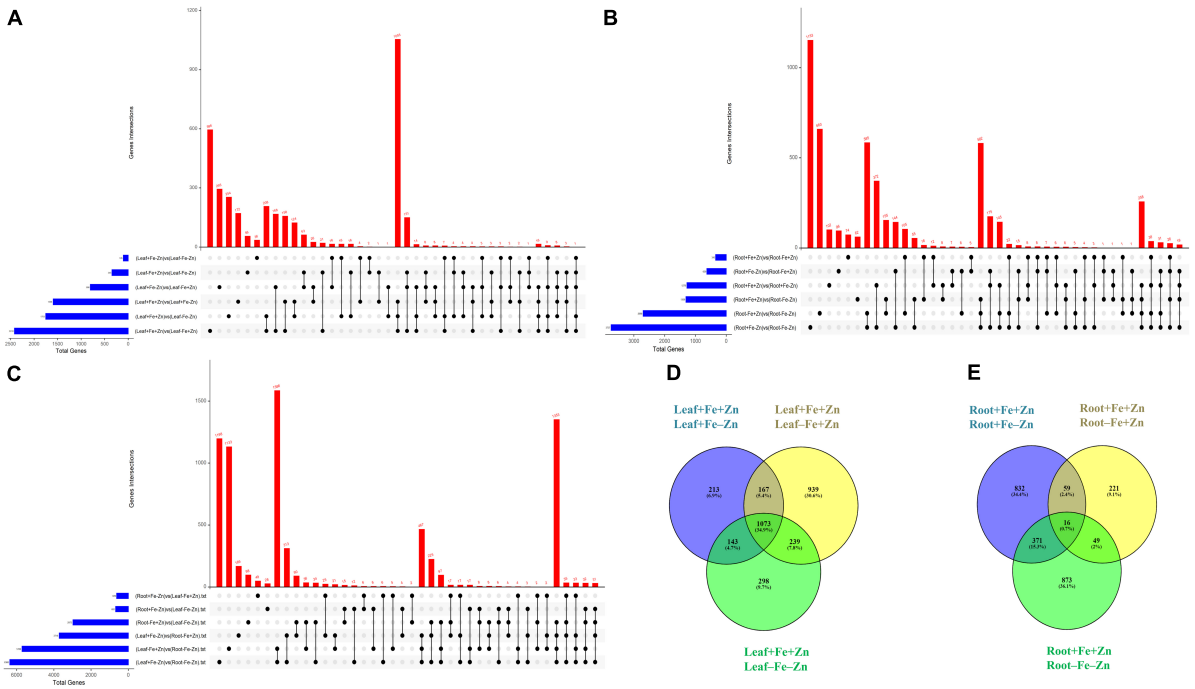

FIGURE 1
Upset plot illustrating the intersections between the set of DEGs identified in response to −Fe, −Zn, −Fe−Zn stresses in **(A)** leaf, **(B)** root, and **(C)** leaf and root. The blue bar on the left side indicates the total number of DEGs expressed under specific stress treatments and the red bar on the right side indicates the DEGs unique to a specific treatment and between the treatments. Dots connect by a black line on the bottom panel indicate the intersections between the treatments and the representation of stress-specific and common DEGs in response to −Fe, −Zn, −Fe −Zn stresses in **(D)** leaf and **(E)** root.

Among the enzymes involved in phytohormones biosynthesis and signaling pathways, *indole-3-glycerol-phosphate synthase* (>1.66), *1-aminocyclopropane-1-carboxylate* (ACC) *synthase* (>2.81), AP2-like ethylene-responsive transcription (>4.13), *and auxin response factor* (ARF >2.15) were highly upregulated in all the stress treatments (−Fe, −Zn, −Fe−Zn). The upregulation of the auxin-responsive protein (ARP >7.45) was observed in −Fe and −Zn treatments. In all Zn-deficient (−Zn, −Fe−Zn) conditions, auxin-responsive factor 23 was upregulated by 2.58-fold (**Supplementary Table 5**). *Xyloglucan endotransglucosylase/hydrolase* (two to sevenfold), *cellulose synthase* (>7.52), and *expansin* (two to fourfold) which are involved in cell wall organization were upregulated in all stress treatments when compared to the control. Moreover, the induced expression of *S-acyltransferases* (four to sixfold), *diacylglycerol O-acyltransferases* (>4.80), and *diacylglycerol kinases* (2.41–3.64-folds) involved in the lipid metabolism were noticed across stress treatments. Further, in our study peroxidases (three to eightfold), mitogen-activated protein kinase (>1.66), NBS-LRR domain-containing proteins (>1.87), and serine/threonine kinases (>2.25) related to biotic and abiotic stress tolerance were upregulated under nutrient-starved leaf treatments. Superoxide dismutase (SOD) involved in scavenging reactive oxygen species (ROS) was threefold downregulated in Zn-deficient leaf (**Figure 2A**) (**Supplementary Table 6**).

Differentially expressed genes in root

Iron-deficiency in root recorded 345 DEGs, Zn-deficiency showed 1,278 DEGs, and −Fe−Zn condition recorded 1,309 DEGs when compared to the control. A total of 16 genes were commonly regulated in all the stress treatments (−Fe, −Zn, −Fe−Zn) while 833, 221, and 873 DEGs were unique to −Zn, −Fe, and −Fe−Zn treatments, respectively (**Figure 1E**). The downregulation of metal ion transmembrane transporter activity genes was observed in all the stress treatments (−Fe, −Zn, −Fe−Zn) when compared to the control. In Fe-deficient conditions, *ferritin* protein, 2-oxoglutarate (2OG), HMA, *solute carrier family 40 protein*, *potassium transporter*, and *copper transporter* were downregulated by several folds. In −Fe root, the induced expression of *3″deamino-3″oxonicotianamine reductase* (2.27), *nicotianamine synthases* (NAS 2.59), *adenine phosphoribosyltransferase* (APRT >2.03 times) genes, and in −Zn root, the upregulation of *ribose 5-phosphate isomerase* (1.74) gene involved in phytosiderophore (PS) synthesis were

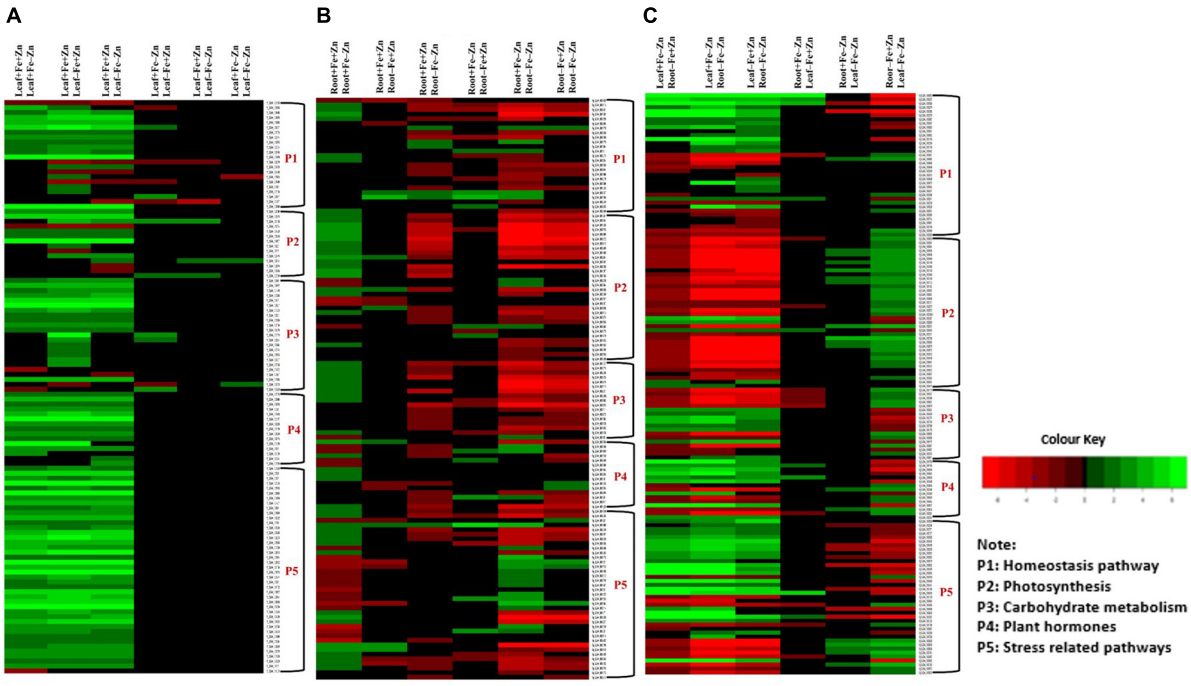

FIGURE 2
Heatmap of the selected differentially expressed genes operating under Fe and Zn stress **(A)** across leaf-pairwise combinations, **(B)** across root-pairwise combinations, **(C)** between leaf and root combinations.

observed. The expression of MYB transcription factor was 2.45-fold induced in −Zn root and in −Fe−Zn condition it was 2.8-fold downregulated. The gene involved in the Zn transport was nearly two to threefold downregulated in the −Zn, −Fe, and −Fe−Zn treatments. *Aspartate aminotransferases* (IDI4) involved in the methionine (Met) cycle were 2.39 times downregulated in −Fe−Zn when compared to the −Zn treatment. The *oligopeptide transporter 3* (OPT3) gene was 1.64 times induced in the roots under the deficiency of Fe and Zn (**Supplementary Table 7**).

The *magnesium chelatase*, *Mg-protoporphyrin IX chelatase,* and *chlorophyll-binding a-b proteins* involved in the chlorophyll biosynthesis pathway were several folds downregulated in the absence of Fe and were upregulated in the presence of Fe. The upregulation of light reaction involved proteins, *ferredoxin* (2.36), *ferredoxin NADP reductase* (>1.69), *ATP-synthase complex assembly* (2.42), and downregulation of *PSII reaction center* (−1.63), *cytochrome c oxidase* subunit (−1.52) and *cytochrome c* (−2.02) were observed in Zn-deficient root. *RUBISCO*, an enzyme involved in the dark reaction is nearly two times upregulated in either of the nutrient deficiency (−Fe or −Zn) but 2.62-fold downregulated under −Fe−Zn treatment (**Supplementary Table 8**).

Genes such as *3-Phosphoglycerate dehydrogenase* (2.45), *phosphoglycerate kinase* (2.07), *malate dehydrogenase* (1.54), *fructose-bisphosphate aldolase* (2.09), *glyceraldehyde-3-phosphate dehydrogenase* (2.41), PEPC (2.21), *phosphoenolpyruvate carboxykinase* (2.33), and *glucose-6-phosphate 1-dehydrogenase* (2.11) involved in the carbohydrate metabolism process were upregulated and *lactate dehydrogenase* (−1.68) was downregulated in the Zn-deficient root. The downregulation of *pyruvate* (−4.53), *3-phosphoglycerate dehydrogenase* (−2.84), *phosphoglycerate kinase* (−1.64), *malate dehydrogenase* (−1.51), *fructose-bisphosphate aldolase* (−3.04), *phosphoenolpyruvate carboxykinase* (−3.68), *phosphoglycerate mutase* (−1.72), *isocitrate lyase* (−1.81), *pyruvate dehydrogenase E1 component* (−1.99), *aconitase hydratase* (−1.64), and *D-fructose-1,6-bisphosphate 1-phosphohydrolase* (−2.45) was observed in −Fe−Zn condition (**Supplementary Table 9**).

In the case of phytohormones, the downregulation of *auxin efflux carrier protein* (−1.59) and ARF (−2.15) was observed in Fe-deficient roots. In the −Zn root, the downregulation of *tryptophan synthase* (−1.52), ARP (−2.23) was recorded. The expression of ARF SAUR36 was induced two to threefold when the root was deficient to −Fe or −Zn. The downregulation of ACC *synthase* (−1.87) was noticed in the −Fe−Zn treatment (**Supplementary Table 10**). The downregulation of *trehalose 6-phosphate phosphatase* (<−1.94) involved in cell wall organization was observed in −Fe and −Zn root treatments, while downregulation of *cellulose synthase* (−1.52), *xyloglucan endotransglucosylase/hydrolase* (<−1.71) were observed in

−Fe−Zn root. In all the root treatments, the *expansin* was nearly twofold upregulated. *Diacylglycerol O-acyltransferases* (−2.21) involved in the lipid metabolism were downregulated in −Fe−Zn condition whereas *S-acyltransferases* (−1.68) were downregulated in Fe-deficient roots. Peroxidases (<−1.7) were downregulated in all the root treatments. Serine/threonine kinases (−2.65) involved in the stress signaling mechanism were downregulated in Fe-deficient conditions (**Figure 2B**) (**Supplementary Table 11**).

Tissue-specific expression of genes

Leaf and root stress treatments were compared to identify the tissue-specific expression of genes involved in uptake and transport activities. The upregulation of PS synthesis enzymes, *formate dehydrogenases* (FDH > 6.73), *3″deamino 3″oxonicotianamine reductase* (>4.46), NAS (five to ninefold), involved in the uptake of Fe and Zn from the rhizosphere and ABC transporter G protein (>1.77) was observed in −Fe and −Fe−Zn root when compared to −Fe and −Zn leaf. FER-like transcription factors, *2′-deoxymugineic-acid 2′-dioxygenase* (IDS3 four to eightfold), heavy metal detoxification proteins (>1.76), bZIP domain-containing proteins (five to sevenfold), calcium ATPase (>2.38) were upregulated while MYB transcription factors (<−5.39), IDS2 (<−3.72) was downregulated in −Fe and −Fe−Zn root when compared to −Fe and −Zn leaf. Downregulation of zinc transporter 5 (−2.59), and zinc transporter 3 (−1.57) was recorded in −Fe root when compared to −Zn leaf. The downregulation of ZIF-like protein (−2.84) and upregulation of *S-adenosyl methionine* (SAM) *synthase* (1.95) and 1, 2-dihydroxy-3-keto-5-methylthiopentene (3.33), 5-methyltetrahydropteroyltriglutamate (homocysteine transferases >1.5) were observed in −Fe−Zn root when compared to −Fe leaf. The gene involved in iron-nicotianamine transmembrane transporter activity was downregulated (−1.79) in −Fe root when compared to −Zn leaf. The APRT (>1.96 times), involved in the ATP production needed for the Met activation process was induced in the root treatment (−Fe, −Fe−Zn) when compared to leaf treatments (−Fe, −Zn). The IDI4 (< −2.38), potassium transporter gene (<−2.19), and *ribose 5-phosphate isomerase* (<−1.60) were downregulated in the root treatment (−Fe, −Fe−Zn) but the same genes were upregulated in −Fe−Zn leaf (**Supplementary Table 12**).

The expression of *delta-aminolevulinic acid dehydratase* (<−1.54) involved in chlorophyll biosynthesis was low in the −Fe, −Fe−Zn root treatments when compared to −Fe and −Zn leaf. The *RUBISCO* (>1.54), an important plant sugar synthesis enzyme of dark reaction was upregulated in −Fe−Zn leaf when compared to root deficient in −Fe or −Zn but downregulated in root −Fe (<−2.5) and −Fe−Zn (<−6.8) when compared to Zn-deficient leaf (**Supplementary Table 13**).

The enzymes, *pyruvate* (two to sevenfold), *3-Phosphoglycerate dehydrogenase* (two to fivefold), *malate dehydrogenase* (two to fivefold), and *phosphoglycerate kinase* (three to fivefold) involved in the carbohydrate metabolism were downregulated in the root treatments (−Fe, −Fe−Zn) when compared to leaf treatments (−Fe, −Zn). The above-mentioned genes were upregulated in −Fe−Zn leaf when compared to −Fe root and downregulated in −Fe leaf when compared to −Zn root. The *glyceraldehyde-3-phosphate dehydrogenase* (−2.72), *pyruvate kinase* (−1.70), PEPC (−2.20), and *pyrophosphate fructose 6-phosphate* (−2.04) were downregulated in −Fe−Zn leaf when compared to −Fe or −Zn leaf (**Supplementary Table 14**). In the case of genes involved in phytohormones synthesis and signaling mechanism, ARP (>3.23), auxin efflux carrier component (three to ninefold), ACC *synthase* (two to threefold), were upregulated and, ARP SAUR36 was two to sixfold downregulated in −Fe and −Fe−Zn root when compared to −Zn and −Fe leaf tissue (**Supplementary Table 15**).

Serine and threonine kinases were nearly 2–5 times upregulated in −Fe, −Fe−Zn root when compared to −Fe and −Zn leaf treatments. *Patatin, laccase, kinesin*, SOD, were two to eightfold upregulated and, *serine/threonine-protein phosphatase, catalase*, and *ascorbate peroxidases* were two to ninefold upregulated in root treatments (−Fe, −Fe−Zn) when compared to leaf treatments (−Fe, −Zn) and four to fivefold downregulated in −Fe−Zn leaf when compared to −Fe root. *Trehalose 6-phosphate phosphatase* (<−3.75), and *peroxidases* (<−3.67) were downregulated in −Fe−Zn leaf when compared to −Fe and −Zn root (**Figure 2C**) (**Supplementary Table 16**).

Chromosomal annotation of identified iron and zinc responsive genes

A total of 68 genes (**Supplementary Table 17**) corresponding to Fe and Zn uptake and transport, identified in our study were distributed on all seven chromosomes (**Figure 3**). The genes related to Fe response and transport were distributed on 2 and 3 chromosomes while for Zn, they were distributed on all the chromosomes except on chromosome 2. The genes of the MA pathway for PS synthesis were distributed on all 7 chromosomes. OPT3 and ferritin were located on chromosome 2 and the transcription factor FER-like was located on chromosome 3.

Identification of orthologs

The identified 68 Fe- and Zn-homeostasis pathway-related genes (**Supplementary Table 17**) in the present study were BLAST searched against *Arabidopsis* spp., rice, maize, sorghum, and foxtail millet genomes for the identification of orthologous genes.

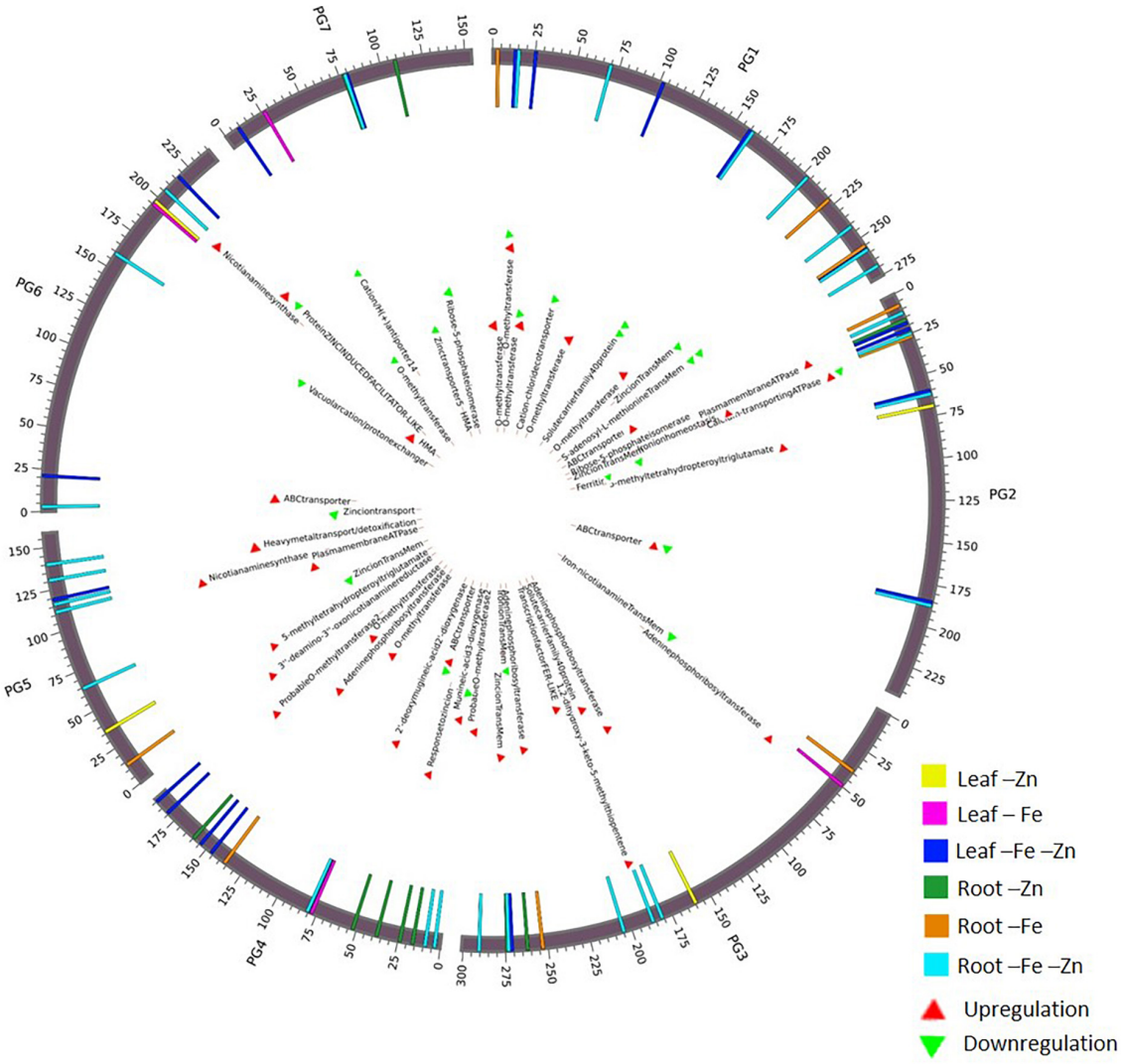

FIGURE 3
Circos plot representing important Fe and Zn homeostasis-related genes along with the differential expression patterns in pearl millet.

Foxtail millet had the maximum homology, sharing 64 orthologs with pearl millet followed by rice (32), maize (33), sorghum (34), and *Arabidopsis* spp. (8). Annotations were assigned to the identified orthologs to know their functionality in respective species. The foxtail millet had the highest similarity to the pearl millet genes by capturing 80 ortholog sequences from 64 genes with 23 sequences of 100% similarity. In rice, 92 ortholog sequences were identified for 58 genes, of which 11 sequences showed 100% similarity and 34 sequences showed >90% similarity to pearl millet genes. Maize had 102 ortholog sequences for the 56 pearl millet genes, of which 11 sequences recorded 100% similarity. The pearl millet to sorghum comparison yielded 93 ortholog sequences from 32 genes, of which 16 sequences showed 100% similarity. In *Arabidopsis* spp. a total of 14 ortholog sequences were identified for 8 genes, of which 10 ortholog sequences recorded >90% similarity (**Figure 4**).

Our analysis also showed more than one ortholog for a given gene. Among food crops, 23 genes out of total identified 58 orthologs in rice reported more than one ortholog sequence. Maize, sorghum, and foxtail millet had 32, 23, and 11 genes, respectively, and had more than one ortholog.

The orthologs of four genes, *Ribose 5-phosphate isomerase*, SAM synthase, FDH, and OPT3 were identified in Arabidopsis and four food crops. The ortholog of a gene, 5-methyltetrahydropteroyltriglutamate—homocysteine was identified in Arabidopsis and three food crops except for sorghum, and the ortholog of one gene, *ABC transporter F* family member was identified in Arabidopsis and three food crops except for foxtail millet. The *plasma membrane*

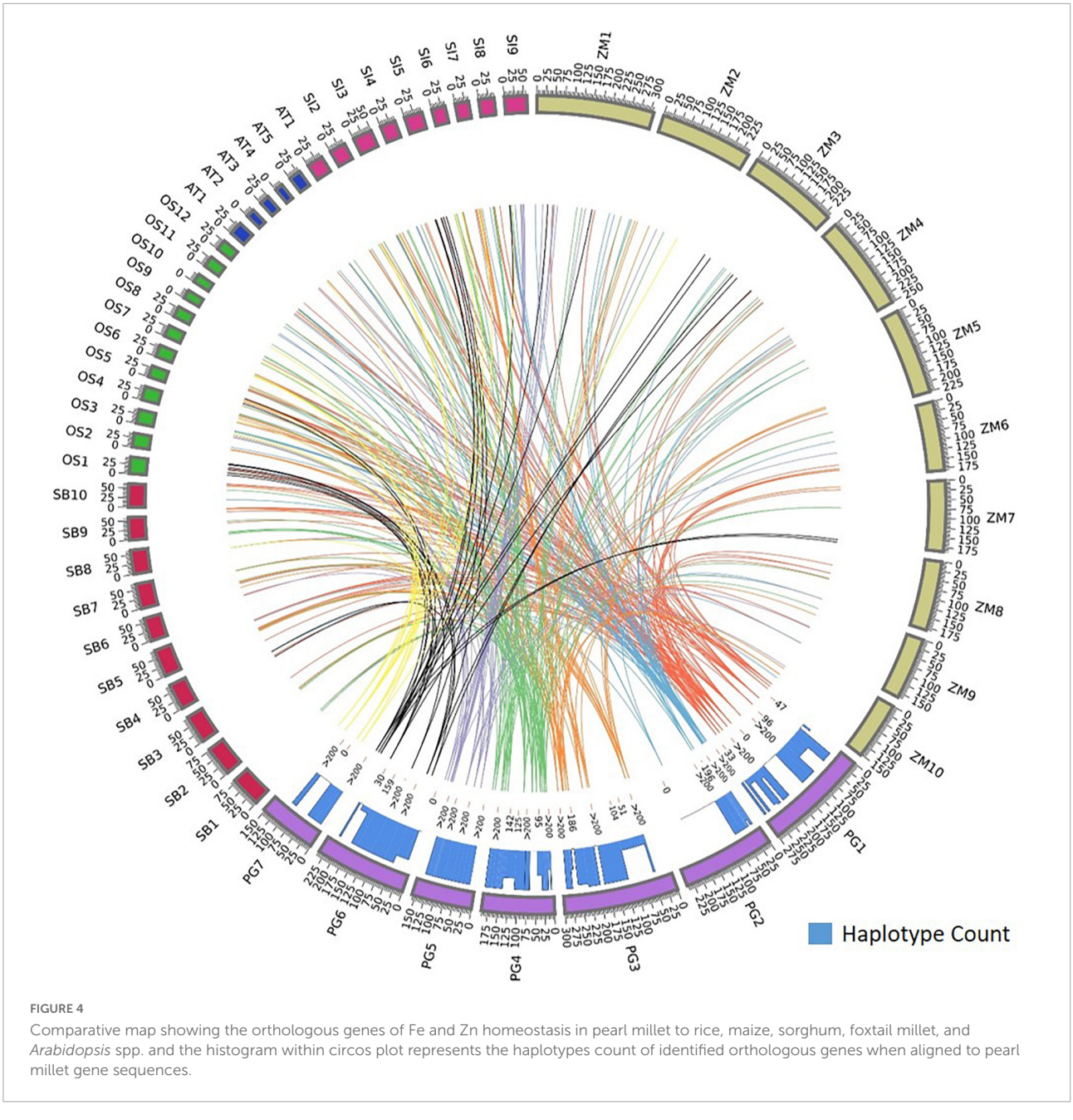

FIGURE 4
Comparative map showing the orthologous genes of Fe and Zn homeostasis in pearl millet to rice, maize, sorghum, foxtail millet, and *Arabidopsis* spp. and the histogram within circos plot represents the haplotypes count of identified orthologous genes when aligned to pearl millet gene sequences.

ATPases orthologs were identified in *Arabidopsis* spp. and three food crops except for rice. More than 40 gene orthologs were identified in all food crops except *Arabidopsis* spp. The orthologs of eight genes were identified in three food crops except for rice and the orthologs of two genes were identified in three food crops except for sorghum.

Identification of haplotypes

The identified ortholog sequences of 68 pearl millet Fe and Zn-related genes across *Arabidopsis* spp. and four food crops were fetched out and aligned for the identification of haplotypes. The ortholog sequences of all four pearl millet genes (*Ribose-5-phosphate isomerase*, SAM synthase, FDH, and OPT3) identified across the *Arabidopsis* spp. and four food crops (rice, maize, sorghum, and foxtail millet) recorded >200 haplotypes (Figure 4). A total of >200 haplotypes were identified in the ortholog sequences of four pearl millet genes-*Plasma membrane ATPases* (except rice), *ABC transporter F family member 1* (except foxtail millet), and two 5-methyltetrahydropteroyltriglutamate—homocysteine (except sorghum), identified across *Arabidopsis* spp. and any of the three

food crops. The maximum haplotypes (>200) were recorded in the ortholog sequences of 29 pearl millet genes with all food crops. The minimum haplotypes (35) were identified in the ortholog sequences of the SAM transmembrane transporter activity gene across four food crops when aligned to pearl millet genes (**Figure 5**).

Discussion

The present study was performed to determine the expression pattern of Fe and Zn-responsive genes in leaf and root tissues under starvation conditions. The expression changes of genes involved in different cellular pathways that consequently effecting the Fe and Zn uptake and transport mechanism have been investigated.

Altered expression of cellular pathways and homeostasis genes under iron deficiency

Plants uptake Fe from the soil by reduction-based strategy at the root surface, wherein expression of metal ion uptake genes FRO2 (ferric chelate reductase oxidase), and IRT2 (iron regulated transporter) were upregulated in Fe starvation to avoid deficiency. The induced expression of a bHLH transcription factor named FER in tomato (34) or FIT1 (Fe-induced transcription factor 1) in Arabidopsis (35), positively controlling the Fe uptake genes was observed in the present study (**Figure 6**). In a reduction-based strategy, the plasma membrane's H^+-ATPase activity of releasing protons to the rhizosphere led to Fe-deficiency to decrease the pH of the soil which solubilizes the Fe^{3+} and drives the Fe ions by generating the electrochemical proton gradient (36). Fe in graminaceous plants is mostly taken by the roots by chelation activity (Strategy II), where plants synthesize the MA family of PS from SAM a conserved pathway (37). The enzymes, SAM synthetase, S adenosylmethionine decarboxylase, NAS, IDS3, and 3″'deamino 3″'oxonicotianamine reductase for the PS production were upregulated in the Fe-deficient root indicating their sensitivity to Fe nutrition. Moreover, IDS2, one of the MA synthesis enzymes, involved in the hydroxylation of the C-3 positions of MA, and 2′-deoxymugineic acid (DMA) were downregulated in Fe-deficient root as it was a Fe-dependent enzyme (38). Hence, for the production of MAs, sufficient quantities of Met molecules are needed, which are generated by the Met cycle. The enzymes, 5 methyltetrahydropteroyltriglutamate (homocysteine methyltransferases), IDI4, and the intermediate product, 1,2-dihydroxy-3-keto-5-methylthiopentene formed by dehydratase-enolase-phosphatase (DEP) enzyme of Met cycle were induced in Fe-deficient root. The FDH, ribose 5-phosphate isomerase, APRT, enzymes synchronously expressed with Met cycle enzymes related to the Met recycling reactions (39), which were also reported to be accumulated in Fe-deficient roots.

The enhanced extrusion of protons and FC-R (ferric chelate-reductase) activity during Fe-deficiency requires a higher rate of NAD(P)H and ATP regeneration aided by carbohydrate catabolism to necessitate the increased uptake (40) (**Figure 6**). The carbohydrate catabolism increases the accumulation of enzymes and intermediates of the glycolytic cycle for the production of ATP needed for the H^+ ATPase activity, increases the H^+ ions in the proton extrusion process, and reduces equivalents for FC-R activity (40). To maintain the glycolytic cycle, the feedback inhibition of *phosphofructokinase* (PFK) can be overcome by the utilization of PEP through PEPC activity (41). PEPC induces the production of organic acids resulting in the acidification of cytoplasm, indeed responsible for the extrusion of H^+ ions from the root surface. In addition to the PEPC activity and organic acids production, an increase in CO_2 fixation (42) and sucrose accumulation under Fe-deficient roots and shoots helped in maintaining the sugar concentrations (PEP) needed for PEPC activity (43).

Moreover, under Fe deficiency, the genes related to several additional metabolic pathways and cytosolic enzymatic activities showed elevated expression for the production of reducing equivalents required to support FC-R activity. In plants, for the transport of Fe molecules from root to shoot, the principal chelator's citrate, malate, NA (nicotianamine), and MAs are required. Here induced expression of PEPC in Fe-deficiency, aids in the Fe uptake and transport by secretion of malate and other organic acids. Fe is known to be transported as Fe^{3+}-chelates (citrate and MAs) in the xylem and as Fe^{2+}-NA in the phloem. The induced expression of the NAS gene aids in NA production required for Fe translocation from root to shoot was well studied (44). The upregulated OPT3 in Fe-deficient root suggests its role in the redistribution between vegetative tissues and is also known to be involved in loading shoot Fe to phloem for transport and movement of Fe to developing seeds (45). This may be a critical part of understanding the proportional Fe uptake of biofortified varieties in comparison to non-biofortified varieties to compensate for available soil Fe concentration during the pearl millet growth and seed filling. As expected, Ferritin was downregulated in Fe-deficient leaf and root tissues since it's a Fe storage protein.

During Fe stress, a reduced amount of ferredoxin fails to activate delta-aminolevulinic acid (ALA), affecting the chlorophyll biosynthesis and resulting in chlorosis (**Figure 6**). Moreover, in the chloroplast, the Fe stress affected the thylakoid proteins by reducing the light-harvesting complexes and overall amount of photosystem I and II, cytochrome complexes, rubisco carboxylation efficiency, and ATPase complex in plants (46). At the root level, some morphological changes such as the development of additional root hairs and transfer cells occur during Fe-deficiency (47), which is known to be regulated by

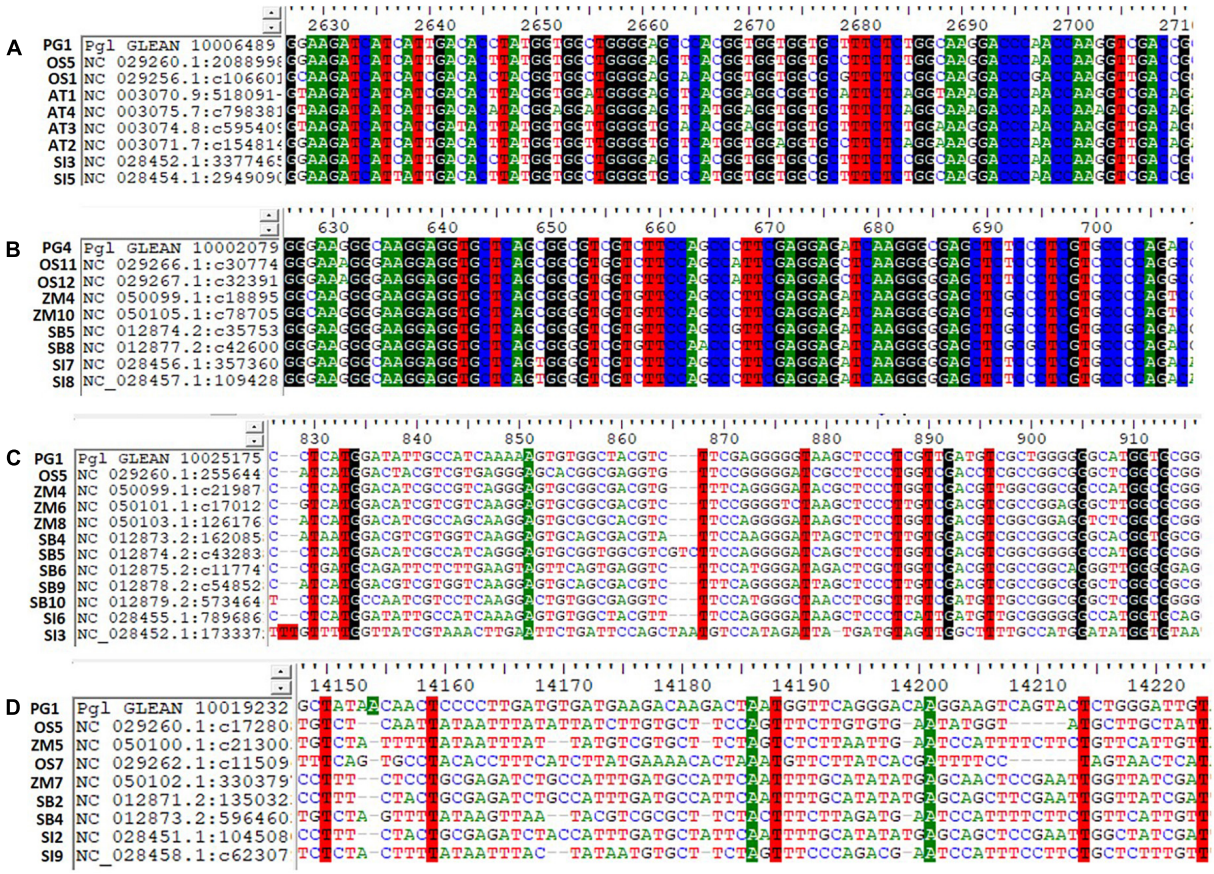

FIGURE 5
Haplotypes representation for the top identified Fe and Zn genes across Arabidopsis and five food crops (AT, *Arabidopsis thaliana*; PG, *Pennisetum glaucum*; OS, *Oryza sativa*; ZM, *Zea mays*; SB, *Sorghum bicolor*; and SI, *Setaria italica*). **(A)** Pgl_GLEAN_10006489 (SAM synthase) with ortholog sequences of *Arabidopsis* spp. and two food crops showing highly conserved regions of a gene, **(B)** Pgl_GLEAN_10002079 (Ferritin) with ortholog sequences of four food crops showing highly conserved regions of a gene, **(C)** Pgl_GLEAN_10025175 (O-methyltransferase activity) with ortholog sequences of four food crops showing higher variability regions with a few haplotypes of a gene, and **(D)** Pgl_GLEAN_10019232 (SAM transmembrane transporter activity) with ortholog sequences of four food crops showing higher variability regions with a few haplotypes of a gene.

ethylene and/or auxin signaling (48). Our study reported the induced expression of ACC *synthase* for ethylene biosynthesis and *Indole-3-glycerol-phosphate synthase* for auxin biosynthesis along with the ARP and efflux carrier protein in the Fe-deficient plant. Studies reported that the accumulation of sucrose acts as a signal for the induction of auxin under Fe-deficiency (49) which in turn is essential for the nitric oxide (NO) synthesis, required for the activation of Fe-deficiency response by acting upstream of FIT (50) (**Figure 6**).

The Fe starvation conditions in the pearl millet seedlings activated several genes namely, *NAS*, *SAM synthases*, *DMA*, *IDS3*, *IDS2*, *IDI4*, and *APRT* in the MA pathway and *FER*-like transcription factor, H^+ *ATPases*, and *OPT3* in the Fe homeostasis mechanism regulating the uptake and transport. Additionally, the genes in cellular pathways indirectly aiding in the uptake and transport of Fe ions in pearl millet were also reported.

Altered expression of cellular pathways and homeostasis genes under zinc deficiency

The rhizosphere acidification process, which lowers the pH of the soil by releasing H^+ ions and organic acids, facilitated the Zn solubilization and uptake. Plants uptake Zn in the form of Zn^{2+} and Zn^{2+}-ligand complexes. The Zn^{2+}-ligand complex uptake is mediated by the synthesis and release of PS, among which NA was reported to be the primary mediator responsible for the uptake and transport (51). So, under the Zn-starved conditions, the genes required for the chelator synthesis were elevated in graminaceous plants to increase the uptake from soil (**Figure 7**) to avoid deficiency effects. Here in our study, *SAM synthetase,* NAS, and *ribose 5-phosphate isomerase genes* for the synthesis of NA were upregulated in Zn-deficient roots similar to previous reports (20). Under Zn deficiency,

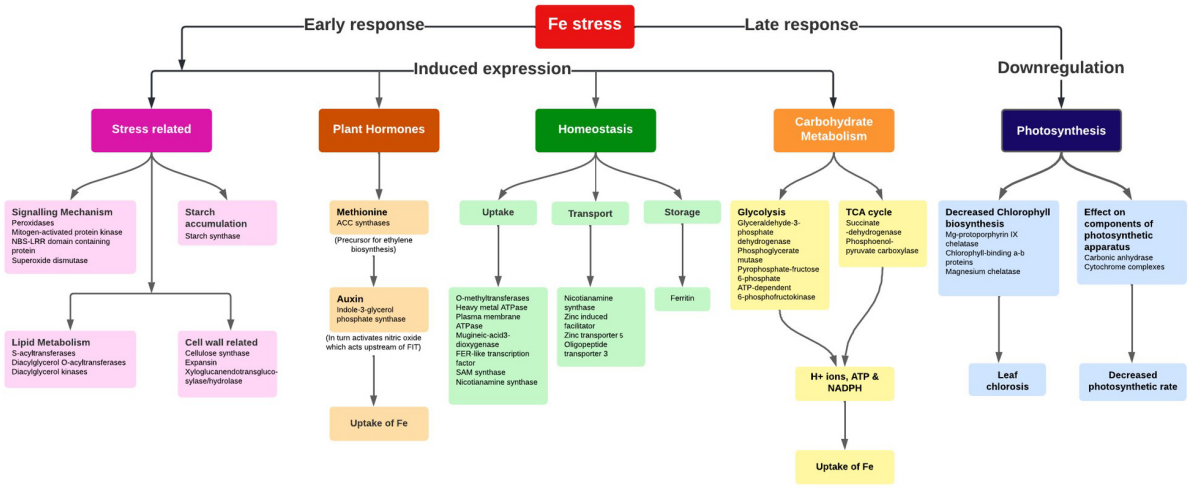

FIGURE 6
Important pathways and their interconnectivity in response to Fe stress in pearl millet.

the ZIP (Zinc, Iron permease family/ZRT-IRT like proteins) family transporters (Zn transporter 3 and 5) were upregulated for the uptake of remaining traces of Zn from the soil in deficiency condition (52). The members of the HMA (P-type ATPase) family for the xylem loading, maintaining the plastid Zn content were upregulated in Zn-deficient leaves (53).

Zinc acts as a co-factor in activating anhydrases, oxidases, and peroxidase enzymes and is involved in nitrogen metabolism, photosynthesis, carbohydrate metabolism, and auxin synthesis in plants (**Figure 7**). Zn-deficiency is known to reduce the chlorophyll content by affecting the chlorophyll biosynthesis pathway causing a decline in the photosynthetic efficiency of plants (54). Moreover, the upregulation of enzymes involved in the starch synthesis was observed which was similar to the previous report (55). The reduced expression of carbonic anhydrases was observed in Zn-deficiency affecting the entire photosynthetic rate (**Figure 7**). Zn-deficiency is known to affect the stomatal conductance as it is involved in maintaining the integrity of cell membrane and K^+ uptake by which the CO_2 assimilation rate is reduced, indirectly affecting the carbohydrate metabolism process (56). The expression of enzymes, *carbonic anhydrase, ribulose 1, 5-bisphosphate carboxylase*, involved in the photosynthesis and *fructose 1, 6-bisphosphate* involved in glycolysis are reduced in Zn starvation, as Zn is an important constituent in activating these enzymes (57). Moreover, the aldolase, sucrose, and starch synthesis enzymes are inhibited by Zn stress in plants. Under Zn deficiency, the reduced expression of SOD in leaves was observed as the enzyme needed Zn ion for the activation. The induced expression of abiotic stress-responsive peroxidases and catalase enzymes for ROS detoxification was noticed under Zn-deficiency (33). The downregulation of the tryptophan synthase enzyme involved in auxin synthesis was reported in Zn-deficiency (**Figure 7**), as the enzyme requires Zn ion as a co-factor, and its reduction causes disturbances in the auxin metabolism process.

Therefore, under the Zn deficiency condition, the expression of NA synthesis genes (*SAM synthetase, NAS,* and *ribose 5-phosphate isomerase* gene), ZIP family proteins, and HMA family proteins regulating the Zn homeostasis mechanism were revealed. The study also disclosed the expression changes of many cellular pathway genes which require Zn ions to activate the respective pathways.

Cross-talks between iron and zinc pathways

The induced expression of chelator synthesis genes (e.g., NAS, DMAS, and SAM) was reported under both Fe and Zn deficiency demonstrating the dual role of PS in Fe and Zn homeostasis mechanisms in pearl millet. Several studies reported the affinity of Fe-transporters in transporting Zn along with the Fe in plants (58). Hence, the upregulation of Fe-transporters under Fe-starvation conditions resulted in increased uptake and accumulation of Zn and vice-versa. The induced expression of transcription factor FER reported under Fe and Zn deficiency aids in activating the expression of transporter genes for the uptake of both nutrients and is considered a principal transcription factor in their homeostasis pathway mechanism.

Iron-deficiency-induced accumulation of Zn ions leads to excess toxic amounts (>0.4 mg g^{-1} dry weight) of Zn in plant cytoplasm (32). Vacuoles are identified to be the main storage and detoxifying organelles for Zn excess in the plant cytoplasm. Metal tolerance protein (MTP3), HMA3, and ZIF

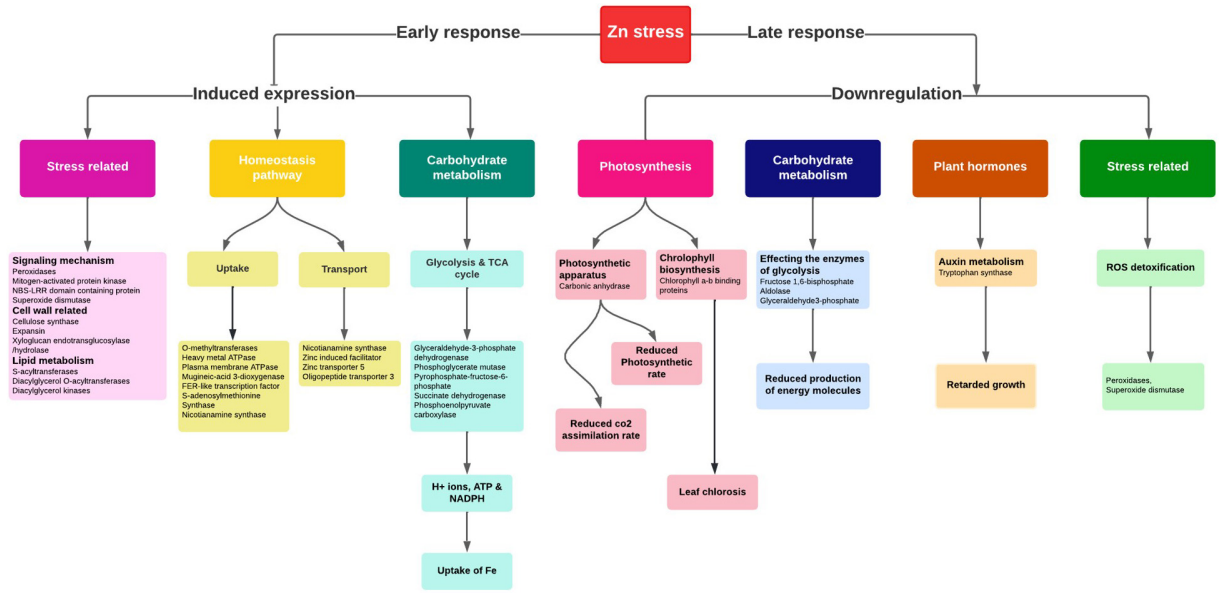

FIGURE 7
Important pathways and their interconnectivity in response to Zn stress in pearl millet.

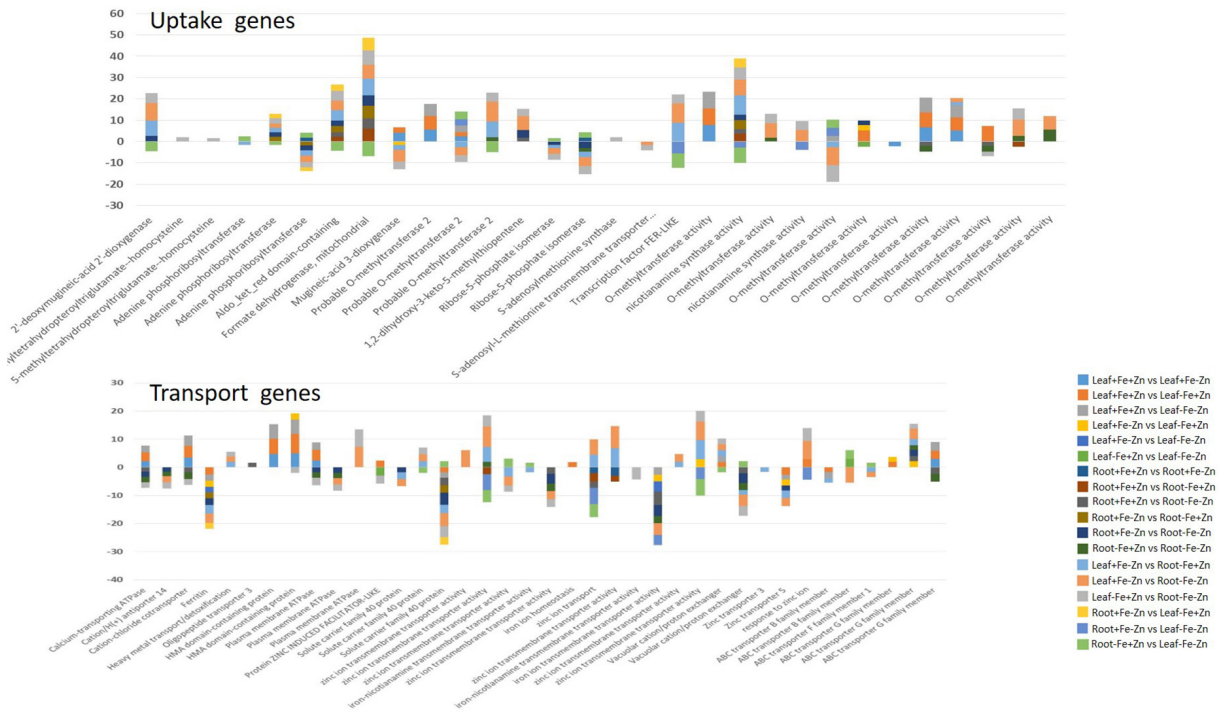

FIGURE 8
Important genes associated with the Fe and Zn uptake and transport in the leaf and root tissues of pearl millet under 18 pairwise stress combinations.

are the vacuolar membrane transporters that aid in Zn tolerance during excess accumulation of Zn in Fe-deficient conditions. Among them, the ZIF1 transporter of the MFS (major facilitator superfamily) family has shown the induced expression in our studies which indirectly aids in the sequestration of Zn molecules by transporting chelator molecules (NA) into the

vacuole (59). In addition, HMA transporters induced in Fe deficiency are probably similar to HMA3 required for the detoxification of Zn (60). This study reported the downregulated expression of zinc transporters 3 and 5 in reducing the Zn content, to avoid toxic effects due to its accumulation under the Fe deficiency condition. The same transporters can be upregulated for increasing the Zn content in target-oriented biofortification processes. Further, the studies reported that the Zn-deficiency will accumulate higher Fe by induced expression of uptake genes in plants (61). NAS involved in PS synthesis and NA production that is needed for the uptake and transport of Fe and Zn intracellularly was upregulated (44) in the current study (**Figure 8**).

Through an *in silico* approach, the 68 important Fe and Zn-related gene orthologs were identified in *Arabidopsis* spp. and four food crops namely rice, maize, sorghum, and foxtail millet (**Figure 4**). The identified ortholog sequences were grouped under pair-wise type orthologs showing a one-to-many (1: m) relationship where one gene of pearl millet has more than one ortholog in *Arabidopsis* spp. and other food crops which imply that the gene may be duplicated in an ancestor, after the event of speciation process (62). In total, the orthologous sequences of 64 genes out of 68 were identified in the foxtail millet crop with a maximum number of orthologs having 100% similarity when compared to *Arabidopsis* spp. and other three food crops explaining the fact that it had a common ancestor during the evolutionary process or belongs to the same clade in a phylogenetic tree. In the other three food crops (rice, maize, and sorghum), the orthologs for more than 32 genes were identified, when compared to *Arabidopsis* spp., which shows that all the food crops and pearl millet are related or grouped under one cluster. The ortholog sequences for the least number of genes were identified in *Arabidopsis* spp. when compared to the other four food crops, which shows that it is distantly related to the pearl millet crop.

Haplotypes are the specific group of jointly inherited DNA regions or nucleotides from a single parent (63). The genes *Ribose-5-phosphate isomerase*, SAM synthase, FDH, and OPT3 identified across the *Arabidopsis* spp. and four food crops showed highly conserved regions with a high number of haplotypes. These are the core genes strongly conserved at the nucleotide sequence level throughout the related genomes. A high number of haplotypes observed in 29 pearl millet genes with all four food crops probably indicated the conservation of these sequences during the evolution process (64). SAM transmembrane transporter activity gene showed higher variability or polymorphism by recording a few haplotypes (35) due to deletion, addition, substitution, or mutation during the process of evolution (64, 65). The continuous series of haplotypes detected for the Fe and Zn responsive genes across the *Arabidopsis* spp. and four food crops could be used for designing the common markers for its utilization across the crop species (66).

Conclusion

A few studies in pearl millet reported a positive and significant correlation between Fe and Zn contents (15, 16), which implies the possible existence of common uptake and regulatory pathways operate to maintain genotypic variations for these two micronutrients within the limit of available soil Fe and Zn concentration during the crop growth and development thereby to seeds. Our current study revealed the expression of *NAS*, *SAM synthases*, *DMA*, *IDS3*, *IDS2*, *IDI4*, and *APRT* in the MA pathway and *FER*-like transcription factor, H^+ *ATPases*, *HMA*, *ZIF1*, *OPT3,* and *Zn transporter 3* and *5* involved in the uptake and transport mechanism of Fe and Zn ions. The expression changes of major cellular pathway genes related to phytohormones, chlorophyll biosynthesis, photosynthesis, stress-induced pathways, carbohydrate metabolism, and their regulation in Fe and Zn homeostasis under stress conditions in pearl millet were revealed. This study is limited to the seedling stage and hence merits further investigation on the field-based study that mimics similar conditions (deficiency of soil Fe and Zn) to validate its practical application in pearl millet breeding and biofortification of varieties. Indian Council of Agricultural Research (ICAR) endorsed the minimum standards for Fe (>42 ppm) and Zn (>32 ppm) in pearl millet variety and hybrid testing and release policy since 2018 (67). Furthermore, the validated genic SNPs associated with Fe and Zn pathways will help in the development of Fe and Zn-efficient biofortified pearl millet lines through a marker-assisted selection program.

Maintaining the higher Fe and Zn with the higher yield is a challenge to the breeders using conventional breeding approaches, therefore, the present study provides the opportunity to develop and explore the genomic-assisted breeding pipelines to deliver more nutritious varieties under varied soil Fe/Zn availability in the crop ecology. Further, the above-identified genes can be used for the enhancement of Fe and Zn contents in other staple crops, which will help to ameliorate malnutrition.

Data availability statement

The data presented in the study are deposited in the Sequence Read Archive repository, accession number PRJNA819827.

Author contributions

CG, VS, MG, and NT conceptualized the experiment and wrote the manuscript. CG, VS, RM, AV, and HK conducted the experiments. CG, AR, JS, SR, and NT performed the data analysis. All authors read and approved the manuscript.

Funding

This experiment was funded by the Bill and Melinda Gates Foundation project (INV-008187), the HarvestPlus Pearl Millet project (HP#5403), and the ICAR-Indian Institute of Millets Research project (CI/2018-23/120). CG acknowledged the PJTSAU, Hyderabad for providing the Ph.D. scholarship.

Conflict of interest

The authors declare that the research was conducted in the absence of any commercial or financial relationships that could be construed as a potential conflict of interest.

Publisher's note

Supplementary material

The Supplementary Material for this article can be found online at: https://www.frontiersin.org/articles/10.3389/fnut.2022.884381/full#supplementary-material

References

1. Muthamilarasan M, Dhaka A, Yadav R, Prasad M. Exploration of millet models for developing nutrient rich graminaceous crops. *Plant Sci.* (2015) 242:89–97. doi: 10.1016/j.plantsci.2015.08.023

2. Taylor, JRN, Emmambux MN. *Gluten-Free Cereal Products and Beverages*. (2008). Available online at: http://www.sciencedirect.com/science/article/pii/B9780123737397500083

3. Boncompagni E, Orozco-Arroyo G, Cominelli E, Gangashetty PI, Grando S, Tenutse Kwaku Zu T, et al. Antinutritional factors in pearl millet grains: phytate and goitrogens content variability and molecular characterization of genes involved in their pathways. *PLoS One.* (2018) 13:e0198394. doi: 10.1371/journal.pone.0198394

4. Govindaraj M, Rai K. Breeding biofortified pearl millet cultivars with high iron density. *Indian Farm.* (2016) 65:53–5.

5. Govindaraj M, Rai KN, Cherian B, Pfeiffer WH, Kanatti A, Shivade H. Breeding biofortified pearl millet varieties and hybrids to enhance millet markets for human nutrition. *Agriculture.* (2019) 9:106. doi: 10.3390/agriculture9050106

6. Stoltzfus, RJ, Mullany L, Black RE. Iron deficiency anaemia. In: Ezzati CLJMM, Lopez AD, Rodgers A editors. *Comparative Quantification of Health Risks: Global and Regional Burden of Disease Attributable to Selected Major Risk Factors*. Geneva: World Health Organization (2004) p. 163–209.

7. Manwaring HR, Bligh HFJ, Yadav R. "The challenges and opportunities associated with biofortification of pearl millet (*Pennisetum glaucum*) with elevated levels of grain iron and zinc. *Front Plant Sci.* (2016) 7:1944. doi: 10.3389/fpls.2016.01944

8. Black RE, Victora CG, Walker SP, Bhutta ZA, Christian P, De Onis M, et al. Maternal and child undernutrition and overweight in low-income and middle-income countries. *Lancet.* (2013) 382:427–51. doi: 10.1016/S0140-6736(13)60937-X

9. Ashok Kumar A, Reddy B, Ramaiah B, Sahrawat K, Pfeiffer W. Genetic variability and character association for grain iron and zinc contents in *Sorghum* germplasm accessions and commercial cultivars. *Eur J Plant Sci Biotechnol.* (2012) 6:1–5.

10. Mallikarjuna MG, Thirunavukkarasu N, Hossain F, Bhat JS, Jha SK, Rathore A, et al. Stability performance of inductively coupled plasma mass spectrometry-phenotyped kernel minerals concentration and grain yield in maize in different agro-climatic zones. *PLoS One.* (2015) 10:e0139067. doi: 10.1371/journal.pone.0139067

11. Kola G, Reddy PCO, Shaik S, Gunti M, Palakurthi R, Talwar HS, et al. Variability in seed mineral composition of foxtail millet (*Setaria italica* l.) landraces and released cultivars. *Curr Trends Biotechnol Pharm.* (2020) 14:239–55. doi: 10.5530/ctbp.2020.3.25

12. Govindaraj M, Rai KN, Shanmugasundaram P, Dwivedi SL, Sahrawat KL, Muthaiah AR, et al. Combining ability and heterosis for grain iron and zinc densities in pearl millet. *Crop Sci.* (2013) 53:507–17. doi: 10.2135/cropsci2012.08.0477

13. Singh S, Gupta SK. Formation of heterotic pools and understanding relationship between molecular divergence and heterosis in pearl millet [*Pennisetum glaucum* (L.) R. Br.]. *PLoS One.* (2019) 14:e0207463. doi: 10.1371/JOURNAL.PONE.0207463

14. Gupta SK, Velu G, Rai KN, Sumalini K. Association of grain iron and zinc content with grain yield and other traits in pearl millet (*Pennisetum glaucum* (L.) R.Br.). *Crop Improv.* (2009) 36:4–7.

15. Govindaraj M, Rai KN, Kanatti A, Upadhyaya HD. Exploring the genetic variability and diversity of pearl millet core collection germplasm for grain nutritional traits improvement. *Sci Rep.* (2020) 10:21177. doi: 10.1038/s41598-020-77818-0

16. Pujar M, Gangaprasad S, Govindaraj M, Gangurde SS. Genome - wide association study uncovers genomic regions associated with grain iron, zinc and protein content in pearl millet. *Sci Rep.* (2020) 10:19473. doi: 10.1038/s41598-020-76230-y

17. Huey SL, Venkatramanan S, Udipi SA, Finkelstein JL, Ghugre P, Haas JD, et al. Acceptability of iron- and zinc-biofortified pearl millet (ICTP-8203)-based complementary foods among children in an urban slum of Mumbai, India. *Front Nutr.* (2017) 4:39. doi: 10.3389/fnut.2017.00039

18. Kanatti A, Rai KN, Radhika K, Govindaraj M, Sahrawat KL, Rao AS. Grain iron and zinc density in pearl millet: combining ability, heterosis and association with grain yield and grain size. *Springerplus.* (2014) 3:1–12. doi: 10.1186/2193-1801-3-763

19. Zheng L, Huang F, Narsai R, Wu J, Giraud E, He F, et al. Physiological and transcriptome analysis of iron and phosphorus interaction in rice seedlings. *Plant Physiol.* (2009) 151:262–74. doi: 10.1104/pp.109.141051

20. Mallikarjuna MG, Thirunavukkarasu N, Sharma R, Shiriga K, Hossain F, Bhat JS, et al. Comparative transcriptome analysis of iron and zinc deficiency in maize (*Zea mays* L.). *Plants.* (2020) 9:1–31. doi: 10.3390/plants9121812

21. Azevedo H, Azinheiro SG, Muñoz-Mérida A, Castro PH, Huettel B, Aarts MMG, et al. Transcriptomic profiling of *Arabidopsis* gene expression in response to varying micronutrient zinc supply. *Genomics Data.* (2016) 7:256–8. doi: 10.1016/j.gdata.2016.01.021

22. Bolger AM, Lohse M, Usadel B. Trimmomatic: a flexible trimmer for Illumina sequence data. *Bioinformatics.* (2014) 30:2114–20. doi: 10.1093/bioinformatics/btu170

23. Varshney RK, Shi C, Thudi M, Mariac C, Wallace J, Qi P, et al. Pearl millet genome sequence provides a resource to improve agronomic traits in arid environments. *Nat Biotechnol.* (2017) 35:969–76. doi: 10.1038/nbt.3943

24. Kim D, Paggi JM, Park C, Bennett C, Salzberg SL. Graph-based genome alignment and genotyping with HISAT2 and HISAT-genotype. *Nat Biotechnol.* (2019) 37:907–15. doi: 10.1038/s41587-019-0201-4

25. Li H, Handsaker B, Wysoker A, Fennell T, Ruan J, Homer N, et al. The sequence alignment/map format and SAMtools. *Bioinformatics.* (2009) 25:2078–9. doi: 10.1093/bioinformatics/btp352

26. Liao Y, Smyth GK, Shi W. FeatureCounts: an efficient general purpose program for assigning sequence reads to genomic features. *Bioinformatics.* (2014) 30:923–30. doi: 10.1093/bioinformatics/btt656

27. Love MI, Huber W, Anders S. Moderated estimation of fold change and dispersion for RNA-seq data with DESeq2. *Genome Biol.* (2014) 15:550. doi: 10.1186/s13059-014-0550-8

28. Kent WJ. BLAT - the BLAST-like alignment tool. *Genome Res.* (2002) 12:656–64. doi: 10.1101/gr.229202

29. Livak KJ, Schmittgen TD. Analysis of relative gene expression data using real-time quantitative PCR and the 2-ΔΔCT method. *Methods.* (2001) 25:402–8. doi: 10.1006/meth.2001.1262

30. Cheong WH, Tan YC, Yap SJ, Ng KP. ClicO FS: an interactive web-based service of Circos. *Bioinformatics.* (2015) 31:3685–7. doi: 10.1093/bioinformatics/btv433

31. Hall TA. BioEdit: a user-friendly biological sequence alignment editor and analysis program for windows 95/98/NT. *Nucleic Acids Symp Ser.* (1999) 41:95–8.

32. Kanai M, Hirai M, Yoshiba M, Tadano T. Iron deficiency causes zinc excess in *Zea mays*. *Soil Sci Plant Nutr.* (2010) 55:271–6. doi: 10.1111/j.1747-0765.2008.00350.x

33. Hajiboland R, Amirazad F. Growth, photosynthesis and antioxidant defense system in Zn-deficient red cabbage plants. *Plant Soil Environ.* (2010) 56:209–17. doi: 10.17221/207/2009-pse

34. Ling HQ, Bauer P, Bereczky Z, Keller B, Ganal M. The tomato fer gene encoding a bHLH protein controls iron-uptake responses in roots. *Proc Natl Acad Sci USA.* (2002) 99:13938–43. doi: 10.1073/pnas.212448699

35. Bauer P, Ling HQ, Guerinot ML. FIT, the fer-like iron deficiency induced transcription factor in *Arabidopsis*. *Plant Physiol Biochem.* (2007) 45:260–1. doi: 10.1016/j.plaphy.2007.03.006

36. Santi S, Cesco S, Varanini Z, Pinton R. Two plasma membrane H+-ATPase genes are differentially expressed in iron-deficient cucumber plants. *Plant Physiol Biochem.* (2005) 43:287–92. doi: 10.1016/j.plaphy.2005.02.007

37. Kobayashi T, Nishizawa NK. Iron uptake, translocation, and regulation in higher plants. *Annu Rev Plant Biol.* (2012) 63:131–52. doi: 10.1146/annurev-arplant-042811-105522

38. Nakanishi H, Yamaguchi H, Sasakuma T, Nishizawa NK, Mori S. Two dioxygenase genes, Ids3 and Ids2, from *Hordeum vulgare* are involved in the biosynthesis of mugineic acid family phytosiderophores. *Plant Mol Biol.* (2000) 44:199–207. doi: 10.1023/A:1006491521586

39. Itai RN, Ogo Y, Kobayashi T, Nakanishi H, Nishizawa NK. Rice genes involved in phytosiderophore biosynthesis are synchronously regulated during the early stages of iron deficiency in roots. *Rice.* (2013) 6:1–13. doi: 10.1186/1939-8433-6-1

40. Espen L, Dell'Orto M, De Nisi P, Zocchi G. Metabolic responses in cucumber (*Cucumis sativus* L.) roots under Fe-deficiency: a 31P-nuclear magnetic resonance in-vivo study. *Planta.* (2000) 210:985–92. doi: 10.1007/s004250050707

41. De Nisi P, Zocchi G. Phosphoenolpyruvate carboxylase in cucumber (*Cucumis sativus* L.) roots under iron deficiency: activity and kinetic characterization. *J Exp Bot.* (2000) 51:1903–9. doi: 10.1093/jexbot/51.352.1903

42. Jin CW, Du ST, Chen WW, Li GX, Zhang YS, Zheng SJ. Elevated carbon dioxide improves plant iron nutrition through enhancing the iron-deficiency-induced responses under iron-limited conditions in tomato. *Plant Physiol.* (2009) 150:272–80. doi: 10.1104/pp.109.136721

43. Lin XY, Ye YQ, Fan SK, Jin CW, Zheng SJ. Increased sucrose accumulation regulates iron-deficiency responses by promoting auxin signaling in *Arabidopsis* plants. *Plant Physiol.* (2016) 170:907–20. doi: 10.1104/pp.15.01598

44. Inoue H, Higuchi K, Takahashi M, Nakanishi H, Mori S, Nishizawa NK. Three rice nicotianamine synthase genes, OsNAS1, OsNAS2, and OsNAS3 are expressed in cells involved in long-distance transport of iron and differentially regulated by iron. *Plant J.* (2003) 36:366–81. doi: 10.1046/j.1365-313X.2003.01878.x

45. Stacey MG, Patel A, McClain WE, Mathieu M, Remley M, Rogers EE, et al. The *Arabidopsis* AtOPT3 protein functions in metal homeostasis and movement of iron to developing seeds. *Plant Physiol.* (2008) 146:589–601. doi: 10.1104/pp.107.108183

46. Andaluz S, López-Millán AF, De Las Rivas J, Aro EM, Abadía J, Abadía A. Proteomic profiles of thylakoid membranes and changes in response to iron deficiency. *Photosynth Res.* (2006) 89:141–55. doi: 10.1007/s11120-006-9092-6

47. Santi S, Schmidt W. Laser microdissection-assisted analysis of the functional fate of iron deficiency-induced root hairs in cucumber. *J Exp Bot.* (2008) 59:697–704. doi: 10.1093/jxb/erm351

48. Schmidt W, Tittel J, Schikora A. Role of hormones in the induction of iron deficiency responses in *Arabidopsis* roots. *Plant Physiol.* (2000) 122:1109–18. doi: 10.1104/pp.122.4.1109

49. Chen PF, Chen L, Jiang ZR, Wang GP, Wang SH, Ding YF. Sucrose is involved in the regulation of iron deficiency responses in rice (*Oryza sativa* L.). *Plant Cell Rep.* (2018) 37:789–98. doi: 10.1007/s00299-018-2267-8

50. Meiser J, Lingam S, Bauer P. Posttranslational regulation of the iron deficiency basic helix-loop-helix transcription factor FIT is affected by iron and nitric oxide. *Plant Physiol.* (2011) 157:2154–66. doi: 10.1104/pp.111.183285

51. Nishiyama R, Kato M, Nagata S, Yanagisawa S, Yoneyama T. Identification of Zn-nicotianamine and Fe-2'-deoxymugineic acid in the phloem sap from rice plants (*Oryza sativa* L.). *Plant Cell Physiol.* (2012) 53:381–90. doi: 10.1093/pcp/pcr188

52. Li S, Zhou X, Huang Y, Zhu L, Zhang S, Zhao Y, et al. Identification and characterization of the zinc-regulated transporters, iron-regulated transporter-like protein (ZIP) gene family in maize. *BMC Plant Biol.* (2013) 13:1. doi: 10.1186/1471-2229-13-114

53. Hussain D, Haydon MJ, Wang Y, Wong E, Sherson SM, Young J, et al. P-type ATPase heavy metal transporters with roles in essential zinc homeostasis in *Arabidopsis*. *Plant Cell.* (2004) 16:1327–39. doi: 10.1105/tpc.020487

54. Zhang J, Wang S, Song S, Xu F, Pan Y, Wang H. Transcriptomic and proteomic analyses reveal new insight into chlorophyll synthesis and chloroplast structure of maize leaves under zinc deficiency stress. *J Proteomics.* (2019) 199:123–34. doi: 10.1016/j.jprot.2019.03.001

55. Suzuki M, Bashir K, Inoue H, Takahashi M, Nakanishi H, Nishizawa NK. Accumulation of starch in Zn-deficient rice. *Rice.* (2012) 5:1–8. doi: 10.1186/1939-8433-5-9

56. Sharma PN, Tripathi A, Bisht SS. Zinc requirement for stomatal opening in cauliflower. *Plant Physiol.* (1995) 107:751–6. doi: 10.1104/pp.107.3.751

57. Marschner P. *Marschner's Mineral Nutrition of Higher Plants*. 3rd ed. Boston, MA: Academic Press, Elsevier (2012).

58. Korshunova YO, Eide D, Clark WG, Guerinot ML, Pakrasi HB. The IRT1 protein from *Arabidopsis thaliana* is a metal transporter with a broad substrate range. *Plant Mol Biol.* (1999) 40:37–44. doi: 10.1023/A:1026438615520

59. Haydon MJ, Cobbett CS. A novel major facilitator superfamily protein at the tonoplast influences zinc tolerance and accumulation in *Arabidopsis*. *Plant Physiol.* (2007) 143:1705–19. doi: 10.1104/pp.106.092015

60. Morel M, Crouzet J, Gravot A, Auroy P, Leonhardt N, Vavasseur A, et al. AtHMA3, a P1B-ATPase allowing Cd/Zn/Co/Pb vacuolar storage in *Arabidopsis*. *Plant Physiol.* (2009) 149:894–904. doi: 10.1104/pp.108.130294

61. Imtiaz M, Alloway BJ, Shah KH, Siddiqui SH, Memon MY, Aslam M, et al. Zinc nutrition of wheat: II: interaction of zinc with other trace elements. *Asian J Plant Sci.* (2003) 2:156–60. doi: 10.3923/ajps.2003.156.160

62. Zahn-Zabal M, Dessimoz C, Glover NM. Identifying orthologs with OMA: a primer. *F1000Research.* (2020) 9:27. doi: 10.12688/f1000research.21508.1

63. Stephens M, Smith NJ, Donnelly P. A new statistical method for haplotype reconstruction from population data. *Am J Hum Genet.* (2001) 68:978–89. doi: 10.1086/319501

64. Panchy N, Lehti-shiu M, Shiu S. Evolution of gene duplication in plants. *Plant Physiol.* (2016) 171:2294–316. doi: 10.1104/pp.16.00523

65. Long M, Betrán E, Thornton K, Wang W. The origin of new genes glimpses from the young. *Nat Rev Genet.* (2003) 4:865–75. doi: 10.1038/nrg1204

66. Patil G, Do T, Vuong TD, Valliyodan B, Lee J. Genomic-assisted haplotype analysis and the development of high-throughput SNP markers for salinity tolerance in soybean. *Sci Rep.* (2016) 6:19199. doi: 10.1038/srep19199

67. Aicrp Pearl Millet. *Proceedings of the 53 rd Annual Group Meeting of ICAR - All India Coordinated Research Project on Pearl Millet Held*. Rajasthan: Agriculture University Jodhpur (2018).

Frontiers in Nutrition

Explores what and how we eat in the context of health, sustainability and 21st century food science

A multidisciplinary journal that integrates research on dietary behavior, agronomy and 21st century food science with a focus on human health.

Discover the latest Research Topics

See more →

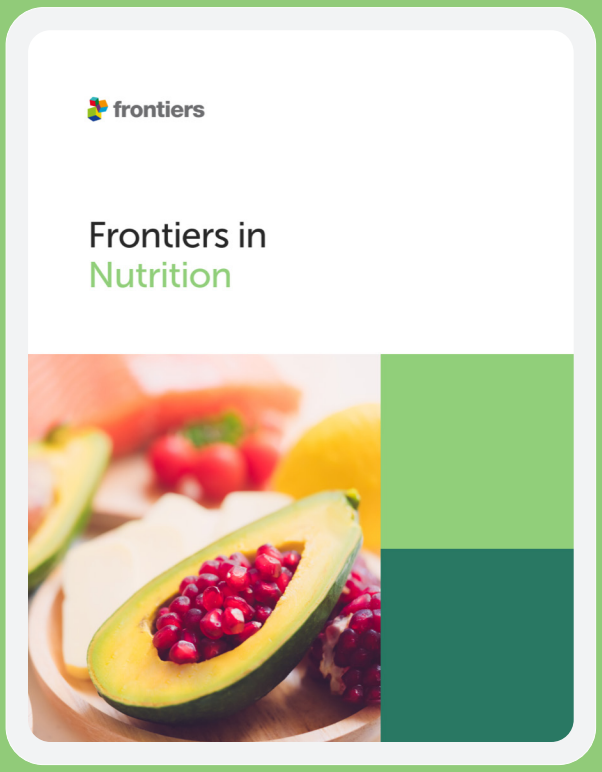

Frontiers

Avenue du Tribunal-Fédéral 34
1005 Lausanne, Switzerland
frontiersin.org

Contact us

+41 (0)21 510 17 00
frontiersin.org/about/contact